Fusion tag-based immobilization methods for the one-step purification and immobilization of enzymes

Inaugural-Dissertation

zur Erlangung des Doktorgrades
der Mathematisch-Naturwissenschaftlichen Fakultät
der Heinrich-Heine-Universität Düsseldorf

vorgelegt von

Johannes Döbber
aus Haselünne

Jülich, April 2018

aus dem Institut für Bio- Geowissenschaften (IBG-1: Biotechnologie)
der Forschungszentrum Jülich GmbH

Gedruckt mit der Genehmigung der
Mathematisch-Naturwissenschaftlichen Fakultät der
Heinrich-Heine-Universität Düsseldorf

Berichterstatter:

1. Prof. Dr. Martina Pohl

2. Prof. Dr. Vlada Urlacher

Tag der mündlichen Prüfung: 12.07.2018

Eidesstattliche Erklärung

Ich versichere an Eides Statt, dass die Dissertation von mir selbständig und ohne unzulässige fremde Hilfe unter Beachtung der „Grundsätze zur Sicherung guter wissenschaftlicher Praxis an der Heinrich-Heine-Universität Düsseldorf“ erstellt worden ist.

Bisher habe ich keine erfolgslosen Promotionsversuche unternommen und diese Dissertation nicht an einer anderen Fakultät vorgelegt.

_____ _____

Ort, Datum Johannes Döbber

Publications in the course of this thesis

Publications in scientific journals

1. Döbber J, Pohl M. 2017. HaloTag™: Evaluation of a covalent one-step immobilization for biocatalysis. *J. Biotechnol.* **241**:170–174.

2. Döbber J, Pohl M, Ley SV, Musio B. 2018. Rapid, selective and stable HaloTag-*Lb*ADH immobilization directly from crude cell extract for the continuous biocatalytic production of chiral alcohols and epoxides. *React. Chem. Eng.* **3**:8–12.

3. Döbber J, Gerlach T, Offermann H, Rother D, Pohl M. 2018. Closing the gap for efficient immobilization of biocatalysts in continuous processes: HaloTag™ fusion enzymes for a continuous enzymatic cascade towards a vicinal chiral diol. *Green Chem.* **20**:544–552.

Oral presentations (Presenting authors are underlined)

1. Rother D, Döbber J, Kloß R., Jäger V, Krauß U, Pohl M. 2016. Enzyme toolboxes & reaction engineering – Solutions for applied biocatalysis. *ProcessNET 2016.* Aachen.

2. Döbber J, Gerlach T, Offermann H, Rother D, Pohl M. 2017. Covalent one-step purification and immobilization by innovative binding tags. *BioTrans 2017.* Budapest, Hungary.

3. Döbber J, Kloß R, Pohl M. 2017. Fusionstags zur Immobilisierung von Enzymen. *Bayer AG*. Leverkusen.

4. Döbber J, Schmieg B, Franzreb M, Pohl M. 2017. Enzyme immobilization approaches for the implementation of a continuous enzymatic cascade. *3rd MIE Evaluation*. Jülich.

5. Döbber J, Musio B, Ley SV, Pohl M. 2018. HaloTag™ fusion enzymes for in situ immobilization in flow. *4th Multistep Enzyme Catalyzed Processes Congress.* Trondheim, Norway.

Poster presentations

1. Döbber J, Pohl M. 2016. New Options for Biocatalysis: Merging Purification and Immobilization through Innovative Binding Tags. *Gordon Research Conference.* Boston, USA.

2. Döbber J, Pohl M. 2016. New Options for Biocatalysis: Merging Purification and Immobilization through Innovative Binding Tags. *ProcessNET 2016.* Aachen.

3. Döbber J, Gerlach T, Offermann H, Rother D, Pohl M. 2017. Efficient Immobilization of Biocatalysts: HaloTag™ fusion enzymes for Continuous Production Processes. *Jahrestagung Biotechnologie 2020+*. Jülich.

Table of contents

Abstract

Immobilization of biocatalysts is an important tool to allow the economical viable use of enzymes through efficient recycling and to establish different reaction concepts. A general methodology applicable for a broad range of enzymes and allowing stable, preferably site-directed and covalent binding to respective supports with high catalytic activity is still elusive. In addition, immobilizates with high enzyme purity can only be achieved via previous time-consuming chromatographic purification steps which drastically increase the overall costs for immobilization. Therefore, tag-based immobilization concepts were evaluated in this thesis as a simple and generic strategy to mediate site-directed immobilization of enzymes.

To evaluate the different tags, various model enzymes were selected comprising the groups of ThDP-dependent enzymes, alcohol dehydrogenases, transaminases as well as aldolases. Among the selected tags, the HaloTag^{TM} mediates covalent binding to carriers exposing chloroalkane residues. This tag is commercially available and was artificially constructed based on a dehalogenase from *Rhodococcus* spec. by respective modification of the active site. The fusion of this tag to the selected model enzymes revealed in all cases good heterologous production with up to 50 % of the soluble total protein content. Second, immobilization proceeded in all cases with high affinity within minutes directly from crude cell extracts yielding covalently bound enzymes with high purity. The residual activity of the immobilized fusion enzymes ranged between 10 % and 100 % compared to the free enzyme variants without HaloTag^{TM} but the majority of immobilized enzymes revealed catalytic activities higher than 50 %. In addition, low residual activity of immobilized aldolases was slightly enhanced by long rigid spacer sequences separating the HaloTag^{TM} and the corresponding model enzyme.
Besides recycling in repetitive batch reactions, the applicability and long-term usage of the immobilized HaloTag^{TM} fusion enzymes were successfully demonstrated in continuous reactions employing plug-flow reactors. Respective reactors were directly loaded in flow due to the high affinity of the HaloTag^{TM} and reactions were started immediately afterwards. This allowed access to valuable products such as mono aldol reaction products or chiral alcohols but most importantly, multi-step reaction sequences were successfully implemented. Incompatibilities of individual steps in such cascades were successfully overcome since each step occurred in specific flow modules under optimal conditions. As a consequence, highly productive reactions were established for the synthesis of chiral epoxides and chiral vicinal diols, respectively, with space-time yields of the individual steps up to 1.8 $kg*L^{-1}*d^{-1}$ and an operational stability up to several weeks.

In comparison, the use of carbohydrate-binding modules (CBMs) which mediate binding towards insoluble carbohydrates also enabled one-step purification and immobilization of the selected model enzymes with similar residual activities. However, the heterologous production of corresponding fusion enzymes was in many cases drastically reduced and a lower purity as well as a lower binding strength to respective carriers was observed.

Therefore, the HaloTag^{TM} was identified as the most suitable candidate. This methodology is simple and broadly applicable to various enzymes and consequently has the potential to facilitate the development of immobilized biocatalysts.

Kurzfassung

Die Immobilisierung von Biokatalysatoren ist ein wichtiges Instrument für die kosteneffiziente Nutzung von Enzymen, da hierdurch sowohl ihre Wiederverwendung als auch verschiedenste Reaktionskonzepte ermöglicht werden. Die derzeitig verfügbaren Methoden sind jedoch kaum generell anwendbar und die Bildung einer gerichteten, vorzugsweise kovalenten Bindung des Enzyms an das Trägermaterial unter Erhaltung der katalytischen Aktivität ist eher selten. Außerdem können derzeit Immobilisate mit hoher Reinheit meist nur durch vorhergehende chromatographische Reinigung der Enzyme hergestellt werden, was mit einem hohen Zeit- und Kostenaufwand verbunden ist. Daher wurden in dieser Arbeit Tag-basierte Methoden als einfache und kostengünstige Alternative für die Immobilisierung von Enzymen evaluiert.

Hierfür wurden Enzyme aus den Familien der ThDP-abhängigen Enzyme, Alkoholdehydrogenasen, Transaminasen sowie Aldolasen als Modellenzyme ausgewählt. Unter den ausgewählten Tags ermöglicht der HaloTag™ eine kovalente Bindung an Trägermaterialien, auf denen entsprechende Chloroalkane exponiert sind. Der Tag ist kommerziell erhältlich und wurde artifiziell durch entsprechende Modifizierung des aktiven Zentrums einer Dehalogenase aus *Rhodococcus* spec. konstruiert. Die Fusion dieses Tags mit den entsprechenden Modellenzymen ergab in allen Fällen eine gute heterologe Produktion mit bis zu 50 % Anteil am löslichen Gesamtproteingehalt. Des Weiteren ermöglicht der HaloTag™ eine schnelle Bindung der Fusionsenzyme direkt aus Rohzellextrakten an die Trägermatrix, was zu Immobilisaten mit hoher Enzymreinheit führte. Alle Modellenzyme waren im Anschluss katalytisch aktiv, wobei die Aktivität im Vergleich zu den freien Referenzenzymen ohne HaloTag™ zwischen 10 % und 100 % variierte. Für die Mehrzahl der untersuchten Enzyme wurde jedoch eine Restaktivität höher als 50 % beobachtet und im Falle der immobilisierten Aldolase konnte die Aktivität durch Auswahl von langen, starren Abstandshaltern, die den HaloTag™ mit dem Modellenzym verknüpften, erhöht werden.
Die so hergestellten Immobilisate wurden im Anschluss sowohl für die Rezyklierung in Satzreaktoren als auch für die Etablierung von kontinuierlichen Reaktionen verwendet. Hierfür wurden effiziente Protokolle entwickelt, die eine direkte Beladung von Strömungsrohr-Reaktoren im Fluss erlauben, sodass Reaktionen direkt im Anschluss durchgeführt werden können. Mithilfe dieser Reaktionskonzepte wurde die effiziente Produktion von beispielsweise Mono-Aldol Reaktionsprodukten oder die Bildung von chiralen Alkoholen ermöglicht. Insbesondere wurden dadurch aber auch erfolgreich Mehrschritt-Reaktionen etabliert, da durch die räumliche Trennung der einzelnen Reaktionsschritte auftretende Inkompatibilitäten erfolgreich überwunden wurden. Dies mündete schließlich in Reaktionen für die Synthese von chiralen Epoxiden oder vicinalen Diolen, für die Raum-Zeit Ausbeuten von bis zu 1,8 $kg*L^{-1}*d^{-1}$ erzielt wurden. Die einzelnen Reaktionen verliefen darüber hinaus bis zu mehrere Wochen stabil.

Im Vergleich dazu wurden Kohlenhydrat-Binde Module (CBMs), welche die Bindung an unlösliche Kohlenhydrate ermöglichen, ebenfalls erfolgreich für die Immobilisierung von Enzymen mit gleichzeitiger Reinigung eingesetzt. Die resultierenden Immobilisate zeigten ähnliche Restaktivitäten wie entsprechende immobiliserte HaloTag™-Fusionsenzyme. Allerdings wurde in vielen Fällen eine geringe Produktion der Fusionsenzyme und eine geringere Reinheit sowie schwächere Bindungsstärke an Cellulose beobachtet.

Daher wurde der HaloTag™ als besonders geeigneter Kandidat für die erfolgreiche Immobilisierung von Enzymen identifiziert. Generell ist diese Methode einfach durchzuführen und auf eine Vielzahl an Modellenzymen anwendbar, was damit das Potential birgt, die oftmals aufwändige Entwicklung von immobilisierten Biokatalysatoren deutlich zu beschleunigen und zu vereinfachen.

List of Figures and Tables

Abbreviations

aa	amino acid
ACN	acetonitrile
APP	1-amino-1-phenylpropane-2-ol
*Bm*TA	ω-transaminase from *B. megaterium* SC6394
BRENDA	Braunschweig Enzyme Database
C. fimi	*Cellulomonas fimi*
CatIB	catalytically active inclusion body
CAZy	carbohydrate-active enzyme database
CBM	carbohydrate-binding module
cip	cellulosomal integrating protein
DC family	decarboxylase family
DMSO	dimethyl sulfoxide
E. coli	*Escherichia coli*
*Ec*DERA	2-deoxyribose-5-phosphate aldolase from *Escherichia coli*
ee	enantiomeric excess
f	flexible
FGE	formylglycine-generating enzyme
GST	glutathione S-transferase
HEPES	4-(2-hydroxyethyl)-1-piperazineethanesulfonic acid
HFCS	high-fructose corn syrup
HPP	2-hydroxy-1-phenylpropanone
ic	isomeric content
IPA	isopropylamine
IPTG	isopropyl β-D-1-thiogalactopyranoside
*Lb*ADH	alcohol dehydrogenase from *Lactobacillus brevis*
LB media	lysogeny broth media
Lbp	large binding pocket
MBP	maltose-binding protein
MTBE	*tert*-butyl methyl ether
$NAD(P)^+$	nicotinamide adenine dinucleotide (phosphate)
NusA	N-utilization substance
PAGE	polyacrylamide gel electrophoresis
*Pf*BAL	benzaldehyde lyase from *Pseudomonas fluorescens*
PLP, PMP	pyridoxal 5-phosphate, pyridoxamine 5-phosphate
POX family	pyruvate oxidase family
PP	pyrophosphate domain
*Pp*BFD	benzoylformate decarboxylase from *Pseudomonas putida*
PPD	1-phenylpropane-1,2-diol
PYR	pyrimidine domain
SBP	small binding pockket
SDS	sodium dodecyl sulfate
TEA	triethanolamine
ThDP	thiamine diphosphate
Tris	tris(hydroxymethyl)aminomethane

1 General Introduction

1.1 Biocatalysis – the use of enzymes for organic synthesis

1.1.1 Biocatalysis as a tool of biotechnology

Biological systems have been utilized by mankind for thousands of years starting with simple applications of microbial cells for the production of food and beverages. On that basis, technical fermentative processes were developed in which microorganisms were used to produce various products of higher value and it became clear that a highly complex system of biochemical activities within these cells was responsible for the effects observed. Many of these biochemical reactions are accelerated by biological macromolecules to which proteins which are called enzymes – a term first introduced by Wilhelm Friedrich Kühne at the end of the 19th century (Kühne, 1876) – contribute mostly. In the field of biocatalysis, the catalytic activity of such enzymes is exploited and directed towards the chemical synthesis of various valuable compounds (Sheldon and Woodley, 2018).

After having understood the catalytic nature of enzymes due to the pioneering work of Emil Fischer (Fischer, 1894), biocatalysis was especially promoted by the establishment of molecular biology tools allowing the artificial recombination of DNA in microbial host cells (Cohen et al., 1973). On that basis, even more sophisticated methods were developed to enable the modification and engineering of biocatalysts towards specific aims and needs in a Darwinian evolution based manner (Arnold, 1996; Stemmer, 1994). Retrospectively, this was the start of the so-called third wave of biocatalysis, which is still making use of advanced protein engineering, gene synthesis and bioinformatic tools to increase the availability (see 1.1.2) of suitable biocatalysts for synthetic chemistry (Bornscheuer et al., 2012).

All these efforts have also resulted in the implementation of biocatalytic processes in different industrial sectors including for example agriculture, food or pharma (Choi et al., 2015; Straathof et al., 2002). For example, glucose isomerase was already implemented in the 20th century for the production of high-fructose corn syrup as a cheap sweetener for the food industry (Bhosale et al., 1996) and is nowadays used to produce high-fructose corn syrup in a scale of more than 1 million tons per year (Bommarius and Riebel, 2004; Crabb and Shetty, 1999). A further example developed later on in the sector of pharma was the application of a transaminase for the production of the antidiabetic compound sitagliptin (Savile et al., 2010). However, the overall amount of industrial biocatalytic processes is still modest and often, biocatalytic solutions are underrepresented (Schmid et al., 2001; Truppo, 2017). Therefore, a closer look on the strength and limitations of biocatalysts will be given in the following chapters to understand this phenomenon.

1.1.2 General strengths and limitations of biocatalysts

Selectivity

One of the biggest strengths of enzymes in comparison to chemical synthesis strategies is their outstanding regio-, chemo- and stereoselectivity enabling precise control of individual functional groups within a complex molecule. To achieve the same high regio- or chemoselectivity, chemical strategies routinely depend on the use of protection groups shielding functional groups from undesired reactivities (Kocienski, 2005). However, such protecting groups increase in all cases the total amount of overall steps to achieve a specific synthetic goal and generally lower the atom economy of a synthesis thereby rendering enzymes a good alternative (Sierra and de la Torre, 2004). In contrast, a high stereoselectivity is often mandatory to produce bioactive compounds. Since biological molecules are characterized by a specific stereochemistry, which is also described as biological homochirality (Blackmond, 2010), bioactivity of compounds is often inherently connected to the spatial orientation of their functional groups. For example, the stereoisomer of a bioactive compound can have no, a much stronger or even a detrimental effect in comparison to its counterpart (Smith, 2009). Stereoselective synthesis routes in organic chemistry can be divided into three different strategies comprising (*i*) chiral pool, (*ii*) resolution of racemates and (*iii*) asymmetric synthesis each of them connected to several drawbacks (Beck, 2002; Faber, 2018). Chiral pool methods are based on the isolation of stereochemically pure natural starting compounds but the availability of such compounds at an affordable price can be limited. Instead, racemates can be produced much easier using classical chemical routes, which can be combined with resolution techniques to achieve enantiomerically pure compounds but 50 % of the product will be discarded. If applicable, kinetic resolution approaches are a good alternative, which iteratively racemise the undesired stereoisomer combined with subsequent resolutions. However, asymmetric synthesis strategies represent the fastest access to enantiomerically pure compounds. Depending on the availability of chiral catalysts or auxiliaries, new chiral centers are incorporated into prochiral substrates in one step (Beck, 2002). For asymmetric synthesis approaches, each reaction has to be evaluated individually if bio- or chemical catalysts lead to a higher stereoselectivity but enzymes are also able to perform chiral functionalizations on non-activated substrates (Bernhardt and Urlacher, 2014) and additionally have the advantage of being non-toxic and biodegradable (see below).

Environmental impact

In 1998, Paul Anastas and John Warner introduced 12 principles for the design and evaluation of reactions with respect to their sustainability and their environmental impact (Anastas and Eghbali, 2010; Anastas and Warner, 1998). These 12 principles of Green Chemistry illustrate ideal processes that spare the use of toxic compounds during synthesis, prevent the formation of waste and high

consumption of energy and resources, start from renewable feed stocks and need as few process steps as possible to reach the synthetic goal. Enzymes as biocatalysts directly address these demands by inherently being non-toxic, degradable catalysts from renewable feed stocks. Additionally, reactions are mostly catalyzed with a high selectivity (see above) at ambient temperatures and pressures leading to step efficient reactions with low energy input. Due to the just described nature of biocatalysts, their "greenness" is often seen as obvious and detailed assessments of their environmental impact are rarely found in literature (Jegannathan and Nielsen, 2013; Kuhn et al., 2010). This was recently critically reviewed and the authors pointed towards the argument of waste generation which is often not discussed in detail (Domínguez de María and Hollmann, 2015). A rational measure to evaluate the amount of waste formed was introduced with the E-factor describing the amount of waste formed per kg of product (Sheldon, 2017). Since many biological reactions are performed usually under aqueous conditions, one has to consider the amount of water as waste, too. Under dilute conditions, the ratio of waste water and formed product is very unfavorable yielding a very high E-factor. Taking this issue into account, the assessment of the environmental impact of biocatalytic reactions becomes more exact and still is often evaluated of being a ´greener´ solution in comparison to conventional process strategies (Jegannathan and Nielsen, 2013; Kuhn et al., 2010).

Availability

During millions of years, evolution has come up with a huge variety of enzymes catalyzing a vast number of different biochemical reactions. Furthermore, the general opinion about enzyme specificity has changed from the paradigm that a single enzyme can only catalyze one distinct reaction towards the acceptance of enzyme promiscuity (Arora et al., 2014; Gupta, 2016). Such promiscuity can be classified into (*i*) substrate, (*ii*) condition or (*iii*) catalytic promiscuity explaining that enzymes catalyze the same kind of reaction with different substrates or display even new catalytic activities in comparison to their native physiological function (Babtie et al., 2010). This huge amount of available functionalities is enhanced by the possibilities offered by modern protein engineering tools. By applying these, the catalytic repertoire of enzymes can be enhanced with designed functions completely unknown to exist in nature or yet impossible to achieve with chemical synthetic strategies (Arnold, 2017) as was just recently shown by discovering carbon-silicon bond formation (Kan et al., 2016) or Anti-Markovnikov alkene oxidation (Hammer et al., 2017). Besides all this catalytic potential, there is still the question of how to find the right enzyme. To answer this question, bioinformatics tools were introduced already more than 30 years ago. For example, the BRaunschweig ENzyme DAtabase (BRENDA) was established in 1987. Today this database provides access to more than 370,000 enzymes and their published biochemical functions (Schomburg et al., 2017). Even though such bioinformatics tools are constantly expanding, the possibility to find the desired biocatalyst especially with activity towards non-physiological substrates is rather low. Furthermore,

each application requires specific properties of a biocatalyst in terms of activity, stability and selectivity. Therefore, the availability of enzymes with all desired characteristics is mostly impossible and optimization by protein engineering is often necessary (Bornscheuer et al., 2012). One major problem that has to be overcome is the identification of the right amino acid exchanges leading to an optimized catalyst. In light of the huge amount of combinatorial possibilities caused by the theoretical option to insert 20 different amino acids at any position of the enzyme, the development of screening methods enabling the fast identification of positive hits from large libraries of altered enzyme variants is a current bottleneck and of major focus (Reetz, 2017). Recent publication for example targeted the increase of screened variants per time frame (Chen et al., 2016) or the development of enzyme assays applicable to a broader range of enzymes (Yan et al., 2017).

1.2 Biocatalytic reaction concepts

As outlined above, the use of biocatalysis for the synthesis of organic compounds is promising due to great selectivity under economically friendly conditions. To fully exploit this potential, reaction concepts are necessary beyond the obvious set-ups of single-step transformation in simple batch reactors which are explained in the following chapters.

1.2.1 Continuous reactions

In a continuous reaction, a fluid is pumped into a reactor where a reaction takes place in flow while the formed products exit the reactor into an environment where no further chemical transformation is intended to occur (Plutschack et al., 2017). In comparison to traditional batch systems, continuous reactions have several advantages that do apply for reactions either using chemical or biological catalysts. Reactions in flow benefit from (*i*) reduced costs for large-scale production (Roberge et al., 2008; Schaber et al., 2011) (*ii*) easier scale-up (Anderson, 2012) (*iii*) improved mixing, heat and mass transfer especially for small scale reactors enabling higher productivities (Baxendale et al., 2006b; Kirschning et al., 2012; Schlange et al., 2011), (*iv*) higher control about parameters such as residence time, mixing, temperature or pressure leading to a more reliable process (Plutschack et al., 2017) (*v*) higher safety (Brahma et al., 2016; Musio et al., 2018; O'Brien et al., 2010), (*vi*) higher sustainability (Ley, 2012; Newman and Jensen, 2013; Wiles and Watts, 2012) as well as (*vii*) the possibility for automation (Fitzpatrick and Ley, 2016; Reizman and Jensen, 2016). However, the establishment of continuous processes can be time-consuming and reactions in batch are usually established much faster (Plutschack et al., 2017).

In biocatalysis, attempts to perform reactions in flow have started early and first examples include the establishment of a process for the continuous resolution of amino acids (Tosa et al., 1966a; Tosa et al., 1966b; Tosa et al., 1967) or the implementation of a continuous stirred tank reactor containing an

ultrafiltration membrane for the retentions of enzymes and cofactors (Wichmann et al., 1981). Today, applications of biocatalysis in flow have diversified and can be classified according to different measures comprising (*i*) size and type of reactor, (*ii*) the flow inside the reactor, and (*iii*) the biocatalyst formulation (Tamborini et al., 2018). As a tool for fast screening applications and rapid process development, microreactors ranging in dimensions of mm- or µm scale have been studied intensively (Bolivar et al., 2011; Laurenti and dos Santos Vianna Jr., 2016; Wohlgemuth et al., 2015). Such reactors are for example based on chips or micro-capillaries and sometimes have additional internal microstructures. To bridge the scale-up towards macroscale reactors usually used for preparative applications, mesoscale reactors such as continuous stirred tank reactors or cylindrical plug-flow reactors at the ml scale were reported (Rao et al., 2009). Inside these different types of reactors, the flow can be mono- or biphasic including a segmentation into different droplets (Tamborini et al., 2018), which is often used to overcome mixing problems (Robertson, 2017). To obtain high enzymatic productivities, the retention of biocatalysts inside flow modules is crucial. Although continuous biocatalytic reactions are sometimes performed without retention of the biocatalyst in the reactor (Cascón et al., 2013), the great majority of reported reactions apply a compartmented biocatalyst. Therefore, efficient methods have to be established to allow compartmentalization of biocatalysts in flow reactors by for example attachment to insoluble particles, coating to the inner wall of reactors or retention with membranes or within polymers (Kazenwadel et al., 2016; Rao et al., 2009; Tamborini et al., 2018; Yuryev et al., 2011).

1.2.2 Multi-step reaction sequences

The production of organic compounds usually involves the combination of several individual reaction steps until the final synthetic goal is reached. Traditionally, the reactions are performed consecutively in batch including the purification of intermediates. However, intermediate product isolation is time-consuming, leads to the accumulation of a huge amount of waste during the whole reaction sequence and reduces the overall yield (Gröger and Hummel, 2014). Therefore, the development of multi-step reaction sequences bypassing such purification steps and allowing direct combination of several steps has become a major field of interest in biocatalysis to enable more sustainable reactions (Schrittwieser et al., 2018). These reactions are also described as biocatalytic cascades and can generally be defined as the combination of at least two different reaction steps without isolation of the intermediates and of which at least one step is catalyzed by an enzyme (Kroutil and Rueping, 2014). Cascades can be subdivided into different subgroups whereby the chronology order of events is very important. They can be run in a simultaneous mode where all components of a reaction are added at the beginning in one reaction vessel without further intervention or in a sequential mode where a temporal or spatial separation of different reaction steps is adjusted (Schrittwieser et al., 2018). The sequential reaction sequence might be necessary due to several reasons and usually arises from incompatible reaction

conditions. First, two different enzymes may have activity towards the same substrate which would drastically diminish the yield of the target product and which is also described as cross-reactivity (Jakoblinnert and Rother, 2014; Wachtmeister et al., 2016). Second, the simultaneous activity of different biocatalysts in one reactor can be hampered by different pH optima, stabilities towards solvents or inactivation by involved reactants (Enoki et al., 2016; Klermund et al., 2017). The latter is especially difficult for the combination of biologically and chemically catalyzed steps when, for example, enzymes and metal catalysts, such as palladium are combined (Denard et al., 2013; Gröger and Hummel, 2014; Sato et al., 2015). Therefore, efficient strategies to establish sequential operation modes for biocatalytic cascades have to be developed. One strategy comprises the compartmentalization of catalysts to perform each reaction in a defined space and environment under optimal conditions (Rulli et al., 2013; Schmidt et al., 2017).

Evidently, the combination of continuous reaction strategies and multi-step reaction sequences can thereby result in highly efficient and sustainable reaction concepts based on biocatalyst compartmentalization as a common element. The reaction would take place in a defined reactor compartment and products would then be transported to further modules and subsequent reactions without intermediate product isolation. In addition, potential incompatibilities would be eliminated while the high reaction control in flow would guarantee highly efficient individual steps and if required the introduction of reactants as well as the removal of undesired compounds from the reaction sequence exactly at the time and place needed (Wegner et al., 2012). However, reports on continuous enzymatic cascades are rare (Gruber et al., 2017; Peschke et al., 2017b) and the majority of examples is based on single-step transformations leaving room for optimization (Schrittwieser et al., 2018).

1.3 Translation of biocatalytic reactions into industrial processes

Based on the just mentioned biocatalytic reaction concepts, different industrial processes have been established (Choi et al., 2015; Huisman and Collier, 2013; Pellis et al., 2018; Straathof et al., 2002; Wohlgemuth, 2009; Wohlgemuth, 2010). As already described in chapter 1.1, biocatalysis comes along with several advantages including a high selectivity and sustainability but the availability of suitable catalysts is limited. In addition to these general strengths and limitations, the existing barriers of translating a biocatalytic reaction into an industrial process are discussed in this chapter.

In 2012, Dach and coworkers aimed to define eight criteria to evaluate processes for the manufacturing of chemicals (Dach et al., 2012). These criteria were assigned to two major groups comprising the cost factors for material as well as conversion and every single criterion was afterwards rated according to its impact on the overall process efficiency. Among these, the criterion of volume-time output was weighed with 40 % constituting by far the most important factor. Translating this estimation on the development of a biocatalytic process, process engineers have to focus on the employment of enzymes which are highly active in the presence of high substrate concentrations to

enable a high productivity. However, enzymes often lack operational stability under such demanding conditions (Iyer and Ananthanarayan, 2008; Schmid et al., 2001). Furthermore, high concentrations of hydrophobic substrates are especially challenging since organic solvents are required for efficient solubilization but the majority of natural enzymes displays lower catalytic activity in such solvents compared to aqueous solutions (Klibanov, 1997; Zaks, 1991). Nevertheless, low operational stability can be overcome by different methods including either (*i*) optimization of the biocatalyst itself by protein engineering, (*ii*) modification of the enzyme structure by for example rigidification (see 1.4) or (*iii*) by establishment of a protective micro-environment as for example achieved by the use of whole cell catalysts (de Gonzalo et al., 2007; Jakoblinnert and Rother, 2014; Li et al., 2015; Serdakowski and Dordick, 2008; Stepankova et al., 2013; Truppo et al., 2012).

Material costs are the second biggest contributing factor for an efficient process according to Dach and coworkers (Dach et al., 2012). Such comprise the costs for all purchased chemicals including the catalyst. Therefore, the costs for the biocatalyst need to be reasonable to render the process economically feasible. Overall, the costs for the production of enzymes are not easy to determine and depend on several factors. First of all, the production scale is decisive and with increasing cultivation volume, the costs for the production of the biocatalyst decrease (Tufvesson et al., 2011). Furthermore, the cultivation yield as well as the production level in the production strain affects the price as well. Therefore, prices for biocatalysts can vary a lot and range between 100 and 100,000 $/kg (Rozzell, 1999). A further contributing factor that influences the catalyst price is the final formulation that is used for the reaction. Biocatalysts can be applied as whole cells, as crude cell extracts containing the target enzyme in crude mixture with other soluble cell components or in a purified form. Whole cell catalyst are the cheapest formulation but costs increase with every additional processing step and especially chromatographic enzyme purification is by almost one order of magnitude more expensive (Tufvesson et al., 2011). However, the choice between different biocatalyst formulations is not only a matter of price and comes along with several advantages and disadvantages affecting the overall process efficiency. Whole cells may carry further undesired catalytic activities potentially causing an increase in by-product formation, if the substrate is similar to physiological ones (Carvalho and Fonseca, 2007). Another disadvantage associated with whole cells is the risk of leaching cell components causing regulatory problems or complicating the downstream processing (Aguilera et al., 2013). Furthermore, the cell membrane constitutes a diffusion barrier, which may slower down the overall reaction and some compounds might even not be able to pass it. These effects do not apply for pure enzymes but on the contrary, whole cells already contain expensive cofactors that can be used for cofactor regeneration and the cell membrane can have a protective effect on the biocatalyst (McAuliffe, 2012; Wachtmeister and Rother, 2016). These arguments clearly indicate that the biocatalyst formulation has a huge impact beyond the point of catalyst production costs and that each process needs individual assessment to find the optimal solution. However, either chemical or biological chiral catalysts are generally not regarded as cheap (Rozzell, 1999). Therefore, the most

economical approach would be to use catalysts as long as possible since they are not consumed during a reaction. One approach is the development of methods to efficiently recycle enzymes in industrial operations (see 1.4) thereby decreasing overall process costs (DiCosimo et al., 2013).
Finally, further factors to successfully translate a biocatalytic reaction into an efficient process depend on the price of the product as well as the time available to find the right biocatalyst. For bulk chemicals, the product price is rather low and was estimated to be about 1 €/kg while products in the pharma sector typically range above 100 €/kg (Tufvesson et al., 2011). Consequently, a biocatalyst used for the production of bulk chemicals has to be much more productive to render the process economically feasible leading to much tougher thresholds for the production of low-priced products. In addition, Matthew Truppo recently reviewed the short time frame for example in the pharmaceutical industry to implement a process and that the time necessary to find, characterize and optimize a certain biocatalyst is usually too long for a significant impact (Truppo, 2017) (see also 1.1.2).
To sum up, the implementation of a highly productive biocatalytic process needs to be fast and would require an ideal biocatalyst that has a high activity as well as high operational stability under challenging conditions, is produced with low production costs and is easily separated from the reaction media for successful long-term use and low product impurities.

1.4 Biocatalyst immobilization

Biocatalyst immobilization can be a solution to the just mentioned issues for the establishment of different reaction concepts and economically viable processes (see 1.2, 1.3) One of the most comprehensive definitions for enzyme immobilization was given by Winfried Hartmeier, who wrote in a review about immobilized biocatalysts:

"*Upon immobilization, biocatalysts are either bound to carriers (or to each other) or physically confined in a definite volume* […]" (Hartmeier, 1985).

This definition reveals the two different strategies of immobilization, comprising either the formation of insoluble catalysts by binding to a support or to itself as well as the entrapment of free and soluble enzymes in a defined compartment (see also Figure 1.4-1).
Biocatalyst immobilization is utilized to target several bottlenecks in biocatalysis. One of the greatest advantages connected with immobilized biocatalysts is a facile recovery of the enzyme from the reaction medium which enables the efficient reuse of enzymes for long-term and economically viable applications (DiCosimo et al., 2013). Furthermore, the biocatalyst stability can be enhanced by immobilization in some cases, leading to enhanced resistance against stress factors like for example organic solvents or extreme pH and temperature (Garcia-Galan et al., 2011; Guzik et al., 2014; Li et al., 2015; Mateo et al., 2007b). Finally, biocatalyst immobilization is an important tool for process

intensification[1] in general. Besides facile recovery, immobilized catalyst allow a greater variety of reactor designs starting from simple batch to sophisticated continuous set-ups, a higher reaction control as for example in multi-step synthesis approaches by easy termination and start of sequenced reactions, and a facilitated down-stream processing accompanied with less catalyst related impurities (Baxendale et al., 2006a; Caddow and Concoby, 2004; Homaei et al., 2013; Tamborini et al., 2018).
In contrast, immobilization can lead to a reduced catalyst activity, which is based on several reasons. In some cases, the immobilization process is rather harsh and the modifications introduced to the enzyme diminish its catalytic activity (see also chapters below) (Mateo et al., 2007a; Sheldon, 2011). Additionally, the used carrier and the functional groups present on its surface may establish an unfavorable micro-environment with respect to charge, pH and hydrophobicity (Liese and Hilterhaus, 2013). For example, in close proximity of a cationic surface, protons are repelled due to the same charge. The resulting alkaline micro environment may affect the enzyme stability and catalytic activity. Finally, potential mass-transport limitations can reduce the activity since enzymes are locally concentrated and substrates have to diffuse in some cases into polymers or porous carriers (Liese and Hilterhaus, 2013). Another important factor is that immobilization leads to enhanced biocatalyst production costs. Among these, the costs for the carrier contribute the most, followed by costs for the respective enzyme, labor and equipment (Tufvesson et al., 2011). Based on these disadvantages, basic guidelines for the development of immobilization methods can be deduced. The ideal immobilization strategy should be gentle to maintain catalytic activity while establishing a strict compartmentalization without enzyme leaching. The choice of the right carrier is rather enzyme specific since it influences the direct environment of an enzyme but should be cheap and inert to guarantee economical immobilization as well as long-term operations. Although a universal immobilization approach would be desirable, the huge variety of complex enzymes with completely different properties represents a great barrier to implement such generic approaches. This may explain the evolution of a vast amount of different immobilization approaches, which are described in the next chapters.

1.4.1 **Overview about existing strategies for biocatalyst immobilization**

Strategies for biocatalyst immobilization are classified into two different groups as depicted in Figure 1.4-1 (Hartmeier, 1985). In the first group, the biocatalyst is bound to a carrier or to itself whereas in the second group, it is confined in a distinct compartment without establishing any bond and entrapment as well as encapsulation methods are distinguished. However, these general ways of immobilization can principally be applied to all kinds of biocatalyst formulations including whole cells, crude cell extracts and purified enzymes. As a consequence, the performance of the immobilized biocatalyst is influenced by the used biocatalyst formulation in terms of production costs and catalytic

[1] Process intensification is understood as the development of "novel apparatuses and techniques that […] bring dramatic improvements in manufacturing and processing […]" (Stankiewicz and Moulijn, 2000).

efficiency as described in 1.3. In the following chapters, the main focus will be placed on methods for the immobilization of enzymes but in principle, most of the methods can be performed starting from whole cells, too (Polakovič et al., 2017; Zajkoska et al., 2013). Therefore, methods for the immobilization of whole cells will be briefly mentioned where appropriate.

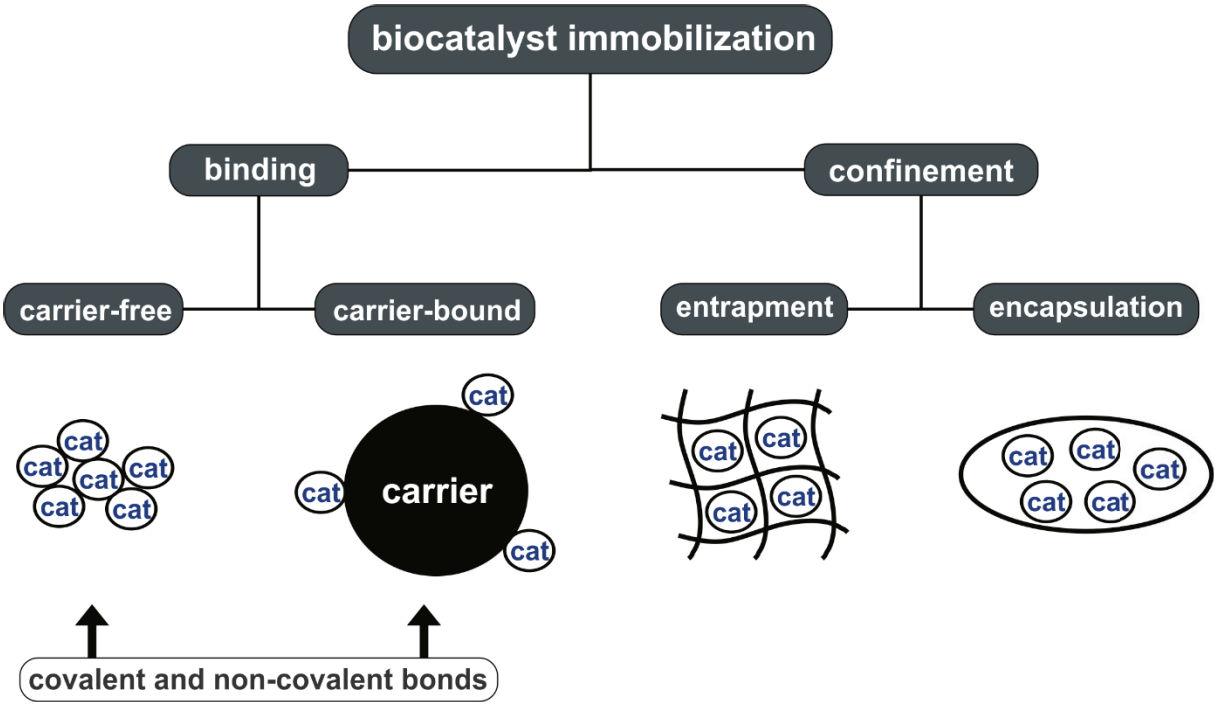

Figure 1.4-1: General strategies for biocatalyst immobilization. Image is based on a general definition about biocatalyst immobilization given by Hartmeier, 1985.

Immobilization methods based on confinement

The confinement of biocatalysts can be divided into different subcategories comprising (*i*) membrane confinement, (*ii*) entrapment and (*iii*) encapsulation. The simplest approach is the confinement of catalysts by membranes inside continuous mesoscale reactors (see 1.2.1). In these approaches, ultrafiltration membranes are used to simply retain catalysts inside reactors for long-term use (Liese et al., 1998; Schroer et al., 2007; Wichmann et al., 1981; Yuryev et al., 2011). However, it is questionable wether such concepts belong to the field of enzyme immobilization although they are covered by the general definition given above. Catalysts experience the same degree of freedom as in a non-immobilized state and the only difference is that they cannot escape from the reactor. Usually biocatalyst immobilization is understood as an immobilization in the smallest space, and therefore, these approaches will not be further discussed here in detail.

By definition, entrapment methods generally refer to the inclusion of biocatalysts in matrices or polymers which are usually formed during the immobilization procedure around the catalyst without establishing any bond (Cao, 2006c). A huge variety of different polymers exists for the efficient

entrapment of either enzymes or whole cells, which can be classified due to their different types of polymers and polymerization methods. In the first group, polymerization is induced chemically. Well-studied carrier materials are for example sol-gels, which are based on the formation of siloxane networks which form upon hydrolyzation of alkoxide percursors, like tetramethoxysilane, followed by subsequent condensation of the resulting silanol groups to siloxanes (Buthe, 2011; Pierre, 2004) or polyacryamide gels, which are formed through radical polymerization of acrylamide (Bilal et al., 2016; Nawaz et al., 2016). In the second group, polymerization is induced by change in temperature, pH or ionic strength. A very simple and often applied method in such approaches involves the use of alginate, which solidifies upon addition of divalent calcium ions (Fraser and Bickerstaff, 1997). Besides, further techniques were developed based on the entrapment of biocatalysts in synthetic polymers such as polyvinyl alcohols which form a stable hydrogen bond network (Krasňan et al., 2016).

In comparison, biocatalyst encapsulation describes the inclusion of biocatalysts inside a spherical container or capsule that allows the flux of substrates and products but retains the catalyst (Cao, 2006d). However, the distinction to entrapment methods is not always clear in literature and the term encapsulation is sometimes also used for methods focusing on the formation of spherical microcapsules, which consist of solid polymeric networks with entrapped biocatalysts. (Rother and Nidetzky, 2014; Vemmer and Patel, 2013). Therefore, a differentiation is made at this point to state that the term encapsulation is understood in this thesis as the formation of a semi-permeable membrane or layer around a liquid enzyme preparation. According to this definition, whole cell formulations carrying catalytic activities, which are surrounded by the cell membrane, are a natural occurring encapsulation method. This can be mimicked by artificially constructing lipo- or polymerosomes starting from amphiphilic lipids like phosphatidylcholines or amphiphilic copolymers as polystyrene-poly(acrylic acid), which form bilayers around catalysts in aqueous solutions (Kuiper et al., 2008; Walde and Ichikawa, 2001). Further approaches are based on coating of micro-core templates and subsequent internal core liquefaction while the biocatalyst is either inside the solid micro-core template or loaded afterwards. Examples are the cross-linking of the outer layer of conventional calcium alginate beads (see above) with poly-lysine followed by a sodium citrate treatment to liquefy the catalyst inside (Prakash and Chang, 1995) or the use of polyelectrolyte capsules that become permeable for enzymes under certain conditions for loading after removal of the sacrificial core template used for capsule manufacturing (Lvov et al., 2001). As a last method for biocatalyst encapsulation, interfacial processes are mentioned, which involve reactions of compounds that are soluble in different, immiscible phases (Cao, 2006d). For example, an emulsion of aqueous droplets containing the catalyst and a water soluble polymer is formed in an organic solvent. Then polymerization of the polymer is induced by the addition of a cross-linker only soluble in the organic phase. Since cross-linker and polymer meet only at the interface of both immiscible phases, spherical membranes are formed leading to encapsulated biocatalysts (Groboillot et al., 1993).

The advantage of entrapment and encapsulation methods is their broad applicability and the immobilization without establishing any bonds. However, enzyme leakage, diffusion constraints inside polymers and through membranes as well as negative effects of compounds used for the preparation of polymers or membranes, such as radical initiators or organic solvents are general problems and often lower the catalytic potential after immobilization (Cao, 2006c; Cao, 2006d). Especially enzyme leakage is often targeted by the combination with further immobilization methods such as covalent or adsorptive binding (Cao, 2006c; Cao, 2006d; Liu and Cao, 2017) which are discussed in the following chapter.

Immobilization methods based on covalent and non-covalent bonds

Immobilization achieved via establishing a covalent bond usually involves a carrier except the catalyst is connected to itself. In such cases, cross-linking agents targeting the intermolecular connection of different functional groups present in enzymes like amino-, carboxyl-, or sulfhydrylgroups are often used (Wong and Jameson, 2011; see also below for further information on reactivity of functional groups). Among these, glutaraldehyde is one of the most prominent representatives (Migneault et al., 2004) and is for example utilized for the formation of cross-linked enzyme aggregates (CLEAs) (Sheldon, 2011). For the preparation of these, enzymes are precipitated and subsequently treated with glutaraldehyde to connect the amino groups of different catalysts with each other. Upon formation of the imine, the formed bonds are reduced by for example sodium borohydride, which results in the formation of a stable amine. In contrast, carrier-free immobilization approaches can also be based on non-covalent interactions without the involvement of chemical cross-linkers. One starting point for the development of such concepts was the observation that intracellular enzyme aggregates, also known as inclusion bodies, still have catalytic activity (Diener et al., 2016; García-Fruitós and Villaverde, 2010; Peternel and Komel, 2011; Worrall and Goss, 1989). The formation of such aggregates can either be natural or artificially induced by different fusion partners (see also 1.4.2) and can lead to stable immobilized biocatalysts (Krauss et al., 2017). In comparison, whole cells are not directly cross-linked with for example glutaraldehyde since this would result in a very dense network accompanied with poor mass-transfer (Zhang et al., 2018). Therefore, additives such as polyethylenimine are added during the cross-linking process to achieve a copolymerization between cells and additives with higher mass-transfer characteristics (Bahulekar et al., 1991; Zhang et al., 2018).

For the binding of a biocatalyst to a carrier, non-covalent and covalent immobilization strategies can be distinguished. In adsorptive immobilization approaches, van der Waals forces, ionic interactions and hydrogen bonding are responsible for the binding of enzymes or cells to the carrier (Jesionowski et al., 2014; Klein and Ziehr, 1990). Very often highly ordered carriers with a porous structure are selected for adsorptive immobilization purposes to achieve a high surface area with pore sizes that match the typical size of catalysts. Especially for the immobilization of enzymes, the individual

properties of the biocatalyst with respect to for example surface charge or hydrophobicity have to be addressed to promote adsorptive binding. This explains that focus in this field was laid on the development of methods to adjust the surface properties according to pore size and surface groups that would benefit the target enzyme most. Nowadays, mesoporous carriers can be made of silicas, metals, carbons or polymers and a huge variety of functional groups can be attached post-synthetically (Hartmann, 2005; Zhou and Hartmann, 2013). However, almost any material can be employed for adsorptive enzyme immobilization provided that the right functional groups are exposed to establish efficient binding (Cao, 2006a). Immobilization performed by such methods is usually very mild, since the biocatalyst is not modified and binding is achieved due to its natural properties. However, the binding strength of adsorptive interactions can be too weak or may change during a reaction since for example the surface charge of an enzyme is also a function of pH. Therefore, biocatalyst leakage is a well-known problem for adsorptive immobilization technologies that are targeted by employing additional immobilization steps after adsorption such as confinement (see above) or covalent binding (see below) (Zhou and Hartmann, 2013).

The covalent binding of biocatalysts to a carrier is based on the coupling of functional groups present in amino acid side chains of enzymes or on the surface of whole cells with functional groups displayed by the carrier. Considering all side chains of the 20 proteinogenic amino acids, only nine side chains display functional groups with theoretical reactivity for interaction with residues exposed on potential carriers (Tischer and Wedekind, 1999; Wong and Jameson, 2011). These are listed in Table 1.4-1 and include for example the lysine ε-amino group and the sulfhydryl group of cysteine. Furthermore, Table 1.4-1 reveals possible reactions mechanisms of the respective functional groups. Most of these reactions are nucleophilic reactions, where lone pairs of valence electrons attack electron-deficient centers for example exposed on the carrier. Among the functional groups, the nucleophilicity of the sulfhydryl group is the highest, followed by amino- and oxygen containing groups (Edwards and Pearson, 1962). However, the reactivity of functional groups depends additionally on their accessibility on the enzyme surface as well as on the surrounding micro-environment (Duggleby and Kaplan, 1975; Means and Feeney, 1990). For example, the pH influences the reactivity of nucleophilic groups strongly since lone electron pairs can bind protons. Therefore, it is difficult to predict which functional groups will be involved in the establishment of covalent bonds. Furthermore, covalent immobilization strategies either involve the direct reaction of groups present on the carrier with groups of amino acid side chains (e.g.: epoxy groups react with amino groups of lysines or maleimide groups with sulfhydryl groups of cysteines) or employ additional cross-linking agents such as glutaraldehyde which react with groups of the enzyme as well as with groups exposed on the carrier to enable immobilization (Cao, 2006e; Wong and Jameson, 2011). Finally, the effect of spacer length to achieve a spatial distance between enzme and carrier and the number of covalent attachment sites are further aspects that have to be considered for covalent immobilization techniques (Hoarau et al., 2017). Spacers are sometimes necessary in case of potential negative effects caused by the surface

characteristics of the carrier and the number of covalent bonds decides about the rigidity of an immobilized enzyme. As a general rule, a higher rigidity may reduce activity but increase stability and vice versa.

Table 1.4-1: Reactive functional groups in proteins for covalent immobilization. Other reactions include (a) iodination, (b) nitration, (c) diazotitation, (d) esterification, (e) amidation and reaction with (f) mercury, (g) dicarbonyls, (h) sulfenyl halides, and (i) cyanogen bromide. *The N- and the C-terminus leads to an additional reactive amino- and carboxylgroup, respectively. Table adapted from Wong and Jameson, 2011.

amino acid	reactive functional group	alkylation/ arylation	acylation	oxidation	other
cysteine	sulfhydryl-	+	+	+	a,d,f,h
lysine	amino*-	+	+	-	c,e,g
methionine	thioether-	+	-	+	i
histidine	imidazolyl-	+	+	+	a,c
tyrosine	phenolic hydroxyl-	+	+	+	a,b,c,d
tryptophan	indolyl-	+	-	+	H
aspartic acid	carboxyl*-	-	+	-	d,c
glutamic acid	carboxyl*-	-	+	-	d,c
arginine	guanidinyl-	-	-	-	g

The main drawback of these approaches is that immobilization can hardly be controlled. Macromolecular biocatalysts usually contain several functional groups of the same type that all can theoretically participate in the interaction with carrier-bound groups. As a consequence, a huge portion of catalytic activity may be lost, since functional groups essential for activity cannot be protected and will be targeted in the same way like groups of minor importance given that they have the same reactivity. Further factors that cannot be influenced since they depend on the position and number of functional groups, are enzyme orientation towards the carrier and multi-point attachments leaving no control about active site accessibility and rigidity of the catalyst (Cao, 2006e). Overall, these factors explain that in some cases a huge amount of catalytic activity is lost in such approaches, although a high binding strength is established (Mateo et al., 2007a; Zhang et al., 2015).

As a consequence, further methods have evolved to specifically control the covalent immobilization in terms of groups involved in binding, orientation towards the carrier and the number of established bonds (Meldal and Schoffelen, 2016). These site-specific approaches usually target the incorporation of functional groups not naturally occurring in proteins to control immobilization sites followed by biorthogonal reactions. The term bioorthogonal reaction was developed by Carolyn Bertozzi and describes chemical reactions that ‘neither interact with nor interfere with a biological system’ (Sletten

and Bertozzi, 2011). Consequently, the involved groups have to react with a high selectivity under biocompatible conditions and a huge variety of different reactions has been developed including reactions of aldehydes with hydrazides or azides and triarylphosphines (Gong and Pan, 2015). However, the introduction of functional groups not naturally occurring in proteins is a crucial bottleneck and not easy to establish. One approach is the manipulation of the protein biosynthetic machinery to allow the introduction of non-canonical amino acids carrying reactive groups for subsequent bioorthogonal reactions (Young and Schultz, 2010). Furthermore, fusion tags can be applied in combination with post-translational modifications to incorporate non-natural groups like aldehydes (Carrico et al., 2007; Frese and Dierks, 2009) (see Table 1.4-2). Nevertheless, the introduction of such unnatural functional groups is still a huge bottleneck, which probably explains why these methods have not yet been broadly established in biocatalysis and why further site-specific methods are required.

1.4.2 Fusion tag-based immobilization approaches

Fusion tag-based immobilization approaches belong to the group of immobilization methods yielding covalently or non-covalently bound biocatalysts. These concepts comprise the genetic fusion of a peptide or protein to the N- or C-terminus of the selected biocatalyst to mediate immobilization. This can result in catalysts either bound to carriers or to each other through covalent bonds or adsorptive interactions and metal-chelate complexes (Barbosa et al., 2015). A huge variety of different tags enabling the immobilization of proteins or enzymes has been developed and a selection of important tags is listed in Table 1.4-2. Nature has invented for example lots of native interactions between proteins and compounds like binding of biotin by the protein streptavidin (Michael Green, 1990), proteins with an intrinsic magnetic moment (Qin et al., 2016) or naturally occurring fusion tags such as carbohydrate-binding modules (CBMs) guiding their fusion partners to their natural carbohydrate substrates like cellulose or chitin (Boraston et al., 2004). In particular, CBMs were already intensively investigated for their use in biocatalysis. The first proof of concept for this technique was made in 1989 by immobilizing a β-glucosidase to cellulose via a genetic fusion of this enzyme to the CBM from xylanase 10A of *C. fimi* (Ong et al., 1989). As one of the first structures, the crystal structure of this CBM, also known as CBD_{Cex}, was resolved in 1995 and it was found that the 110 amino acids are mainly arranged in two β-sheets consisting of four and five anti-parallel β-strands, respectively (Xu et al., 1995). The high selectivity as well as strong interaction with microcrystalline cellulose is predominantly caused by solvent exposed tryptophan residues, which contribute with their hydrophobic aromatic rings to the selective binding to cellulose (Bray et al., 1996; McLean et al., 2000). On that basis, a vast amount of further CBMs has been identified so far which were categorized into more than 60 families based on structure similarities (CAZypedia Consortium, 2018; Lombard et al., 2014). Furthermore, each CBM can be classified according to its binding mode comprising (*i*) the

planar binding on the surface of insoluble polysaccharides, (*ii*) the attachment to single glycan chains by forming a cleft or (*iii*) the affinity towards mono- or disaccharides (Boraston et al., 2004). Application of CBMs in biocatalysis for enzyme immobilization consequently focuses on CBMs with affinity towards insoluble sugars. Since some CBMs are additionally able to induce the formation of inclusion bodies (Krauss et al., 2017) (see 1.4.1), the identification of appropriate binding modules is crucial. Nevertheless, many applications for the immobilization of several enzymes such as heparinases (Shpigel et al., 1999), organophosphate hydrolases (Richins et al., 2000), invertases (Santiago-Hernández et al., 2006), β-galactosidases (Lu et al., 2012) and hydroxynitrile lyases (Kopka et al., 2015) were reported. In addition, immobilized CBM fusion enzymes have already successfully been used for the implementation of continuous reaction set-ups including packed-bed reactors for the production of (*R*)-phenylacetyl-carbinol (Engel et al., 2005) as well as (*S*)-2-chloro-phenylalanine (Dreßen et al., 2017).

But not only nature has invented tags useful for the immobilization of proteins and enzymes. Many tags were specifically designed or engineered to result in a stable binding between enzymes and ligand ranging from simple ionic tags with respective charge for ionic binding (see Table 1.4-2) towards more complex enzymatic tags like the HaloTag™, which are based on an enzymatic suicide mechanism. Such enzyme-tags can only catalyze the conversion of one substrate molecule, which remains covalently bound in the active site. In detail, the HaloTag™ was engineered starting from the monomeric haloalkane dehalogenase from *Rhodococcus rhodocrous*. This enzyme catalyzes the irreversible hydrolysis of simple, linear haloalkanes to the corresponding alcohols in several steps (Schindler et al., 1999). As shown in Figure 1.4-2, the halogen is displaced by nucleophilic attack of an aspartate side residue leading to the formation of an intermediate ester bond between substrate and enzyme. Subsequently, the ester is hydrolyzed by a hydroxide ion, which results from the interaction of a neighboring histidine in the active site with a water molecule. As a consequence, a primary alcohol is released from the active site. To install a suicide mechanism and to develop a useful tag, the catalytic histidine was exchanged by phenylalanine, which maintained the initially formed ester bond (Encell et al., 2012) (see Figure 1.4-2). Based on this first variant, further protein engineering was initiated to increase the affinity towards chloroalkane ligands as well as the heterologous, soluble protein production (Encell et al., 2012; Ohana et al., 2009). After seven rounds of optimization, the final HaloTag™ version was established revealing a similar affinity to its ligands as streptavidin exhibits towards biotin (HaloTag™: $2.7*10^6$ $M^{-1}s^{-1}$; Streptavidin: $8.5*10^6$ $M^{-1}s^{-1}$) (Los et al., 2008). Furthermore, this variant promotes the soluble production of respective fusions with proteins and enzymes, which are otherwise only producible as inactive inclusion bodies (Peterson and Kwon, 2013; Sun et al., 2015). Despite these interesting characteristics, the HaloTag™ was not yet investigated in detail for biocatalysis and the great majority of reports focused on its application in cell imaging and protein localization (Los et al., 2008).

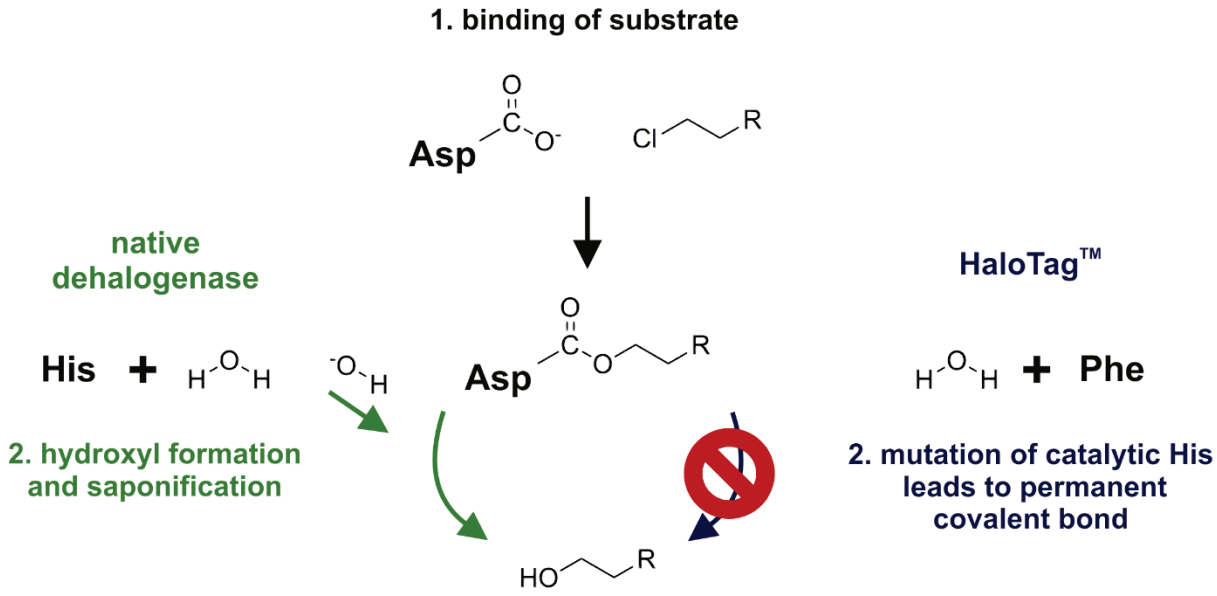

Figure 1.4-2: Suicide mechanism of the HaloTag™ in comparison to the native dehalogenase. After binding of a chloroalkane substrate to an aspartate residue in the active site, a hydroxyl ion is formed upon interaction of the catalytic histidine residue with water, which results in saponification of the ester bond and release of a primary alcohol in case of the native enzyme (green scheme). In the HaloTag™, the catalytic histidine is replaced by an unreactive phenylalanine leading to a suicide mechanism (blue scheme). Scheme based on Encell, et al. 2012.

The last class of fusion tags mentioned in Table 1.4-2 leads to the *in vivo* immobilization of enzymes and their attachment to insoluble cell parts like CatIBs or liposomes. The number of different techniques was recently reviewed and generally involves fusion of biocatalysts to proteins which are naturally associated with intracellular compartments or deposits (Rehm et al., 2018). However, it is also possible to use fusion tags for the immobilization of complete microbial cells. These techniques usually involve the display of fusion tags on the cell surface for immobilization onto several supports (Peschke et al., 2017a).

The advantage of such tag-based immobilization approaches is the site-directed manner of immobilization leaving the biocatalyst untouched. Unlike other strategies, no functional groups with catalytic function are involved in the establishment of the binding interaction. In addition, fusion tags can easily be introduced by genetic fusion and enable distinction of the target enzyme from all other proteins inside the microbial host cell. Therefore, immobilization can directly start from crude cell mixtures resulting in the selective binding of the target enzyme thereby omitting expensive previous chromatographic enzyme purification steps (see 1.3). The binding will usually take place under physiological conditions, which lowers the risk of enzyme inactivation during the immobilization process. However, the fusion of a peptide or protein tag may influence the heterologous enzyme production as well as the enzyme conformation and flexibility leading to a reduced catalytic activity. Furthermore, the binding strength and affinity depend on the selected tag and have to be assessed individually to guarantee fast and strong binding without enzyme leakage. Finally, substrates or surfaces recognized by the respective tags should be rather simple since coating of carriers with

chemically complex binding sites would lead to undesired increased costs for the preparation of respective immobilizates.

Table 1.4-2: Fusion tags enabling binding of enzymes or proteins to respective carriers, to each other or to intracellular compartments.

tag	size	mode of immobilization	references
non-covalent interactions			
His-tag	6 – 10 aa	formation of a chelate complex between histidines and divalent metal ions; commercialized for biocatalyst immobilization by EnginZyme	Engelmark Cassimjee et al., 2014
Strep-tag I/II	8 aa	peptide sequence with binding affinity towards streptavidin coated beads	Schmidt et al., 1996; Schmidt and Skerra, 1993
Avi-tag	15 aa	tag induces posttranslational biotinylation of enzymes which allows binding to streptavidin coated beads	Beckett et al., 1999; Cronan, 1990
silica binding tags (CotB1, Si-tag)	10 – 15 aa	introduction of charged amino acid residues allows ionic binding to surfaces of opposite charge (e.g. positive charge of arginine allows binding to negatively charged silicas)	Abdelhamid et al., 2014; Taniguchi et al., 2007
ionic tags (Poly-Arg, Z_{basic2})	9 aa – 7 kDa		Bolivar and Nidetzky, 2012; Fuchs and Raines, 2009; Wiesbauer et al., 2011
GST-tag	26 kDa	glutathione S-transferase (GST) binds to glutathione exposed on carrier surfaces	Smith and Johnson, 1988
PS-tag	10 aa	tag with affinity towards polystyrene	Kumada et al., 2006; Kumada et al., 2009
Calmodulin-tag	16 kDa	calmodulin binds to the drug phenothiazine exposed on carrier surfaces	Schauer-Vukasinovic and Daunert, 1999
CBMs	30 – 200 aa	carbohydrate-binding module (CBMs) allow binding to various carbohydrates (e.g. cellulose or chitin)	Guillén et al., 2010; Levy and Shoseyov, 2002
Magnetic tag	14 kDa	intrinsic magnetic moment allows direct binding on iron beads	Jiang et al., 2017; Qin et al., 2016

covalent interactions			
Aldehyde-tag	5 aa	generation of an aldehyde moiety through posttranslational enzymatic modification of a cysteine within the tag sequence; the aldehyde group can be used for subsequent bioconjugation (see 1.4.1)	Carrico et al., 2007; Frese and Dierks, 2009
SNAP-tag	20 kDa	modified DNA repair proteins; recognize benzylguanine or benzylcytosine moieties on surfaces for covalent binding	Gautier et al., 2008; Keppler et al., 2003; commercialized by NEB
CLIP-tag	20 kDa		
HaloTag™	34 kDa	engineered dehalogenase; recognizes chloroalkanes on surfaces for covalent binding	Encell et al., 2012; Promega
SpyCatcher	15 kDa	interacts with a 13 aa long peptide sequence; upon contact, an amid bond between amino acid residues is spontaneously formed; used for construction of biocatalytic biofilms	Botyanszki et al., 2015; Zakeri et al., 2012
Tags inducing in vivo anchoring in…			
…CatIBs	diverse	tag induced formation of catalytically active inclusion bodies (CatIBs); various tags are known for CatIB formation: e.g. CBMs, coiled-coil domains, artificial peptides	Krauss et al., 2017
…liposomes	194 aa	fusion to phasin PhaP1 leads to association of fusion partners to intracellular triacylglyceride inclusions	Hänisch et al., 2006
…magnetosomes	124 aa	magnetotactic bacteria produce intracellularly magnetic nanoparticles covered by a lipid bilayer; Msm13 is a protein tightly associated with these particles; fusion with MsM13 leads to display of fusion partners on magnetic particles	Honda et al., 2015; Yoshino and Matsunaga, 2006
…cell membranes	43 aa	enzymes are fused to a protein anchored to the inner surface of the cell membrane, upon cell lysis, membranes are used for biocatalysis	Sührer et al., 2015

1.4.3 Immobilized biocatalysts in industrial applications

As presented in the previous chapters, enzyme immobilization is an important tool to allow an economical long-term use of biocatalysts through easy recycling, to introduce operational stability under demanding conditions and to enable the design of a large set of different reactor concepts. These arguments suggest that immobilizates are especially appealing for technical applications. Indeed, several immobilized biocatalysts were successfully introduced in industrial applications, such as immobilized nitrile hydratases for the synthesis of acrylamide from acrylonitrile (Zheng et al., 2010), immobilized lipases for food oil processing (Xu et al., 2006) or immobilized penicillin G acylases for the modification of antibiotics (Kallenberg et al., 2005). Among these, immobilized glucose isomerase for the production of high-fructose corn syrup (HFCS) is known as the most successful example for immobilized catalysts in industry (DiCosimo et al., 2013). HCFS are utilized as a cheap sweetener for the food industry and are produced in a scale of more than 10^7 tons per year (Bommarius and Riebel, 2004). Consequently, a huge demand for immobilized glucose isomerase exists leading to an annual production of around 500 tons (DiCosimo et al., 2013). Different forms of this immobilized catalyst are currently sold employing various immobilization techniques. For example, glucose isomerase was adsorbed to an anion exchange resin giving the possibility to reuse this carrier (GENSWEET®SGI sold by DuPont Industrial Biosciences). In this business model, the carrier is only leased by the respective HCFS producing company and can be reused after enzyme inactivation or leakage by addition of new enzyme sold by DuPont (DiCosimo et al., 2013). However, this formulation was mostly exchanged against a carrier-free immobilization method consisting of glutaraldehyde cross-linked microbial cells employing polyethylenimine as a copolymer (GENSWEET®IGI sold by DuPont Industrial Biosciences) (DiCosimo et al., 2013). Several driving forces explain the utilization of immobilized catalysts for this industrial application. Glucose isomerase was immobilized because (*i*) it is involved in the production of a large-scale product worth returning the expenses invested into developing a suitable immobilization method (Bommarius and Riebel, 2004), (*ii*) it offered greatly enhanced process economics by the introduction of continuous manufacturing (DiCosimo et al., 2013) and (*iii*) enzyme recovery is needed since high enzyme amounts are necessary to achieve good conversion in a reasonable time-frame due to the high K_m of the enzyme towards glucose (> 0.1 M) (Chen, 1980).

Although enzyme immobilization seems to be highly advantageous for industry, only few surveys analyzed the share of immobilized catalysts among all processes implemented in industrial biocatalysis. Researchers from DuPont aimed to specifically address this question and found out that only less than 20 % of biocatalytic applications apply immobilized catalyst (DiCosimo et al., 2013). This raises the question why this result is lower than expected. According to the author's opinion, the development of a suitable immobilized biocatalyst is highly enzyme-specific, consequently leading to tedious and time-consuming research projects to find appropriate methods. In addition, immobilized biocatalysts are usually more expensive leading to a higher initial investment that has to be balanced

with the improvements gained by enzyme immobilization. Therefore, the production of immobilized biocatalysts at a reasonable price is of utmost importance. These arguments are supported by researches from Merck who also addressed the problem of developing an immobilized biocatalyst by stating that "a general methodology for the rapid and inexpensive immobilization of biocatalysts still eludes us" (Truppo, 2017). As a consequence, the development of simple and cheap immobilization methods with broad applicability for different enzymes would be highly beneficial.

1.5 Model enzymes to evaluate immobilization concepts

Enzymes are complex catalysts each of them characterized by specific properties. They differ not only in their sequence and structure leading to different phenotypes regarding size, surface charge and hydrophobicity but also to different quaternary structures covering a large range from mono- to multimeric active units. In addition, many enzymes depend on essential cofactors, which are either recycled or consumed during the reaction. For the latter, cofactor regeneration concepts are required for an economic application. Therefore, a set of various representatives of different enzymatic prototypes has to be selected to evaluate the potential of immobilization concepts. In the following chapters, a set of different enzymes appearing in this thesis will be presented.

1.5.1 ThDP-dependent enzymes

Thiamine diphosphate (ThDP) is an essential cofactor required for many biochemical activities in important metabolic pathways and assists in the cleavage and formation of C-S, C-H, C-N and C-C bonds (Frank et al., 2007). As shown in Figure 1.5-1, it consists of three main moieties: (*i*) the aminopyrimidine ring, (*ii*) the thiazolium ring and (*iii*) the diphosphate group. ThDP-dependent enzymes utilize the catalytic potential of this cofactor for the formation or breaking of C-C, C-O, C-N and C-S bonds by binding the cofactor in a constrained so-called "V-conformation" (Dobritzsch et al., 1998; Lindqvist et al., 1992; Muller and Schulz, 1993). This conformation places the N4 atom of the pyrimidine ring in proximity to the C2 atom of the thiazolium ring, which allows an abstraction of a proton at C2. Proton abstraction yields an activated nucleophilic ylide and enables subsequent attack of for example electrophilic carbonylgroups (Jordan, 2003). Subsequently the carboligation reaction is described in more detail: Carbonylsubstrates like aldehydes or α-keto acids are called donor substrates and are directly deprotonated or decarboxylated after nucleophilic attack. In the formed intermediate, the originally electrophilic C-atom of the carbonylgroup becomes nucleophilic and is able to attack a second electrophilic acceptor substrate (Kluger and Tittmann, 2008). This leads to a broad range of C-C bond forming reactions giving access to various α-hydroxy ketones (Müller et al., 2009; Pohl et al., 2002).

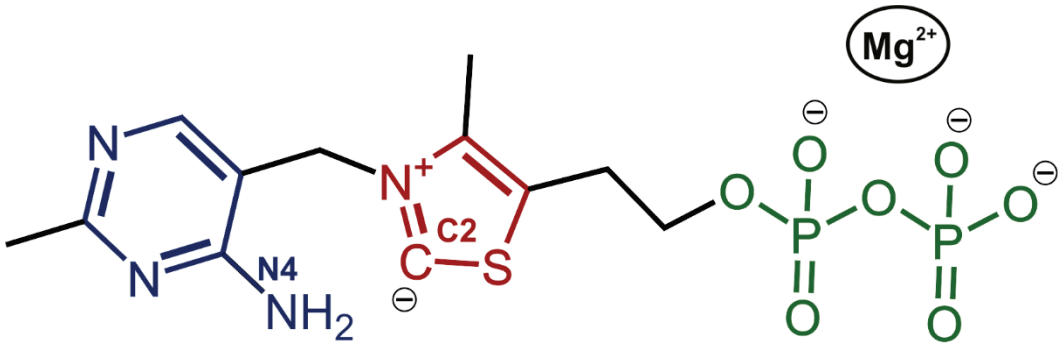

Figure 1.5-1: Activated ylide form of ThDP. ThDP consists of three main moieties: (*i*) the aminopyrimidine ring (blue), (ii) the thiazolium ring (red) and (iii) the diphosphate group (green). The activated ylide is formed by placing the N4 atom of the pyrimidine ring in close distance to the C2 atom of the thiazolium ring resulting in proton abstraction at the C2 position. Divalent magnesium ions are responsible for binding of ThDP and interact with the diphosphate group. Scheme based on Frank et al., 2007.

Among all ThDP-dependent enzymes, two highly conserved protein domains were found. The pyrimidine domain (PYR) is responsible for the binding of the aminopyrimidine ring of ThDP whereas the pyrophosphate domain (PP) interacts with divalent cations like Mg^{2+}, which in turn are involved in the binding of the diphosphate group of ThDP (Duggleby, 2006; Vogel and Pleiss, 2014). Active sites are often formed at the interface of two enzyme monomers by binding of two ThDP molecules via the neighboring PYR and PP domains of respective monomers but further arrangements were reported (Muller et al., 1993; Vogel and Pleiss, 2014). In general, ThDP-dependent enzymes are classified into nine superfamilies depending on sequence similarities and the arrangement of the conserved protein domains (Vogel and Pleiss, 2014). For example, a major difference between these superfamilies is the location of genes encoding for the PYR and PP domain (Widmann et al., 2010). They can be located on separate open reading frames such as in superfamily 2 (α-keto dehydrogenases) or in one single open reading frame as for the decarboxylase family (DC family). In this thesis, only representatives of the DC family were applied which are described in the section below. This group was originally named the POX family since pyruvate oxidase (POX) was one of the first ThDP-dependent enzymes of the DC family which was structurally characterized (Muller and Schulz, 1993). Later on, it was found out that most of the representatives catalyze the decarboxylation of α-keto acids and consequently, this group was renamed into the DC family (Duggleby, 2006).

The benzaldehyde lyase from *Pseudomonas fluorescens* (*Pf*BAL) is a well-studied enzyme belonging to the DC superfamily. It was first described in 1989 motivated by the observation that *Pseudomonas fluorescens* is able to grow on benzoin as the sole carbon and energy source (Gonzalez and Vicuna, 1989). Besides the presence of ThDP, the addition of Mn^{2+}, Mg^{2+} or Ca^{2+} cations was required for optimal activity of this tetrameric enzyme. Demir and coworkers further exploited the catalytic potential of *Pf*BAL in the following years and demonstrated that the catalytic repertoire of this enzyme did not only include benzoin cleavage but also C-C bond formation (Demir et al., 2001). *Pf*BAL is able to catalyze the formation of a huge set of α-hydroxy ketones using various aromatic and

herteroaromatic aldehydes as donor and aliphatic as well as aromatic aldehydes as acceptor. The resulting products are symmetric and mixed benzoins as well as mixed aliphatic 2-hydroxy ketones. In all cases, *Pf*BAL is strictly *R*-selective (Demir et al., 2001; Demir et al., 2002; Demir et al., 2003; Demir et al., 2004; Dünkelmann et al., 2002). Among all *Pf*BAL-catalyzed carboligation reactions, the mixed carboligation of benzaldehyde and acetaldehyde towards (*R*)-2-hydroxy-1-phenylpropanone ((*R*)-HPP) was intensively studied. The effect of cosolvents, pH and the optimal ratio between benzaldehyde and acetaldehyde were studied to enable high productivities in first preparative scale approaches (Domínguez de María et al., 2006). In addition, this reaction was also exploited with different biocatalyst formulations and reaction set-ups including continuous reactions with immobilized *Pf*BAL (Kurlemann and Liese, 2004) as well as the use of whole cell catalysts in bi- and monophasic media allowing for high substrate concentrations (Domínguez de María et al., 2008; Jakoblinnert and Rother, 2014; Wachtmeister et al., 2016).

Another tetrameric enzyme belonging to the DC-family is the benzoylformate decarboxylase from *Pseudomonas putida* (*Pp*BFD). The BFD catalyzes the non-oxidative decarboxylation of benzoylformate to benzaldehyde and is part of the mandelate degradation pathway in *Pseudomonas* strains, which was discovered first during growth studies of *Pseudomonas fluorescens* (Gunsalus et al., 1953; Stanier, 1948). Later on, the same pathway was also investigated in *Pseudomonas putida* and *Pp*BFD was described and characterized (Hegeman, 1966; Hegeman, 1970). In 1992, *Pp*BFD was applied for the first time in synthetic approaches to produce (*S*)-HPP starting from benzoylformate and an excess of acetaldehyde (Wilcocks et al., 1992; Wilcocks and Ward, 1992). On that basis, further studies were performed and the acceptance of various benzaldehyde derivatives as well as hetero aromatic and aliphatic aldehydes in mixed carboligations with acetaldehyde was shown (Dünnwald et al., 2000; Iding et al., 2000). In addition, *Pp*BFD gives access to a broad range of different (*R*)-benzoins (Demir et al., 1999) but is also able to catalyze carboligations involving longer aliphatic, branched chain or unsaturated aldehydes. In case of the latter, *Pp*BFD is strictly *S*-selective (Cosp et al., 2008; Domínguez de María et al., 2007). These properties were even expanded by several protein engineering approaches leading to the identification of variants with altered substrate specificity as well as increased activity and enantioselective (Lingen et al., 2002; Lingen et al., 2003). Regarding the production of (*S*)-HPP, the variant L476Q was one of the best hits with 5-fold higher carboligase activity and increased activity in ethanol and DMSO in comparison to the unaltered *Pp*BFD. Further application-based investigations concentrated on the immobilization of *Pp*BFD applying covalent and non-covalent carrier-based immobilization techniques (Hilterhaus et al., 2008; Peper et al., 2011; Tural et al., 2014) and its use as a whole cell catalyst in micro-aqueous reaction systems enabling high substrate loadings (Domínguez de María et al., 2008; Jakoblinnert and Rother, 2014; Wachtmeister et al., 2016).

1.5.2 Alcohol dehydrogenases

Alcohol dehydrogenases (ADH) belong to the group of oxidoreductases and catalyze the reversible reduction of aldehydes or ketones to the respective alcohols (Zheng et al., 2017). Therefore a reduced nicotinamide cofactor is essential to deliver a hydride ion as reduction equivalent. The reduction of a carbonyl group starts with a nucleophilic attack of the hydride ion and can occur in four different orientations, which influence the stereochemistry of the product (Matsuda et al., 2009; Musa and Phillips, 2011; Prelog, 1964). Two different phenomena are responsible for the existence of these four different reaction pathways. As demonstrated in Figure 1.5-2, the carbonyl group can be differently oriented in the active site leading to a potential nucleophilic attack either from the *re* or *si* face. Second, enzymes are able to differentiate between the two stereotropic hydrogens in the reduced nicotinamide cofactor revealing overall four different combinations. A nucleophilic attack from the *re* face involving the pro-*R* hydrogen is defined as the Prelog rule and known for many ADHs (Prelog, 1964). However, some ADHs follow the anti-Prelog rule by enabling attack from the *si* face leading to inversed stereospecific orientation (Bradshaw et al., 1992a; Bradshaw et al., 1992b).

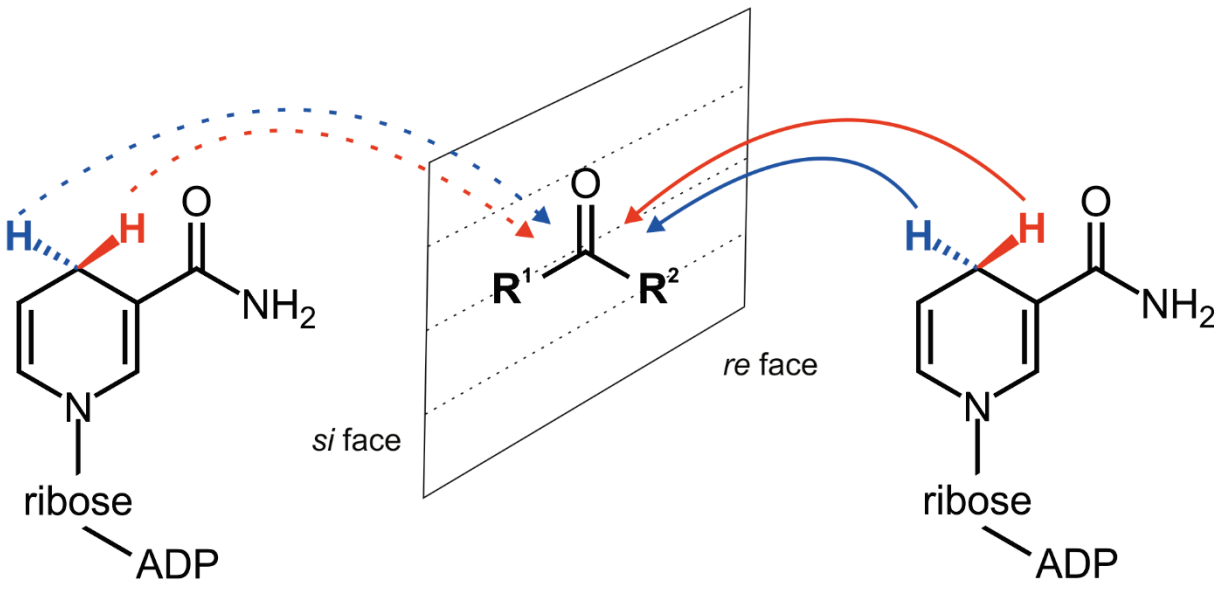

Figure 1.5-2: Possible orientations of the NADH-cofactor relative to a carbonyl substrate in the active site of an alcohol dehydrogenases. Hydride transfer can occur via the *re* or *si* face by employing both stereotropic hydrogens (red and blue). For simplification, the non-phosphorylated nicotinamide cofactor is schematically shown (ADP = adenosine diphosphate). Figure based on Musa and Phillips, 2011.

In general, ADHs are classified into two different super-families consisting of short- and medium-chain dehydrogenases of which the latter are mostly zinc dependent (Auld and Bergman, 2008; Jörnvall et al., 1981; Jörnvall et al., 2015). Short-chain dehydrogenase are characterized by a great functional diversity and most of them form either dimers or tetramers (Jörnvall et al., 1995; Kallberg et al., 2002). They have a more simple architecture in comparison to the medium-chain ADHs since

they are composed of one-domain subunits while medium-chain ADHs consist of two-domain subunits responsible for cofactor binding and catalysis, respectively (Eklund and Ramaswamy, 2008; Ladenstein et al., 2008). In general, evolutionary biologist believe that all types of ADHs have consecutively evolved while small-chain dehydrogenases appeared first, followed by zinc-free and zinc-dependent medium-chain dehydrogenases (Jörnvall et al., 2010). An important issue for all ADHs in biocatalysis is the efficient regeneration of expensive nicotinamide cofactors to render oxido-reductions economically feasible. Several methods are available that can be assigned to different general subgroups including (*i*) co-substrate coupled, (*ii*) enzyme coupled or (*iii*) reaction-internal regeneration (Hummel and Gröger, 2014). In the first two approaches, a sacrificial substrate is selected, which is either converted by the same enzyme catalyzing the main reaction (co-substrate coupled) or by an additional enzyme (enzyme coupled) thereby regenerating respective cofactors. For example, 2-propanol is often used in combination with certain ADHs to reduce oxidized cofactors (Leuchs and Greiner, 2011). 2-propanol is cheap and the resulting acetone is relatively volatile enabling its removal to overcome thermodynamic limitations (Constantinou et al., 2014; Stillger et al., 2002). However, this cosubstrate has to be supplemented in a large excess to shift the equilibrium of such reactions to the product site. In comparison, the use of so-called “smart cosubstrates” elegantly solves this problem by using diols like 1,4-butanediol that undergo lactonization after oxidation, which renders cofactor regeneration irreversible (Kara et al., 2013b; Kara et al., 2013c). In contrast, the use of a second enzyme for cofactor regeneration has to be evaluated carefully in terms of process costs due to the addition of a second catalyst plus cosubstrate. However, several concepts are well-established using for example glucose dehydrogenase and formate dehydrogenase with glucose and formate as cosubstrates, respectively (Hummel and Gröger, 2014; Kara et al., 2013a). In addition, enzyme coupled techniques may also involve the electrochemical regeneration of nicotinamide cofactors where electrons are transported via mediators from an electrode to the cofactor regenerating enzyme (Kara et al., 2013a). Finally, reaction sequences can be designed as such that two or more enzymes with complementary redox state are combined with each other rendering the whole cascade self-sufficient (Hummel and Gröger, 2014). This was for example established by combining an ADH with a Bayer-Villiger monooxygenases, which either need the oxidized or reduced nicotinamide cofactor, respectively (Mallin et al., 2013).

In this thesis, the ADH from *Lactobacillus brevis* (*Lb*ADH) was applied. It belongs to the superfamily of short-chain ADHs, forms a tetramer and strongly depends on divalent magnesium ions (Niefind et al., 2000; Niefind et al., 2003). The *Lb*ADH was first described by Bettina Riebel and acts in an anti-Prelog manner using phosphorylated nicotinamide cofactors (Prelog, 1964; Riebel, 1996). The enzyme possesses two different hydrophobic binding pockets of different size and of which the bigger one is capable of binding even bulky substrate moieties such as phenyl rings (Schlieben et al., 2005). Consequently, acetophenone and derivatives thereof are well accepted by the *Lb*ADH (Rodríguez et al., 2014). Overall, *Lb*ADH accepts a broad range of different substrates including for example

aliphatic ketones, diketones, ketoesters, propargylic ketones as well as α-hydroxyketones (Leuchs and Greiner, 2011). Due to the acceptance of α-hydroxyketones, the *Lb*ADH was already successfully combined with ThDP-dependent enzymes for the production of vicinal diols in enzymatic cascades (Kihumbu et al., 2002; Wachtmeister et al., 2016). Another important fact is its high stability in different solvent systems including a high stability in organic solvents (Leuchs and Greiner, 2011; Villela Filho et al., 2003). This additionally enabled the successful implementation of several continuous reaction systems such as the production of 2,5-hexanediol or 2-butanol in membrane reactors (Erdmann et al., 2014; Schroer and Lütz, 2009). The versatility of *Lb*ADH was finally demonstrated by several successful immobilization procedures including the immobilization on glass beads (Ferloni et al., 2004), on amino-epoxy supports (Hildebrand and Lütz, 2006) or in absorbing polymers (Jeromin, 2009).

1.5.3 Transaminases

Transaminases catalyze the transfer of an amino group from a donor molecule to the carbonyl group of an acceptor and require the essential cofactor pyridoxal phosphate (PLP) (Berglund et al., 2012). PLP is a versatile and highly reactive cofactor mediating several reactions due to its ability to form imines with amino groups via its aldehyde group and its capability to withdraw electrons from bound substrates via its pyridinium ring (John, 1995). PLP-dependent enzymes establish a unique environment to channel this reactivity towards a specific reaction (Mozzarelli and Bettati, 2006).
In transaminases as in many other PLP-dependent enzymes, the cofactor is covalently bound via the just mentioned aldehyde group to the amino group of an active site lysine, as demonstrated in Figure 1.5-3 (Kirsch et al., 1984; Mehta et al., 1993). In the first half of transaminase-catalyzed reactions, this imine is attacked by the donor molecule and the amino group is transferred to PLP yielding the aminated cofactor pyridoxamine phosphate (PMP). In the second half, PMP acts as an amino donor and aminates the acceptor substrate, thereby regenerating PLP for further catalytic cycles (Silverman, 2002). The active site of transaminase is usually formed at the interface of two monomers and most of the transaminase form dimers containing two active sites and two molecules of PLP (Jansonius, 1998). In general, transaminases can be classified according to different subgroups depending on their fold-type among PLP-dependent enzymes (Denesyuk et al., 2002), on primary sequence similarities (Finn et al., 2010; Mehta et al., 1993) or on their region-specificity. The latter classification system is often applied since it allows fast assessment of the substrate range of respective transaminases and reveals if they act on amino groups in α-, β-, γ- or ω-position, respectively. However, this classification is not always strict and often only distinguishes between α-transaminases acting on amino groups in α-position next to a carboxylic or carbonyl groups and ω-transaminases including all other remaining possibilities (Berglund et al., 2012; Ward and Wohlgemuth, 2010). As a consequence, ω-

transaminases are of much higher interest for industrial applications since they are not restricted to α-amino acids and the corresponding ketones (Kelly et al., 2018).

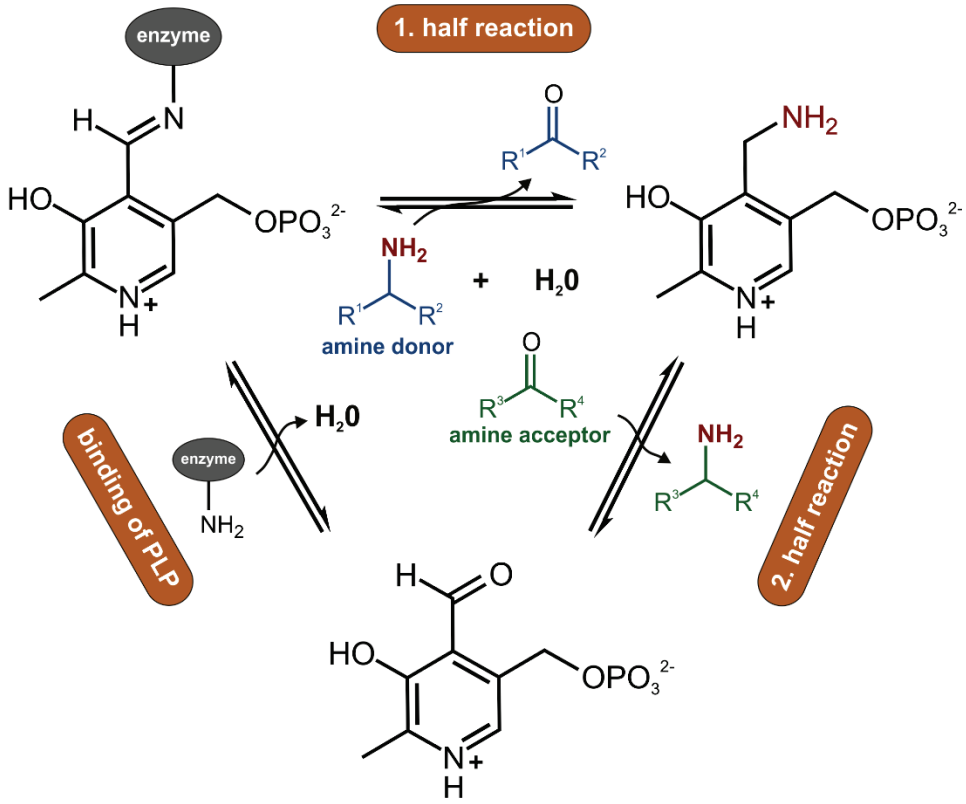

Figure 1.5-3: Reaction mechanism of PLP-dependent transaminases. After binding of the cofactor PLP to the transaminase, the amino group of an amine donor is transferred in the first half reaction to PLP yielding the aminated form PMP. In the second half reaction, PLP is regenerated and the amino group is transferred to an amino acceptor. Scheme was simplified according to Sayer et al., 2014.

In this thesis, the ω-transaminases from *Bacillus megaterium* SC6394 (*Bm*TA) was used. It was discovered in 2008 while searching for appropriate biocatalysts for the preparation of (*R*)-1-cyclopropylethylamine starting from racemic mixtures (Hanson et al., 2008). Just recently, the structure as well as the substrate range of this *Bm*TA was analyzed (van Oosterwijk et al., 2016). The experiments showed that *Bm*TA has a preference for substrates with large planar aromatic substituents such as (*S*)-naphthylethylamines or (*S*)-methylbenzylamines. This was explained by a tunnel leading to the active site that provides the required space. Furthermore, *Bm*TA forms an active homotetramer organized as dimer of dimers. Besides the investigation of the substrate range for the production of optically pure (*S*)-amines, the enzyme was barely characterized. (Koszelewski et al., 2009; Koszelewski et al., 2010a; Koszelewski et al., 2010b).

1.5.4 Aldolases

Aldolases catalyze the stereospecific reaction between an aldehyde acceptor and a carbonyl donor which results in formation of a new C-C bond (Wong and G., 1994). They are found in many essential metabolic pathways for the production or degradation of for example carbohydrates or keto acids (Dean et al., 2007). In general, they can be classified into two major classes according to their reaction mechanism (Rutter, 1964). Class I aldolases are ubiquitous and activate their donor substrates by the formation of a Schiff base via an active site lysine as shown in Figure 1.5-4. Then, the formed enamine tautomer attacks the corresponding acceptor aldehyde via its activated double bond leading to the aldol product, which is still bound to the active site lysine. Hydrolyzation of this imine releases the product (Gefflaut et al., 1995). In contrast, class II aldolases activate the corresponding carbonyl donors through active site bound divalent metal ions that act as a Lewis acid (Fessner et al., 1996). Aldolases bind their donor substrates with high specificity, while they are promiscuous with respect to their acceptor substrates. This allows further classification based on donor specificity (Dean et al., 2007). According to this classification, four different groups based on the donor substrates (*i*) dihydroxyacetone phosphate, (*ii*) pyruvate, (*iii*) acetaldehyde and (*iv*) glycine can be distinguished.

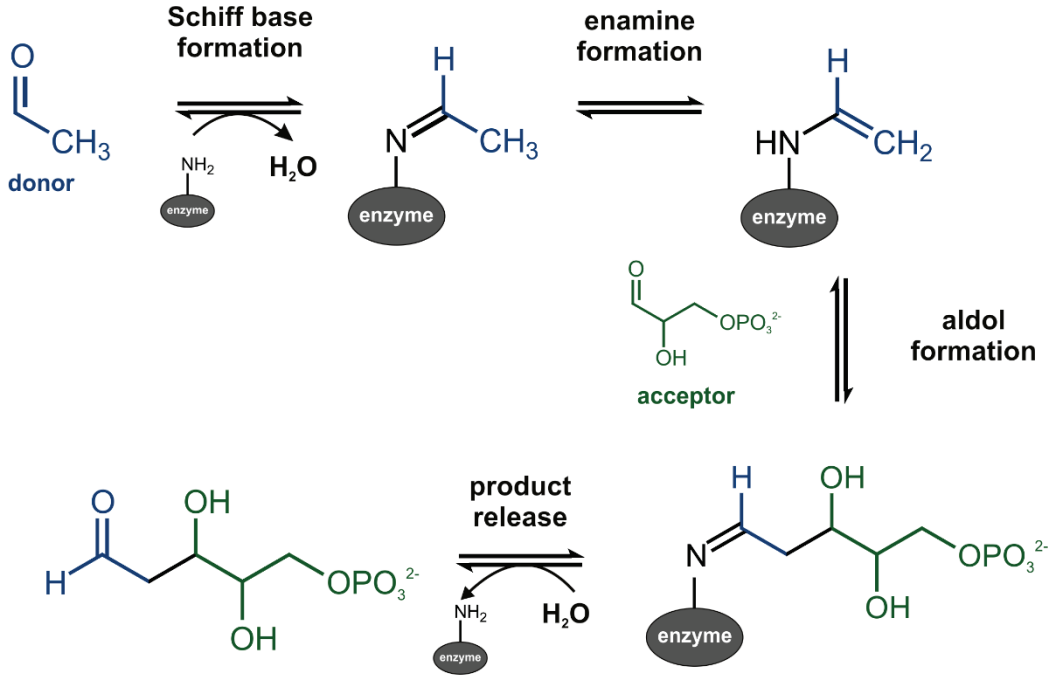

Figure 1.5-4: Catalytic mechanism of class I aldolases exemplarily shown for the formation of 2-desoxyribose-5-phosphate catalyzed by *Ec*DERA. First, the donor molecule (acetaldehyde, blue) is activated by Schiff base formation with an active site lysine. Subsequently, the enamine tautomer attacks respective acceptor molecules (glyceraldehyde-3-phosphate, green) resulting in aldol formation and product release. Scheme based on Heine et al., 2001.

In this thesis, 2-deoxy-D-ribose-5-phosphate aldolase from *Escherichia coli* was applied (*Ec*DERA). It is involved in the metabolism of deoxyribose-5-phosphate, the sugar moiety of DNA, by catalyzing

the reversible aldol reaction between glyceraldehyde-3-phosphate and acetaldehyde (Racker, 1952). For a long time, DERAs were considered to be the only type of aldolases using aldehydes as donors (Dean et al., 2007). However, recent reports proved the existence of further enzymes capable of accepting aldehyde donors (Garrabou et al., 2009; Roldán et al., 2017). The *Ec*DERA was found to occur either in a monomeric form or as a dimer (Heine et al., 2004). The enzyme belongs to class I aldolases and establishes a Schiff base with donor substrates via an active site lysine to initiate respective aldol reactions (Heine et al., 2001; Heine et al., 2004; Stura et al., 1995). Besides acetaldehyde, acetone, fluoroacetone, and propionaldehyde are additionally accepted as donor substrates for the aldol reaction with different aliphatic, mainly linear aldehydes and some halogenated derivatives thereof (Barbas et al., 1990; Chen et al., 1992). However, the activity on these unnatural and non-phosphorylated substrates is relatively low. Furthermore, *Ec*DERA is able to catalyze the sequential addition of two acetaldehyde molecules to one acceptor substrate leading subsequently to spontaneous cyclisation of the formed products (Gijsen and Wong, 1994). A major disadvantage of *Ec*DERA for the use in asymmetric synthesis approaches is its instability and irreversible inactivation in presence of higher acetaldehyde concentrations (Hoffee et al., 1965). It was shown that the aldol product of two acetaldehyde molecule forms a covalent bridge between the active site lysine responsible for donor activation and a cysteine present at position 47 (Dick et al., 2016). Consequently, introduction of mutations at position 47 led to much higher stability towards acetaldehyde (Bramski et al., 2017).

1.6 Scope and objectives of this thesis

As described above, biocatalysts allow the access to valuable compounds due to their outstanding selectivity under mild and sustainable conditions (see 1.1). Currently, great efforts are invested to harness these benefits by establishing suitable reactions for the efficient and sustainable production of such chemicals in new applications. Among other factors, a stable and economically reasonable biocatalyst formulation with low impurities is of utmost importance which additionally allows a versatile set of different reaction concepts according to the specific demands of each individual process (see 1.2, 1.3). In general, carrier-bound biocatalysts have the potential to fulfill these requirements (see 1.4). After binding of the enzyme to the carrier, an insoluble catalyst is formed, which allows repetitive reuse and high enzyme specific productivities due to easy separation from liquid reaction media. Furthermore, compartments can easily be established to implement continuous reactions as well as multi-step synthesis approaches. However, existing immobilization methods struggle to implement a strong connection of biocatalysts to respective supports while maintaining a high catalytic activity for a broad range of different catalysts (see 1.4). Generally, the development of immobilizates with such characteristics is tedious and time-consuming since generic methodologies for the fast and inexpensive immobilization are missing (see 1.4.3). In addition, there is a lack of

methods to establish pure immobilizates in a cost-efficient manner without the need for previous chromatographic purification steps.

To contribute to the solutions of these general problems in the field of biocatalyst immobilization, the objective of this thesis was to identify and evaluate fusion tags as a simple and generic immobilization approach, which allow the efficient combination of enzyme purification and immobilization in one step and concomitantly mediate strong binding to respective supports accompanied by retaining a high level of catalytic activity for a broad range of enzymes. In detail, the tags and immobilizates should comprise the following characteristics:

- The tag should not reduce the heterologous production of corresponding fusion enzymes in microbial host cells and high production yields should easily be achieved.
- The tag should selectively bind directly from crude cell extracts to achieve a high purity and immobilization in one step.
- The tag should bind rapidly to respective supports through strong (preferably covalent) interactions under conditions optimal for each model enzyme.
- The tag should recognize either cheap and available carriers or simply built ligands on the surface of respective supports to keep the carrier costs at a minimum.
- The immobilizates should maintain a high catalytic activity after immobilization.
- The immobilizates should have a high stability which allows efficient reuse in long-term applications.
- The immobilizates should simplify the implementation of continuous reaction concepts.
- The immobilizates should facilitate the establishment of biocatalytic cascades.

To fulfill these aims, three different tags were selected including (*i*) the HaloTag^{TM}, (*ii*) carbohydrate-binding modules and (*iii*) the Aldehyde-tag. The evaluation of these different tags is presented in the following chapters.

2 Results

2.1 HaloTag-*Pf*BAL

Results presented in this chapter were published as:

HaloTag™: Evaluation of a covalent one-step immobilization for biocatalysis.

J. Döbber and M. Pohl

Journal of Biotechnology,

2017, volume 241, pages 170 – 174

DOI: 10.1016/j.jbiotec.2016.12.004

Context:

In this publication, *Pf*BAL was immobilized with the HaloTag™ immobilization concept and activity of the immobilizates, purity after immobilization, binding speed to the support as well as biocatalyst recycling in repetitive batches were investigated. It provides the first proof of concept for this immobilization strategy and is consequently the basis for the immobilization of further model enzymes.

Contributions:

Johannes Döbber planned and performed the experiments. Martina Pohl conceptually planned and supervised the project. Both authors wrote the manuscript.

Journal of Biotechnology 241 (2017) 170–174

Contents lists available at ScienceDirect

Journal of Biotechnology

journal homepage: www.elsevier.com/locate/jbiotec

Short communication

HaloTag™: Evaluation of a covalent one-step immobilization for biocatalysis

Johannes Döbber, Martina Pohl*

IBG-1: Biotechnology, Forschungszentrum Jülich GmbH, D-52425 Jülich, Germany

ARTICLE INFO

Article history:
Received 8 July 2016
Received in revised form
28 November 2016
Accepted 1 December 2016
Available online 5 December 2016

Keywords:
Benzaldehyde lyase
Covalent enzyme immobilization
Repetitive batch
C–C bond formation
Economizing production process
Enzyme fusion

ABSTRACT

Easy, fast and gentle immobilization for the efficient reuse of important biocatalysts is highly demanded. We used the commercially available HaloTag™ technology (Promega), so far relatively unknown in the context of biocatalysis, to immobilize the benzaldehyde lyase from *P. fluorescence* (*Pf*BAL). Immobilization mediated by this fusion tag proceeds rapidly within minutes from crude extracts yielding covalently attached enzymes in high purity, making expensive and laborious previous chromatographic purification steps obsolete, which strongly reduces the costs for biocatalyst immobilization. Further, we introduce a novel design of HaloTag fusions and demonstrate the positive effect of the tag on soluble expression and activity of *Pf*BAL. The immobilized biocatalyst was stable at 4 °C for months and was successfully reused in several repetitive batches for the carboligation of aggressive aldehydes.

1. Introduction

The use of enzymes for the sustainable production of chiral compounds in industry is of rapidly growing interest (Choi et al., 2015). However, there are still several drawbacks that hinder their unlimited implementation. Besides specificity and catalytic efficiency, especially their long-term use and operational stability are known bottlenecks that have to be overcome. Enzyme immobilization can be a solution to these challenges by often increasing the stability of enzymes and enabling their efficient reuse in consecutive processes (Sheldon and van Pelt, 2013).

Ideally, the enzyme is immobilized in a fast, gentle and site-directed way, thereby offering the highest potential to maintain maximal residual activity after immobilization. Further, only the enzyme of interest should bind to the carrier to allow maximal binding of the target enzyme and to avoid the formation of undesired by-products through other catalytic activities. The usual strategy to achieve this goal is (chromatographic) enzyme purification prior to immobilization, which is laborious, costly, and time-consuming. One option to achieve the direct immobilization of enzymes directly from crude cell extracts is the selective absorption through non-covalent or covalent binding on hydrophobic supports that were previously reported for lipases (Bastida et al., 1998; Mihailović et al., 2014) However, a selective method combining purification and covalent site-directed immobilization for a broad range of enzymes in one step is highly demanded. Therefore, fusions of catalysts with respective protein tags are useful (Barbosa et al., 2015). Whereas most of these fusions mediate non-covalent attachment to respective supports, the HaloTag™ system from Promega enables covalent binding without usage of aggressive crosslinking agents such as glutaraldehyde (Migneault et al., 2004).

The HaloTag is a specifically designed suicide variant of the haloalkane dehalogenase from *Rhodococcus rhodocrous*. It recognizes terminal chloroalkanes displayed on any carrier within minutes and forms a covalent ester bond to an aspartate residue in the active site (Encell et al., 2012), which would enable a fast, gentle, and site-directed immobilization directly from crude cell extracts. So far, the HaloTag is mainly used for various biomedical applications, e.g. the *in vivo* detection of protein interactions and cell imaging (Los et al., 2008; England et al., 2015). In 2010, an initial study of this tag for biocatalysis was published using a monomeric lipase from *Bacillus thermocatenulatus* bound to magnetic beads. However, the authors faced several problems concerning the soluble production of the fusion enzyme. (Motejadded et al., 2010). Meanwhile, the HaloTag was optimized and a new variant was

Abbreviations: MBP, maltose binding protein; *Pf*BAL, benzaldehyde lyase from *Pseudomonas fluorescence*; HPP, hydroxy-1-phenylpropan-1-one; ThDP, Thiamine diphosphate.

* Corresponding author.
E-mail address: ma.pohl@fz-juelich.de (M. Pohl).

http://dx.doi.org/10.1016/j.jbiotec.2016.12.004
0168-1656/

established (Ohana et al., 2009). Additional reports underline the positive rather than negative effect of this new HaloTag variant on the soluble production of recombinant enzymes (Peterson and Kwon, 2012; Sun et al., 2015).

Our goal is to exploit fusions with the latest HaloTag version as a generic strategy for the immobilization of enzymes in biocatalysis. The strategy is currently evaluated for a broad range of enzymes with different complexity. Here we present first results on the thiamine diphosphate-dependent homotetrameric benzaldehyde lyase from *Pseudomonas fluorescence* (*Pf*BAL), an important catalyst for the production of 2-hydroxy ketones (Pohl et al., 2014), to demonstrate the functionality of the HaloTag strategy also for complex enzymes. Besides the immobilization directly from crude cell extracts, we demonstrate the application and reusability of immobilized *Pf*BAL for the stereoselective carboligation of aggressive aldehydes like benzaldehyde and acetaldehyde towards (*R*)-hydroxy-1-phenylpropan-1-one ((*R*)-HPP) in repetitive batch reactions, which is not possible with the wildtype enzyme due to fast inactivation (Schwarz , 2010).

2. Results and discussion

For the design of the HaloTag fusion enzyme, the DNA sequence of the HaloTag was optimized using the GENEius software to facilitate soluble protein production in *E. coli*. The final construct contained the HaloTag fused to the N-terminus of *Pf*BAL and separated by a helical linker consisting of 25 amino acids (Chen et al., 2014; Arai et al., 2001). Additionally, *Pf*BAL carries also a C-terminal hexahistidine tag (His-tag) (cf. SI). The resulting HaloTag-*Pf*BAL-His was solubly produced in high amounts in *E.coli* BL21 (DE3), which was demonstrated by SDS-PAGE (Fig. 1), showing a prominent band at about 95 kDa corresponding to one monomer of the fusion enzyme.

Afterwards, the fusion enzyme was successfully purified by Ni-NTA chromatography to simplify the analysis of the immobilization. First, the immobilization of HaloTag-*Pf*BAL-His on HaloLink™ resin was investigated. This carrier consists of Sepharose® beads displaying the corresponding ligand recognized by the HaloTag (Promega) (Fig. 2). As demonstrated in Fig. 3, we measured the amount of fusion enzyme in the supernatant as well as on the Sepharose® beads to follow the interaction. Under the conditions

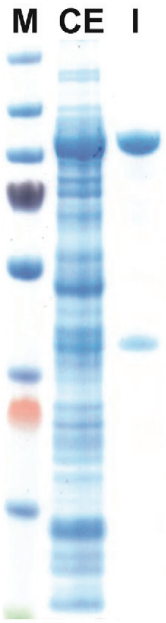

Fig. 1. Purity of HaloTag-*Pf*BAL-His after immobilization from crude cell extracts. Crude cell extract (CE) containing HaloTag-*Pf*BAL-His was mixed with 1 mg of HaloLink™ Resin for immobilization in a total volume of 250 µl BAL buffer. Afterwards, all proteins including covalently bound HaloTag-*Pf*BAL-His were released by treatment with SDS and NaOH (cf. Methods) and analyzed by SDS-PAGE (I). PageRuler™ Prestained Protein Ladder (Thermo Scientific™) was used as a standard (M).

applied the binding of HaloTag-*Pf*BAL-His to the HaloLink carrier occurred fast and after five minutes more than 50% was already bound. After 30 min, no further increase of protein concentration on the carrier was observed, whereas the protein concentration in the supernatant was still slightly decreasing. The latter could be

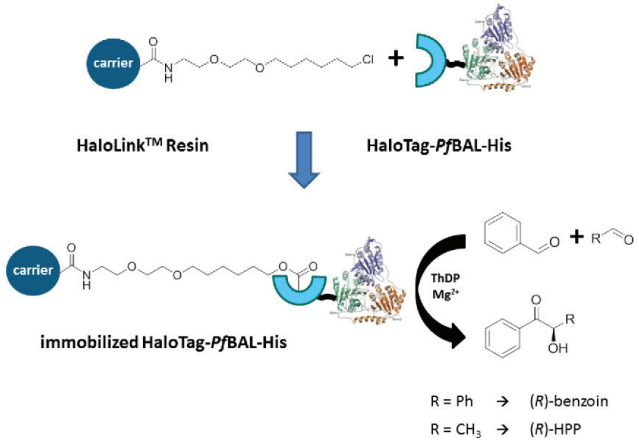

Fig. 2. Schematic presentation of the immobilization procedure of HaloTag-*Pf*BAL-His on HaloLink Resin and the carboligation reactions studied in this work.

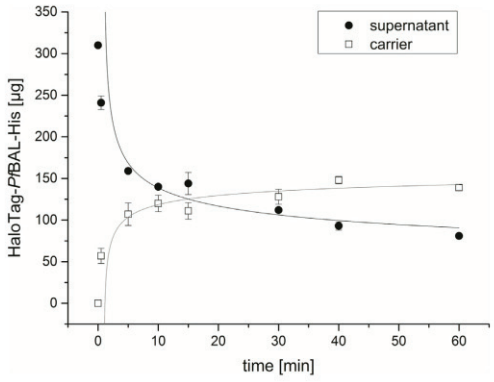

Fig. 3. Binding of HaloTag-*Pf*BAL-His to HaloLink™ Resin. 300 µg of purified HaloTag-*Pf*BAL-His were incubated with 1 mg of HaloLink™ Resin in 250 µl BAL buffer. Immobilization was stopped after different time points by sedimentation of the carrier through centrifugation. The protein amount in the supernatant as well as on the carrier after washing (5 times with 1 ml BAL buffer) were determined. Both data sets were fitted with Origin. Experiments were performed in triplicate.

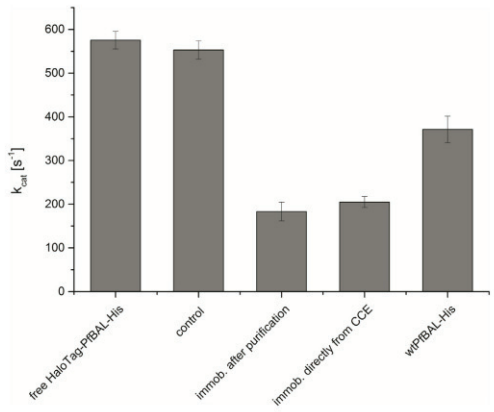

Fig. 4. Activities of wild-type, tagged and immobilized *Pf*BAL-His. Activities were measured by following the conversion of benzaldehyde to (*R*)-benzoin and are given astotal turnover number (k_{cat} [s^{-1}]). Activities were determined for wild-type *Pf*BAL-His (wtPfBAL-His), free HaloTag-*Pf*BAL-His and for HaloTag-*Pf*BAL-His immobilized on HaloLink™ Resin either starting from crude cell extracts (immob. directly from CCE) or after previous chromatographic purification (immob. after purification). Free HaloTag-*Pf*BAL-His incubated under immobilization conditions (cf. Methods) but without carrier was taken as a control to detect possible denaturation at high shaking speeds and in presence of Triton X-100. Experiments were performed in triplicate.

explained by unspecific interactions of the fusion enzyme with the carrier, which was afterwards removed by washing, and thus not accessible by protein determination and activity measurements. Under these conditions, the protein load with this large tetrameric fusion enzyme (380 kDa) amounted to around 10% of the total dry weight of the immobilizate.

Subsequently, the activity of HaloTag-*Pf*BAL-His before and after binding was analyzed. For this purpose, we followed the conversion of benzaldehyde to (*R*)-benzoin by HPLC. As depicted in Fig. 4, the HaloTag has a rather positive influence on the activity of *Pf*BAL and the HaloTag-*Pf*BAL-His is 50% more active than *Pf*BAL-His. However, the activity clearly decreased through immobilization resulting in a residual activity of around 30% compared to the free HaloTag-*Pf*BAL-His. Since the control (free HaloTag-*Pf*BAL-His incubated without carrier) lost almost no activity under immobilization conditions, this activity loss must have been caused by the immobilization. However, enzyme inactivation for other covalent immobilization strategies such as epoxy-activated supports is usually known to be even higher or at least in the same range (Tural et al., 2014; Zhang et al., 2015). It is also noteworthy to mention that the immobilized HaloTag-*Pf*BAL-His still retains 50% of the activity found for *Pf*BAL-His (Fig. 4).

Subsequently, the selective one-step immobilization of the fusion enzyme directly from cell-free crude extracts was tested. To analyze the purity of immobilized enzyme under these conditions, the immobilizate was incubated under alkaline conditions to remove all bound proteins including HaloTag-*Pf*BAL-His (cf. Methods). As demonstrated in Fig. 1, the fusion enzyme was cleaved from the carrier after the immobilization was performed from crude extracts. Besides an intense protein band referring to HaloTag-*Pf*BAL-His, only one additional protein band at about 40 kD appeared indicating the high purity (ca. 90%) of HaloTag-*Pf*BAL-His on the HaloLink resin. Comparison of the activities starting from either crude extracts or purified enzyme did not show a significant difference. However, the amount of enzyme bound to the carrier after immobilization from crude extracts was reduced by 30%.

The stability of the immobilized fusion enzyme was analyzed by measuring the residual benzoin-forming activity of stored immobilizates over several months. As demonstrated in Fig. 5A, the immobilized HaloTag-*Pf*BAL-His is stable for months at 4 °C, if stored in buffer. Finally, the process stability of immobilized HaloTag-*Pf*BAL-His in the presence of aggressive aldehyde substrates was tested. Previous studies have shown that *Pf*BAL is rapidly inactivated in the presence of aliphatic and aromatic aldehydes (Schwarz, 2010). The specific carboligation of benzaldehyde and acetaldehyde towards (*R*)-HPP (Fig. 2) was chosen as a model reaction performed as repetitive batch using the same immobilized catalyst. Fig. 5B clearly shows that the immobilized enzyme was highly active. Around 120 µg of immobilized enzyme on 1 mg HaloLink catalyzed the formation of 12 µmol (*R*)-HPP with almost full (98%) conversion and with an excellent enantiomeric excess (ee) of 99% within one hour in the first cycle. With every further cycle, the reaction proceeded slower and the initial activity decreased by around 30–40% (Fig. 5C). Most likely, this loss of activity partly results from the inactivation caused by the aldehyde substrates benzaldehyde and acetaldehyde. However, the inactivation is much lower compared to the soluble wildtype enzyme (Schwarz, 2010). A further reason for the loss of activity in repetitive batch reactions is loss of immobilizate during washing steps between the single reactions. Nevertheless, the same high conversion and ee as in the first cycle were reached in all repetitive batches. Since the reaction time increased fivefold in the last cycle in comparison to the first batch, the experiment was stopped at this point although the catalyst was still active.

To conclude: For the first time, we here studied the latest HaloTag variant for the use in biocatalysis. The presented data indicates the low interference of the HaloTag on the soluble production and activity of recombinant fusion enzymes as well as the simplicity to purify and immobilize even complex homotetrameric enzymes like *Pf*BAL covalently with this strategy in one step. Similar studies with further enzymes are currently conducted in our lab to further evaluate the suitability of this immobilization strategy for biocatalysis.

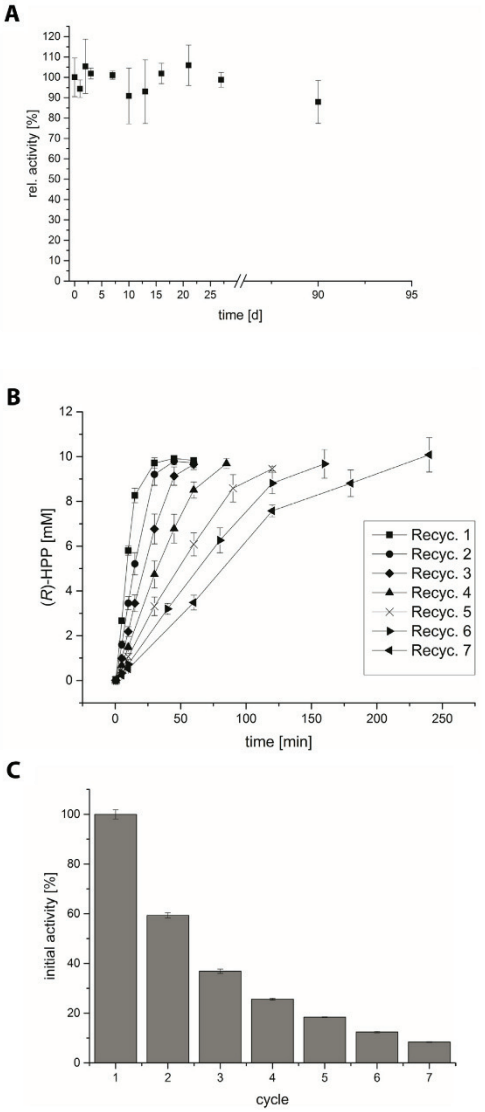

Fig. 5. Stability of immobilized HaloTag-*Pf*BAL-His bound to HaloLink™ Resin. A: the storage stability at 4 °C in BAL buffer is shown. Activities were determined by following the conversion of benzaldehyde to (*R*)-benzoin (cf. Methods). The activity directly after immobilization was defined as 100%. B: process stability of immobilized HaloTag-*Pf*BAL-His in seven repetitive batches catalyzing the carboligation of benzaldehyde and acetaldehyde towards (*R*)-HPP. Batches were performed over 10 days and in between stored at 4 °C. C: initial activity in each cycle of the same repetitive batch mentioned in B. The initial activity in the first cycle was defined to be 100%. All experiments were performed in triplicate.

3. Materials and methods

3.1. Materials

If not otherwise stated, all chemicals were purchased from Sigma-Aldrich at the highest available purity. Benzaldehyde was distilled prior to use. Clone Manager Professional (Version 8, Sci-Ed Software) was used for design of expression plasmids and figures were made with Origin (Version 9.1, OriginLab).

3.2. Construction of expression plasmid, cell cultivation and chromatographic purification

The expression plasmid pET28a-*halotag-pfbal-his* was constructed with the Gibson Assembly® Cloning Kit (NEB). Protein production was performed in LB media at 20 °C and HaloTag-*Pf*BAL-His was purified by means of immobilized metal ion chromatography. Detailed information is given in the SI.

3.3. Immobilization

The HaloLink™ Resin (Promega) consists of Sepharose® beads with a particle size of 45–165 μm. The HaloTag® binding ligand is covalently attached to the surface of these beads via a carbamide linkage using an eleven-atom linker (see Fig. 2). For immobilization, a suspension (200 μl) of the HaloLink™ Resin (corresponding to ~1 mg of dry carrier) was transferred into a 1.5 ml microreaction tube. To remove any residual ethanol, the carrier was washed several times with 1 ml BAL buffer, consisting of 50 mM potassium phosphate buffer, pH 8.0, containing 2.5 mM $MgSO_4$ and 0.15 mM ThDP. In addition, 0.5% v/v Triton X-100 was added to the BAL buffer to prevent attachment of the carrier to the surface of the microreaction tubes and pipette tips. Then, immobilization was performed in a total volume of 250 μl using various amounts of either crude cell extracts or purified fusion enzyme. This mixture was incubated for 1 h at 25 °C and 1200 rpm in a ThermoMixer® (Eppendorf) and subsequently washed 5 times with 1 ml of BAL buffer containing 0.5% v/v Triton X-100. The immobilized catalyst was stored in BAL buffer at 4 °C.

3.4. Purity of immobilized HaloTag-Pf*BAL-His*

For immobilization directly from crude cell extracts, the purity of immobilized HaloTag-*Pf*BAL-His was analyzed after washing. Therefore, the carrier was incubated in lysis buffer of the GeneJET Plasmid Miniprep Kit (ThermoFisher Scientific) at 20 °C for 15 min. This lysis buffer contains SDS and NaOH. Treatment with SDS denatures all bound proteins, thus removing non-specifically bound proteins and additionally leading to an exposure of the ester bonds connecting the HaloTag with the carrier. NaOH results in saponification of this ester bond to release covalently bound HaloTag fusions. After this treatment, the samples were centrifuged and the supernatant was analyzed by SDS-PAGE.

3.5. Analytics

Protein concentrations of free and immobilized proteins were determined with the BC Assay Protein Quantitation Kit (Interchim) according to the manufacturerís instructions with slight adaptations. Assays were performed with 25 μl of the respective sample and 200 μl of BC assay reagent in a 1.5 ml microreaction tube. After incubation at 37 °C for 30 min and 1200 rpm in a ThermoMixer® (Eppendorf), the samples were shortly centrifuged to pellet the immobilizates and 150 μl of the supernatant was transferred into a 96 well microtiter plate. The absorption of this solution was mea-

sured at 562 nm using a TECAN Infinite® M200 reader and protein concentrations were determined using BSA as a standard.

Activity of HaloTag-*Pf*BAL-His was determined by HPLC on a Chiralpak IE column using an Agilent 1260 Infinity Quarternary LC system (Agilent Technologies) equipped with a 1260 Diode Array Detector. Toluene was used as an internal standard detected at 215 nm. For the analysis of (*R*)-benzoin formation, the column was operated with a mobile phase of 50% v/v acetonitrile and 50% v/v pure water at a flow of 1 ml/min and 20 °C. Benzaldehyde and benzoin were detected at 250 nm with approximate retention times of 5.2 min and 7.3 min, respectively. For the carboligation of acetaldehyde and benzaldehyde towards (*R*)-HPP, the column was operated with a mobile phase of 35% v/v acetonitrile and 65% v/v pure water at a flow of 1 ml/min and 20 °C. (*R*)-HPP, (*S*)-HPP, benzaldehyde and (*R*)-benzoin were detected at 250 nm with approximate retention times of 6.3 min, 6.8 min, 8.3 min and 18.1 min, respectively.

3.6. Activity assays and stability tests

Storage stability was analyzed by storing immobilized HaloTag-*Pf*BAL-His at 4 °C in BAL buffer over several months. Samples were taken at different time points and the residual activity was measured. For this purpose, 0.001 mg/ml of immobilized enzyme was incubated with 50 mM benzaldehyde in 500 µl BAL buffer containing 10% v/v DMSO at 25 °C and 1200 rpm (ThermoMixer, Eppendorf). Benzoin formation was detected by HPLC as described above. One unit (U) of activity is defined as the amount of enzyme which catalyzes the formation of 1 µmol benzoin per minute under these conditions.

Process stability of immobilized HaloTag-*Pf*BAL-His was determined by following the carboligation of benzaldehyde and acetaldehyde to (*R*)-HPP (Fig. 2). For this purpose, 120 µg of immobilized enzyme (immobilized on 1 mg of HaloLink resin) were mixed with 10 mM benzaldehyde and 60 mM acetaldehyde in BAL buffer containing 10% (v/v) DMSO in a total volume of 1.2 ml. Reaction was performed at 25 °C and 1200 rpm in a ThermoMixer (Eppendorf) until no further increase in product formation was observed (40–250 min), which was measured by HPLC as described above. After the reaction was completed, aldehydes were removed by intense washing (5 times) with 1 ml BAL buffer containing 0.5% v/v Triton X-100 and the immobilized enzyme was stored at 4 °C in BAL buffer until the next reaction cycle was started. In total, immobilized HaloTag-*Pf*BAL-His was reused for seven repetitive batches performed over ten days.

Acknowledgment

This project was funded by the German Federal Ministry of Education and Research (BMBF) within the project "Molecular Interaction Engineering" (funding code 031A095).

Appendix A. Supplementary data

Supplementary data associated with this article can be found, in the online version, at http://dx.doi.org/10.1016/j.jbiotec.2016.12.004.

References

Arai, R., Ueda, H., Kitayama, A., Kamiya, N., Nagamune, T., 2001. Design of the linkers which effectively separate domains of a bifunctional fusion protein. Protein Eng. Des. Sel. 14, 529–532, http://dx.doi.org/10.1093/protein/14.8.529.

Barbosa, O., Ortiz, C., Berenguer-Murcia Á, Torres, R., Rodrigues, R.C., Fernandez-Lafuente, R., 2015. Strategies for the one-step immobilization–purification of enzymes as industrial biocatalysts. Biotechnol. Adv. 33, 435–456, http://dx.doi.org/10.1016/j.biotechadv.2015.03.006.

Bastida, A., Sabuquillo, P., Armisen, P., Fernández-Lafuente, R., Huguet, J., Guisán, J.M., 1998. A single step purification, immobilization, and hyperactivation of lipases via interfacial adsorption on strongly hydrophobic supports. Biotechnol. Bioeng. 58, 486–493.

Chen, Xiaoying, Zaro, Jennica, Shen, W.-C., 2014. Fusion protein linkers: property, design and functionality. NIH Public Access 65, 1357–1369, http://dx.doi.org/10.1016/j.addr.2012.09.039.

Choi, J.-M., Han, S.-S., Kim, H.-S., 2015. Industrial applications of enzyme biocatalysis: current status and future aspects. Biotechnol. Adv. 33, 1–12, http://dx.doi.org/10.1016/j.biotechadv.2015.02.014.

Encell, L.P., Friedman Ohana, R., Zimmerman, K., Otto, P., Vidugiris, G., Wood, M.G., Los, G.V., McDougall, M.G., Zimprich, C., Karassina, N., Learish, R.D., Hurst, R., Hartnett, J., Wheeler, S., Stecha, P., English, J., Zhao, K., Mendez, J., Benink, H.A., Murphy, N., Daniels, D.L., Slater, M.R., Urh, M., Darzins, A., Klaubert, D.H., Bulleit, R.F., Wood, K.V., 2012. Development of a dehalogenase-based protein fusion tag capable of rapid, selective and covalent attachment to customizable ligands. Curr. Chem. Genomics 6, 55–71, http://dx.doi.org/10.2174/1875397301206010055.

England, C.G., Luo, H., Cai, W., 2015. HaloTag technology: a versatile platform for biomedical applications. Bioconjug. Chem. 26, 975–986, http://dx.doi.org/10.1021/acs.bioconjchem.5b00191.

Los, G.V., Encell, L.P., McDougall, M.G., Hartzell, D.D., Karassina, N., Zimprich, C., Wood, M.G., Learish, R., Ohana, R.F., Urh, M., Simpson, D., Mendez, J., Zimmerman, K., Otto, P., Vidugiris, G., Zhu, J., Darzins, A., Klaubert, D.H., Bulleit, R.F., Wood, K.V., 2008. HaloTag: a novel protein labeling technology for cell imaging and protein analysis. ACS Chem. Biol. 3, 373–382, http://dx.doi.org/10.1021/cb800025k.

Migneault, I., Dartiguenave, C., Bertrand, M.J., Waldron, K.C., 2004. Glutaraldehyde: behavior in aqueous solution, reaction with proteins, and application to enzyme crosslinking. Biotechniques 37, 790–802, http://dx.doi.org/10.2144/3705A0790.

Mihailović, M., Stojanović, M., Banjanac, K., Carević, M., Prlainović, N., Milosavić, N., Bezbradica, D., 2014. Immobilization of lipase on epoxy-activated Purolite® A109 and its post-immobilization stabilization. Process Biochem. 49, 637–646, http://dx.doi.org/10.1016/j.procbio.2014.01.013.

Motejadded, H., Kranz, B., Berensmeier, S., Franzreb, M., Altenbuchner, J., 2010. Expression, one-step purification, and immobilization of HaloTagTM fusion proteins on chloroalkane-functionalized magnetic beads. Appl. Biochem. Biotechnol. 162, 2098–2110, http://dx.doi.org/10.1007/s12010-010-8985-1.

Ohana, R.F., Encell, L.P., Zhao, K., Simpson, D., Slater, M.R., Urh, M., Wood, K.V., 2009. HaloTag7: a genetically engineered tag that enhances bacterial expression of soluble proteins and improves protein purification. Protein Expression Purif. 68, 110–120, http://dx.doi.org/10.1016/j.pep.2009.05.010.

Peterson, S.N., Kwon, K., 2012. The HaloTag: improving soluble expression and applications in protein functional analysis. Curr. Chem. Genomics 6, 8–17.

Pohl, M., Wechsler, C., Müller, M., 2014. Acyloin, benzoin, and related reactions. In: Faber, K., Fessner, W.-D., Turner, N.J. (Eds.), Science of Synthesis: Biocatalysis in Organic Synthesis 2. Georg Thieme Verlag KG, Stuttgart, pp. 93–131.

M. Schwarz 2010. Einflussfaktoren auf die Stabilität und Aktivität der Benzaldehydlyase aus Pseudomonas fluorescens in Carboligasereaktionen mit aromatischen Aldehyden. Heinrich-Heine University, Düsseldorf.

Sheldon, R.A., van Pelt, S., 2013. Enzyme immobilisation in biocatalysis: why, what and how. Chem. Soc. Rev. 42, 6223–6235, http://dx.doi.org/10.1039/c3cs60075k.

Sun, C., Li, Y., Taylor, S.E., Mao, X., Wilkinson, M.C., Fernig, D.G., 2015. HaloTag is an effective expression and solubilisation fusion partner for a range of fibroblast growth factors. PeerJ 3, e1060, http://dx.doi.org/10.7717/peerj.1060.

Tural, B., Tarhan, T., Tural, S., 2014. Covalent immobilization of benzoylformate decarboxylase from *Pseudomonas putida* on magnetic epoxy support and its carboligation reactivity. J. Mol. Catal. B Enzym. 102, 188–194, http://dx.doi.org/10.1016/j.molcatb.2014.02.016.

Zhang, D.H., Peng, L.J., Wang, Y., Li, Y.Q., 2015. Lipase immobilization on epoxy-activated poly(vinyl acetate-acrylamide) microspheres. Colloids Surf. B Biointerfaces 129, 206–210, http://dx.doi.org/10.1016/j.colsurfb.2015.03.056.

Supporting Information

HaloTag™: Evaluation of a covalent one-step immobilization for biocatalysis

Johannes Döbber, Martina Pohl*

IBG-1: Biotechnology, Forschungszentrum Jülich GmbH, D-52425 Jülich, Germany

* Corresponding author

Phone: +49-02461-614388

Fax: +49-2461-613870

Table of content

Primer sequences:

Primer A: gcgaaagcggccgcgGCGATGATTACAGGCGGC

Primer B: ccgtaccaatttctgcCATGGTATATCTCCTTC

DNA sequence of *halotag-pfbal-his*

Sequence encoding for the HaloTag™: green; spacer: red, *Pf*BAL: blue

ATGGCAGAAATTGGTACGGGATTTCCGTTTGACCCGCATTATGTGGAGGTTCTGGGTGAACGCATGCACTACGT
GGATGTTGGTCCGCGCGATGGCACACCGGTGCTGTTTCTGCATGGTAATCCGACCTCCAGCTATGTTTGGCGCA
ACATTATTCCGCATGTCGCCCCAACGCATCGCTGTATTGCCCCAGATCTCATTGGCATGGGCAAAAGCGACAAA
CCGGATTTGGGCTACTTCTTCGACGATCACGTACGGTTTATGGACGCCTTTATCGAGGCTCTGGGACTCGAGGA
AGTAGTGCTGGTTATTCATGACTGGGGCTCTGCATTAGGCTTTCACTGGGCTAAACGGAACCCAGAACGCGTCA
AGGGGATTGCCTTCATGGAGTTCATCCGTCCGATTCCGACCTGGGATGAATGGCCCGAATTTGCCCGTGAAACC
TTTCAGGCGTTTCGTACCACGGATGTTGGCCGTAAGCTCATCATCGACCAAAACGTGTTCATTGAGGGCACTCT
TCCCATGGGAGTAGTGCGTCCTTTAACCGAAGTCGAGATGGACCACTATCGCGAACCCTTCCTGAATCCGGTTG
ATCGCGAACCGCTGTGGCGCTTCCCGAATGAGCTGCCTATTGCTGGTGAACCGGCGAATATCGTGGCACTTGTG
GAAGAATACATGGATTGGCTGCATCAGAGTCCAGTCCCTAAGCTGTTGTTTTGGGGTACACCTGGCGTGTTGAT
TCCGCCTGCAGAAGCTGCTCGCTTAGCGAAAAGCTTGCCCAACTGCAAAGCGGTCGATATTGGGCCAGGTCTG
AACCTGTTACAGGAGGATAACCCGGATCTGATCGGGAGTGAAATCGCGCGTTGGCTGTCAACTCTGGAAATCT
CGGGTCTTGCAGAAGCAGCGGCCAAAGAAGCTGCGGCCAAAGAGGCAGCCGCGAAAGAAGCAGCGGCGAAA
GCGGCCGCGGCGATGATTACAGGCGGCGAACTGGTTGTTCGCACCCTAATAAAGGCTGGGGTCGAACATCTGT
TCGGCCTGCACGGCGCGCATATCGATACGATTTTTCAAGCCTGTCTCGATCATGATGTGCCGATCATCGACACC
CGCCATGAGGCCGCCGCAGGGCATGCGGCCGAGGGCTATGCCCGCGCTGGCGCCAAGCTGGGCGTGGCGCTG
GTCACGGCGGGCGGGGGATTTACCAATGCGGTCACGCCCATTGCCAACGCTTGGCTGGATCGCACGCCGGTGC
TCTTCCTCACCGGATCGGGCGCGCTGCGTGATGATGAAACCAACACGTTGCAGGCGGGGATTGATCAGGTCGC
GATGGCGGCGCCCATTACCAAATGGGCGCATCGGGTGATGGCAACCGAGCATATCCCACGGCTGGTGATGCAG
GCGATCCGCGCCGCGTTGAGCGCGCCACGCGGGCCGGTGTTGCTGGATCTGCCGTGGGATATTCTGATGAACC
AGATTGATGAGGATAGCGTCATTATCCCCGATCTGGTCTTGTCCGCGCATGGGGCCAGACCCGACCCTGCCGAT
CTGGATCAGGCTCTCGCGCTTTTGCGCAAGGCGGAGCGGCCGGTCATCGTGCTCGGCTCAGAAGCCTCGCGGA
CAGCGCGCAAGACGGCGCTTAGCGCCTTCGTGGCGGCGACTGGCGTGCCGGTGTTTGCCGATTATGAAGGGCT
AAGCATGCTCTCGGGGCTGCCCGATGCTATGCGGGGCGGGCTGGTGCAAAACCTCTATTCTTTTGCCAAAGCCG
ATGCCGCGCCAGATCTCGTGCTGATGCTGGGGGCGCGCTTTGGCCTTAACACCGGGCATGGATCTGGGCAGTT
GATCCCCCATAGCGCGCAGGTCATTCAGGTCGACCCTGATGCCTGCGAGCTGGGACGCCTGCAGGGCATCGCT
CTGGGCATTGTGGCCGATGTGGGTGGGACCATCGAGGCTTTGGCGCAGGCCACCGCGCAAGATGCGGCTTGGC
CGGATCGCGGCGACTGGTGCGCCAAAGTGACGGATCTGGCGCAAGAGCGCTATGCCAGCATCGCTGCGAAATC
GAGCAGCGAGCATGCGCTCCACCCCTTTCACGCCTCGCAGGTCATTGCCAAACACGTCGATGCAGGGGTGACG
GTGGTAGCGGATGGTGCGCTGACCTATCTCTGGCTGTCCGAAGTGATGAGCCGCGTGAAACCCGGCGGTTTTCT
CTGCCACGGCTATCTAGGCTCGATGGGCGTGGGCTTCGGCACGGCGCTGGGCGCGCAAGTGGCCGATCTTGAA
GCAGGCCGCCGCACGATCCTTGTGACCGGCGATGGCTCGGTGGGCTATAGCATCGGTGAATTTGATACGCTGG
TGCGCAAACAATTGCCGCTGATCGTCATCATCATGAACAACCAAAGCTGGGGGGCGACATTGCATTTCCAGCA
ATTGGCCGTCGGCCCCAATCGCGTGACGGGCACCCGTTTGGAAAATGGCTCCTATCACGGGGTGGCCGCCGCC
TTTGGCGCGGATGGCTATCATGTCGACAGTGTGGAGAGCTTTTCTGCGGCTCTGGCCCAAGCGCTCGCCCATAA
TCGCCCCGCCTGCATCAATGTCGCGGTCGCGCTCGATCCGATCCCGCCCGAAGAACTCATTCTGATCGGCATGG
ACCCCTTCGCACTCGAGCACCACCACCACCACCACTGA

Amino acid sequence of HaloTag-*Pf*BAL-His

HaloTag™: green; spacer: red, *Pf*BAL: blue

MAEIGTGFPFDPHYVEVLGERMHYVDVGPRDGTPVLFLHGNPTSSYVWRNIIPHVAPTHRCIAPDLIGM
GKSDKPDLGYFFDDHVRFMDAFIEALGLEEVVLVIHDWGSALGFHWAKRNPERVKGIAFMEFIRPIPTW
DEWPEFARETFQAFRTTDVGRKLIIDQNVFIEGTLPMGVVRPLTEVEMDHYREPFLNPVDREPLWRFPN
ELPIAGEPANIVALVEEYMDWLHQSPVPKLLFWGTPGVLIPPAEAARLAKSLPNCKAVDIGPGLNLLQE
DNPDLIGSEIARWLSTLEISGLAEAAAKEAAAKEAAAKEAAAKAAAAMITGGELVVRTLIKAGVEHLFG
LHGAHIDTIFQACLDHDVPIIDTRHEAAAGHAAEGYARAGAKLGVALVTAGGGFTNAVTPIANAWLDR
TPVLFLTGSGALRDDETNTLQAGIDQVAMAAPITKWAHRVMATEHIPRLVMQAIRAALSAPRGPVLLD
LPWDILMNQIDEDSVIIPDLVLSAHGARPDPADLDQALALLRKAERPVIVLGSEASRTARKTALSAFVAA

TGVPVFADYEGLSMLSGLPDAMRGGLVQNLYSFAKADAAPDLVLMLGARFGLNTGHGSGQLIPHSAQ
VIQVDPDACELGRLQGIALGIVADVGGTIEALAQATAQDAAWPDRGDWCAKVTDLAQERYASIAAKSS
SEHALHPFHASQVIAKHVDAGVTVVADGALTYLWLSEVMSRVKPGGFLCHGYLGSMGVGFGTALGA
QVADLEAGRRTILVTGDGSVGYSIGEFDTLVRKQLPLIVIIMNNQSWGATLHFQQLAVGPNRVTGTRLE
NGSYHGVAAAFGADGYHVDSVESFSAALAQALAHNRPACINVAVALDPIPPEELILIGMDPFALEHHHH
HH

Construction of expression plasmid

The amino acid sequence of the HaloTag and the linker sequence $A(EAAAK)_4AAA$ was converted into an optimized DNA sequence by the GENEius software (eurofins genomics). The corresponding DNA sequence was synthesized as linear fragments and directly used for ligation with the linearized pET28a plasmid backbone already containing the gene encoding *Pf*BAL-His. Linearization was performed by PCR using Phusion® High-Fidelity DNA Polymerase (NEB) according to the manufacturer´s instructions and with primers A and B. These contained specific overhangs complementary to the ends of the linear fragments encoding for the HaloTag and the linker sequence $A(EAAAK)_4AAA$ to enable ligation of both DNA fragments by using the Gibson Assembly® Cloning Kit (NEB) according to the manufacturer´s instructions.

Cell cultivation and chromatographic purification

E. coli BL21 (DE3) cells were transformed with the expression plasmid pET28a-*halotag-pfBAL-his*. Heterologous production of HaloTag-*Pf*BAL-His was performed in LB media by inducing enzyme production with 0.1 mM IPTG at the end of exponential growth phase. Cells were then harvested after further incubation for 24 h at 20 °C and stored at -20 °C. Purification of HaloTag-*Pf*BAL-His was performed by means of immobilized metal ion chromatography. First, cells were disrupted by sonification using a Branson Sonifier equipped with a 5 mm microtip. Sonification was performed for 10 min with a pulse time of 2 sec and an amplitude of 60 % followed by 8 sec without pulse. After centrifugation at 15000 x g for 30 min, the crude cell extract was applied to the Ni-NTA column (Qiagen; bed volume, 20 ml), which was previously equilibrated with potassium phosphate buffer (50 mM, pH=7.0) containing 2.5 mM $MgSO_4$, 0.15 mM ThDP and 300 mM sodium chloride. Weakly bound enzymes were washed from the column with 10 mM imidazole and elution of HaloTag-*Pf*BAL-His was performed with 250 mM of imidazole. Imidazole and NaCl were removed in a desalting step on a G25 Sephadex column (GE Healthcare; bed volume, 1L) using potassium phosphate buffer (10 mM, pH 7.0). Afterwards, elution fractions containing HaloTag-*Pf*BAL-His were lyophilized and stored at -20 °C.

2.2 HaloTag-*Bm*TA

Results presented in this chapter are part of a cooperation with the group of Dörte Rother at IBG-1: Biotechnology. As final studies have to be performed by the cooperation partner, the respective manuscript could not be finalized until this thesis was submitted. Thus, this chapter comprises a manuscript draft focusing on the results obtained by Johannes Döbber. Where necessary for an understanding, the results of others were included, which was indicated respectively.

Context:

This chapter describes how HaloTag™ fusion enzymes can contribute to enable an efficient two-step enzymatic cascade, which was established in the working group of Dörte Rother (specific contributions see below). In this cascade, *Pp*BFD and *Bm*TA were combined for the production of a chiral 1,2-amino-alcohol. The main task was the immobilization of *Bm*TA and the optimization of reaction conditions to apply immobilized HaloTag-*Bm*TA for reductive amination. Immobilization of the *Pp*BFD was optimized earlier and is described in chapter 2.4.

In general, results focus on the usefulness of the HaloTag™ immobilization concept to combine enzymes for multi-step synthesis approaches in simple batch reaction systems. Individual reaction steps are easily separated through immobilization to circumvent negative interferences of the reaction conditions with each other.

Contributions:

The enzymatic cascade towards corresponding amino alcohols was investigated and established by K. Mack[1], V. Erdmann[1] and U. Mackfeld[1]. Immobilization of involved enzymes and optimization of the established cascade was performed by J. Döbber[2] and K. Mack. T. Gerlach[2] assisted in construction of the expression plasmid to produce HaloTag-*Bm*TA and R. Agular Rocha[1] helped to identify optimal conditions for recycling of *Bm*TA. The present manuscript was written by J. Döbber, V. Erdmann, K. Mack, M. Pohl[2] and D. Rother[1].

[1] Group of Dörte Rother, IBG-1: Biotechnology, Forschungszentrum Jülich, Germany
[2] Group of Martina Pohl, IBG-1: Biotechnology, Forschungszentrum Jülich, Germany

2.2.1 Introduction

Biocatalysis is an interesting alternative to chemical synthesis due to its outstanding selectivity providing access to optically pure compounds. Amines and amino alcohols are valuable chiral building blocks for more complex molecules or directly reveal pharmaceutical activity such as the sympathomimetics cathine or metaraminol (Breuer et al., 2004; Höhne et al., 2008; Höhne and Bornscheuer, 2009; Sehl et al., 2014; Simon et al., 2014). They can be produced via transaminases catalyzing the reductive amination of respective carbonyl substrates (Malik et al., 2012).

Transaminases exhibit a broad substrate scope for many different aliphatic or aromatic substrates (Both et al., 2016; Calvelage et al., 2017; Koszelewski et al., 2008; Park et al., 2012). In general, the active site of transaminases consists of a large and a small binding pocket as demonstrated in Figure 2.2-1. Usually, their large binding pocket accepts small as well as bulky substituents. Besides, large substituents of the substrate don´t fit into the small binding pocket of the active site, which is for most enzymes restricted to methyl and ethyl groups (Kohls et al., 2014; Savile et al., 2010).

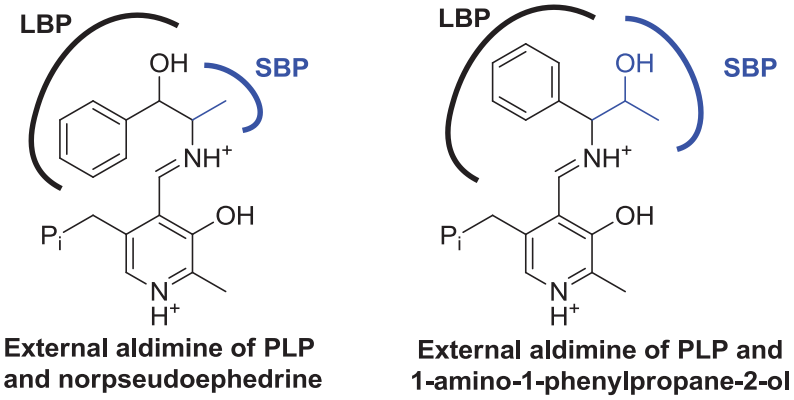

Figure 2.2-1: Active site requirements for the transaminase-catalyzed production of nor(pseudo)ephedrine and 1-amino-1-phenylpropane-2-ol (APP). Generally, active sites in transaminases consist of a small and large binding pocket for the binding of different substituents (SBP, LBP). Reductive amination of 2-hydroxy-1-phenylpropanone to produce APP (right) requires a more flexible SBP in comparison to reductive amination of phenylacetylcarbinol to produce nor(pseudo)ephedrine (left) as indicated in form of respective PLP-bound intermediates. The figure is based on Höhne and Bornscheuer, 2009.

Therefore, the biocatalytical production of amines with bulky side chains is restricted. For example, no biocatalyst is available for the synthesis of 1-amino-1-phenylpropane-2-ol (APP) from 2-hydroxy-1-phenyl-1-propanone (HPP). While its regioisomer and pharmaceutically active drug nor(pseudo)-ephedrine was already accessible via amination of the less stereochemically demanding 1-hydroxy-1-phenylpropan-2-one (phenylacetylcarbinol) (Sehl et al., 2013; Sehl et al., 2014), the carbonyl group in HPP is located between the phenyl ring and the hydroxyethyl group, which requires a much larger binding pocket as demonstrated in Figure 2.2-1. Recently, a search for suitable transaminases was

performed to identify appropriate candidates for the production of APP isomers[1]. For this purpose, wild-type enzymes were screened, which are more flexible in their active site and tolerate even larger substituents in their small binding pocket (Koszelewski et al., 2008; Koszelewski et al., 2010a; Koszelewski et al., 2010b; Simon et al., 2014). Among these, the transaminase of *Bacillus megaterium* (*Bm*TA, see 1.5.3) enabled access to (1*R*,2*S*)-APP by a combination with a previous C-C-bond forming step using the benzoylformate decarboxylase from *Pseudomonas putida* (*Pp*BFD, see 1.5.1) in a two-step enzymatic cascade. As demonstrated in Figure 2.2-2, *Pp*BFD catalyzes the carboligation of benzaldehyde and acetaldehyde yielding (*S*)-HPP (Iding et al., 2000). Then, *Bm*TA is applied to perform a reductive amination towards (1*R*,2*S*)-APP using isopropylamine as an amine donor.

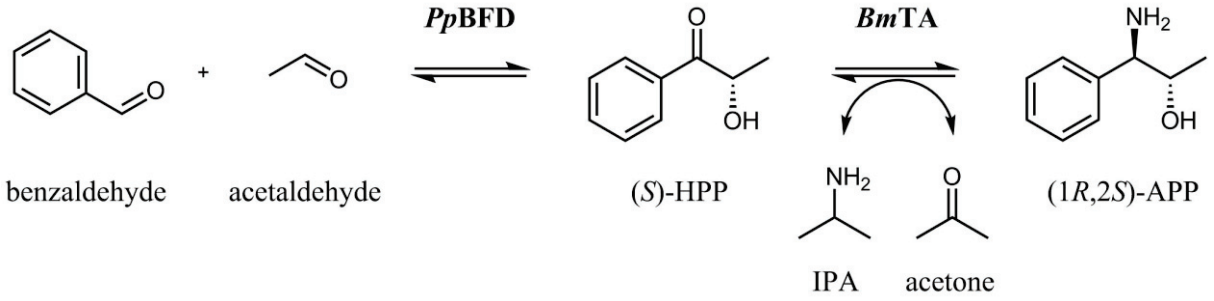

Figure 2.2-2: Two-step enzymatic cascade towards (1*R*,2*S*)-APP. In the first step, *Pp*BFD catalyzes the carboligation of benzaldehyde and acetaldehyde towards (*S*)-HPP, which is converted in the second step into (1*R*,2*S*)-APP by *Bm*TA using isopropylamine (IPA) as an amine donor.

Such cascades generally offer the great advantage to circumvent waste-generating and tedious intermediate product purification steps but require compatible reaction conditions for all involved biocatalysts (see 1.2.2) (Gröger and Hummel, 2014; Schrittwieser et al., 2018). However, lowered cascade efficiencies due to incompatible conditions of the individual reaction steps are often observed and demand efficient strategies to overcome such issues (Rulli et al., 2013; Schmidt et al., 2017). Among these, enzyme immobilization represents an appropriate solutions since an insoluble biocatalyst is formed, thereby allowing easy separation of single reaction steps to increase the efficiency of the cascade (Klermund et al., 2017; Schrittwieser et al., 2018). In addition, enzyme immobilization further enables reuse of the biocatalyst and contributes to a greater operational stability (DiCosimo et al., 2013; Sheldon and van Pelt, 2013). A general problem for immobilization methods is the establishment of strong binding forces between biocatalyst and carrier without disturbing its catalytic activity (Cao, 2006b). Recently, we introduced the HaloTag™ immobilization concept for biocatalytic applications and demonstrated the fast and covalent immobilization of different enzymes

[1] A biocatalytic cascade towards three different APP isomers was established by K. Mack, V. Erdmann, U. Mackfeld and D. Rother (unpublished results). Respective results are shortly summarized here to understand the necessity for the optimization of this cascade using immobilized enzymes. The results presented in this chapter focus on the employment of immobilized HaloTag™ fusion enzymes for the production of (1*R*,2*S*)-APP.

under mild conditions accompanied with high residual activity (Döbber et al., 2018b; Döbber and Pohl, 2017). In this concept, the HaloTag™ is fused to one terminus of the enzyme and mediates the covalent binding to carriers exposing specific chloroalkane residues (Encell et al., 2012). As a consequence, immobilization can be performed directly from crude cell extracts and thereby additionally offers purification and immobilization in one step.
Consequently, the HaloTag™ immobilization approach was selected to optimize the cascade towards the production of (1*R*,2*S*)-APP. HaloTag-*Pp*BFD and HaloTag-*Bm*TA fusion enzymes were constructed to enable fast and covalent immobilization and established immobilizates were used for efficient (*R*,*S*)-APP synthesis with biocatalyst recycling.

2.2.2 Methods

Construction of expression plasmids and production of enzymes

For HaloTag™ fusion enzymes, cloning strategy, production of fusion enzymes and preparation of crude cell extracts were performed as described previously but with minor adjustments (Döbber et al., 2018b; Döbber and Pohl, 2017). Briefly summarized, expression plasmids were constructed via the Gibson Assembly® Cloning Kit (NEB, Frankfurt, Germany). DNA encoding for both enzymes (*Pp*BFD L476Q and *Bm*TA) was amplified by PCR using primers with specific overhangs as published elsewhere (Döbber et al., 2018b). In a next step, these fragments were mixed with the plasmid backbone (pET22b) containing already the information for the HaloTag™ and a ligation was performed. Further detailed information about all sequences is given in 2.2.4.
Fusion enzymes were then produced in *E. coli* BL21 (DE3) in LB medium at 20 °C upon induction with 0.1 mM IPTG. Afterwards, cells were harvested and lysed by sonification. For sonification, cells containing HaloTag-*Pp*BFD fusion enzymes were resuspended in 50 mM potassium phosphate buffer, pH 7, supplemented with 0.1 mM ThDP and 2.5 mM $MgSO_4$. Cells containing HaloTag-*Bm*TA fusion enzymes were resuspended in 10 mM Tris buffer, pH 7.5, 0.1 mM PLP. After centrifugation, the supernatant of lysed cells was frozen at -20 °C and lyophilized.
For the production of the non-immobilized His-tagged enzymes, construction of expression plasmids, heterologous production in *E. coli* as well as chromatographic purification via immobilized metal ion affinity chromatography are described elsewhere (Erdmann, 2018; Gocke et al., 2008; Lingen et al., 2002).

Immobilization of HaloTag™ fusion enzymes, purity, and protein determination

Immobilization of fusion enzymes and subsequent determination of the purity and the amount of bound proteins were performed as described elsewhere with minor adjustments (Döbber et al., 2018b;

Döbber and Pohl, 2017). In brief, lyophilized crude cell extracts were solubilized in respective buffers. For immobilization of HaloTag-*Bm*TA, 175 mg of lyophilized crude cell extract was dissolved in 1 ml Tris-buffer (50 mM, pH 7.5, 0.1 mM PLP). HaloLink™ Resin (Promega, USA) was then equilibrated with the same buffer supplemented with 0.1 vol% Triton X-100 and 200 µl of crude cell extract solution were mixed with 50 µl of resin. Immobilization was performed at 1200 rpm in a ThermoMixer® (Eppendorf, Hamburg, Germany) at 25 °C for 1h. Afterwards, the resin was washed with 100 mM HEPES buffer, pH 8, supplemented with 0.1 mM PLP and 0.1 vol% Triton X-100. Immobilization of HaloTag-*Pp*BFD was performed similarly but 40 mg of crude cell extract were dissolved in 1 ml HEPES buffer (100 mM, pH 8, 1 mM ThDP, 2.5 mM $MgSO_4$) and resin equilibration as well as washing were performed with the same buffer supplemented with 0.1 vol % Triton X-100. Bound fusion enzymes were then released by saponification of the ester bond connecting HaloTag™ and HaloLink™ Resin due to incubation in SDS and NaOH. The amount of bound proteins was determined with the BC Assay Protein Quantitation Kit (Interchim, France) as recently described (Döbber and Pohl, 2017).

Activity test

To analyze the activtiy of free and immobilized *Bm*TA, the conversion of pyruvate to alanine using α-methylbenzylamine as an amino donor was used as a model reaction. For this purpose, 2.5 mM α-methylbenzylamine, 5 mM pyruvic acid, 0.1 mM PLP, 100 mM HEPES, pH 8, 0.1 vol% Triton X-100 and 20 – 50 µg enzyme were mixed in a quartz cuvette in a total volume of 3 ml. The solution was stirred by a small magnetic stirrer bar during the measurement in the photometer at 25 °C and production of acetophenone was followed at 300 nm. One Unit (U) of specific activity is defined as the amount of enzyme in mg which catalyzes the formation of 1 µmol alanine per minute under the described conditions. To compare the activity of both enzyme variants with different molecular weight, the activity was related to one µmol of enzyme. The molecular weight of one subunit was used for respective calculations (53 kDa).

Analytics

Detection of benzaldehyde and (*S*)-HPP to follow the carboligation step was performed as described in (Döbber et al., 2018b). The conversion of (*S*)-HPP towards (1*R,2S*)-APP was analyzed by HPLC (Agilent 1260 Infinity Quarternary LC system equipped with a 1260 Diode ArrayDetector) on a LiChrospher® 100 RP-18 (5µm) column (Merck, Darmstadt, Germany) using deionized water and acetonitrile (ACN) as solvents, which were supplemented with 0.1 % diethylamine and 0.075 % trifluoroacetic acid. To separate respective compounds, the following protocol was performed: injection volume 10 µl; pumping speed 0.75 ml/min; 25 °C; 25 min; 0 – 3 min, 80 % water/20 %

ACN; 3 – 6 min, 65 % water/35 % ACN; 6 – 11 min, 65 % water/35 % ACN; 11 – 11.5 min, 80 % water, 20 % ACN; 11.5 – 13 min, 80 % water/20 % ACN; 13 – 14 min, 40 % water/60 % ACN; 14 – 17 min, 40 % water/60 % ACN; 17 – 18 min, 80 % water/20 % ACN. Retention times were 4.3 min for *anti*-APP, 5.2 min for *syn*-APP, 11.6 min for HPP and 14.7 min for benzaldehyde. All components were detected at 210 nm and 2-methylbenzaldehyde was used as an internal standard (12 µl/L, retention time 20 min). Samples from biotransformations were diluted in 50 % water/50 % ACN and then applied to the HPLC.

The absolute configuration of APP stereoisomers was analyzed by SFC using two columns (Chirapak AD-H and Chiralpak IA column, Daicel, Japan) in tandem. An isocratic method was developed using 85 % supercritical CO_2 and 15 % methanol under addition of 1 % DEA in the mobile phase. The flowrate was set to 0.75 mL/min at 30 °C and an injection volume of 5 µL was used. The method was run for 45 min. Compounds were detected at 220 nm and retention times were as follows: 15.6 min (1*S*,2*S*)-APP, 16.9 min (1*R*,2*R*)-APP, 19.2 min (1*R*,2*S*)-APP, 20.1 min (1*S*,2*R*)-APP. Samples were prepared as follows: 50 µL of the reaction mixture was frozen in liquid nitrogene to stop the reaction. The samples were dried in an Eppendorf Concentrator (Eppendorf, Hamburg, Germany) at 30°C. The dried sample was resuspended in 100 µL methanol (containing 0.1 mg/mL of the internal standard 3,5-dimethoxy-benzaldehyde). The sample was centrifuged for 1 min in an Eppendorf 5424 centrifuge (Eppendorf, Hamburg, Germany) at 20,000 x *g* and then analyzed immediately.

Two-step enzymatic cascade towards (1R,2S)-APP using free enzymes

Carboligation was performed in 2 ml glass vials in a total volume of 1 ml at 30 °C and 750 rpm in a ThermoMixer® (Eppendorf, Hamburg, Germany). 1.75 mg/ml purified *Pp*BFD variant L461A was used to produce (*S*)-HPP starting from 30 mM benzaldehyde, 60 mM acetaldehyde in 100 mM HEPES, pH 8, 0.1 mM ThDP and 2.5 mM $MgSO_4$. After 90 min of incubation, the reaction mixture was heated to 60 °C for 30 min to inactivate the *Pp*BFD variant and to remove excess acetaldehyde. Then, purified *Bm*TA, isopropylamine and PLP were added to a final concentration of 3.5 mg/ml, 100 mM and 0.1 mM, respectively. Again, the reactions were performed in 2 ml glass vials at 30 °C and 750 rpm but with open lid to enable evaporation of acetone and in a volume of 1.25 ml. After 48 h, the reaction was stopped.

Two-step enzymatic cascade towards (1R,2S)-APP using immobilized enzymes

Carboligation was performed in 2 ml glass vials in a total volume of 1 ml at 25 °C and 1000 rpm in a ThermoMixer® (Eppendorf, Hamburg, Germany). 0.5 mg/ml immobilized HaloTag-*Pp*BFD L476Q was used to produce (*S*)-HPP starting from 30 mM benzaldehyde, 90 mM acetaldehyde in 100 mM HEPES, pH 8, 1 mM ThDP, 2.5 mM $MgSO_4$ and 0.1 vol% Triton X-100. After 90 min of incubation,

the reaction was stopped, the supernatant was removed and the carrier was washed three times with 1 ml of fresh buffer. Then, it was either reused for the next carboligation step or stored at 4 °C for further use (three batches were performed per day). The supernatant of each carboligation step was heated to 60 °C for 30 min in a glass vial to remove excess acetaldehyde and 700 µl were transferred to a second 2 ml glass vial containing 4 mg immobilized HaloTag-*Bm*TA. Reductive amination was performed in a total volume of 1 ml at 30 °C, 750 rpm. PLP and isopropylamine were added to a final concentration of 100 mM and 0.1 mM, respectively. Reactions were performed without a lid to allow acetone evaporation. Every 24 h the reaction vial was weighed and water was added until the original weight at t_0 was reached to keep the volume constant. After 72 h of incubation the reaction was stopped by sedimentation of the carrier, the supernatant was removed and the carrier was washed three times with 1 ml of buffer (100 mM HEPES, pH 8, 0.1 mM PLP, 0.1 vol% Triton X-100). Then, immobilizates were either reused for the next reaction or stored at 4 °C for further use (one batch was performed per week).

2.2.3 Results and discussion

Two-step enzymatic cascade towards (1R,2S)-APP using free enzymes

The two-step cascade towards (1*R,*2*S*)-APP was established by K. Mack, V. Erdmann and U. Mackfeld. Briefly summarized, *Pp*BFD catalyzed the carboligation of benzaldehyde and acetaldehyde yielding (*S*)-HPP with almost full conversion and an *ee* > 96 % in less than one hour. Acetaldehyde was applied in excess to shift the carboligation to the product site. Afterwards, *Pp*BFD was inactivated by heating to 60 °C and *Bm*TA was added to perform the second reaction step towards (1*R,*2*S*)-APP. As the activity of the *Bm*TA was rather low, incubation for 48 h was necessary to achieve a conversion of around 93 % and an *ic*[1] higher than 90 %.

The implementation of the enzymatic cascade towards (1*R,*2*S*)-APP as shown above was accompanied by several problems. The production of APP was drastically diminished during the second cascade step in the presence of catalytically active *Pp*BFD. Since *Bm*TA is more active towards benzaldehyde compared to (*S*)-HPP, residual amounts of benzaldehyde from the first reaction step were converted into benzylamine. As a consequence, the reaction equilibrium was shifted and the *Pp*BFD catalyzed the cleavage of (*S*)-HPP, which finally led to the accumulation of benzylamine and drastically diminished the formation of (1*R,*2*S*)-APP. In addition, *Bm*TA was rapidly inhibited by low concentrations of acetaldehyde, which had to be removed efficiently after the first cascade step. Due to the low boiling point of acetaldehyde, heating of the open reaction vessel to 60 °C was applied to concomitantly remove acetaldehyde and inactivate the soluble *Pp*BFD. However, this procedure resulted in a low productivity for the *Pp*BFD since active enzyme is wasted. Also the second cascade step showed low productivity, since *Bm*TA had to be applied in high concentration (3.5 mg/ml) for a

[1] *ic* (isomer content) is defined as the fraction of the target isomer in a mixture of multiple stereoisomers.

long reaction time (48 h) to achieve high conversion. Therefore, strategies to reuse the enzymes of both steps had to be found. Besides, the cascade was performed with purified enzymes, which required tedious and time-consuming chromatographic purification. Thus, faster strategies to achieve high enzyme purity are needed. Both goals could be achieved using the respective HaloTag™ fusion enzymes. The HaloTag™ immobilization approach was used to allow (*i*) easy and fast removal of *Pp*BFD after the first cascade step, (*ii*) subsequent thermal acetaldehyde removal without enzyme inactivation, (*iii*) circumvention of tedious enzyme purification steps since the HaloTag™ mediates covalent immobilization directly from crude cell extracts, and (*iv*) enhanced catalyst productivities due to efficient reuse.

Enzyme immobilization and characterization of immobilizates

The HaloTag™ was N-terminally fused to the *Pp*BFD as well as the *Bm*TA both involved in the production of *(*1*R*,2*S*)-APP. HaloTag-*Pp*BFD fusion enzymes have previously been investigated and the resulting immobilizates revealed a high purity as well as a high residual activity of around 65 % in comparison to free *Pp*BFD (Döbber et al., 2018b). However, transaminases have not yet been immobilized by this technique. After successful genetic fusion of the HaloTag™ to the N-terminus of *Bm*TA, we first analyzed the heterologous production of respective fusion enzymes since fusion of a tag might lead to the formation of undesired inclusion bodies (Krauss et al., 2017).

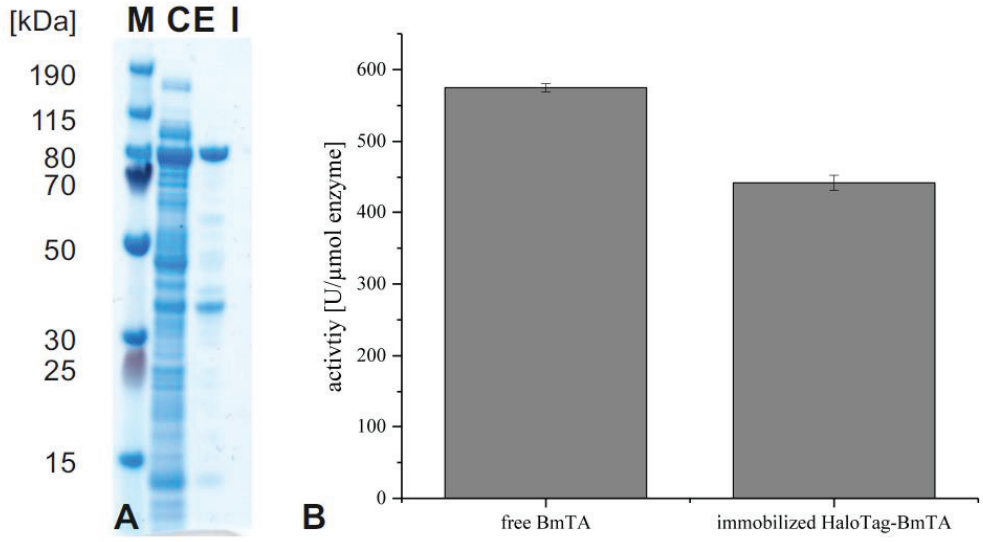

Figure 2.2-3: Production and immobilization of HaloTag-*Bm*TA. Immobilization was performed directly from crude cell extracts on HaloLink™ Resin (Promega). A: SDS-PAGE; M: PageRuler Plus Prestained Protein Ladder (Thermo Scientific); CE: crude cell extract after production of HaloTag-*Bm*TA in *E. coli* BL21 (DE3); I: proteins released from the HaloLink™ Resin by saponification. B: Activity of free *Bm*TA without HaloTag™ and immobilized HaloTag-*Bm*TA; initial rate activities [U/µmol enzyme] were determined for amination of pyruvate to alanine using α-methylbenzylamine as an amine donor; error bars represent the variance of three activity measurements from the same sample.

As depicted in Figure 2.2-3, HaloTag-*Bm*TA fusion enzymes were successfully produced in *E. coli* BL21 (DE3) cells and an intense protein band close to the 80 kDa standard, which corresponds to one monomer of the fusion enzyme, indicates good production yields. In addition, a high purity was achieved after immobilization underlining that protein purification was efficiently performed without employing tedious chromatographic purification steps. The additional protein band appearing above the 30 kDa standard (see Figure 2.2-3A) might be caused by truncated HaloTag™ fusion enzymes. Since the HaloTag™ (34 kDa) was fused to the N-terminus and is consequently expressed first, truncated fusion enzymes could contain a functional HaloTag™, which allows binding to the HaloLink™ Resin (see 3.3.2). Further characterization of formed HaloTag-*Bm*TA fusion enzymes concerned the activity of established immobilizates in comparison to the free enzyme without HaloTag™. As shown in Figure 2.2-3, a high activity of around 75 % was achieved, which is the highest activity obtained so far for all selected model enzymes (see Figure 3.4-1). In general, immobilization often results in reduced catalytic activity due to rigidification, mass-transfer limitations or negative influences of the carrier (Liese and Hilterhaus, 2013). This effect is even more pronounced for conventional covalent immobilization approaches, which are based on the randomized binding of amino acid side chains to respective supports. These approaches offer no site control and may thus result in a huge loss of activity if for example essential catalytic residues are modified (Mateo et al., 2007a). Therefore, the HaloTag™-based approach represents a good strategy to immobilize *Bm*TA with high purity, high binding stability and high residual activity.

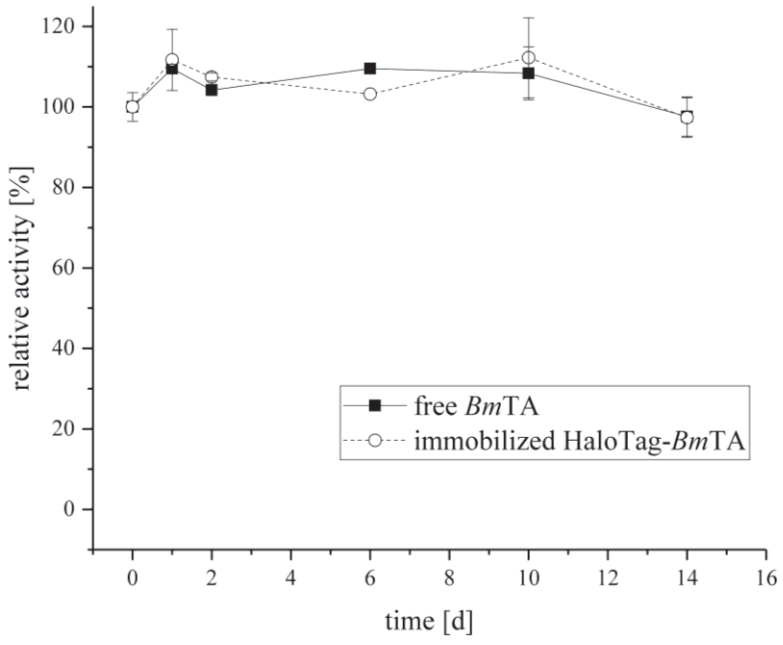

Figure 2.2-4: Stability of immobilized and free *Bm*TA at 30 °C. Free *Bm*TA as well as immobilized HaloTag-*Bm*TA were incubated at 30 °C in 100 mM HEPES buffer, pH 8, containing 0.1 mM PLP. Reaction tubes were shaken at 1200 rpm in a ThermoMixer® (Eppendorf, Hamburg, Germany) and samples were continuously taken at the indicated points in time to measure residual activity. Initial rate activities were determined for the formation of alanine starting from pyruvate and using α-methylbenzylamine as an amino donor. Measured activities were related to the initial activity when starting the experiment. Error bars represent the variance of two activity measurements from the same sample.

Since the second cascade step with free enzymes required long reaction times (48 h) due to the low activity of the *Bm*TA towards (*S*)-HPP (see above), high enzyme stability is required to enable recycling. Therefore, free *Bm*TA as well as immobilized HaloTag-*Bm*TA were incubated at 30 °C and samples were continuously taken to measure the residual activity over time. As depicted in Figure 2.2-4, *Bm*TA revealed a high stability over two weeks and almost no activity was lost. Furthermore, no difference between free *Bm*TA and immobilized HaloTag-*Bm*TA was found, indicating that the enzyme properties were not essentially altered by immobilization and that efficient recycling could be possible.

Two-step enzymatic cascade towards (1R,2S)-APP using immobilized enzymes

In a next step, the two-step enzymatic cascade was investigated using immobilized HaloTag-*Pp*BFD and HaloTag-*Bm*TA in repetitive batch experiments to produce (1*R*,2*S*)-APP. Conditions guaranteeing high *Pp*BFD stability were already optimized previously (Döbber et al., 2018b) and consequently, immobilized HaloTag-*Pp*BFD was efficiently recycled with no activity loss over at least 13 batches as demonstrated in Figure 2.2-5. In each cycle, almost full conversion and a high *ee* > 96 % were achieved for the formation of (*S*)-HPP. After each carboligation batch, the immobilized biocatalyst was easily separated from the reaction media by centrifugation and acetaldehyde removal was subsequently performed at 60 °C. Afterwards, the reaction solution was transferred to the immobilized HaloTag-*Bm*TA and PLP as well as isopropylamine were added for the 2nd cascade step. As demonstrated in Figure 2.2-6, high conversion of (*S*)-HPP towards (1*R*,2*S*)-APP was achieved with immobilized HaloTag-*Bm*TA. The *ic* of the formed (1*R*,2*S*)-APP was higher than 90 % indicating that the reaction was performed with the same conversion and stereoselectivity as observed for free enzymes. However, lower conversions were observed in the following batches and consequently, the experiment was stopped after four cycles. Probably, residual amounts of acetaldehyde resulting from the first carboligation step, isopropylamine or (*S*)-HPP are responsible for slow inactivation since incubation in only buffer does not lead to a reduced activity within weeks (see Figure 2.2-4). Nevertheless, immobilized HaloTag-*Bm*TA revealed a good stability and a half-life of around 288 h since each batch required incubation for at least 3 days to obtain high conversion of (*S*)-HPP. Since the immobilizates were also stored in between, the immobilized biocatalyst showed activity over several weeks.

To conclude, enzyme immobilization with the HaloTag^{TM}-based approach simplified the whole cascade set-up and utilized catalytic activity more efficiently. In the next steps, the considerable low activity of the *Bm*TA towards (*S*)-HPP should be targeted by for example protein engineering methods. Although reuse of the *Bm*TA through immobilization enabled longer use of this enzyme, high enzyme loadings and long incubation times markedly reduced the productivity of the second cascade step and optimization is required in this case.

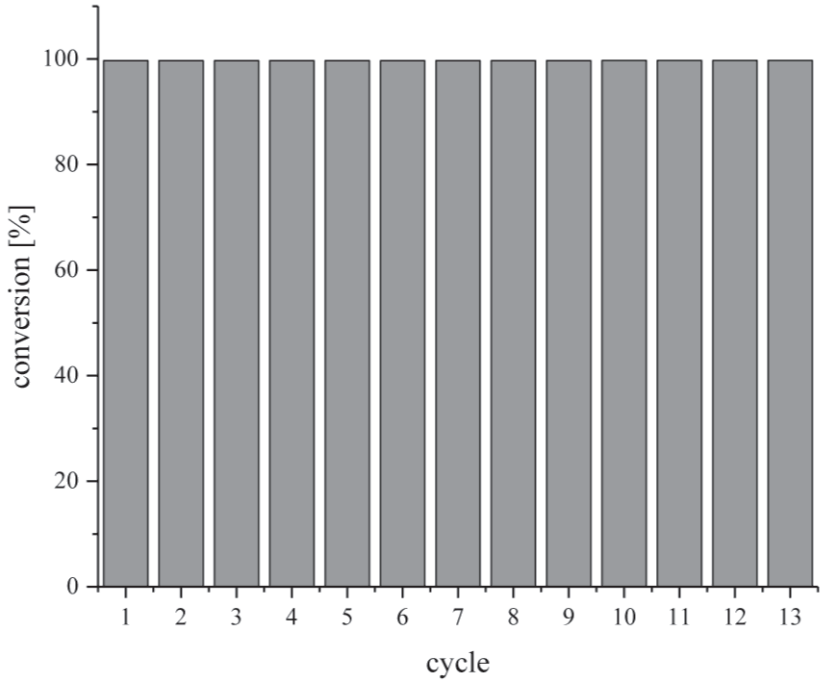

Figure 2.2-5: Recycling of HaloTag-*Pp*BFD for the production of (*S*)-HPP. 500 µg of immobilized HaloTag-*Pp*BFD were used for the carboligation of benzaldehyde (30 mM) and acetaldehyde (90 mM). Reactions were performed in 1 ml at 25 °C and in the presence of 100 mM HEPES, pH 8, 0.1 vol% Triton-X 100, 1 mM ThDP as well as 2.5 mM $MgSO_4$. Each cycle lasted 90 min and the carrier was washed 3x with 1 ml fresh buffer between each cycle. 3 cycles were performed per day and the carrier was stored over the night at 4 °C. Experiments were performed in triplicate and the average conversion per cycle is given in the diagram.

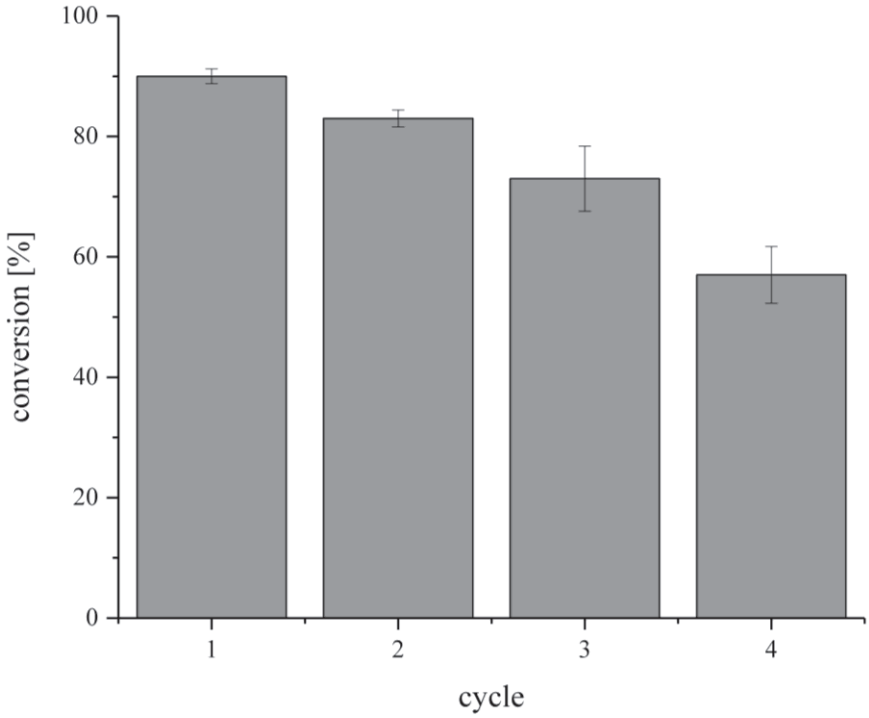

Figure 2.2-6: Recycling of HaloTag-*Bm*TA for the production of (1*R*,2*S*)-APP. Reactions were performed in 1 ml at 30 °C employing 4 mg of immobilized HaloTag-*Bm*TA, 700 µl of (*S*)-HPP solution after carboligation and acetaldehyde removal (see above), 100 mM isopropylamine, 0.1 mM PLP, 100 mM HEPES, pH 8, 0.1 vol% Triton-X 100. Each cycle lasted 72 h and the immobilizate was washed 3x with 1 ml buffer between each cycle. Experiments were performed in triplicate and the average conversion per cycle is given in the diagram.

2.2.4 Supporting information

DNA and protein sequences

a) HaloTag-*Pp*BFD L476Q

Sequences are published elsewhere (Döbber et al., 2018b).

b) HaloTag-*Bm*TA

DNA sequence encoding for the HaloTag™: green; spacer: red, *Bm*TA: blue

atgaaacatcaccatcaccatcacgcagaaattggtacgggatttccgtttgacccgcattatgtggaggttctgggtgaacgcatgcactacgtggatgttggtccgcgcgatggcaca
ccggtgctgtttctgcatggtaatccgacctccagctatgtttggcgcaacattattccgcatgtcgccccaacgcatcgctgtattgccccagatctcattggcatgggcaaaagcgaca
aaccggatttgggctacttcttcgacgatcacgtacggtttatggacgcctttatcgaggctctgggactcgaggaagtagtgctggttattcatgactggggctctgcattaggctttcact
gggctaaacggaacccagaacgcgtcaaggggattgccttcatggagttcatccgtccgattccgacctgggatgaatggcccgaatttgcccgtgaaacctttcaggcgtttcgtacc
acggatgttggccgtaagctcatcatcgaccaaaacgtgttcattgagggcactcttcccatgggagtagtgcgtcctttaaccgaagtcgagatggaccactatcgcgaacccttcctg
aatccggttgatcgcgaaccgctgtggcgcttcccgaatgagctgcctattgctggtgaaccggcgaatatcgtggcacttgtggaagaatacatggattggctgcatcagagtccagt
ccctaagctgttgttttggggtacacctggcgtgttgattccgcctgcagaagctgctcgcttagcgaaaagcttgcccaactgcaaagcggtcgatattgggccaggtctgaacctgtta
caggaggataacccggatctgatcgggagtgaaatcgcgcgttggctgtcaactctggaaatctcgggtcttgcagaagcagcggccaaagaagctgcggccaaagaggcagccg
cgaaagaagcagcggcgaaagcggccgcgagcctgaccgtgcagaaaattaattgggaacaggtgaaagaatgggatcgcaaatatctgatgcgtacctttagcacccagaatga
atatcagccggttccgattgaaagcaccgaaggcgattatctgattatgccggatggcacccgtctgctggatttttttaatcagctgtattgcgttaatctgggccagaaaaaccagaaag
tgaacgcagcaattaaagaagcactggatcgttacggttttgtgtgggatacctatgccaccgattataaagcaaaagccgcaaaaattattattgaagatattctgggcgatgaagattg
gcctggtaaagttcgttttgttagcaccggtagcgaagcagttgaaaccgcactgaatattgcacgtctgtataccaatcgtccgctggttgttacccgtgaacatgattatcatggttggac
cggtggtgcagcaaccgttacccgtctgcgtagctatcgtagcggtctggttggtgaaaatagcgaaagctttagcgcacagattccgggtagcagctataatagcgcagttctgatgg
caccgagcccgaatatgtttcaggattccgatggtaatctgctgaaagatgaaaatggtgaactgctgtccgttaaatatacccgtcgcatgattgaaaattatggtccggaacaggttgc
agcagttattaccgaagttagccagggtgcaggtagcgcaatgcctccgtatgaatatattccgcagattcgtaaaatgaccaaagaactgggtgttctgtggattaatgatgaagtgctg
accggttttggtcgtaccggtaaatggtttggctatcagcattatggtgttcagccggatattattaccatgggtaaaggtctgagcagcagcagcctgcctgcaggtgcagttctggttag
caaagaaatcgcagcctttatggataaacatcgttgggaaagcgttagcacctatgcaggtcatccggttgcaatggcagcagtttgtgcaaatctggaagtgatgatggaagaaaatttt
gtggaacaggccaaagatagcggtgaatatatccgtagcaaactggaactgctgcaggaaaaacataaaagcattggcaattttgatggttatggcctgctgtggattgttgatattgtga
atgccaaaaccaaaaccccgtatgttaaactggatcgcaattttacccatggcatgaatccgaatcagattccgacccagattatcatgaaaaaagccctggaaaaaggtgttctgattgg
tggtgttatgccgaataccatgcgtattggtgcaagcctgaatgttagccgtggcgatattgataaagcaatggatgcactggattatgccctggattatctggaaagcggtgaatggcag
taa

Protein sequence for the HaloTag™: green; spacer: red, *Bm*TA: blue

MKHHHHHHHAEIGTGFPFDPHYVEVLGERMHYVDVGPRDGTPVLFLHGNPTSSYVWRNIIPHVAPTHRC
IAPDLIGMGKSDKPDLGYFFDDHVRFMDAFIEALGLEEVVLVIHDWGSALGFHWAKRNPERVKGIAFM
EFIRPIPTWDEWPEFARETFQAFRTTDVGRKLIIDQNVFIEGTLPMGVVRPLTEVEMDHYREPFLNPVDR
EPLWRFPNELPIAGEPANIVALVEEYMDWLHQSPVPKLLFWGTPGVLIPPAEAARLAKSLPNCKAVDIG
PGLNLLQEDNPDLIGSEIARWLSTLEISGLAEAAAKEAAAKEAAAKEAAAKAAASLTVQKINWEQVKE
WDRKYLMRTFSTQNEYQPVPIESTEGDYLIMPDGTRLLDFFNQLYCVNLGQKNQKVNAAIKEALDRYG
FVWDTYATDYKAKAAKIIIEDILGDEDWPGKVRFVSTGSEAVETALNIARLYTNRPLVVTREHDYHGW
TGGAATVTRLRSYRSGLVGENSESFSAQIPGSSYNSAVLMAPSPNMFQDSDGNLLKDENGELLSVKYTR
RMIENYGPEQVAAVITEVSQGAGSAMPPYEYIPQIRKMTKELGVLWINDEVLTGFGRTGKWFGYQHYG
VQPDIITMGKGLSSSSLPAGAVLVSKEIAAFMDKHRWESVSTYAGHPVAMAAVCANLEVMMEENFVE
QAKDSGEYIRSKLELLQEKHKSIGNFDGYGLLWIVDIVNAKTKTPYVKLDRNFTHGMNPNQIPTQIIMK
KALEKGVLIGGVMPNTMRIGASLNVSRGDIDKAMDALDYALDYLESGEWQ

2.3 HaloTag-*Lb*ADH

Results presented in this chapter were published as:

Rapid, selective and stable HaloTag-*Lb*ADH immobilization directly from crude cell extract for the continuous biocatalytic production of chiral alcohols and epoxides.

J. Döbber, M. Pohl, S. V. Ley and B. Musio

Reaction Chemistry and Engineering

2018, volume 3, issue 1, pages 8 – 12

DOI: 10.1039/C7RE00173H

Context:

In this publication, immobilized HaloTag-*Lb*ADH was used for the continuous production of chiral alcohols and for the establishment of a continuous two-step chemo-enzymatic cascade leading to a chiral epoxide. Protocols were established for the easy loading of plug-flow reactors in flow prior to the intended reaction. Therefore, this publication proves the fast establishment of biocatalytic flow modules with the HaloTag™ strategy. Enzyme compartments can be prepared easily for further modular combination with subsequent reaction steps that are detrimental for catalytic activity, which guarantees optimal efficiency for each individual reaction.

Contributions:

J. Döbber and B. Musio planned and performed the experiments. J. Döbber constructed and produced *Lb*ADH fusion enzymes, optimized the immobilization conditions, characterized immobilizates in different solvent systems in batch and initially screened for optimal conditions in flow for different ketones. The solvent system was further optimized by B. Musio and reactions to produce chiral alcohols and epoxides were performed by B. Musio as well. S. V. Ley and M. Pohl conceptually planned and supervised the project. All authors wrote the manuscript.

Reaction Chemistry & Engineering

COMMUNICATION

View Article Online
View Journal | View Issue

Cite this: *React. Chem. Eng.*, 2018, 3, 8

Received 16th October 2017,
Accepted 7th December 2017

DOI: 10.1039/c7re00173h

rsc.li/reaction-engineering

Rapid, selective and stable HaloTag-*Lb*ADH immobilization directly from crude cell extract for the continuous biocatalytic production of chiral alcohols and epoxides†

J. Döbber,[ab] M. Pohl,[a] S. V. Ley [b] and B. Musio *[b]

A strategy for biocatalyst immobilization in flow directly from the crude cell extract is described. The efficiency and the stability of the immobilized enzyme were demonstrated during the asymmetric reduction of a range of ketones. The cascade two-step chemo-enzymatic preparation of chiral epoxides was possible through the initial ketone bioreduction to an intermediate halohydrin followed by its intramolecular cyclization.

The use of biocatalytic methods in continuous processes for more sustainable chemistry applications has been growing over the last few years.[1] The benefits arising from the continuous biotransformations are clear in terms of reusability of non-toxic catalysts, high selectivity, mild and accurately controlled reaction conditions, reduction of protection–deprotection steps and easy scale-up through improved downstream processing.[2] However, the implementation of continuous biocatalytic processes demands a high operational stability of enzymes, which is still an existing concern especially in the presence of conventional media such as organic solvents.[3] Furthermore, the availability and stability of enzymes can be limiting.

Enzyme immobilization technologies, which lead to the formation of an insoluble biocatalyst, in some cases can aid efficient recycling and an enhanced operational stability. Ideally, enzyme immobilization should proceed rapidly to maintain enzyme activity and result in a biocatalyst formulation that does not leach. Additionally, the ideal arrangement would be cheap to produce and would avoid excessive waste.[4]

Particularly interesting for flow applications is the prospect of preparing plug-flow reactors containing the desired immobilized biocatalyst using simple procedures.

Recently, we reported on an innovative immobilization strategy based on the commercially available HaloTag™ technology (Promega).[5] The HaloTag™ is a modified dehalogenase enzyme from *Rhodococcus* species[6] that can be genetically fused to an enzyme to effect rapid binding from a crude cell extract. This fusion tag recognizes terminal chloroalkane substituents exposed on the surface of the HaloLink™ resin and affords a stable covalent ester bond *via* a self-terminating mechanism thereby immobilizing the target enzyme (Fig. 1). We applied this concept successfully for the one-step purification and immobilization of the benzaldehyde lyase from *Pseudomonas fluorescence* (*Pf*BAL) and could prove its usefulness for the efficient recycling of *Pf*BAL in repetitive batch reactions.[5]

Here we extend the HaloTag™ method to a continuous biocatalytic production process involving the alcohol dehydrogenase from *Lactobacillus brevis* (*Lb*ADH).[7] *Lb*ADH is a complex biocatalyst system consisting of four subunits forming a tetramer to achieve the active conformation. The non-covalently bound cofactor NADPH is also essential for catalysis and must be recycled efficiently to make the corresponding biotransformations economically viable. For the *Lb*ADH, different strategies for cofactor regeneration have

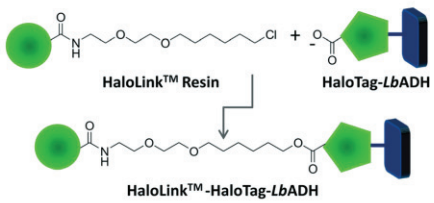

Fig. 1 Schematic overview of the HaloTag-*Lb*ADH enzyme immobilization on the HaloLink™ resin. The HaloLink™ resin consists of Sepharose beads and is visualized as green spheres. The HaloTag™ was genetically fused to the *Lb*ADH and recognizes the terminal chloroalkane ligands to establish a covalent ester bond thereby immobilizing the biocatalyst.

[a] *IBG-1: Biotechnology, Forschungszentrum Jülich, 52425 Jülich, Germany*
[b] *Department of Chemistry, University of Cambridge, Cambridge, CB21EW, UK. E-mail: bm450@cam.ac.uk*

† Electronic supplementary information (ESI) available. See DOI: 10.1039/c7re00173h

been developed, including enzyme engineering or substrate-coupled approaches.[8]

In this study we demonstrate an easy and rapid preparation of a packed-bed flow reactor by immobilizing the fusion enzyme directly from the crude cell extracts from the respective recombinant *E. coli* production host immediately prior to conducting the biotransformation. Furthermore, we evaluate the performance of the immobilized biocatalyst for the continuous asymmetric reduction of a range of ketones to the corresponding chiral alcohols. Finally, we demonstrate the high operational stability of the new immobilized HaloTag-*Lb*ADH and its use in organic solvents for possible multi-step transformations.

In the first stage, the HaloTag™ was genetically fused to the *N*-terminus of the *Lb*ADH resulting in the fusion enzyme HaloTag-*Lb*ADH. After successful production of this fusion enzyme in *E. coli* BL21 (DE3) cells, we verified its activity as a biocatalyst in comparison to the non-immobilized, untagged *Lb*ADH. Thus, HaloTag-*Lb*ADH was immobilized in batch to the HaloLink™ resin directly from the crude cell extract by incubation for 1 h at 25 °C (see ESI† for more details). The activity was analyzed following the reduction of benzaldehyde to benzyl alcohol in an aqueous buffer (Fig. 2, conditions A). The immobilized HaloTag-*Lb*ADH exhibited a residual activity of 35% by comparison to the reference. A similar reduced activity of an immobilized biocatalyst with respect to the free reference system is a common outcome and can be explained by different reasons. First, the physical confinement of the enzyme on the support can lead to a reduced flexibility, thus affecting the activity. Additionally, the immobilization and the high local concentration of an enzyme on a support may cause mass-transfer limitations in comparison to soluble systems. Importantly, in the case of complex tetrameric enzymes carrying four individual HaloTags, such as HaloTag-*Lb*ADH, steric hindrance of the active site, may be an issue. In this case the size per subunit of the enzyme was more than doubled by the HaloTag-fusion from 252 amino acids (26.76 KDa) for the native enzyme to 581 amino acids (63.58 KDa) for the HaloTag-*Lb*ADH fusion enzyme. By contrast, the previously immobilized tetrameric HaloTag-*Pf*BAL fusion enzyme[5] revealed a residual activity of 65% indicating that the influence of the tag cannot be predicted and seems to depend on the relative sizes and overall conformation of the particular fusion partners. Then, we investigated the influence of the sacrificial co-substrate 2-propanol on the activity of the free *Lb*ADH and the immobilized HaloTag-*Lb*ADH (Fig. 2, conditions B). 2-Propanol is generally used for the substrate-coupled cofactor regeneration, being oxidized to acetone by *Lb*ADH thereby reducing $NADP^+$ to NADPH.[8a] Both enzyme variants were less active in the presence of 2-propanol (10 vol%). However, the activity of the free, untagged *Lb*ADH was reduced by 75%, while the immobilized HaloTag-*Lb*ADH variant lost only half of its activity. This observation indicates that the immobilized HaloTag-*Lb*ADH was relatively more stable against the detrimental effects of 2-propanol and that immobilization of the enzyme led to the formation of a more robust catalyst. We also compared the activity of the free, untagged *Lb*ADH with the activity of the immobilized HaloTag-*Lb*ADH in a buffer/THF/2-propanol system (Fig. 2, conditions C).

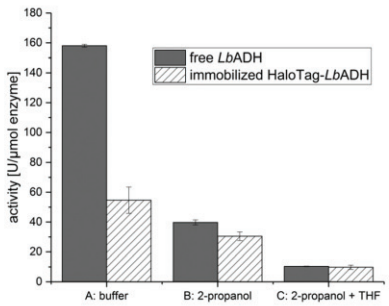

Fig. 2 Activity of immobilized HaloTag-*Lb*ADH in different solvent systems compared to the free, untagged *Lb*ADH. Initial rate activities were analyzed by HPLC following the reduction of benzaldehyde (20 mM) to benzyl alcohol in a total volume of 1 ml at 25 °C. Conditions A: NADPH (20 mM), KPi 50 mM (pH 7.0), $MgCl_2 \cdot H_2O$ (1 mM); conditions B: NADPH (0.5 mM), 2-propanol (10 vol%), KPi 50 mM (pH 7.0), $MgCl_2 \cdot H_2O$ (1 mM); conditions C: NADPH (0.5 mM), 2-propanol (10 vol%), THF (10 vol%), KPi 50 mM (pH 7.0), $MgCl_2 \cdot H_2O$ (1 mM). Error bars represent the variance of three activity measurements from the same sample.

The activity of the free *Lb*ADH as well as of the immobilized HaloTag-*Lb*ADH decreased further in the presence of THF. However, no difference in activity between both the free and the immobilized enzyme was observed although the difference in the buffered system was shown to be about 65% (Fig. 2, conditions A).

As a next step, the preparation of a packed-bed reactor was investigated. Thus, an Omnifit® column (30 MM × 50 MM) was filled with HaloLink™ resin (360 mg wet weight) and connected to an Asia Syringe Pump (Syrris, Royston, United Kingdom) to drive the flow streams. The column was then loaded with a solution of crude cell extract containing the HaloTag-*Lb*ADH fusion enzyme. The efflux was re-circulated and its UV absorption (282 nm) was continuously monitored in-line by a UV/Vis detector (Flow-UVTM, Uniqsis Ltd) provided with a high pressure flow cell and a 220–1050 nm Xenon pulsing lamp (Fig. 3a). The solid packed bed appeared to be saturated with HaloTag-*Lb*ADH after 216 min of continuous recirculation of the crude cell extract solution as was indicated by a constant UV absorbance (Fig. 3b, solid line). Then, the reactor was washed to elute all the non-specifically bound proteins until the absorbance of the efflux reached the baseline (Fig. 3b, dashed line). Finally, the resin was removed from the column to evaluate the immobilization and to determine the purity of the bound enzyme. Thus, the ester bond connecting the HaloTag™ with the HaloLink™ resin was saponified by treatment with sodium dodecyl sulfate (SDS) and NaOH and a

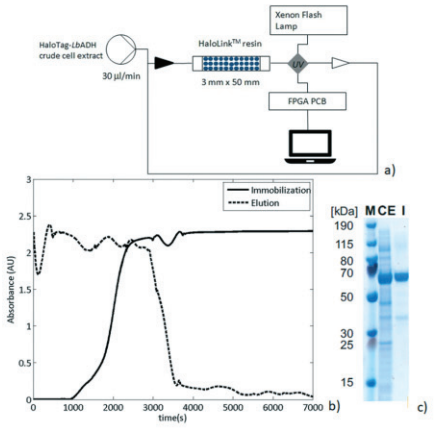

Fig. 3 a) Set-up for the immobilization of the HaloTag-*Lb*ADH directly from the crude cell extracts with in-line UV analysis at 282 nm (Field Progammable Gate Array, FPGA; Printed Circuit Board, PCB). b) In-line monitoring during the immobilization step (solid line) during the unbound proteins elution step (dashed line). c) SDS-PAGE analysis of HaloTag-*Lb*ADH before (CE) and after immobilization (I). M: PageRuler™ Plus Prestained Ladder (ThermoFisher Scientific, Germany).

sodium dodecyl sulfate polyacrylamide gel electrophoresis (SDS-PAGE) analysis was performed.

The HaloTag-*Lb*ADH was efficiently immobilized with a very high purity since almost no contamination was observed on the HaloLink™ resin and the protein band corresponding to one monomer of the HaloTag-*Lb*ADH (63 kDa per monomer) predominated markedly (Fig. 3c).

The total amount of protein (4 mg) present on 360 mg wet resin was determined by using the bicinchoninic acid (BCA) assay.

Once the feasibility of preparing a biocatalytic packed-bed bioreactor directly from the crude cell extracts was demonstrated, its efficiency in catalyzing the asymmetric reduction of a range of ketones was explored particularly in terms of reaction conditions and stability of the bioreactor. First, we aimed to find the appropriate 2-propanol concentration necessary for optimal cofactor regeneration, thereby enabling highest conversion and maximal enzyme activity and stability. Thus, the reduction of acetophenone **1a** to (*R*)-phenylethanol **2a** was first studied in batch mode. As the 2-propanol concentration influences the thermodynamic equilibrium of the reaction, usually an excess is necessary to reach a high conversion. However, a high 2-propanol concentration may affect the enzyme activity as well as stability. We observed a decreased activity of the immobilized HaloTag-*Lb*ADH with increasing concentrations of 2-propanol, though the biocatalyst remained remarkably active even in presence of 2-isopropanol 90 vol% (Fig. S1 in ESI†). Aiming at understanding the effect of 2-propanol on the stability of the immobilized HaloTag-*Lb*ADH, repetitive reactions were performed by examining the same batch of immobilized biocatalyst in the presence of different concentrations of 2-propanol ranging between 10 vol% and 90 vol%. In general, the enzyme was highly stable under all the test conditions. No loss of activity between the repetitive reactions was observed for reactions with 2-propanol 10–25 vol%, and only a slight decrease after the fourth cycle was observed for reactions performed with higher concentrations up to 90 vol% (Fig. S2–S6 in ESI†). With this evidence in hand, we moved on to study the reduction of acetophenone **1a** in flow using the prepared HaloTag-*Lb*ADH packed-bed reactor. The corresponding (*R*)-phenylethanol **2a** could be obtained with 95% conversion when a solution of acetophenone (50 mM) and NADPH (0.5 mM) in a mixture of Kpi 50 mM (90 vol%) and 2-propanol (10 vol%) was passed continuously through the packed-bed reactor (flow rate 30 µl min^{-1}). Higher substrate concentrations (50–100 mM) and faster flow rates (up to 100 µl min^{-1}) were also tested, but the reaction occurred in all cases with lower conversion. More importantly, this reaction was continued over several days and stopped after 138 h, with no loss in activity (see ESI† for experimental details).

To enable the reduction of other ketones, which were less soluble in the buffer/2-propanol solvent system, the addition of conventional co-solvents was considered. Methyl *tert*-butyl ether (MTBE), dimethyl sulfoxide (DMSO), acetonitrile (ACN), dimethylformamide (DMF) and tetrahydrofuran (THF) were evaluated for the reduction of 4′-bromoacetophenone **1b** as a test case. It was found that the formation of a biphasic or emulsion solvent system was not favorable for the reaction. Among the solvents screened, only THF (30 vol%) gave encouraging results giving access to the corresponding (*R*)-4′-bromophenylethanol **2b** with high yield (94%) and excellent ee (>99%). When a lower THF concentration was added to the reaction mixture, the substrate and the product were partially trapped within the packed bed, as demonstrated by UV absorption of the efflux and by the low mass recovery after the reaction work-up. Next, starting from a range of prochiral ketones, we demonstrated the generality of this synthetic strategy for the preparation of a number of chiral alcohols (Fig. 4). The immobilized HaloTag-*Lb*ADH system exhibited a good catalytic activity towards a range of substrates, including substituted aromatic ketones (**1a–1l**), an aliphatic ketone (**1m**, the *ee* of **2m** was determined by HPLC analysis of the corresponding benzoate derivative), a β-ketoester (**1n**) and an alkynyl ketone (**1o**).

The obtained results are in excellent agreement with the reported data describing the dependence of the relative activity of *Lb*ADH on the steric and electronic effects due to the substrate nature and on the thermodynamic stability of the products.[9] The activity of the bioreactor remained constant under these reaction conditions, as demonstrated by the continuous production of (*R*)-(−)-**2n** starting from benzylacetoacetate **1n**, with a total amount of pure compound equated to 420 mg (2.16 mmol) produced over 24 h. After a washing step with buffer, the biocatalytic solid bed

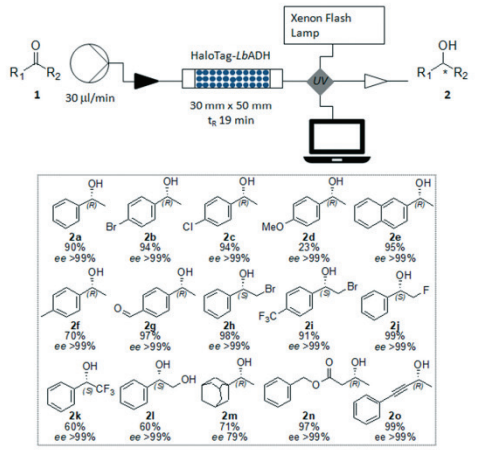

Fig. 4 Asymmetric reduction of ketones by using the immobilized HaloTag-*Lb*ADH in flow. Reaction conditions: ketones **1a–1o** (50 mM), NADPH (0.5 mM), 2-propanol (10 vol%), THF (30 vol%), KPi 50 mM (pH 7.0), $MgCl_2{\cdot}H_2O$ (1 mM), flow rate (30 µl min^{-1}). Isolated yields after purification. The *ee* were determined by GC or HPLC as described in the experimental procedure.

demonstrated to be still active and efficient for another reaction.

Finally, we explored the feasibility of an enantioselective two-step chemo-enzymatic synthesis of the chiral epoxide (*S*)-**5**, using the bio-reduction to form the intermediate halohydrin **2h**, which was immediately cyclized in a glass microreactor under basic conditions (pH 13, Fig. 5). The corresponding (*S*)-2-phenyloxirane **5** could be obtained in a short time (35 minutes) with high conversion (98%) and excellent *ee* (98%). This experiment demonstrated the advantages of the flow-plug technology in multi-step processes, allowing a quick change of the reaction conditions and an efficient compartmentalization of the synthetic steps.

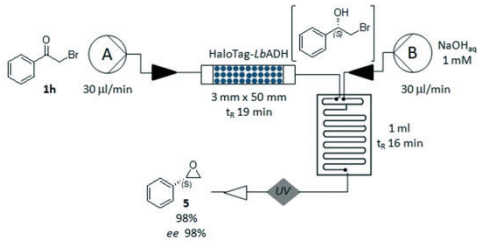

Fig. 5 Two-step chemo-enzymatic synthesis of (*S*)-2-phenyloxirane **5**. Pump A loading the packed-bed reactor containing immobilized HaloTag-*Lb*ADH: flow rate 30 µl min^{-1}, ketone **1h** (50 mM), NADPH (0.5 mM), 2-propanol (10 vol%), THF (30 vol%), KPi 50 mM (pH 7.0), $MgCl_2{\cdot}H_2O$ (1 mM). Pump B loading the glass microreactor (2 inputs, 1 ml): flow rate 30 µl min^{-1}, NaOH (1 mM, pH 13). Conversion determined by ^{1}H-NMR.

In conclusion, we have designed a new methodology for the fast preparation of cartridges containing a stable, covalently immobilized enzyme, starting directly from the crude cell extracts without any need of previous enzyme chromatographic purification step. The resulting packed bed bioreactor was then used for the continuous enantioselective production of chiral alcohols with the re-use of the catalyst. The application of this bioreactor to multi-step processes was demonstrated during the two-step chemo-enzymatic transformation of 2-bromoacetophenone into (*S*)-2-phenyloxirane, with benefits resulting from improved downstream processing. The relative ease of construction of the bioreactor and its robustness, even in the presence of THF as co-solvent, opens up wider opportunities for synthesis.

This work was supported by the EPSRC (Award No. EP/K009494/1 and EP/K039520/1) and by the German Federal Ministry of Education and Research (BMBF) within the project "Molecular Interaction Engineering" (funding code 031A095).

Conflicts of interest

The authors declare no conflicts of interest.

Notes and references

1 (*a*) L. Hajba and A. Guttman, *J. Flow Chem.*, 2016, **6**, 8–12; (*b*) A. Brahma, B. Musio, U. Ismayilova, N. Nikbin, S. Kamptmann, P. Siegert, G. Jeromin, S. V. Ley and M. Pohl, *Synlett*, 2015, 262–266; (*c*) J. C. Thomas, M. D. Burich, P. T. Bandeira, A. R. Marques de Oliveira and L. Piovan, *Biocatalysis*, 2017, **3**, 27–36; (*d*) G. Gasparini, I. Archer, E. Jones and R. Ashe, *Org. Process Res. Dev.*, 2012, **16**, 1013–1016; (*e*) K. Schroer, U. Mackfeld, I. A. W. Tan, C. Wandrey, F. Heuser, S. Bringer-Meyer, A. Weckbecker, W. Hummel, T. Daußmann, R. Pfaller, A. Liese and S. Lütz, *J. Biotechnol.*, 2007, **132**, 438–444.

2 (*a*) P. D. de María and F. Hollmann, *Front. Microbiol.*, 2015, **6**, 6–10; (*b*) S. Wenda, S. Illner, A. Mell and U. Kragl, *Green Chem.*, 2011, **13**, 3007; (*c*) M. D. Truppo, *ACS Med. Chem. Lett.*, 2017, **8**, 476–480; (*d*) P. Tufvesson, J. Lima-Ramos, M. Nordblad and J. M. Woodley, *Org. Process Res. Dev.*, 2011, **15**, 266–274; (*e*) A. Madhavan, R. Sindhu, P. Binod, R. K. Sukumaran and A. Pandey, *Bioresour. Technol.*, 2017, **245**(Part B), 1304–1313; (*f*) A. Schmid, J. S. Dordick, B. Hauer, A. Kiener, M. Wubbolts and B. Witholt, *Nature*, 2001, **409**, 258–268; (*g*) R. O. M. A. de Souza, L. S. M. Miranda and U. T. Bornscheuer, *Chem. – Eur. J.*, 2017, 1–25; (*h*) A. P. Green and N. J. Turner, *Perspect. Sci.*, 2016, **9**, 42–48.

3 (*a*) J. M. Guisan, *Immobilization of Enzymes and Cells IN Series Editor*, 2013, vol. 1051; (*b*) V. Bansal, Y. Delgado, M. D. Legault and G. Barletta, *Molecules*, 2012, **17**, 1870–1882; (*c*) U. Hanefeld, L. Gardossi and E. Magner, *Chem. Soc. Rev.*, 2009, **38**, 453–468; (*d*) R. A. Sheldon and S. Van Pelt, *Chem. Soc. Rev.*, 2013, **42**, 6223–6235.

4 (*a*) I. Eş, J. D. G. Vieira and A. C. Amaral, *Appl. Microbiol. Biotechnol.*, 2015, **99**, 2065–2082; (*b*) C. Mateo, J. M. Palomo, G. Fernandez-Lorente, J. M. Guisan and R. Fernandez-Lafuente, *Enzyme Microb. Technol.*, 2007, **40**, 1451–1463; (*c*) R. C. Rodrigues, C. Ortiz, Á. Berenguer-Murcia, R. Torres and R. Fernández-Lafuente, *Chem. Soc. Rev.*, 2013, **42**, 6290–6307; (*d*) C. Mateo, V. Grazú, B. C. C. Pessela, T. Montes, J. M. Palomo, R. Torres, F. López-Gallego, R. Fernández-Lafuente and J. M. Guisán, *Biochem. Soc. Trans.*, 2007, **35**, 1593–1601; (*e*) A. Liese and L. Hilterhaus, *Chem. Soc. Rev.*, 2013, **42**, 6236–6249.

5 J. Döbber and M. Pohl, *J. Biotechnol.*, 2017, **241**, 170–174.

6 L. P. Encell, R. Friedman Ohana, K. Zimmerman, P. Otto, G. Vidugiris, M. G. Wood, G. V. Los, M. G. McDougall, C. Zimprich, N. Karassina, R. D. Learish, R. Hurst, J. Hartnett, S. Wheeler, P. Stecha, J. English, K. Zhao, J. Mendez, H. A. Benink, N. Murphy, D. L. Daniels, M. R. Slater, M. Urh, A. Darzins, D. H. Klaubert, R. F. Bulleit and K. V. Wood, *Curr. Chem. Genomics*, 2012, **6**, 55–71.

7 B. Riebel, *PhD dissertation*, 1996, Heinrich-Heine University Düsseldorf.

8 (*a*) S. Leuchs and L. Greiner, *Chem. Biochem. Eng. Q.*, 2011, **25**, 267–281; (*b*) W. Kroutil, H. Mang, K. Edegger and K. Faber, *Curr. Opin. Chem. Biol.*, 2004, **8**, 120–126.

9 (*a*) C. Rodríguez, W. Borzęcka, J. H. Sattler, W. Kroutil, I. Lavandera and V. Gotor, *Org. Biomol. Chem.*, 2014, **12**, 673–681; (*b*) F. R. Bisogno, E. García-Urdiales, H. Valdés, I. Lavandera, W. Kroutil, D. Suárez and V. Gotor, *Chem. – A Eur. J.*, 2010, **16**, 11012–11019.

Supporting Information

Rapid, selective and stable HaloTag-*Lb*ADH immobilization directly from crude cell extract for the continuous biocatalytic production of chiral alcohols

Johannes Döbber[a, b], Martina Pohl[a], Steven V. Ley[b], Biagia Musio[b]*

[a] IBG-1: Biotechnology, Forschungszentrum Jülich, 52425 Jülich, Germany.

[b] Department of Chemistry, University of Cambridge, Cambridge, CB21EW, UK.

*bm450@cam.ac.uk

Content

S1. General

All reagents and solvents were obtained from commercial sources and used without further purification. Flash column chromatography was performed using high-purity grade silica gel (Merck grade 9385) with a pore size 60 Å and 230–400 mesh particle size under air pressure. Analytical thin layer chromatography (TLC) was performed using silica gel 60 F254 pre-coated glass backed plates and visualized by ultraviolet radiation (254 nm) and/or potassium permanganate solution as appropriate. 1H NMR spectra were recorded on a 600 MHz Avance 600 BBI Spectrometer as indicated. Chemical shifts are reported in ppm with the resonance resulting from incomplete deuteration of the solvent as the internal standard (CDCl3: 7.26 ppm). 13C NMR spectra were recorded on the same spectrometer with complete proton decoupling. Chemical shifts are reported in ppm with the solvent resonance as the internal standard (13CDCl3: 77.16 ppm, t). 19F NMR spectra were recorded on a 376 MHz Avance III HD Spectrometer with complete proton decoupling. Chemical shifts are reported in ppm with CFCl3 as the external standard (CFCl3: 0.00 ppm). Specific optical rotation was recorded on a Perkin-Elmer Model 343 digital polarimeter, using a Na/Hal lamp set at 589 nm and with a path length of 100 mm. $[\alpha]_D$ values were measured using spectroscopy grade solvent at the specified concentration (in g/100 mL) and temperature. If not otherwise stated, chiral HPLC analysis was conducted on an Agilent 1100 Series Chromatography system using mixtures of hexane/2-propanol as eluent on Chiralpak OD-H, ChiralART SA or ChiralART SB columns. Chiral GC analysis was conducted on anAgilent Technologies 6890N system equipped with a β-cyclodextrin column (CP-Chiralsil-Dex CB 25 m, 0.25 mm) and an FID detector.

S2. Construction of expression plasmid, cell cultivation and preparation of lyophilized crude cell extracts

The construction of the expression plasmid pET22b-*halotag*-*lbadh* was performed with the Gibson Assembly ® Cloning Kit (NEB). The DNA sequence encoding for the HaloTag and the linker for the connection to the *Lb*ADH was synthesized as linear fragments (Eurofins Genomics, Ebersberg, Germany). Specific overhangs for the integration of this sequence into pET22b which was opened by restriction digestion with NdeI were introduced by PCR (Primer 1, 2; see S11). After successful ligation, the DNA sequence encoding for the *Lb*ADH was amplified and again, specific overhangs were introduced by PCR for the integration into pET22b-*halotag* (Primer 3, 4; see S11). pET22b-*halotag* was linearized by PCR, too (Primer 5, 6; see S11), and ligation was performed according to the instructions given by NEB.

E.coli BL21 (DE3) cells were transformed with pET22b-*halotag*-*lbadh* and production of the resulting fusion enzyme was performed in LB medium at 20 °C. For cell disruption, cells were resuspended in 50 mM potassium phosphate buffer, pH 7.0, containing 1 mM $MgCl_2$. A detailed protocol about the

cell cultivation and disruption is described in Döbber & Pohl 2017.[1] The resulting crude cell extract was frozen at -20 °C and lyophilized (Alpha 1-4 LD plus, Christ, Osterode am Harz, Germany). The lyophilized crude cell extract was stored at -20 °C for further use.

Cloning, cell cultivation and chromatographic purification of the untagged *Lb*ADH are described elsewhere.[2]

S3 General batch procedure for the immobilization of HaloTag-*Lb*ADH on the HaloLink™ resin

Immobilization in batch was performed on HaloLink™ Resin (Promega, Madison, WI, USA). Lyophilized crude cell extract (25mg/ml) was dissolved in 50 mM potassium phosphate buffer, pH 7.0, containing 1 mM $MgCl_2x6H_2O$ and 0.5 vol% Triton X-100. 200 µl of the HaloLink™ slurry were transferred into a 1.5 ml microreaction tube (Eppendorf, Hamburg, Germany). The resin was washed three times with 1 ml of the mentioned phosphate buffer (see above) and finally suspended in 100 µl buffer. Immobilization was started by adding 100 µl of the crude cell extract solution (25 mg/ml, see above) and the mixture was incubated for 1h at 25 °C and 1200 rpm in a ThermoMixer® (Eppendorf, Hamburg, Germany). Afterwards, the resin was washed three times with 1 ml phosphate buffer (see above) and immobilizates were directly used or stored at 4 °C.

S4. Determination of protein concentration and activity assay

Protein concentrations of free and immobilized proteins were determined with the BC Assay Protein Quantitation Kit (Interchim, Montluçon, France)) as described elsewhere.[1]

For the characterization of the immobilizates in comparison to the untagged, free *Lb*ADH, the activity was determined by following the conversion of benzaldehyde to benzyl alcohol. Assays were performed with 20 mM benzaldehyde in a total volume of 1ml containing 50 mM potassium phosphate, pH 7.0, and 1 mM $MgCl_2x6H_2O$ at 25 °C as well as 1200 rpm in a ThermoMixer® (Eppendorf). 100 µg of immobilized HaloTag-*Lb*ADH and 20 µg of free, untagged *Lb*ADH, respectively, were used for one assay. NADPH was added either equimolar with respect to benzaldehyde or was used in a concentration of 0.5 mM together with 10 % (v/v) 2-propanol when cosubstrate based cofactor regeneration was applied. Benzaldehyde and benzyl alcohol were detected by HPLC on a Chiralpak IE column using an Agilent 1260 Infinity Quarternary LC system (Agilent Technologies, Santa Clara, CA, USA) equipped with a 1260 Diode Array Detector. The column was operated with a mobile phase consisting of 50 % (v/v) acetonitrile and 50 % (v/v) deionized ultra-pure water with an isocratic flow of 1 ml/min at 20 °C. Benzaldehyde was detected at 250 nm with an

[1] J. Döbber and M. Pohl, *J. Biotechnol.*, 2017, **241**, 170-174
[2] L. Kulishova, PhD Thesis, Heinrich-Heine University Düsseldorf, 2010

approximate retention time of 5.2 min and benzyl alcohol was detected at 215 nm with a retention time of 3.9 min. Toluene was used as an internal standard and was detected at 215 nm with a retention time of 6.3 min. One Unit (U) of specific activity is defined as the amount of enzyme in mg which catalyzes the formation of 1 µmol benzyl alcohol per minute under the described conditions.

S5. General procedure for the HaloTag-*Lb*ADH catalyzed reduction of acetophenone 1a in repetitive batch in the presence of different 2-propanol concentrations

To analyze the activity and stability of immobilized HaloTag-*Lb*ADH in the presence of 2-propanol, a repetitive batch was performed. Reactions were performed in 1.5 ml microreaction tubes (Eppendorf, Hamburg, Germany) in a total volume of 1 ml. Reaction tubes were shaken at 1200 rpm and 25 °C in a ThermoMixer® (Eppendorf). Reactions were performed with 30 mM acetophenone 1a, 0.5 mg immobilized HaloTag-*Lb*ADH, 0.5 mM NADPH, 50 mM potassium phosphate, pH 7.0, 1 mM $MgCl_2x6H_2O$ and different 2-propanol concentrations (10 vol%, 25 vol%, 50 vol%, 75 vol%, 90 vl%). The reaction solution was incubated for 5 h a day. Then, the reaction was stopped by centrifugation and the supernatant was removed from the immobilized HaloTag-*Lb*ADH. Afterwards, immobilized HaloTag-*Lb*ADH was washed three times with 1 ml buffer (50 mM potassium phosphate, pH 7.0, 1 mM $MgCl_2x6H_2O$, 0.5 vol% Triton X-100) and stored at 4 °C until the next cycle was started the next day. Acetophenone 1a and phenylethanol 2a were detected by HPLC on a Chiralpak IE column using an Agilent 1260 Infinity Quarternary LC system (Agilent Technologies, Santa Clara, CA, USA) equipped with a 1260 Diode Array Detector. The column was operated with a mobile phase consisting of 50 % (v/v) acetonitrile and 50 % (v/v) deionized ultra-pure water with an isocratic flow of 1 ml/min at 20 °C. Acetophenone was detected at 250 nm with an approximate retention time of 5.4 min and phenylethanol was detected at 215 nm with a retention time of 4.1 min. Toluene was used as an internal standard and was detected at 215 nm with a retention time of 6.3 min.

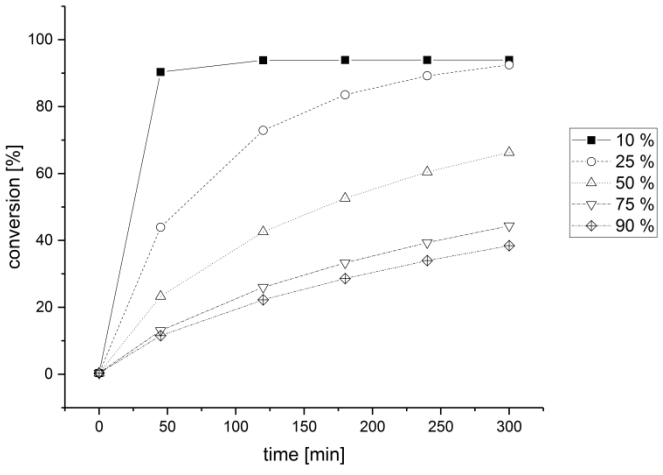

Fig. S1. Effect of 2-propanol on the activity of HaloTag-*Lb*ADH. Assay: acetophenone (30 mM), 2-propanol (10 – 90 vol%), NADPH (0.5 mM), Triton X-100 (0.5 vol%), KPi 50 mM (pH 7.0), MgCl2·H2O (1 mM). Acetophenone and 1-phenylethanol were detected by HPLC.

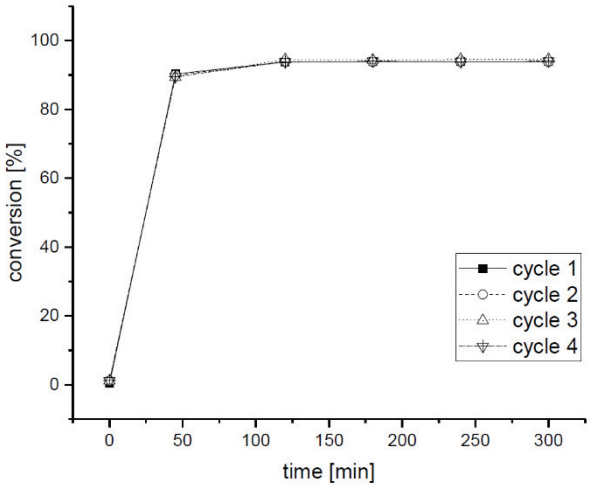

Fig. S2. Repetitive conversion of acetophenone in batch by immobilized HaloTag-*Lb*ADH in the presence of 10 vol% 2-propanol. Four consecutive cycles were performed over 4 days and storage in between at 4 °C. Reaction: 0.5 mg/ml immobilized HaloTag-*Lb*ADH, 30 mM acetophenone, 10 vol% 2-propanol, 0.5 mM NADPH, 0.5 vol% Triton X-100, 50 mM KPi buffer, pH 7.0, 1 mM $MgCl_2x6H_2O$, V = 1ml, T = 25 °C. Acetophenone 1a and phenylethanol 2a were detected by HPLC.

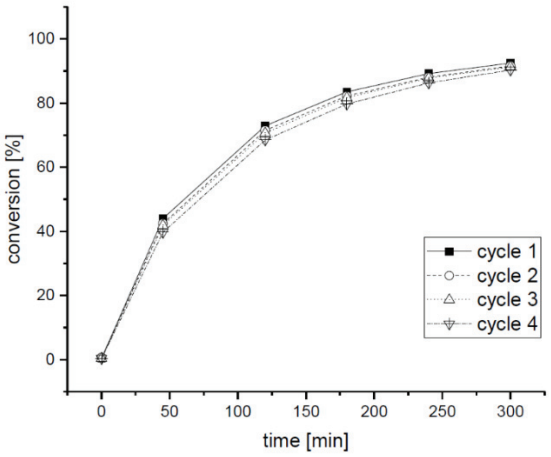

Fig. S3. Repetitive conversion of acetophenone in batch by immobilized HaloTag-*Lb*ADH in the presence of 25 vol% 2-propanol (see Figure S2).

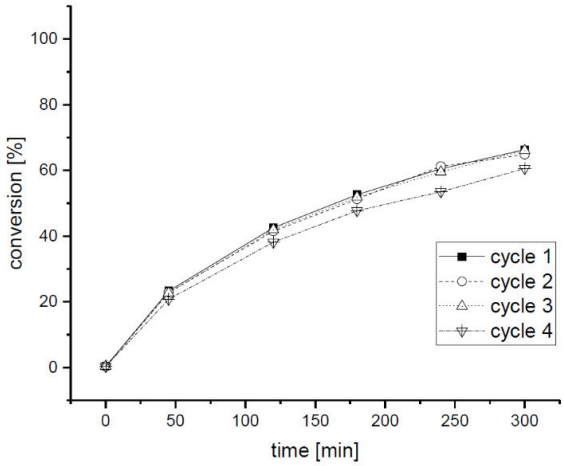

Fig. S4. Repetitive conversion of acetophenone in batch by immobilized HaloTag-*Lb*ADH in the presence of 50 vol% 2-propanol (see Figure S2).

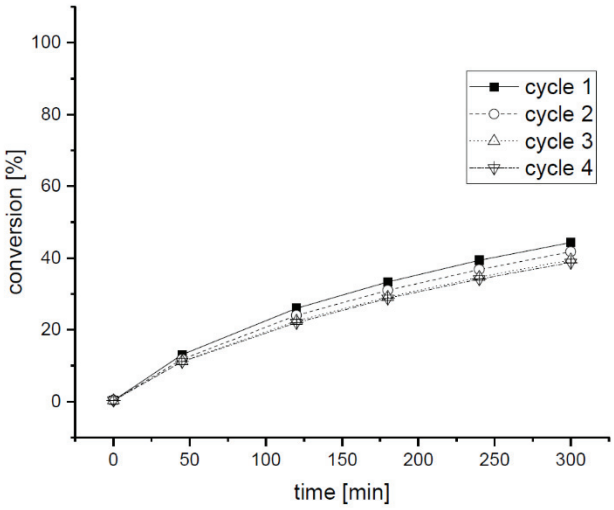

Fig. S5. Repetitive conversion of acetophenone in batch by immobilized HaloTag-*Lb*ADH in the presence of 75 vol% 2-propanol (see Figure S2).

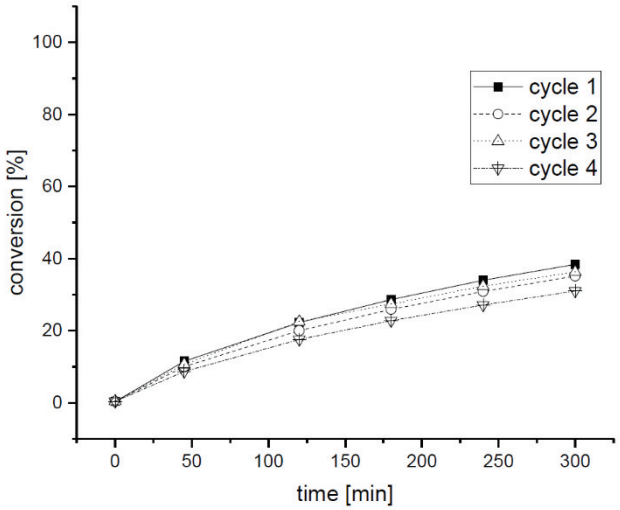

Fig. S6. Repetitive conversion of acetophenone in batch by immobilized HaloTag-LbADH in the presence of 90 vol% 2-propanol (see Figure S2).

S6. General procedure for the immobilization of HaloTag-*Lb*ADH on the HaloLink™ resin in flow

A glass Omnifit® column (Kinesis, Benchmark microbore column 3 MM / 50 MM 2 X F) was loaded with wet HaloLink™ resin (360 mg), allowing particles sedimentation. The reactor was connected to the pump (Syrris Asia Syringe Pumps, equipped with Asia Blue Syringes of 500 µl / 1 ml)[1] by PTFE tubing and end fittings. The resin was washed with Kpi 50 mM pH 7 for 1h (flow rate 30 µl/min). Then, a solution (5 ml) of the cell crude extract (250 mg) in Kpi (50 mM, pH 7) containing

[1] http://syrris.com/flow-products/asia-modules/asia-syringe-pump

$MgCl_2x6H_2O$ (1.0 mM) was pumped continuously through the packed bed. The efflux was monitored in real-time by a UV/Vis detector (Flow-UVTM, Uniqsis Ltd).[1]

S7. General procedure for the HaloTag-*Lb*ADH catalyzed reduction of ketones 1a-1p in flow

A solution of the ketone (50 mM), $MgCl_2x6H_2O$ (1.0 mM) and NADPH (0.5 mM) in Kpi (60% V/V, 50 mM, pH 7), 2-propanol (10% V/V) and THF (30% V/V) was pumped (flow rate 30 µl/min) through the HaloTag-*Lb*ADH packed bed reactor, prepared according to the procedure in section S6. The efflux was monitored in real-time by a UV/Vis detector. The collected solution was extracted with pentane and the organic phase was dried over $MgSO_4$ and concentrated *in vacuo*. The crude was purified as described for each compound.

To analyze the long-term stability of the HaloTag-*Lb*ADH, the conversion of acetophenone **1a** in flow in the presence of 2-propanol was investigated. Acetophenone **1a** and phenylethanol **2a** were detected by HPLC as described in S5.

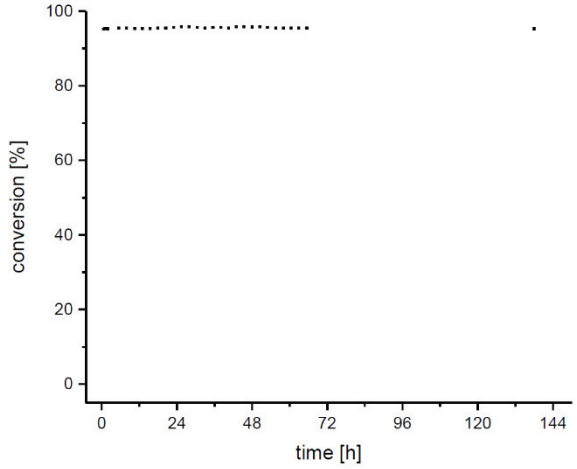

Figure S7: Long-term stability of HaloTag-*Lb*ADH. A packed-bed reactor (5 cm Omnifit® column, V = 350 µl) containing 4 mg HaloTag-*Lb*ADH immobilized on 360 mg of wet HaloLinkTM Resin was prepared and the conversion of acetophenone into phenylethanol was investigated.

S8. General procedure for the preparation of (*S*)-2-phenyloxirane by a two-step chemoenzymatic transformation in flow

A solution of the ketone **1h** (50 mM), $MgCl_2x6H_2O$ (1.0 mM) and NADPH (0.5 mM) in Kpi (60% V/V, 50 mM, pH 7), 2-propanol (10% V/V) and THF (30% V/V) was pumped (flow rate 30 µl/min) through the HaloTag-*Lb*ADH packed bed reactor, prepared according to the procedure in section S6. The efflux was mixed with a second stream containing an aqueous solution of NaOH (1 mM, flow rate 30 µl/min). The resulting mixture was passed through a 2-inputs glass microreactor (1.0 ml). The

[1] http://www.uniqsis.com/paProductsDetail.aspx?ID=Flow-UV

collected solution was extracted with pentane and the organic phase was dried over $MgSO_4$ and concentrated *in vacuo*. The crude was analyzed by ^{1}H-NMR and chiral GC.

S9. General procedure for the preparation of the racemic compounds (±)-2a-p and (±)-5.

Compounds **(±)-2a**, **(±)-2b**, **(±)-2c**, **(±)-2d**, **(±)-2e**, **(±)-2f**, **(±)-2k**, **(±)-2l**, **(±)-2m**, **(±)-2o** and **(±)-5** were obtained from commercial sources and used without further purification as reference for GC and HPLC analyses. Compounds **(±)-2g**,[1] **(±)-2h**,[2] **(±)-2i**,[3] **(±)-2j**,[3] and **(±)-2n**[6] were prepared according to the reported procedure.

S10. Spectral characterization of compounds 2a-2p and 5

(*R*)-(+)-1-Phenylethanol, 2a. Isolated by flash cromatography (hexane/AcOEt 80/20), 90% yield. The optical purity of **2a** was assessed by GC analysis, using the following method: initial temperature 40 °C holded for 13 min, ramp 15 °C/min to 180 °C holded for 10 min, post run 180 °C for 1 min. (*R*)-isomer, t_R 19.910 min; (*S*)-isomer, t_R 20.037 min., >99% *ee*. $[\alpha]^{20}_{589}$= +49.3 (c = 0.82 g/100ml, $CHCl_3$). The configuration was assigned by comparison with the commercial available (*R*)-(+)-1-phenylethanol. The NMR spectra are in accordance with the reported data.[3]

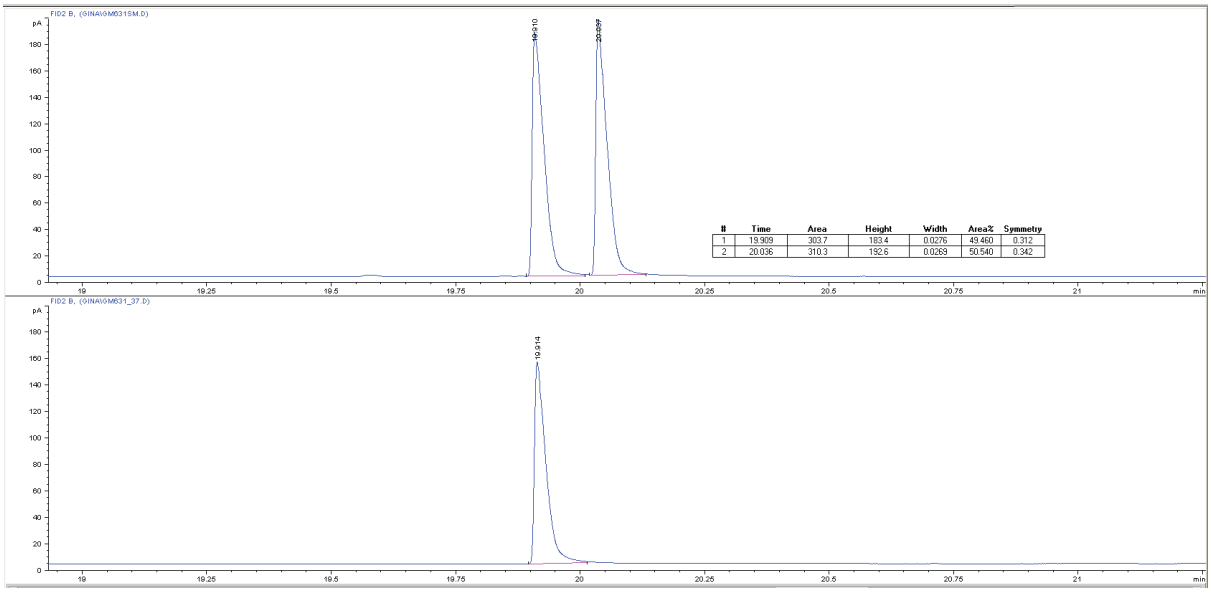

[1] K. Yahata, M. Minami, Y. Yoshikawa, K. Watanabe and H. Fujioka, *Chem. Pharm. Bull. (Tokyo).*, 2013, **61**, 1298–307.
[2] G. Hostetler, D. Dunn, B. A. McKenna, K. Kopec and S. Chatterjee, *Bioorganic Med. Chem. Lett.*, 2014, **24**, 2094–2097.
[3] W. Li, X. Sun, L. Zhou and G. Hou, *J. Org. Chem.*, 2009, **74**, 1397–1399.

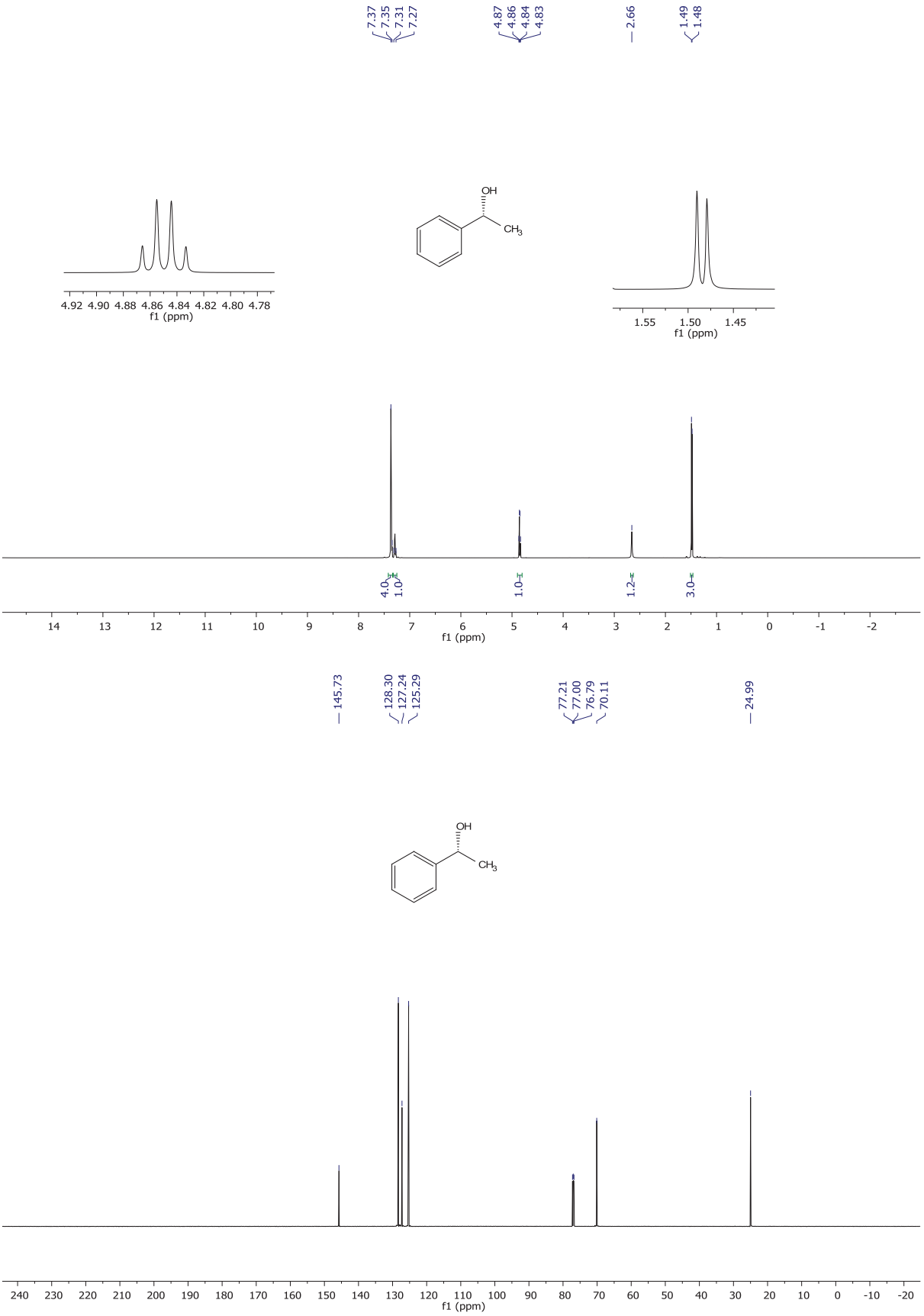

(*R*)-(+)-1-(4-Bromophenyl)ethanol, 2b. Isolated by cromatography (hexane/AcOEt 80/20), 94% yield. The optical purity of **2b** was assessed by GC analysis, using the following method: initial temperature 40 °C holded for 13 min, ramp 15 °C/min to 180 °C holded for 10 min, post run 180 °C

for 1 min. t_1 22.376 min; t_2 22.501 min., >99% *ee*. $[\alpha]^{20}_{589}$= +28 (c = 0.5 g/100ml, $CHCl_3$). The NMR spectra are in accordance with the reported data.[1]

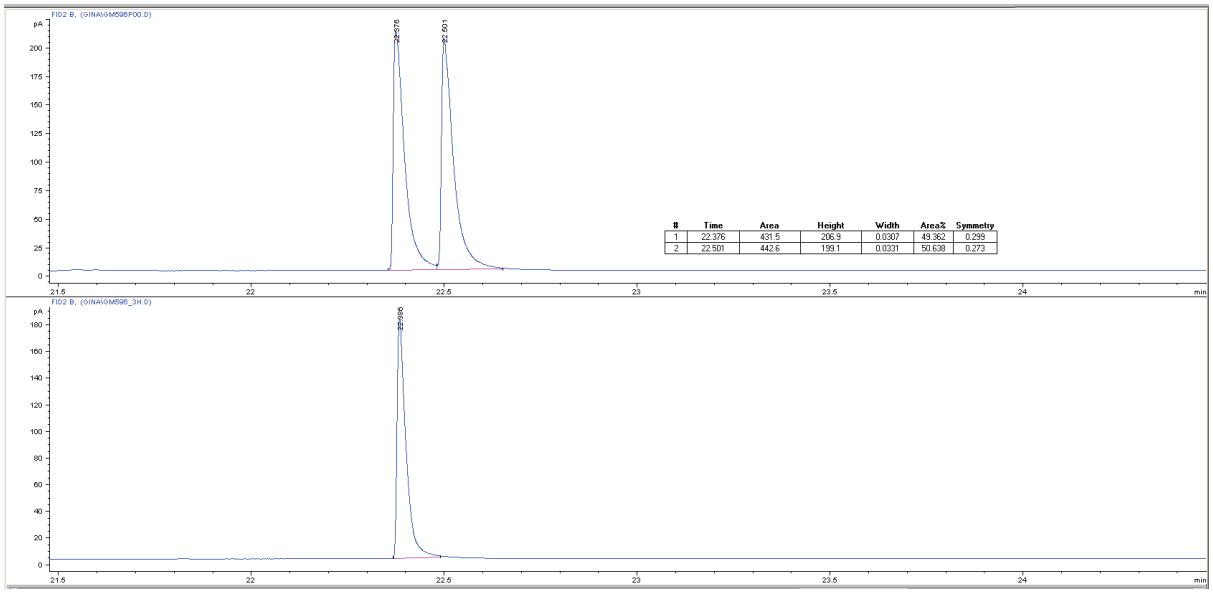

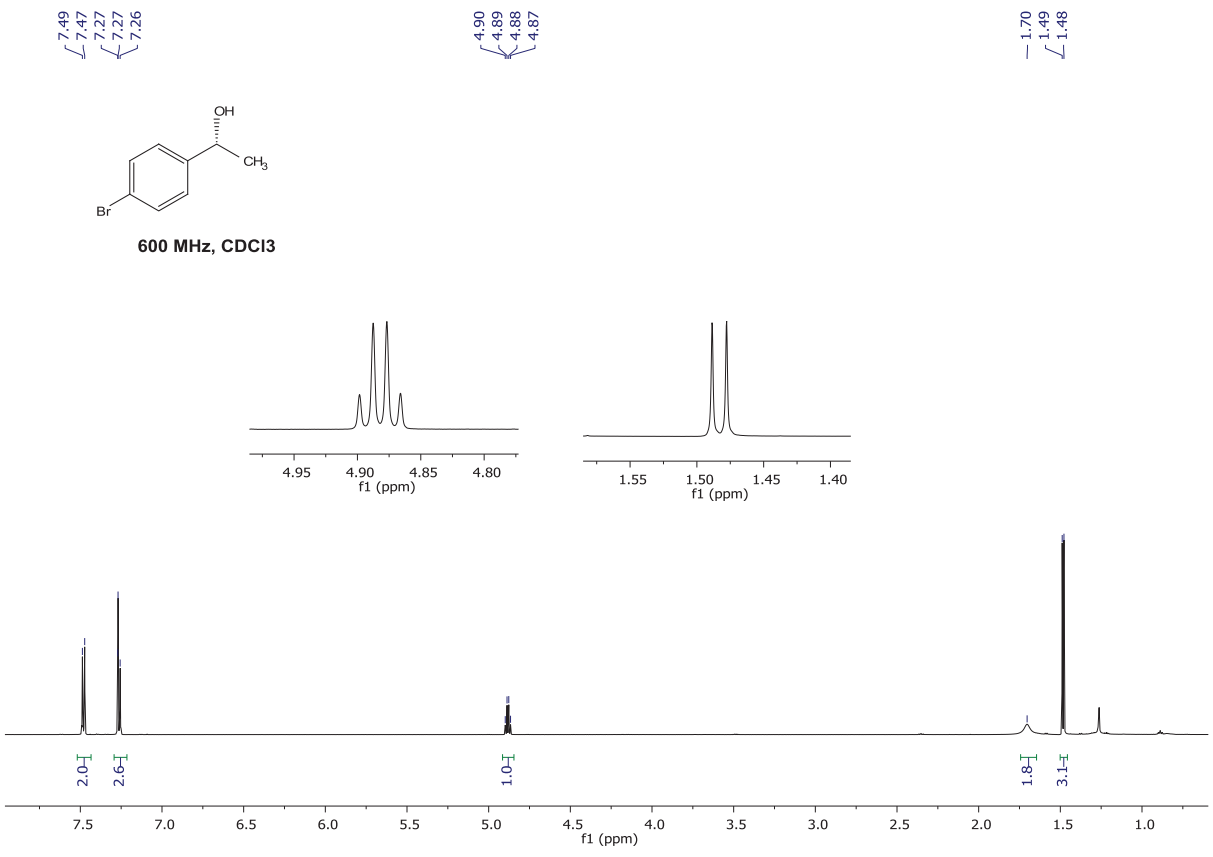

[1]I. P. Query, P. A. Squier, E. M. Larson, N. A. Isley and T. B. Clark, *J. Org. Chem.*, 2011, **76**, 6452–6456.

(*R*)-(+)-1-(4-Chlorophenyl)ethanol, 2c. Isolated by chromatography (hexane/AcOEt 80/20), 94% yield. The optical purity of **2c** (*ee* > 99%) was assessed by GC analysis, using the following method: initial temperature 40 °C holded for 13 min, ramp 15 °C/min to 180 °C holded for 10 min, post run 180 °C for 1 min. t_1 21.650 min; t_2 21.797 min., >99% *ee*. $[\alpha]^{20}_{589}$= +48 (c = 0.715 g/100ml, $CHCl_3$). The NMR spectra are in accordance with the reported data.[1]

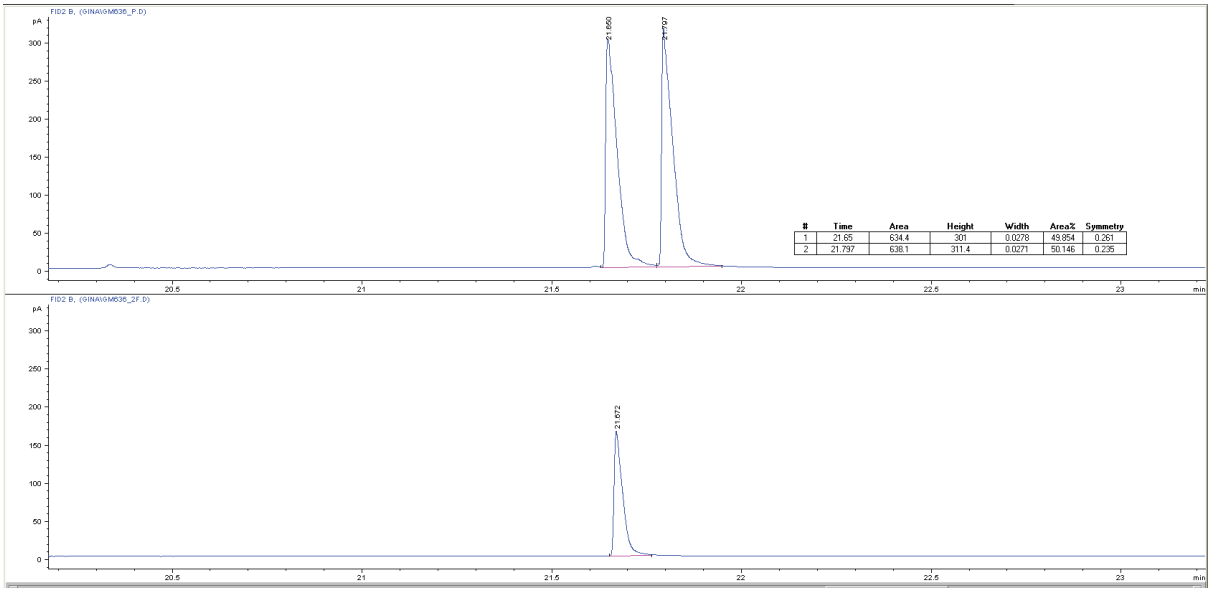

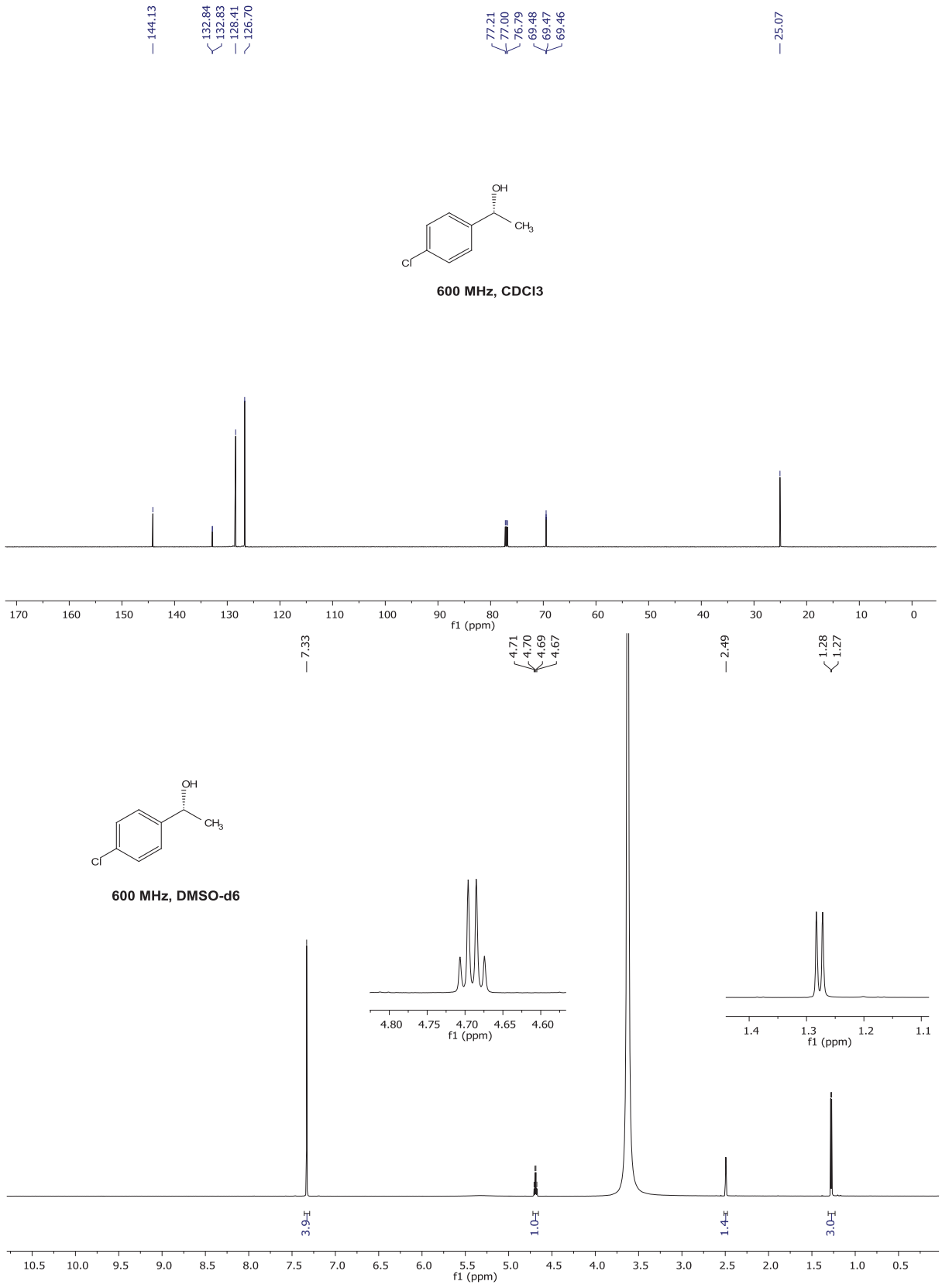

(*R*)-(+)-1-(4-Methoxyphenyl)ethanol, 2d. Isolated by chromatography (hexane/AcOEt 80/20), 23% yield. The optical purity of **2d** was assessed by GC analysis, using the following method: initial temperature 40 °C holded for 13 min, ramp 15 °C/min to 180 °C holded for 10 min, post run 180 °C

for 1 min. t_1 21.650 min; t_2 21.73 min., >99% *ee*. $[\alpha]^{20}_{589}$= +28.5 (c = 1.76 g/100ml, $CHCl_3$). The NMR spectra are in accordance with the reported data.[1]

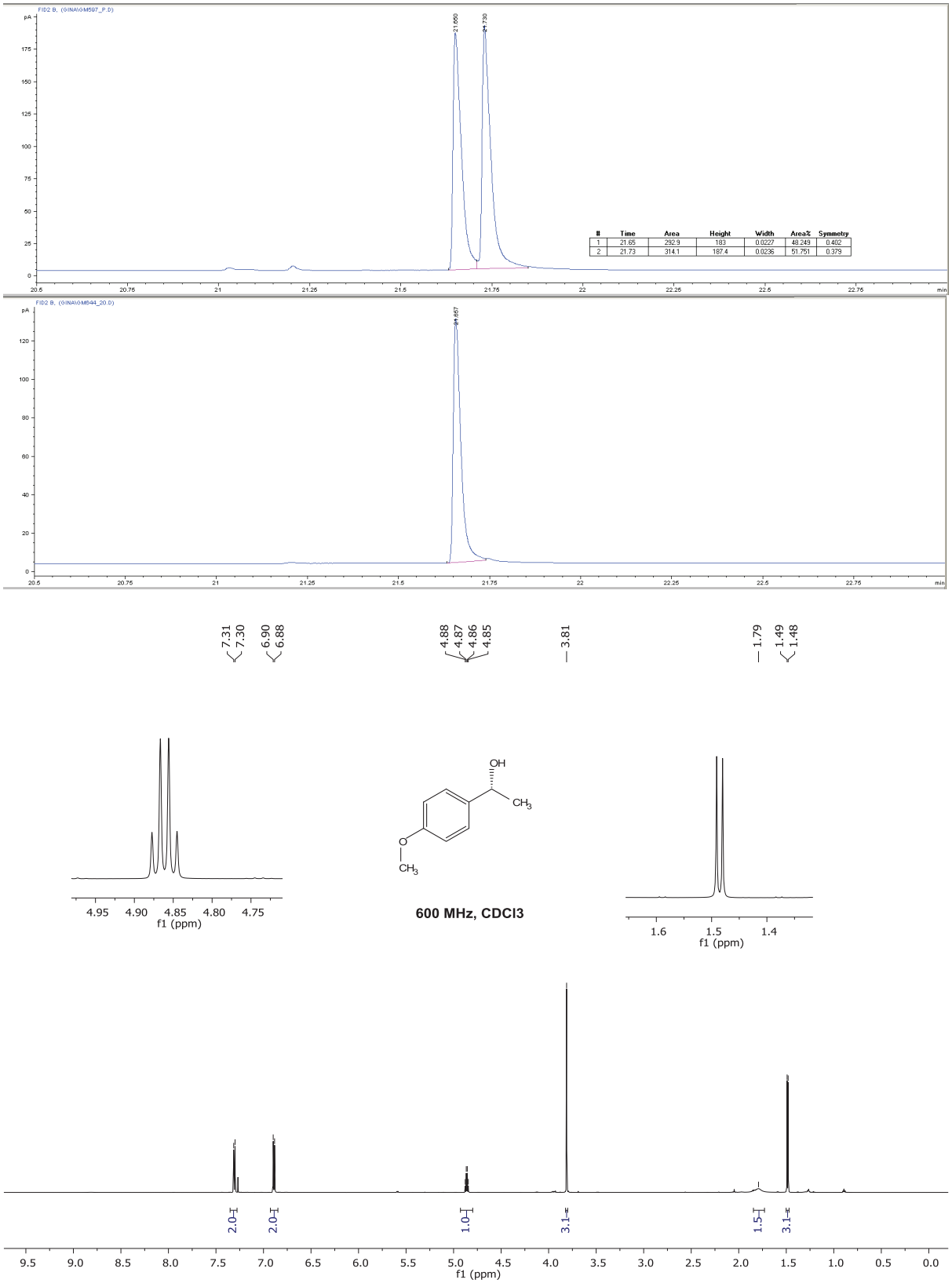

[1]K. E. Jolley, A. Zanotti-Gerosa, F. Hancock, A. Dyke, D. M. Grainger, J. A. Medlock, H. G. Nedden, J. J. M. Le Paih, S. J. Roseblade, A. Seger, V. Sivakumar, I. Prokes, D. J. Morris and M. Wills, *Adv. Synth. Catal.*, 2012, **354**, 2545–2555.

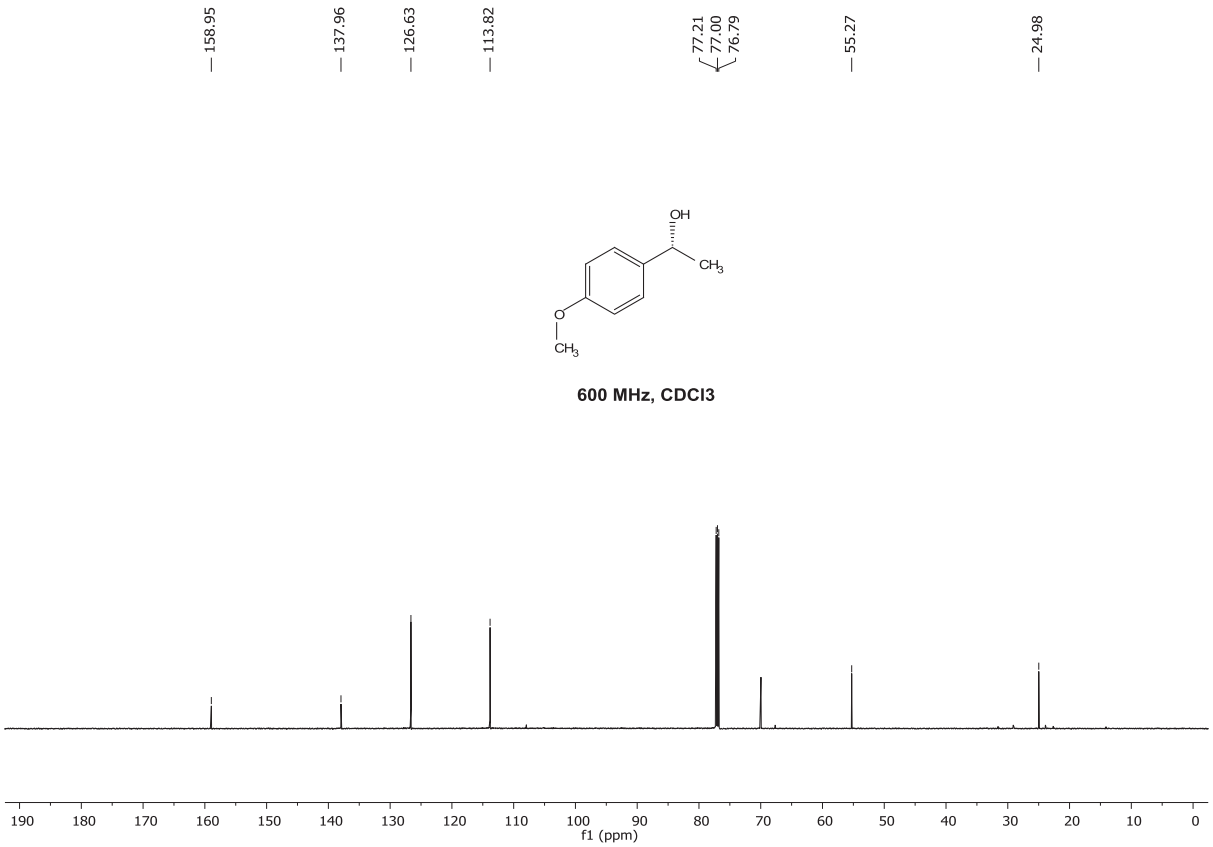

(*R*)-(+)-1-(Naphthalene-2-yl)ethanol, 2e. Isolated by chromatography (hexane/AcOEt 80/20), 95% yield. The optical purity of **2e** (*ee* > 99%) was assessed by GC analysis, using the following method: initial temperature 40 °C holded for 13 min, ramp 15 °C/min to 180 °C holded for 10 min, post run 180 °C for 1 min. t_1 24.534 min; t_2 24.657 min., >99% *ee*. $[\alpha]^{20}_{589}$= +40 (c = 0.3 g/100ml, $CHCl_3$). The NMR spectra are in accordance with the reported data.[1]

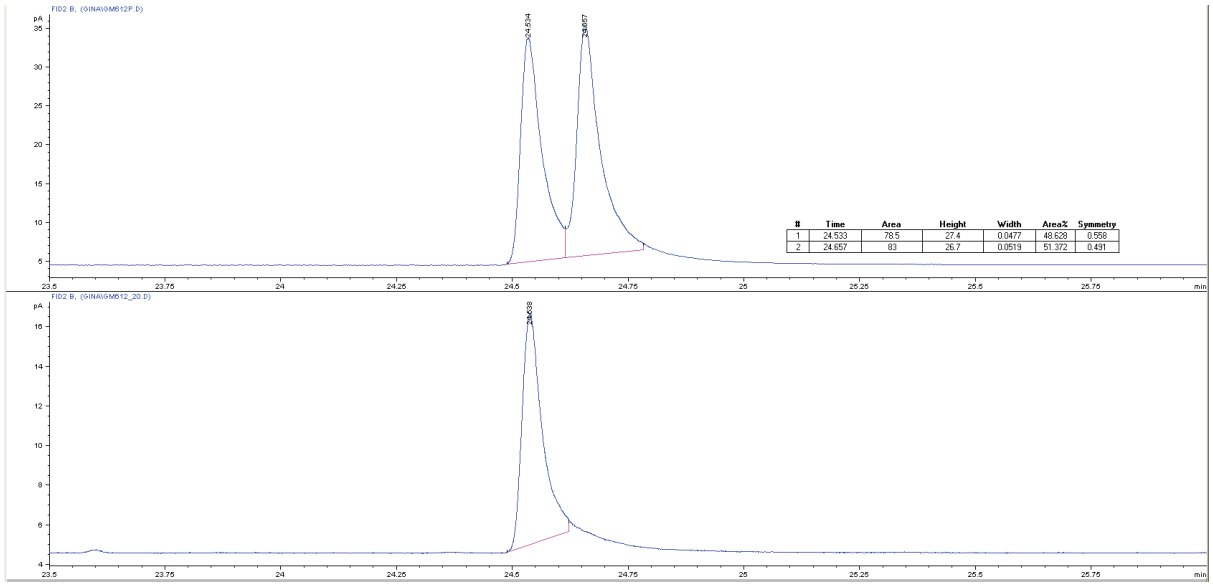

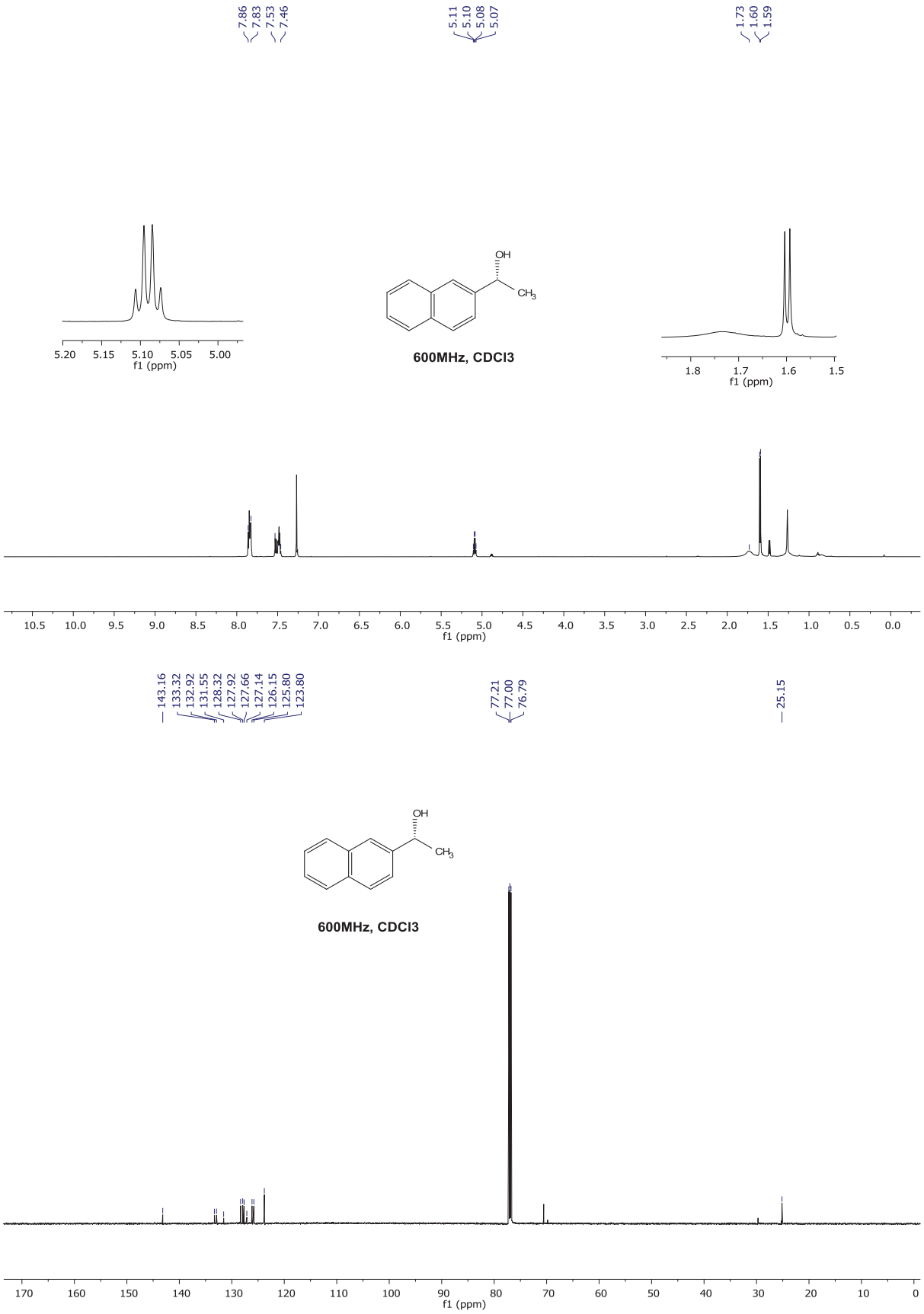

(*R*)-(+)-1-(Tol-4-yl)ethanol, 2f. Isolated by chromatography (hexane/AcOEt 80/20), 70% yield. The optical purity of **2g** was assessed by GC analysis, using the following method: initial temperature 40 °C holded for 13 min, ramp 15 °C/min to 180 °C holded for 10 min, post run 180 °C for 1 min. t_1

20.42 min; t_2 20.583 min., 99% *ee*. $[\alpha]^{20}_{589}$= +54.4 (c = 0.69 g/100ml, $CHCl_3$). The NMR spectra are in accordance with the reported data.[1]

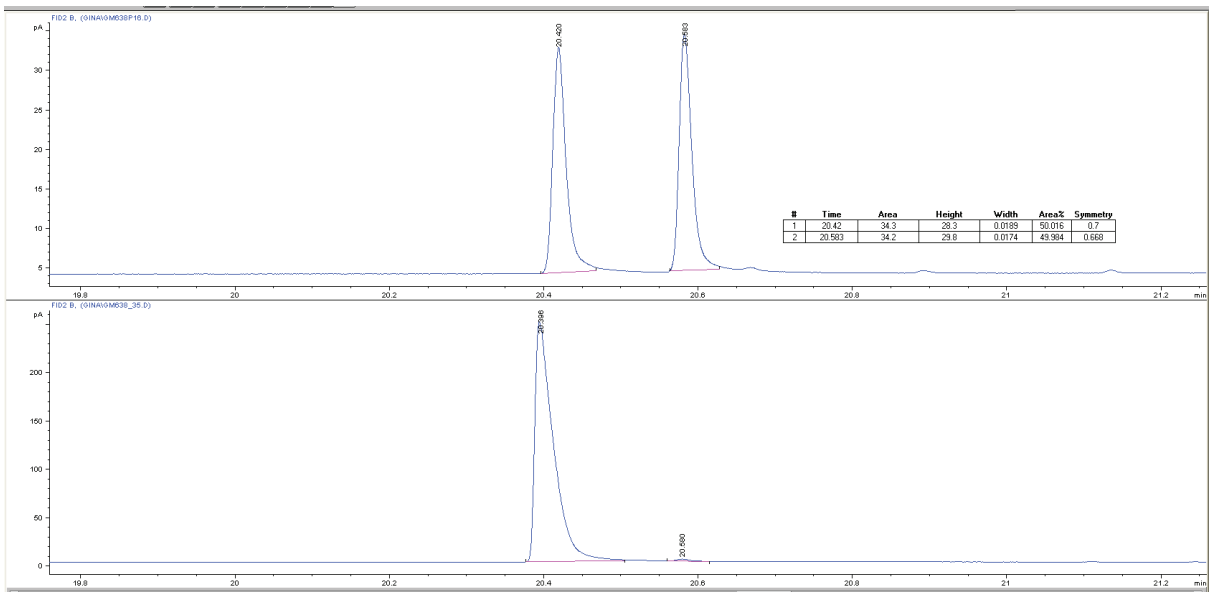

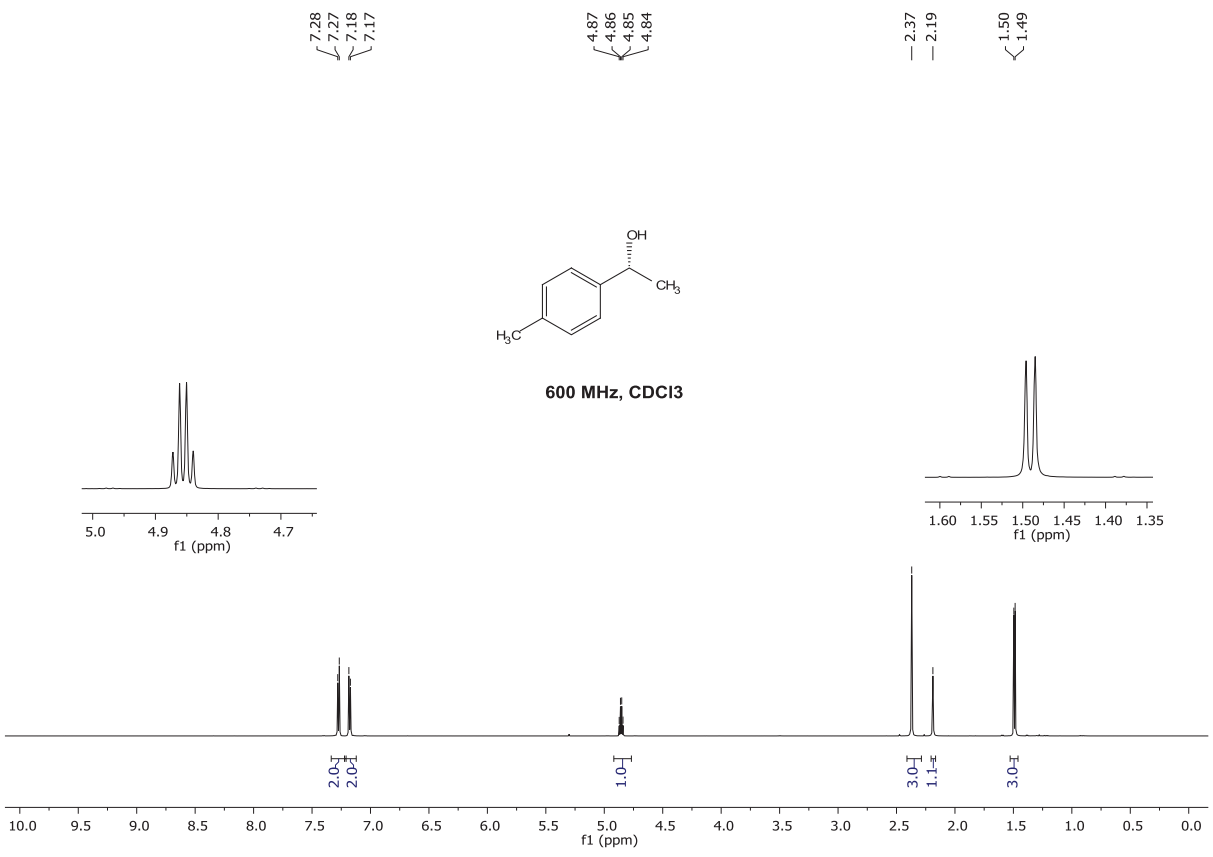

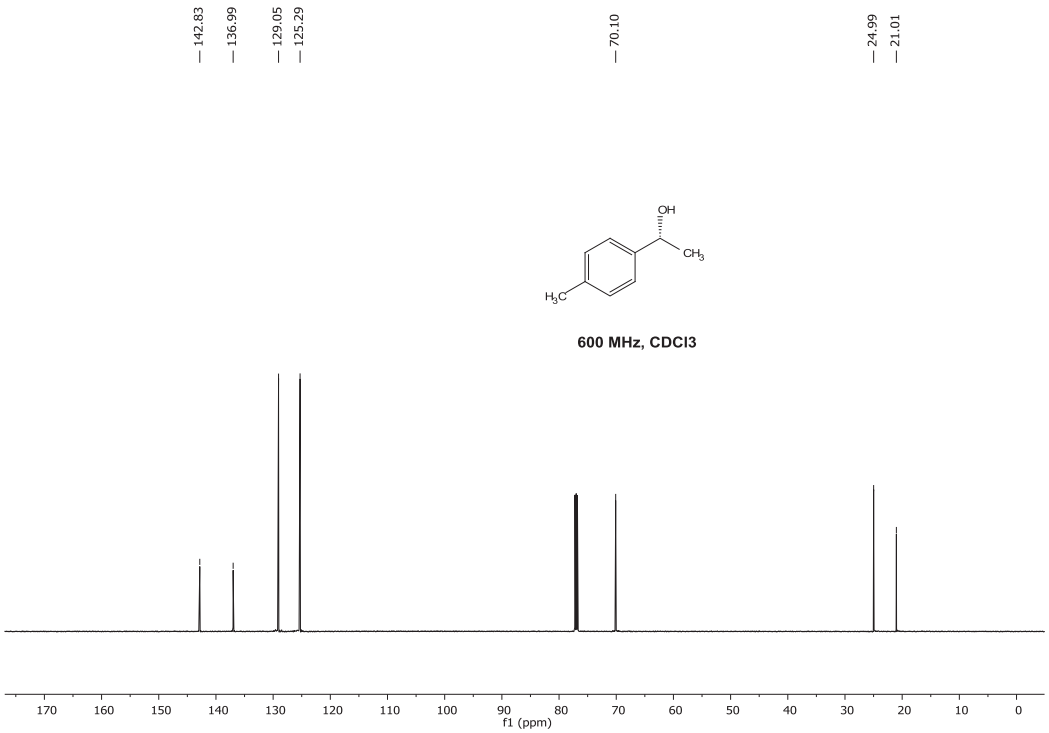

(*R*)-(+)-4-(1-Hydroxyethyl)benzaldehyde, 2g. Isolated by chromatography (hexane/AcOEt 80/20), 97% yield. The optical purity of **2g** (*ee* > 99%) was assessed by GC analysis, using the following method: initial temperature 40 °C holded for 13 min, ramp 15 °C/min to 180 °C holded for 10 min, post run 180 °C for 1 min. t_1 21.063 min; t_2 23.24 min., >99% *ee*. $[\alpha]^{20}_{589}$= +40 (c = 0.3 g/100ml, $CHCl_3$). The NMR spectra are in accordance with the reported data.[1]

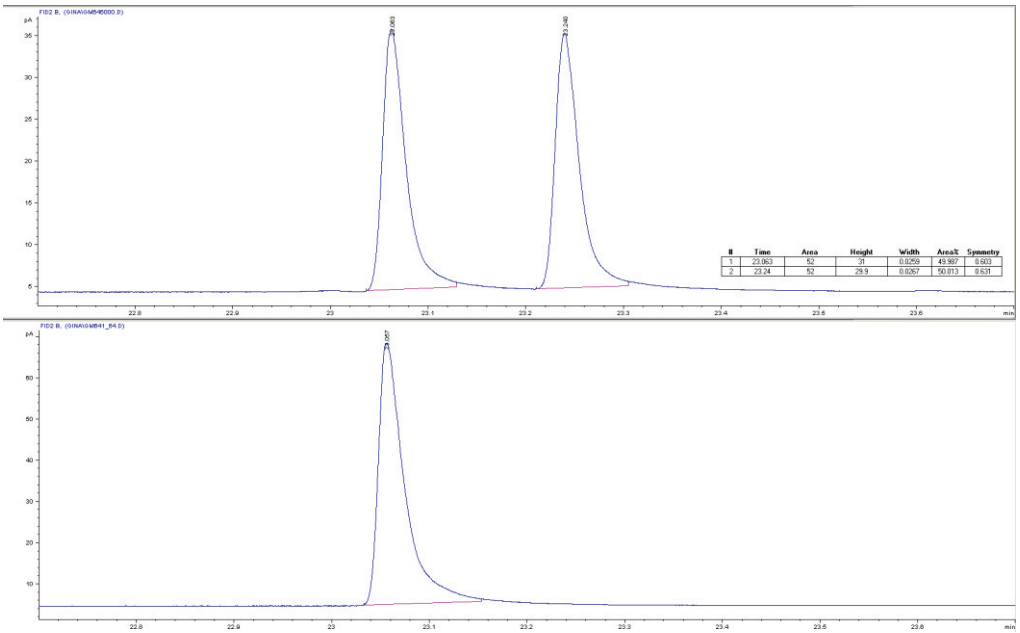

[1]K. Yahata, M. Minami, Y. Yoshikawa, K. Watanabe and H. Fujioka, *Chem. Pharm. Bull. (Tokyo).*, 2013, **61**, 1298–307.

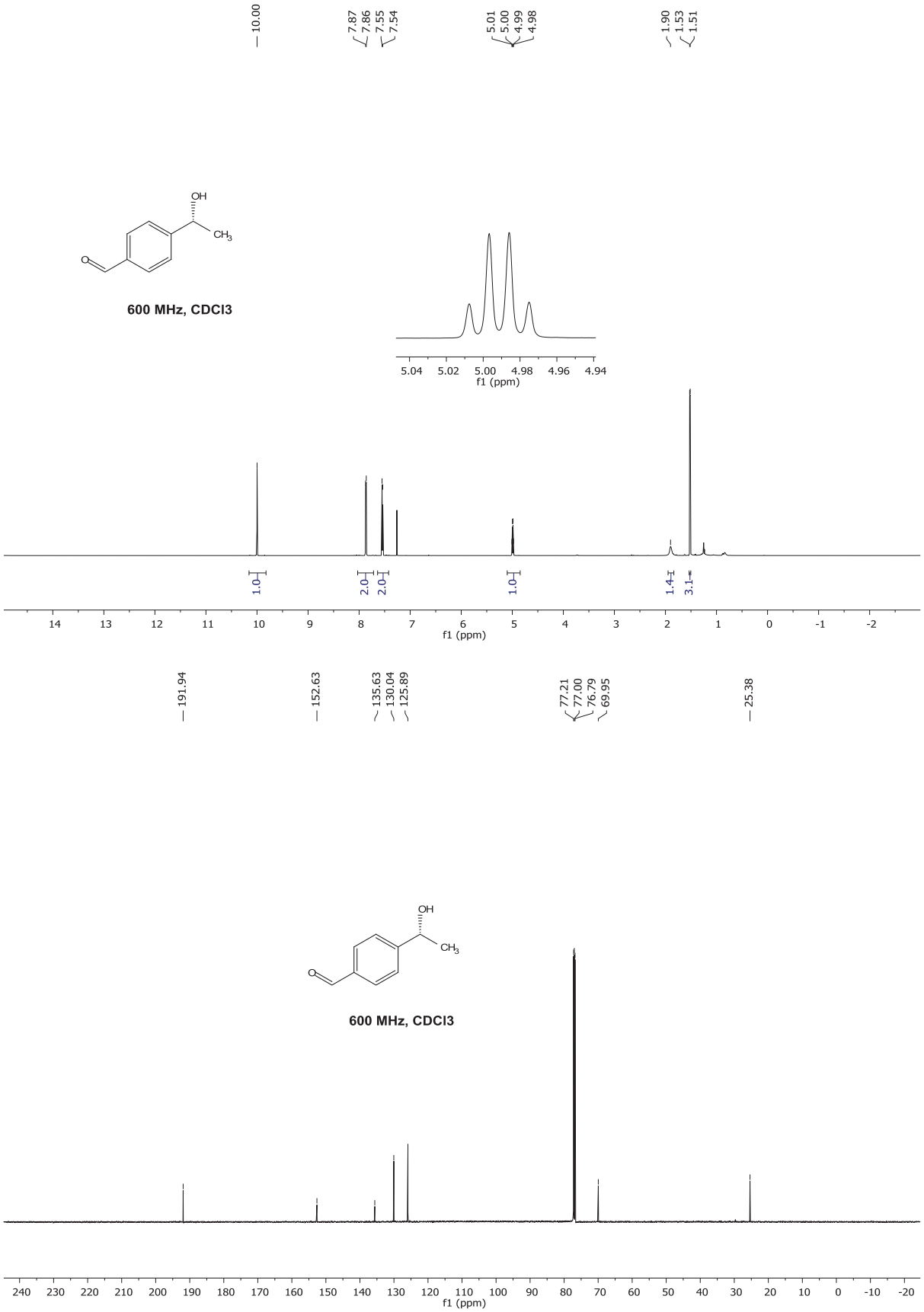

(*S*)-(+)-2-Bromo-1-phenylethanol, 2h. Isolated by chromatography (hexane/AcOEt 80/20), 98% yield. The optical purity of **2h** was assessed by GC analysis, using the following method: initial temperature 40 °C holded for 13 min, ramp 15 °C/min to 180 °C holded for 10 min, post run 180 °C

for 1 min. t_1 22.530 min; t_2 22.602 min., >99% *ee*. $[\alpha]^{20}_{589}$= +49.4 (c = 1.1 g/100ml, $CHCl_3$). The NMR spectra are in accordance with the reported data.[1]

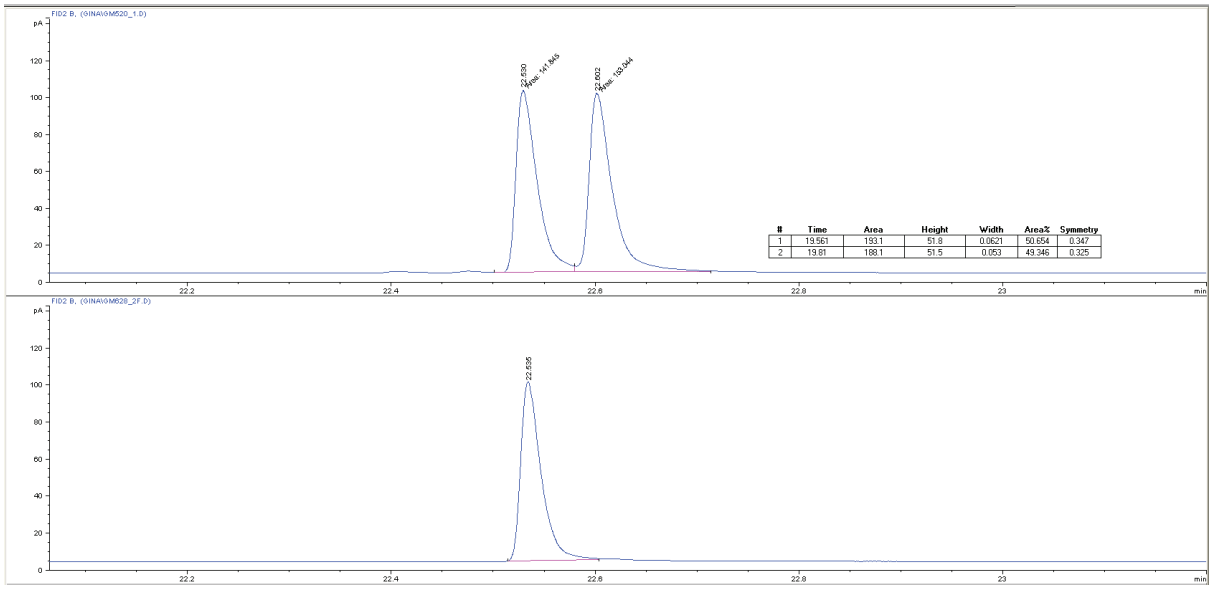

#	Time	Area	Height	Width	Area%	Symmetry
1	19.561	193.1	51.8	0.0621	50.654	0.347
2	19.81	188.1	51.5	0.053	49.346	0.325

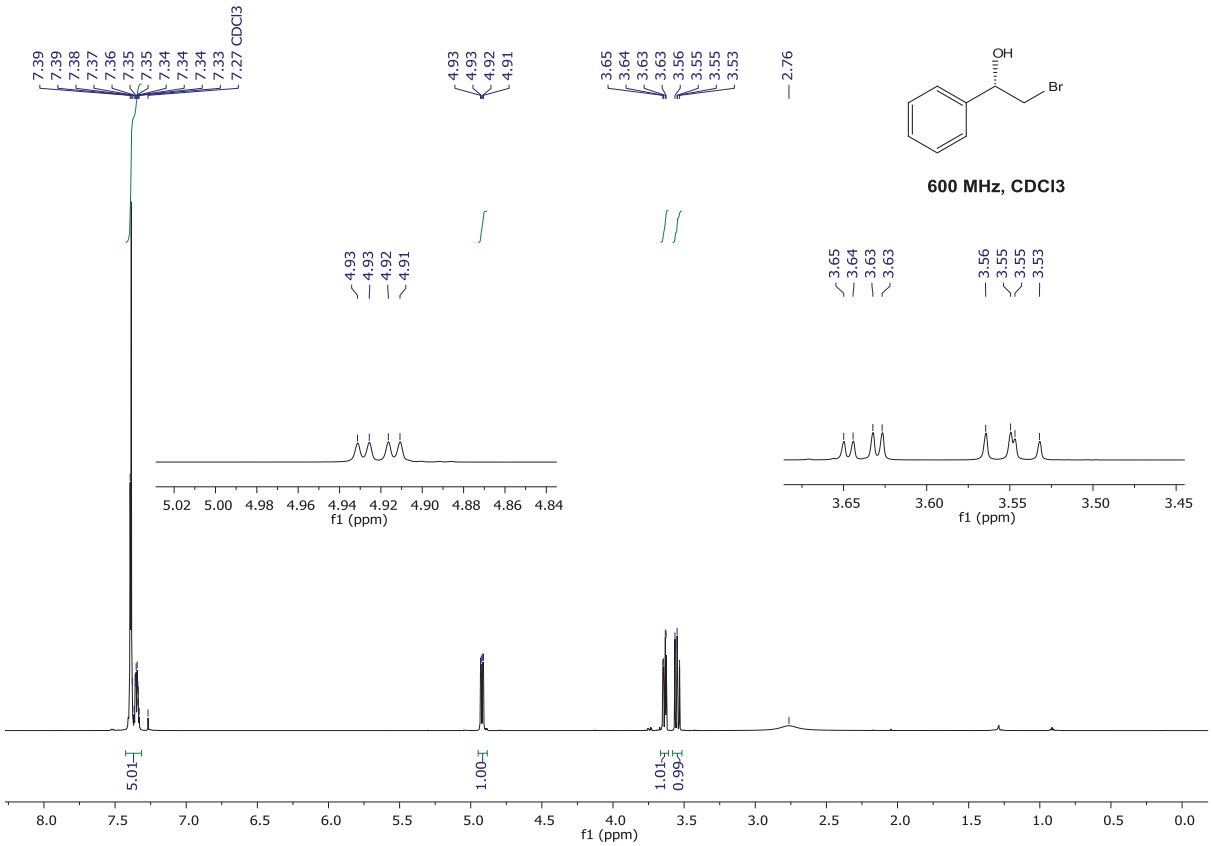

[1]Y. Ma, H. Liu, L. Chen, X. Cui, J. Zhu and J. Deng, *Org. Lett.*, 2003, **5**, 2103–2106.

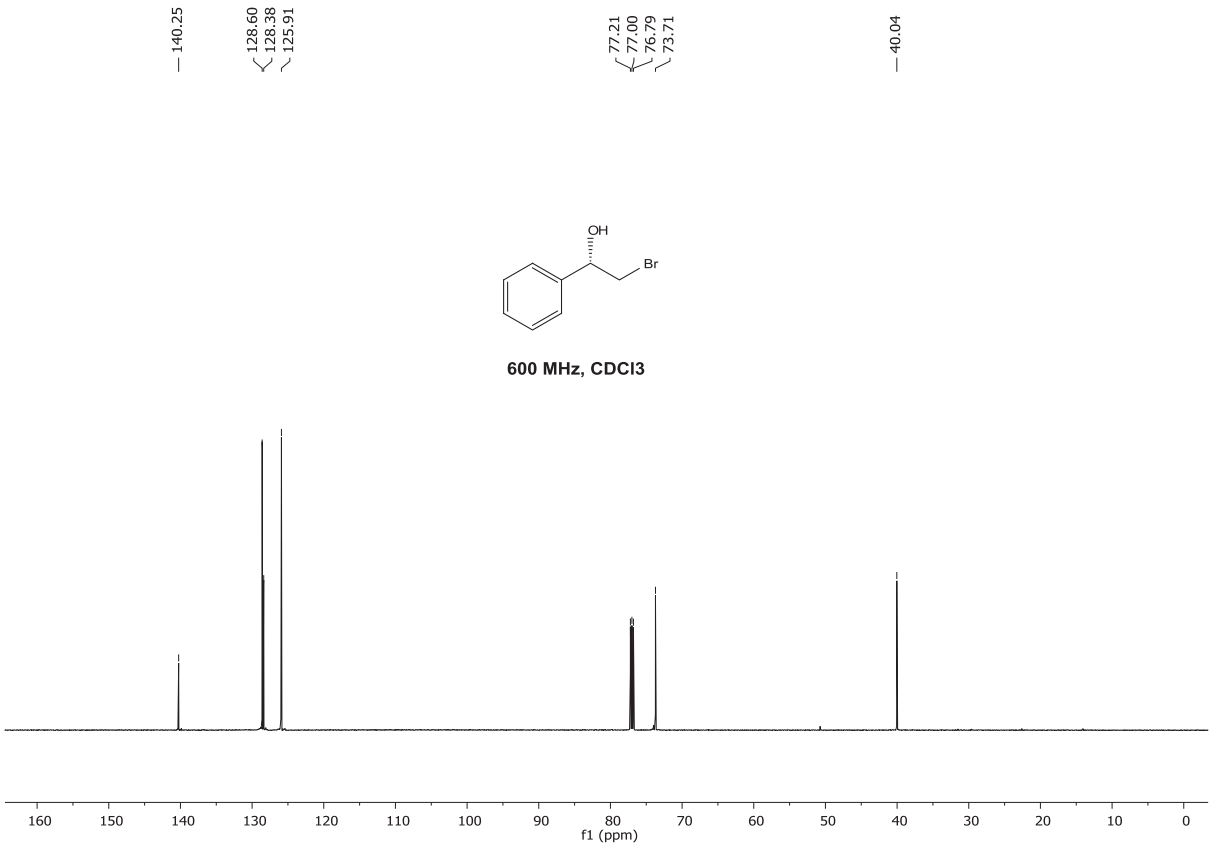

(*S*)-(+)-2-Bromo-1-[4-trifluoromethyl)phenyl]ethanol, 2i. Isolated by chromatography (hexane/AcOEt 80/20), 91% yield. The optical purity of **2i** was assessed by GC analysis, using the following method: initial temperature 40 °C holded for 13 min, ramp 15 °C/min to 180 °C holded for 10 min, post run 180 °C for 1 min. t_1 23.065 min; t_2 23.226 min., >99% *ee*. $[\alpha]^{20}_{589}$= +35.5 (c = 0.4 g/100ml, $CHCl_3$). The NMR spectra are in accordance with the reported data.[1]

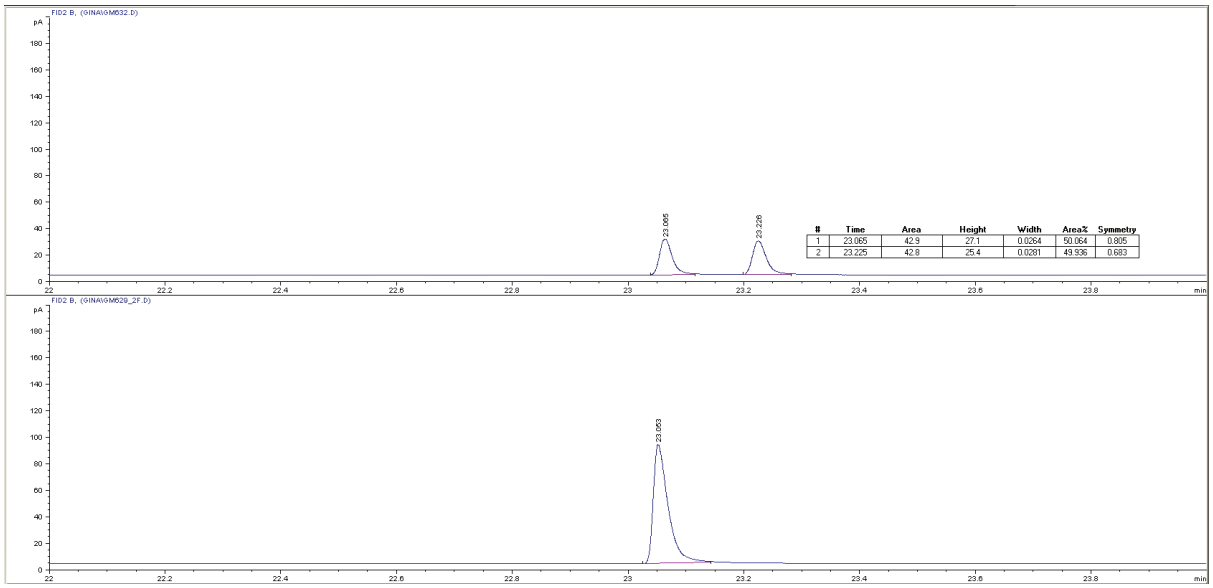

[1]A. G. Hortmann, D. A. Robertson and B. K. Gillard, *J. Org. Chem*, 1979, **87**, 322–324.

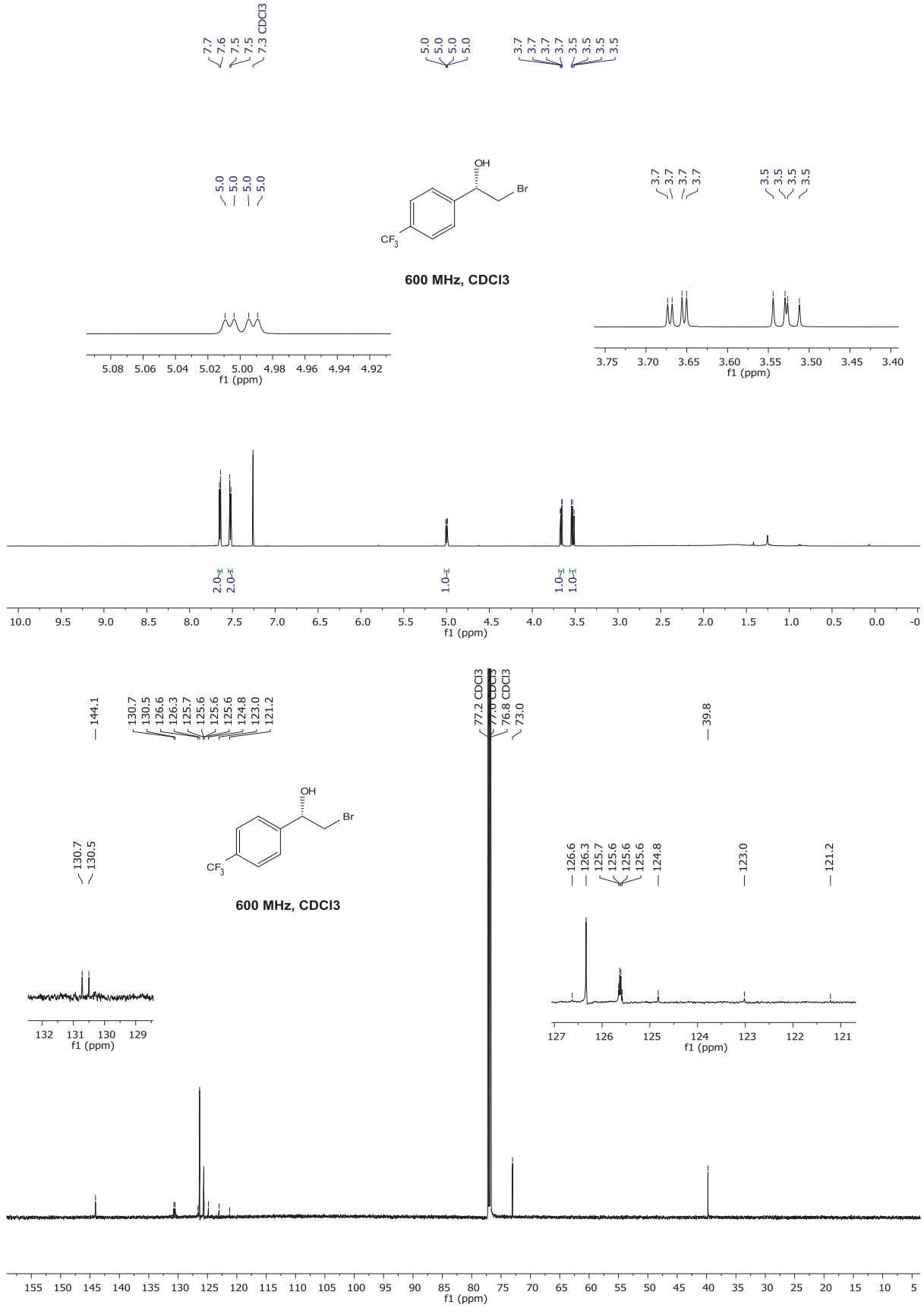
7.7
7.6
7.5
7.5
7.3 CDCl3
5.0
5.0
5.0
5.0
3.7
3.7
3.7
3.7
3.5
3.5
3.5
3.5
OH
Br
CF3
600 MHz, CDCl3
f1 (ppm)
2.0
2.0
1.0
1.0
144.1
130.7
130.5
126.6
126.3
125.7
125.6
125.6
124.8
123.0
121.2
77.2 CDCl3
77.0 CDCl3
76.8 CDCl3
73.0
39.8

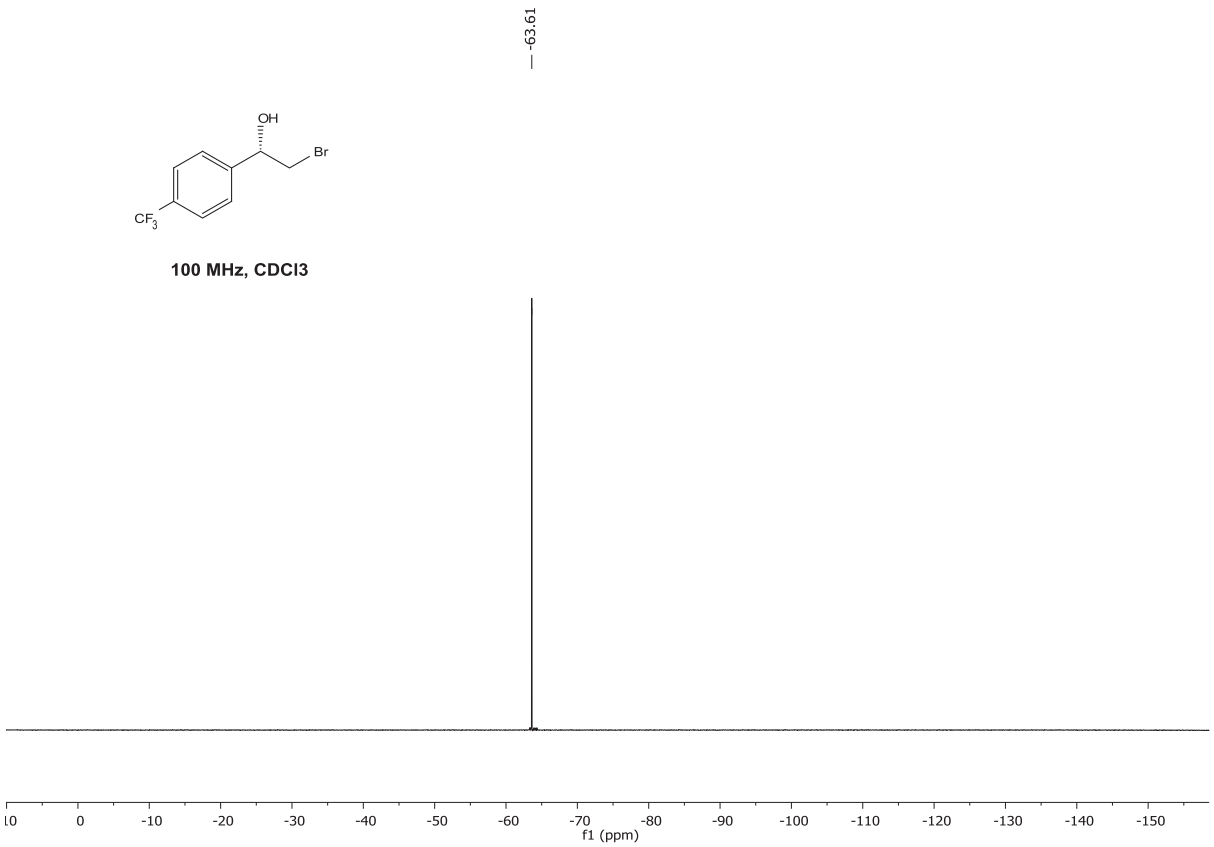

(*S*)-(+)-2-Fluoro-1-phenylethanol, 2j. Isolated by chromatography (hexane/AcOEt 80/20), 99% yield. The optical purity of **2j** was assessed by GC analysis, using the following method: initial temperature 40 °C holded for 13 min, ramp 15 °C/min to 180 °C holded for 10 min, post run 180 °C for 1 min. t_1 20.706 min; t_2 20.815 min., >99% *ee*. $[\alpha]^{20}_{589}$= +16.1 (c = 0.75 g/100ml, $CHCl_3$). The NMR spectra are in accordance with the reported data.[1]

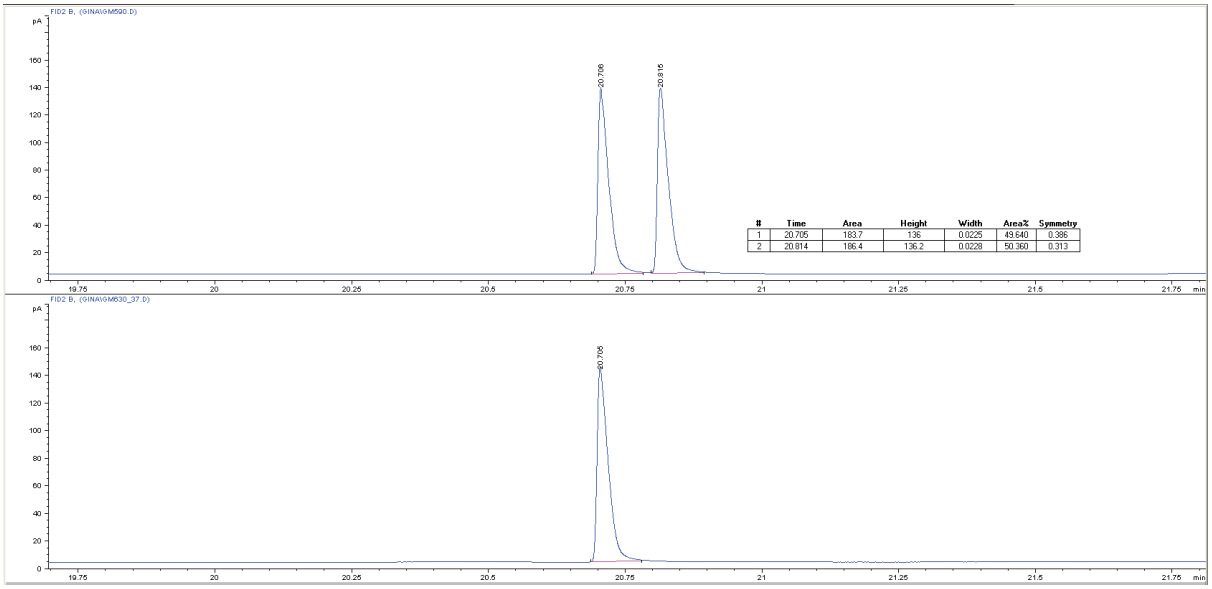

[1]G. Stavber, M. Zupan, M. Jereb and S. Stavber, *Org. Lett.*, 2004, **6**, 4973–6.

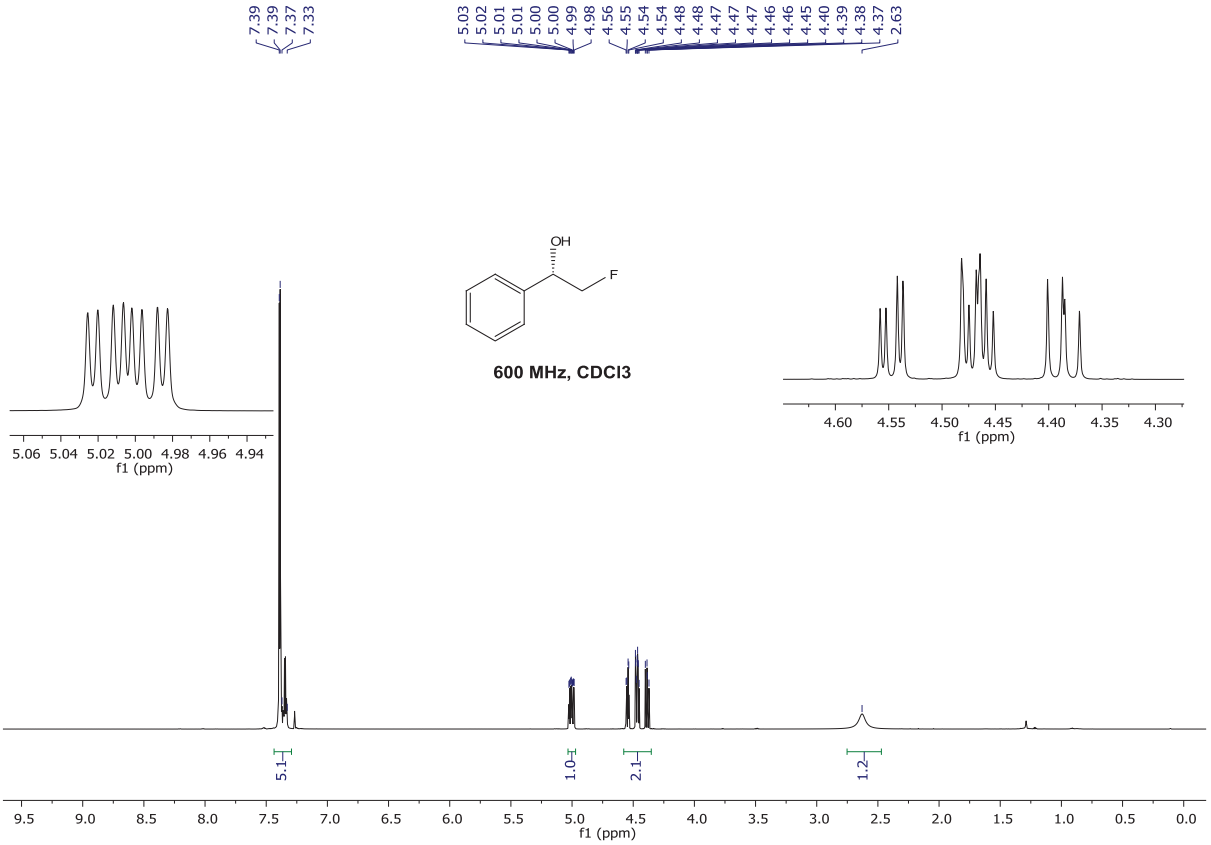
7.39
7.39
7.37
7.33
5.03
5.02
5.01
5.01
5.00
5.00
4.99
4.98
4.56
4.55
4.54
4.54
4.48
4.48
4.47
4.47
4.47
4.46
4.46
4.45
4.40
4.39
4.38
4.37
2.63
OH
F
600 MHz, CDCl3
5.06 5.04 5.02 5.00 4.98 4.96 4.94
f1 (ppm)
4.60 4.55 4.50 4.45 4.40 4.35 4.30
f1 (ppm)
5.1
1.0
2.1
1.2
9.5 9.0 8.5 8.0 7.5 7.0 6.5 6.0 5.5 5.0 4.5 4.0 3.5 3.0 2.5 2.0 1.5 1.0 0.5 0.0
f1 (ppm)

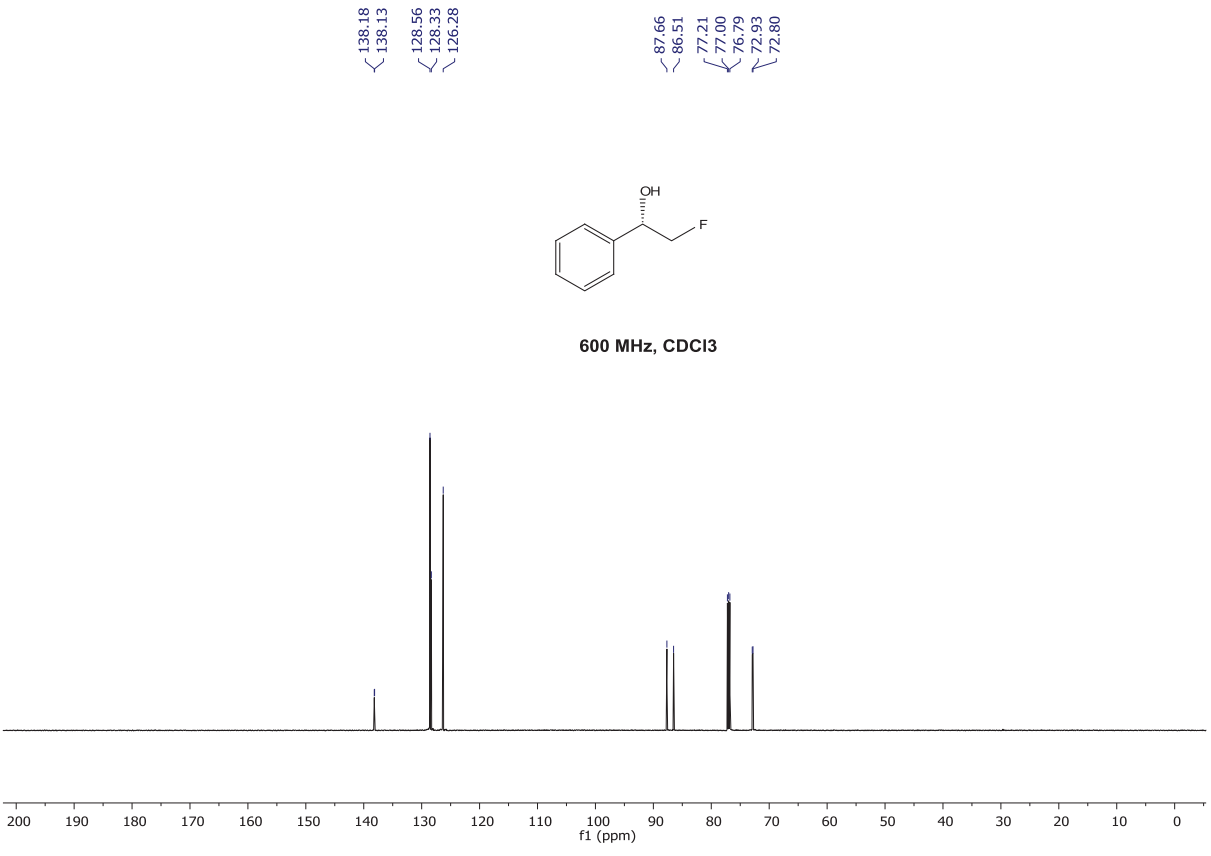
138.18
138.13
128.56
128.33
126.28
87.66
86.51
77.21
77.00
76.79
72.93
72.80
OH
F
600 MHz, CDCl3
200 190 180 170 160 150 140 130 120 110 100 90 80 70 60 50 40 30 20 10 0
f1 (ppm)

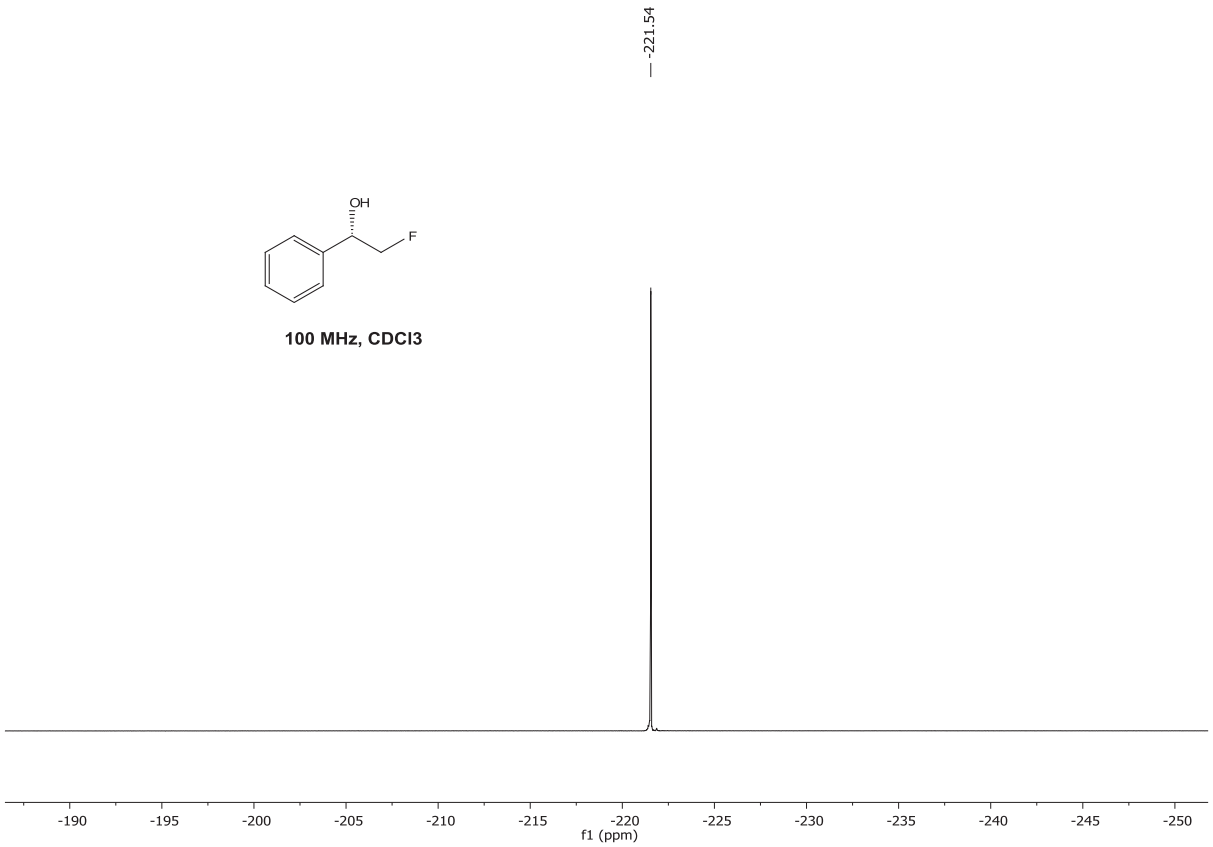

(*R*)-(+)-2,2,2-Trifluoro-1-[4-trifluoromethyl)phenyl]ethanol, 2k. Isolated by cromatography (hexane/AcOEt 80/20), 60% yield. The optical purity of **2k** was assessed by GC analysis, using the following method: initial temperature 40 °C holded for 13 min, ramp 15 °C/min to 180 °C holded for 10 min, post run 180 °C for 1 min. t_1 20.770 min; t_2 20.841 min., >99% *ee*. $[\alpha]^{20}_{589}$= +17.8 (c = 1.2 g/100ml, $CHCl_3$). The NMR spectra are in accordance with the reported data.[1]

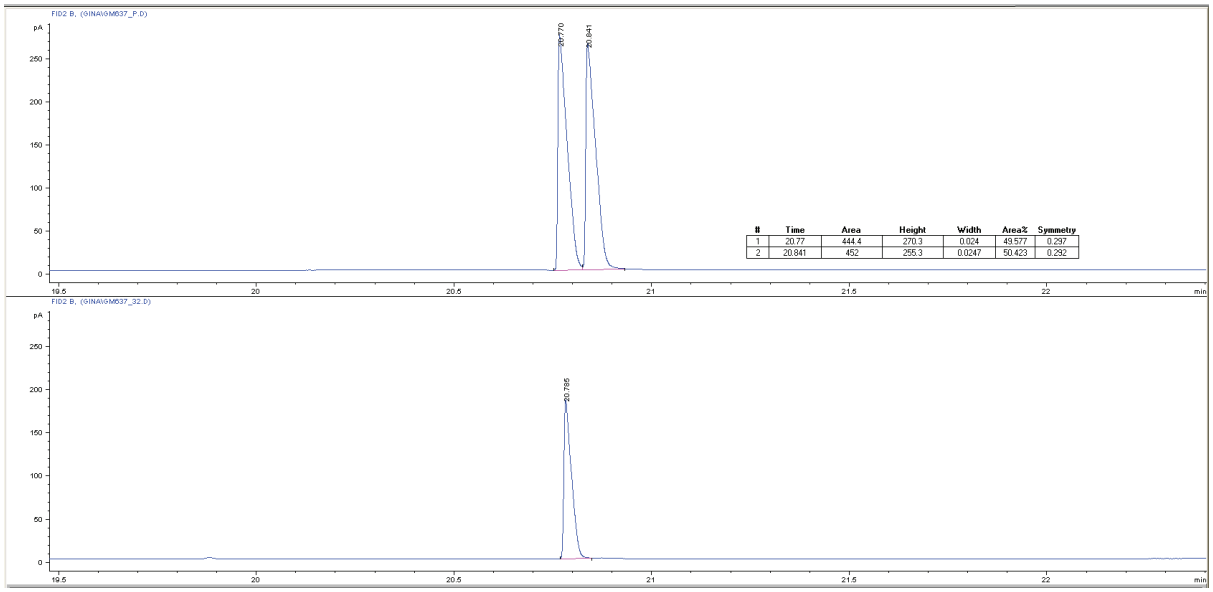

[1]H. Zhao, B. Qin, X. Liu and X. Feng, *Tetrahedron*, 2007, **63**, 6822–6826.

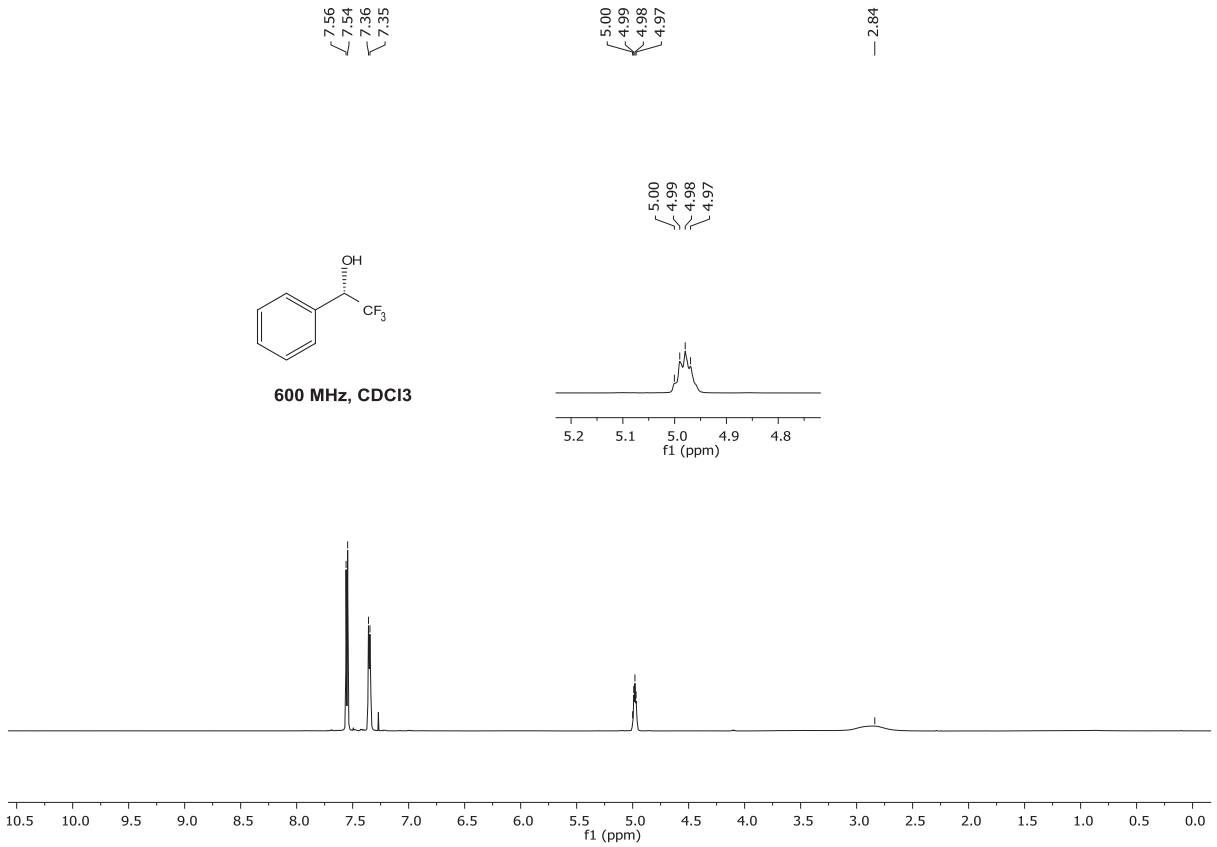
7.56
7.54
7.36
7.35
5.00
4.99
4.98
4.97
2.84
OH
CF3
600 MHz, CDCl3
f1 (ppm)

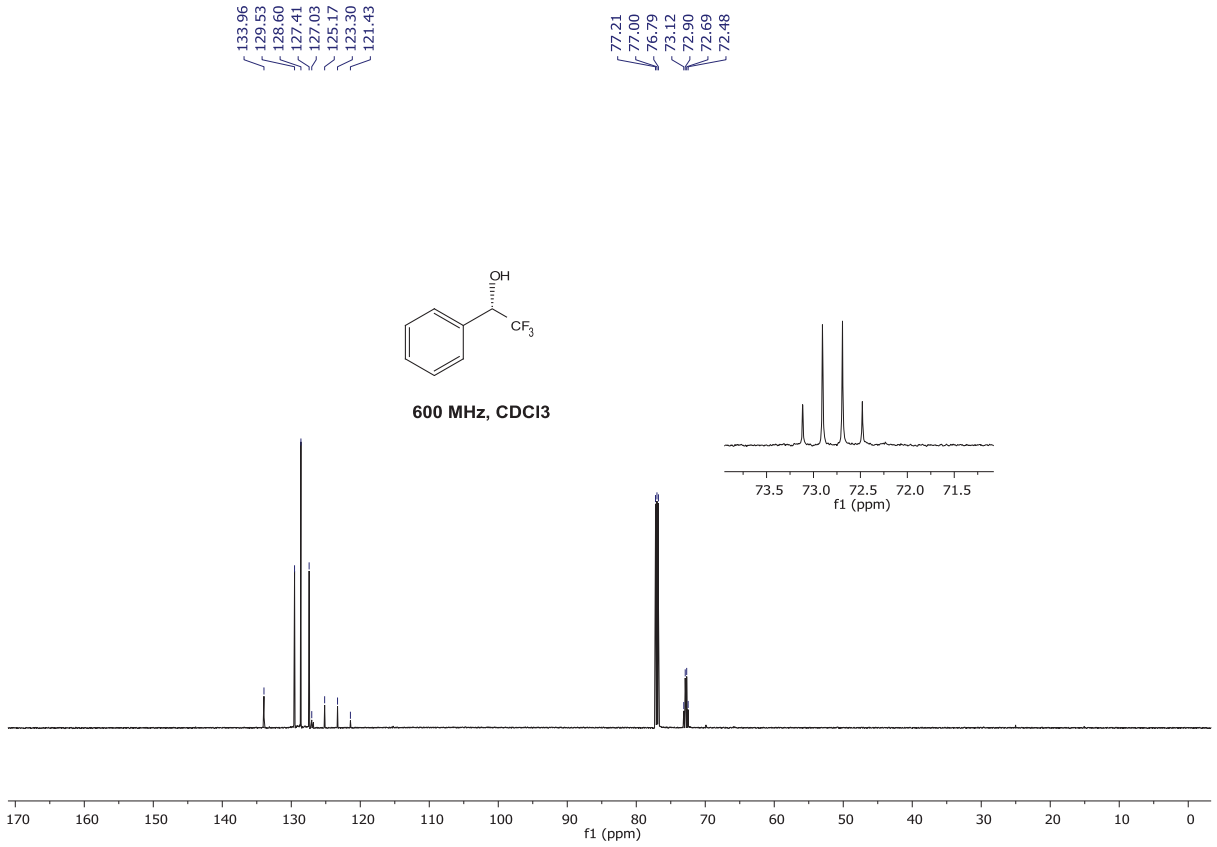
133.96
129.53
128.60
127.41
127.03
125.17
123.30
121.43
77.21
77.00
76.79
73.12
72.90
72.69
72.48
OH
CF3
600 MHz, CDCl3
f1 (ppm)

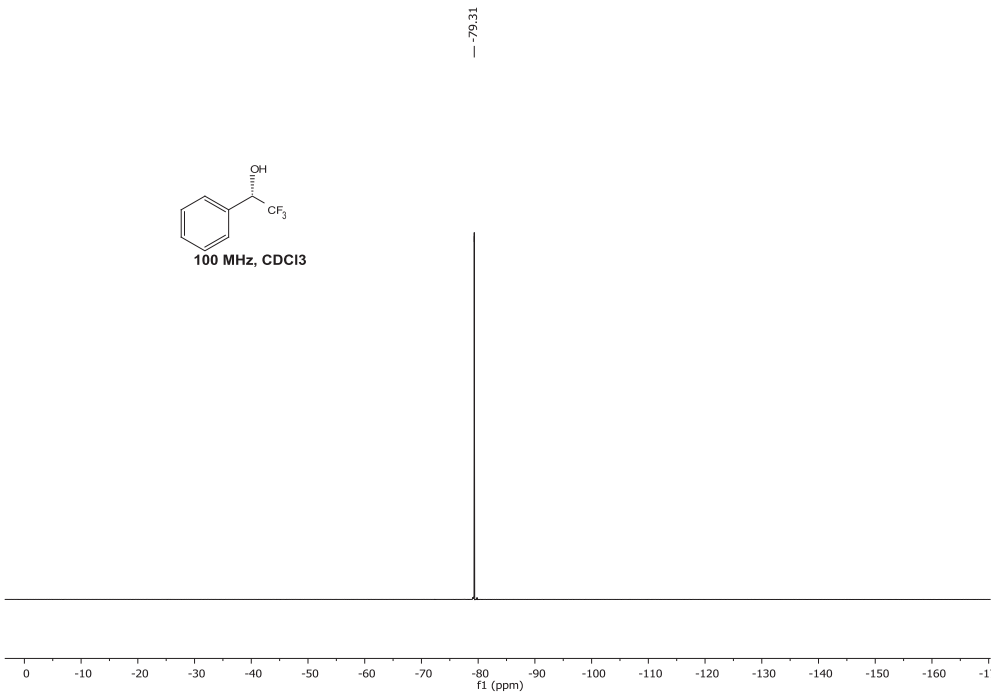

(*S*)-(-)-1-Phenylethane-1,2-diol, 2l. Isolated by chromatography (hexane/AcOEt 80/20), 40% yield. The optical purity of **2l** was assessed by HPLC analysis, using a ChiralART SC column, hexane/2-2-propanol 95/5, flow rate 1.0 ml/min. t_1 20.115 min; t_2 21.322 min., >99% *ee*. $[\alpha]^{20}_{589}$= +65.5 (c = 0.6 g/100ml, $CHCl_3$). The configuration was assigned by comparison with the commercial available (*R*)-(-)-1-phenylethane-1,2-diol.The NMR spectra are in accordance with the reported data.[1]

[1]S. Haubenreisser, T. H. Wöste, C. Martínez, K. Ishihara and K. Muñiz, *Angew. Chemie - Int. Ed.*, 2016, **55**, 413–417.

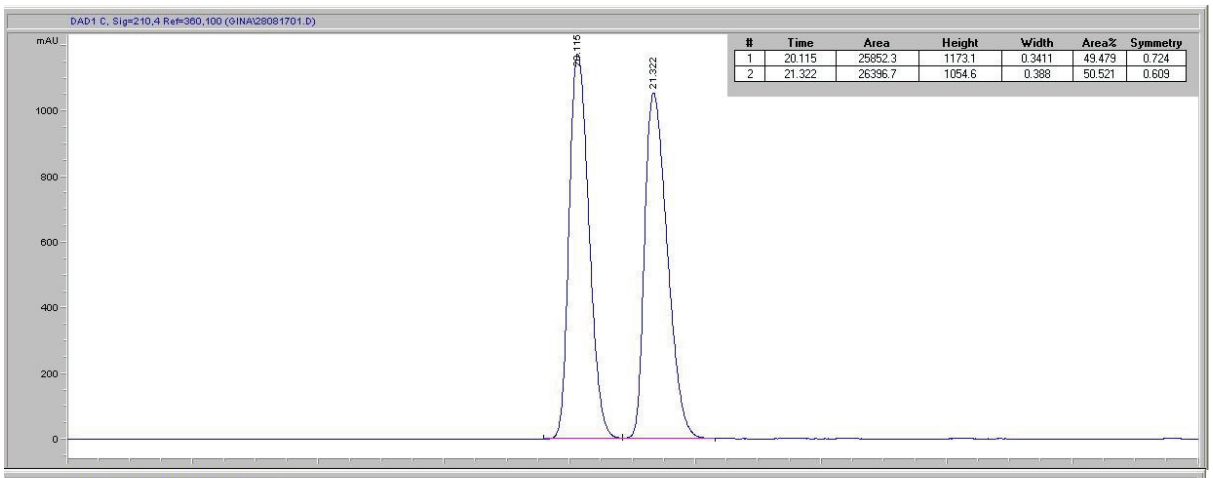
DAD1 C, Sig=210,4 Ref=360,100 (GINA\28081701.D)
mAU
20.115
21.322
Time Area Height Width Area% Symmetry
1 20.115 25852.3 1173.1 0.3411 49.479 0.724
2 21.322 26396.7 1054.6 0.388 50.521 0.609

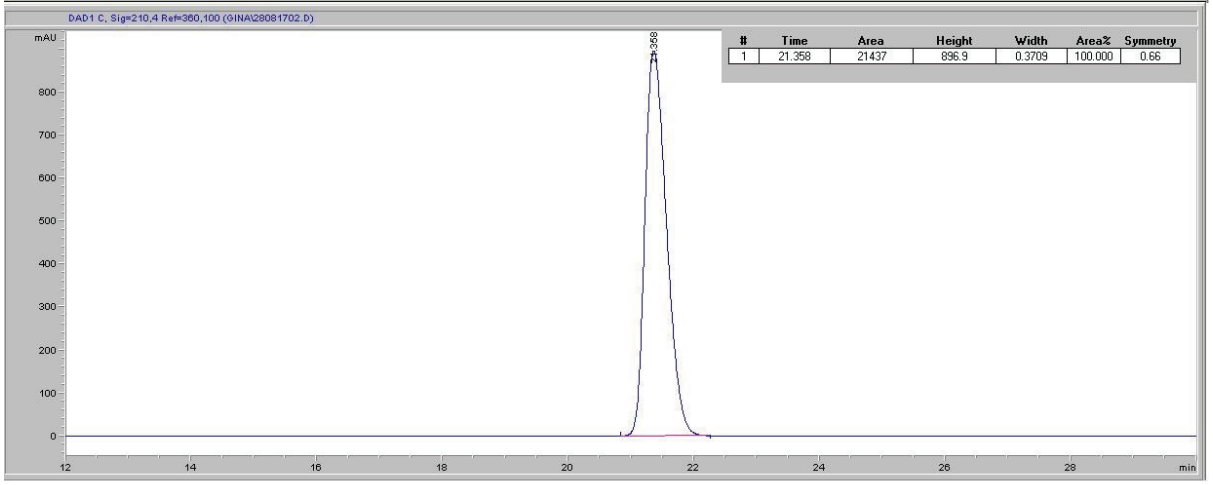
DAD1 C, Sig=210,4 Ref=360,100 (GINA\28081702.D)
mAU
21.358
Time Area Height Width Area% Symmetry
1 21.358 21437 896.9 0.3709 100.000 0.66
min

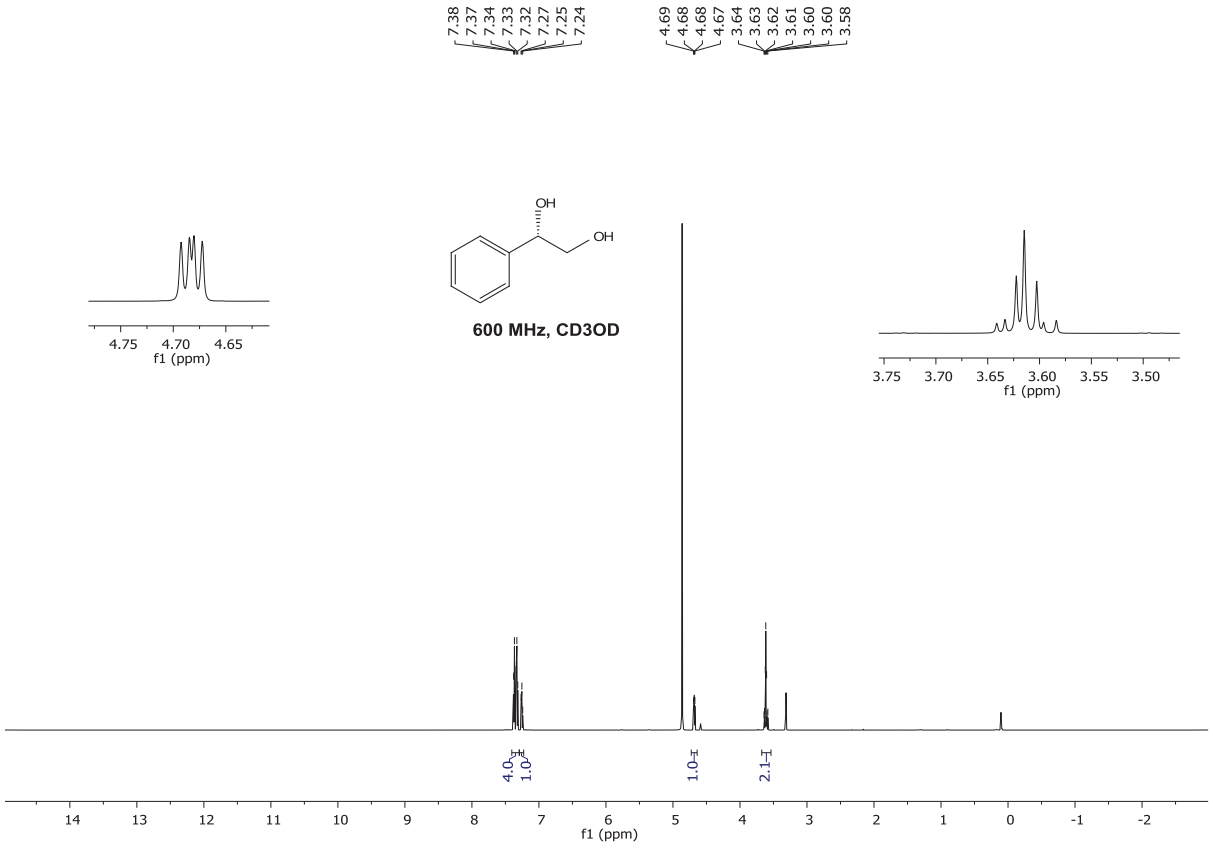
7.38 7.37 7.34 7.33 7.32 7.27 7.25 7.24
4.69 4.68 4.68 4.67 3.64 3.63 3.62 3.61 3.60 3.60 3.58
OH
OH
600 MHz, CD3OD
4.75 4.70 4.65
f1 (ppm)
3.75 3.70 3.65 3.60 3.55 3.50
f1 (ppm)
4.0
1.0
1.0
2.1
f1 (ppm)

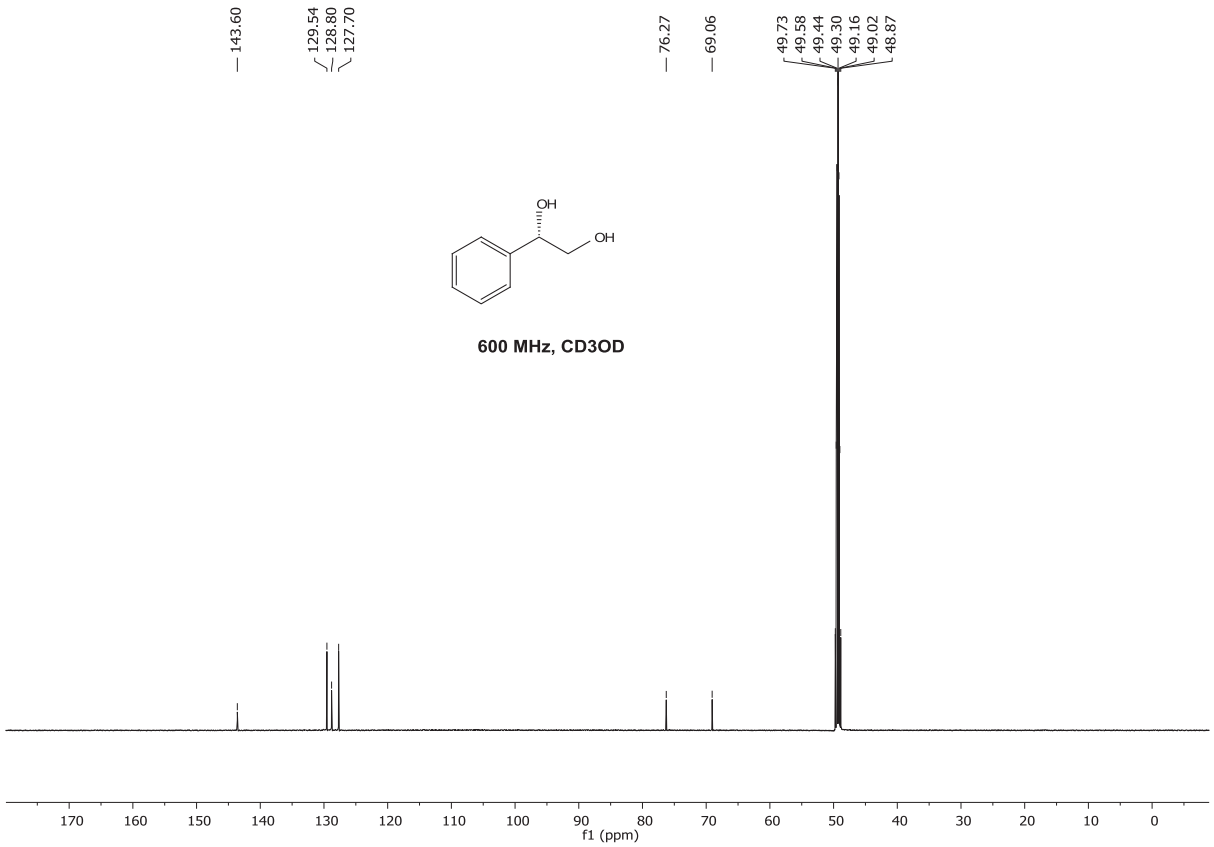

(*R*)-(+)-1-(1-Adamanthyl)ethanol, 2m. PS-Tosyl hydrazine (2.39 mmol/g, 0.6 g) was added to a mixture of the reaction crude (obtained according to the general procedure described in S5) and AcOH (5%) in THF (2 mL). This mixture was stirred for 30min, then filtered and washed with MeOH (8 mL). The compound **2m** was obtained with 71 % yields. The % *ee* of the benzoate derivative, prepared according to the reported procedure, was determined by HPLC analysis, using a ChiralART SA column, hexane/2-2-propanol 97/3, flow rate 0.5 ml/min. t_1 8.144 min; t_2 8.673 min., 79% *ee*. $[\alpha]^{20}_{589}$= +1.25 (c = 0.98 g/100ml, $CHCl_3$). The NMR spectra of **2m** are in accordance with the reported data.[1]

[1]H. N. Hoang, Y. Nagashima, S. Mori, H. Kagechika and T. Matsuda, *Tetrahedron*, 2017, **73**, 2984–2989.

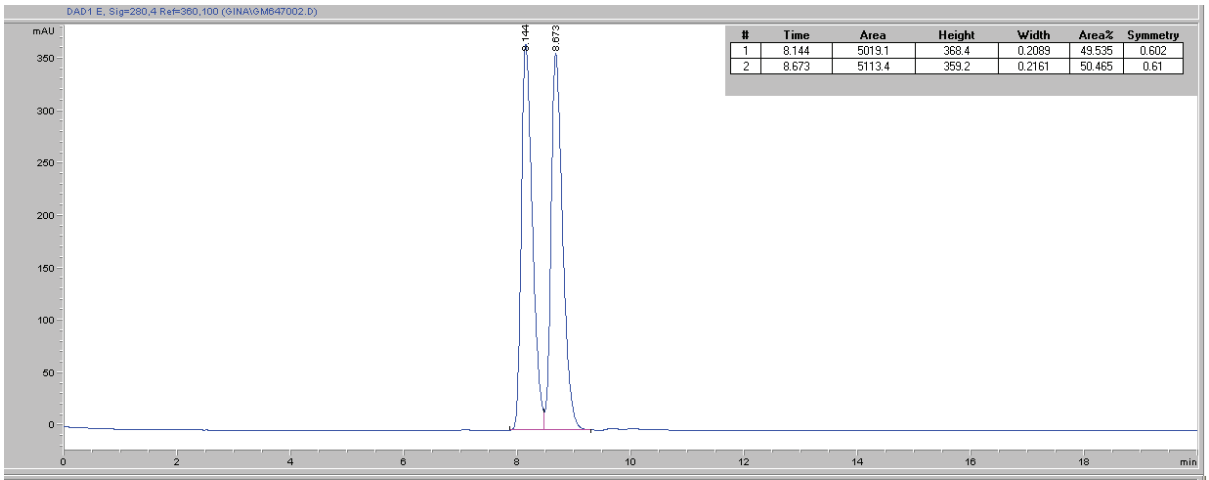

#	Time	Area	Height	Width	Area%	Symmetry
1	8.144	5019.1	368.4	0.2089	49.535	0.602
2	8.673	5113.4	359.2	0.2161	50.465	0.61

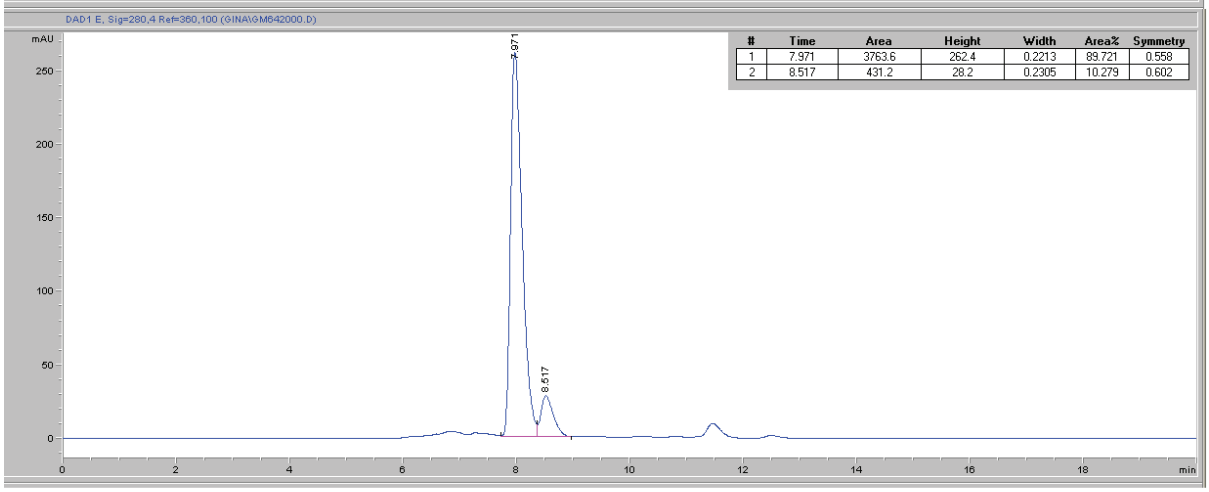

#	Time	Area	Height	Width	Area%	Symmetry
1	7.971	3763.6	262.4	0.2213	89.721	0.558
2	8.517	431.2	28.2	0.2305	10.279	0.602

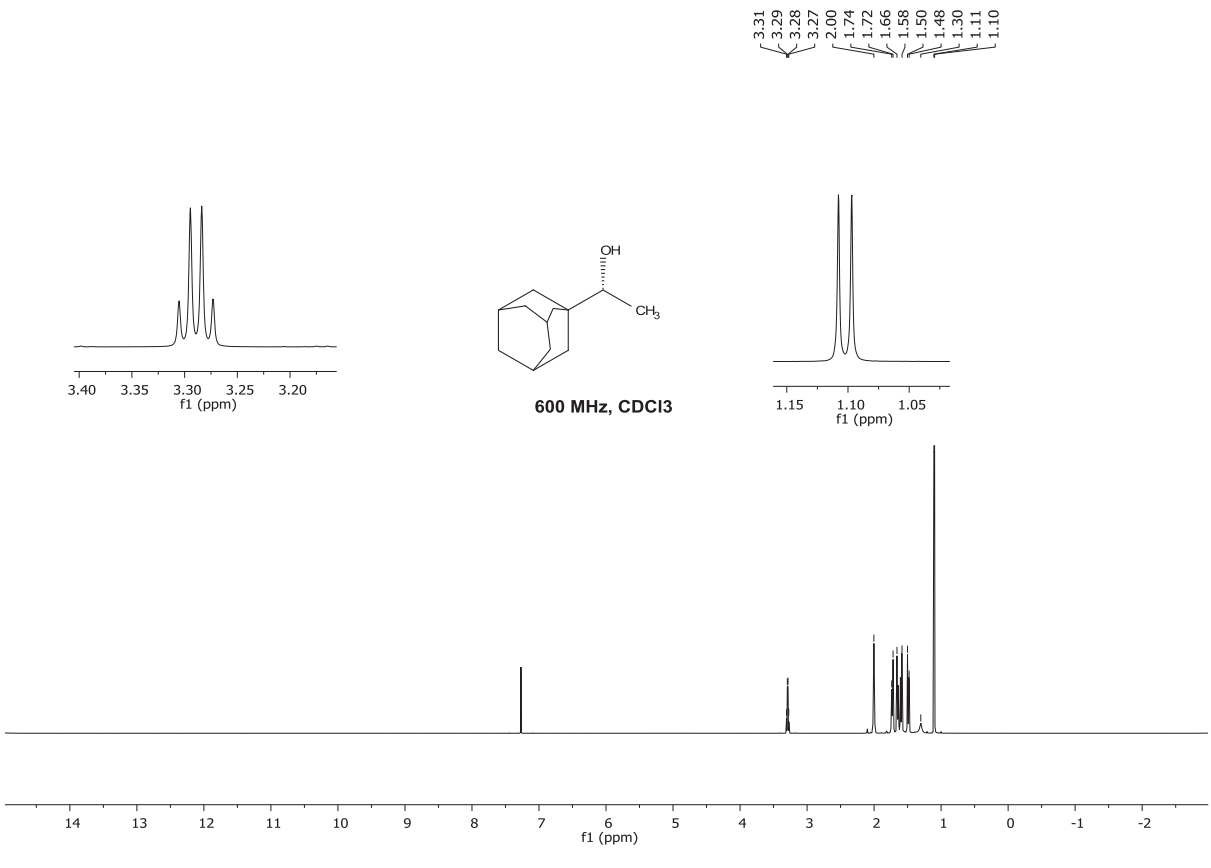

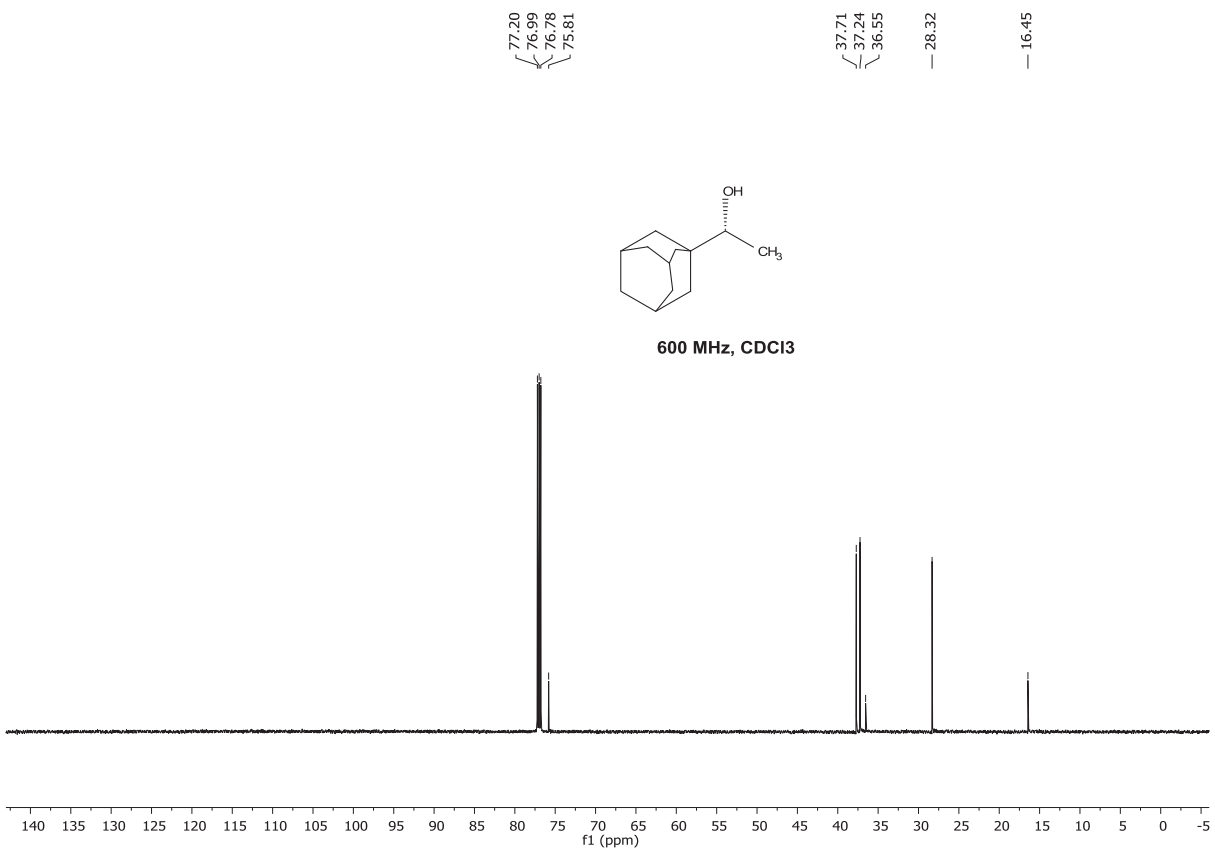

(*R*)-(-)-Benzyl-3-hydroxybutanoate, 2n. Isolated by cromatography (hexane/AcOEt 80/20), 97% yield. The optical purity of **2n** was assessed by HPLC, using a Chiralpak OD-H column, hexane/2-propanol 98/2, flow rate 0.5 ml/min. t_1 50.918 min; t_2 73.901 min, >99% *ee*. $[\alpha]^{20}_{589}$= -30 (c = 0.84 g/100ml, $CHCl_3$). The NMR spectra are in accordance with the reported data.[1]

[1]T. Shiomi, T. Adachi, K. Toribatake, L. Zhou and H. Nishiyama, *Chem. Commun.*, 2009, 5987–5989.

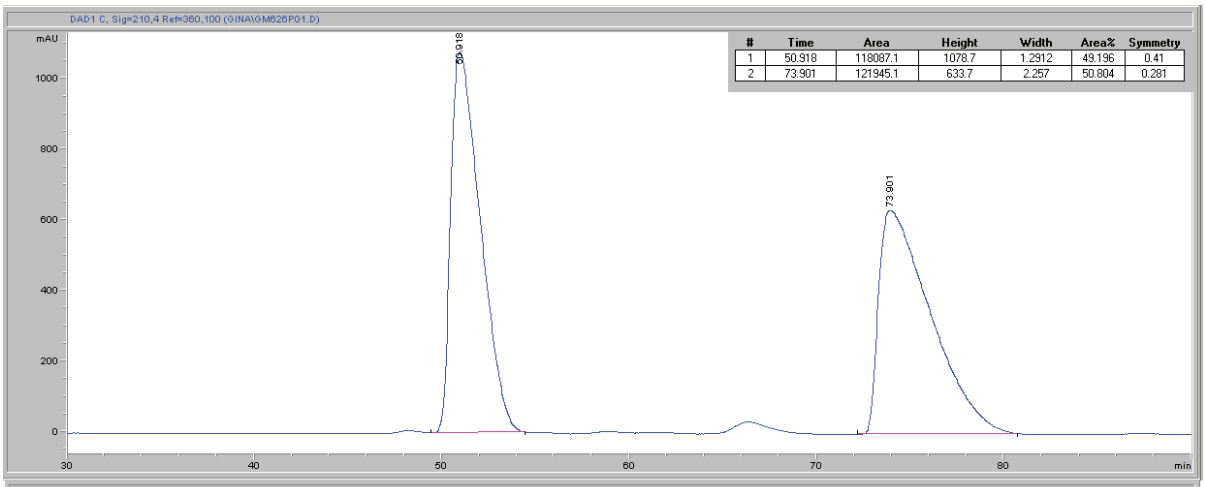
DAD1 C, Sig=210,4 Ref=360,100 (GINA\GM626P01.D)
mAU
1000
800
600
400
200
0
50.918
73.901
30
40
50
60
70
80
min
Time Area Height Width Area% Symmetry
1 50.918 118087.1 1078.7 1.2912 49.196 0.41
2 73.901 121945.1 633.7 2.257 50.804 0.281

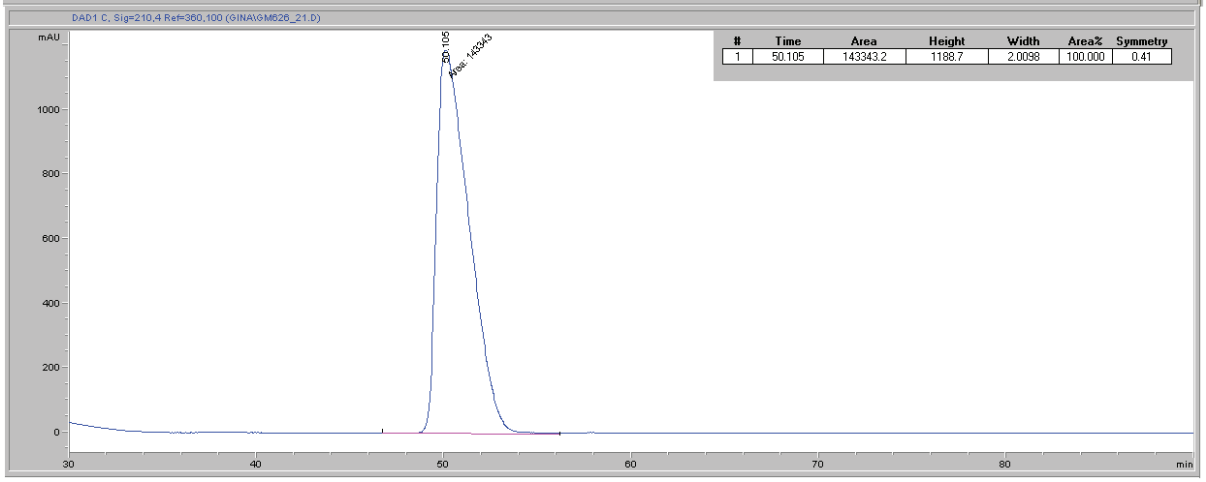
DAD1 C, Sig=210,4 Ref=360,100 (GINA\GM626_21.D)
mAU
1000
800
600
400
200
0
50.105
Area: 143343
30
40
50
60
70
80
min
Time Area Height Width Area% Symmetry
1 50.105 143343.2 1188.7 2.0098 100.000 0.41

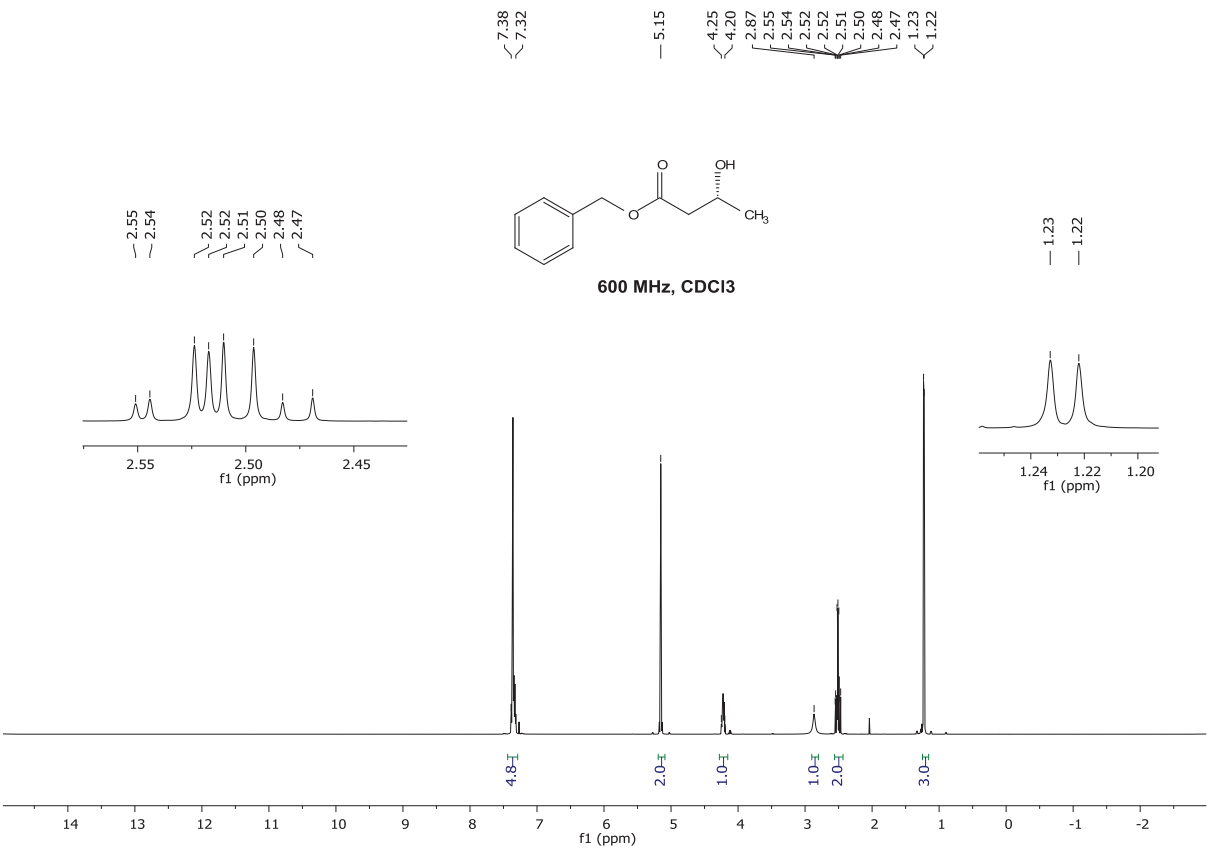
7.38
7.32
5.15
4.25
4.20
2.87
2.55
2.54
2.52
2.52
2.51
2.50
2.48
2.47
1.23
1.22
O
OH
O
CH3
600 MHz, CDCl3
2.55
2.54
2.52
2.52
2.51
2.50
2.48
2.47
1.23
1.22
2.55
2.50
2.45
f1 (ppm)
1.24
1.22
1.20
f1 (ppm)
4.8
2.0
1.0
1.0
2.0
3.0
14
13
12
11
10
9
8
7
6
5
4
3
2
1
0
-1
-2
f1 (ppm)

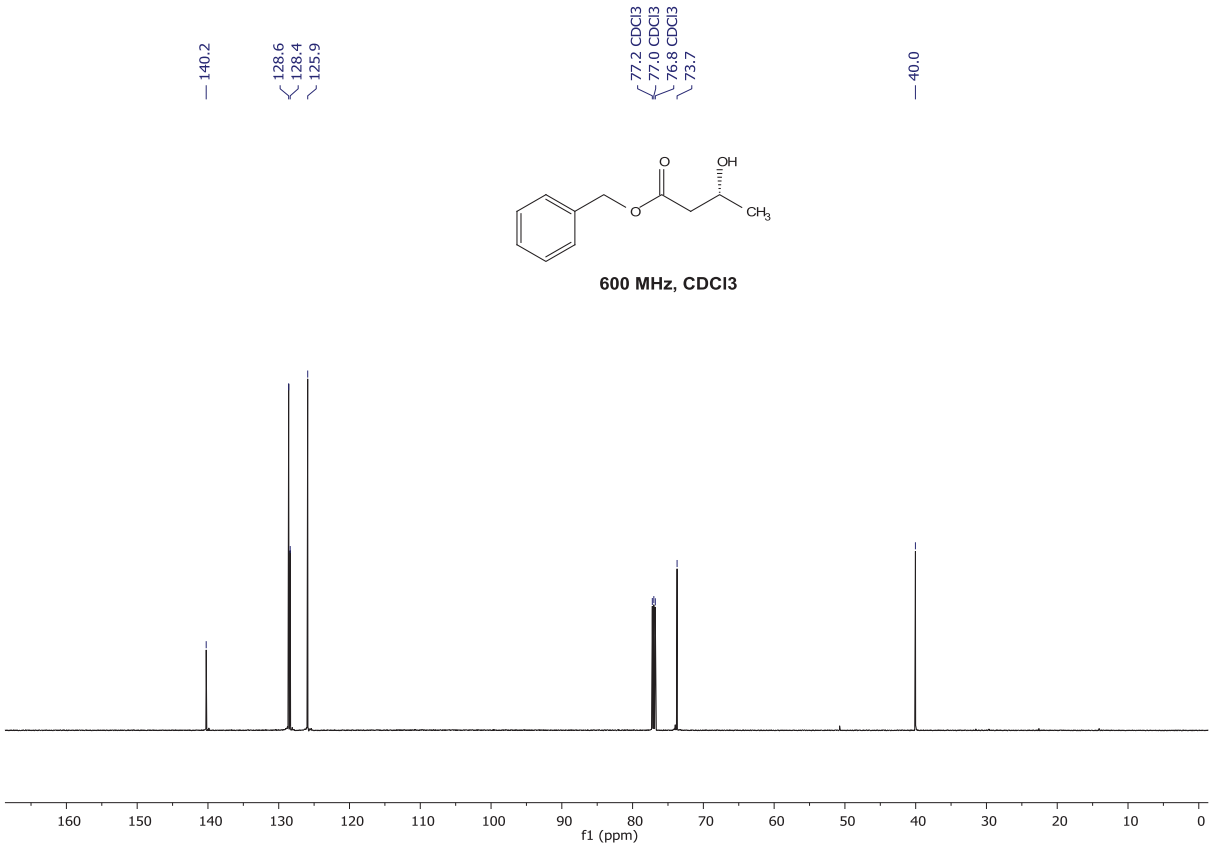

(*R*)-(+)-Phenylbut-3-yn-2-ol, 2o. Isolated by chromatography (hexane/AcOEt 80/20), 99% yield. The optical purity of **2o** was assessed by HPLC, using a ChiralART SB column, hexane/2-2-propanol 95/5, flow rate 0.5 ml/min. t_1 19.469 min; t_2 42.1 min., >99% *ee*. $[\alpha]^{20}_{589}$= +32.4 (c = 0.9 g/100ml, $CHCl_3$). The NMR spectra are in accordance with the reported data.[1]

[1]S. Eagon, C. Delieto, W. J. McDonald, D. Haddenham, J. Saavedra, J. Kim and B. Singaram, *J. Org. Chem.*, 2010, **75**, 7717–7725.

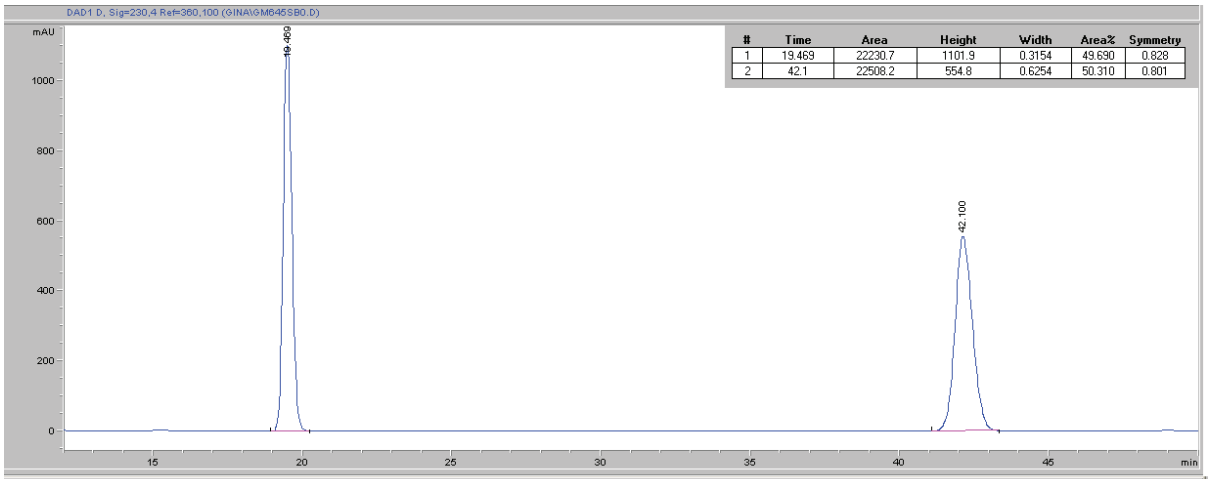

#	Time	Area	Height	Width	Area%	Symmetry
1	19.469	22230.7	1101.9	0.3154	49.690	0.828
2	42.1	22508.2	554.8	0.6254	50.310	0.801

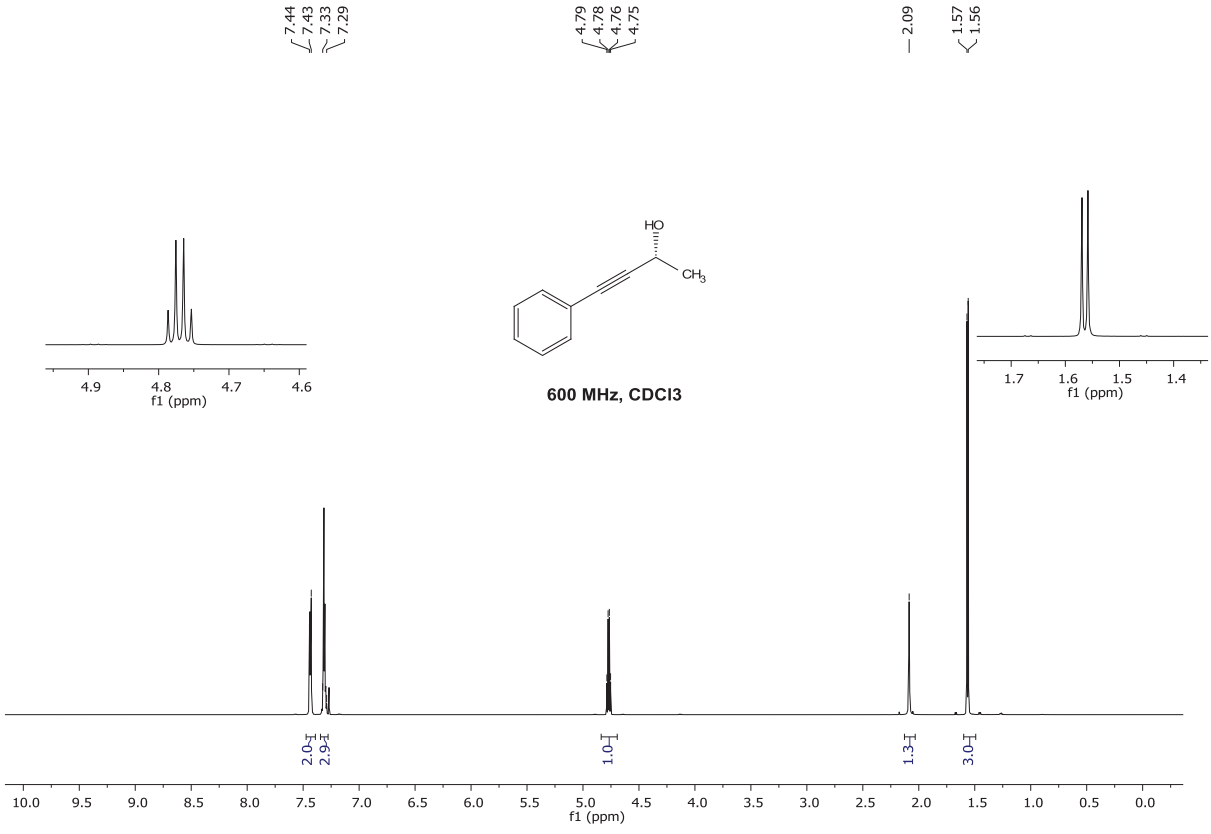

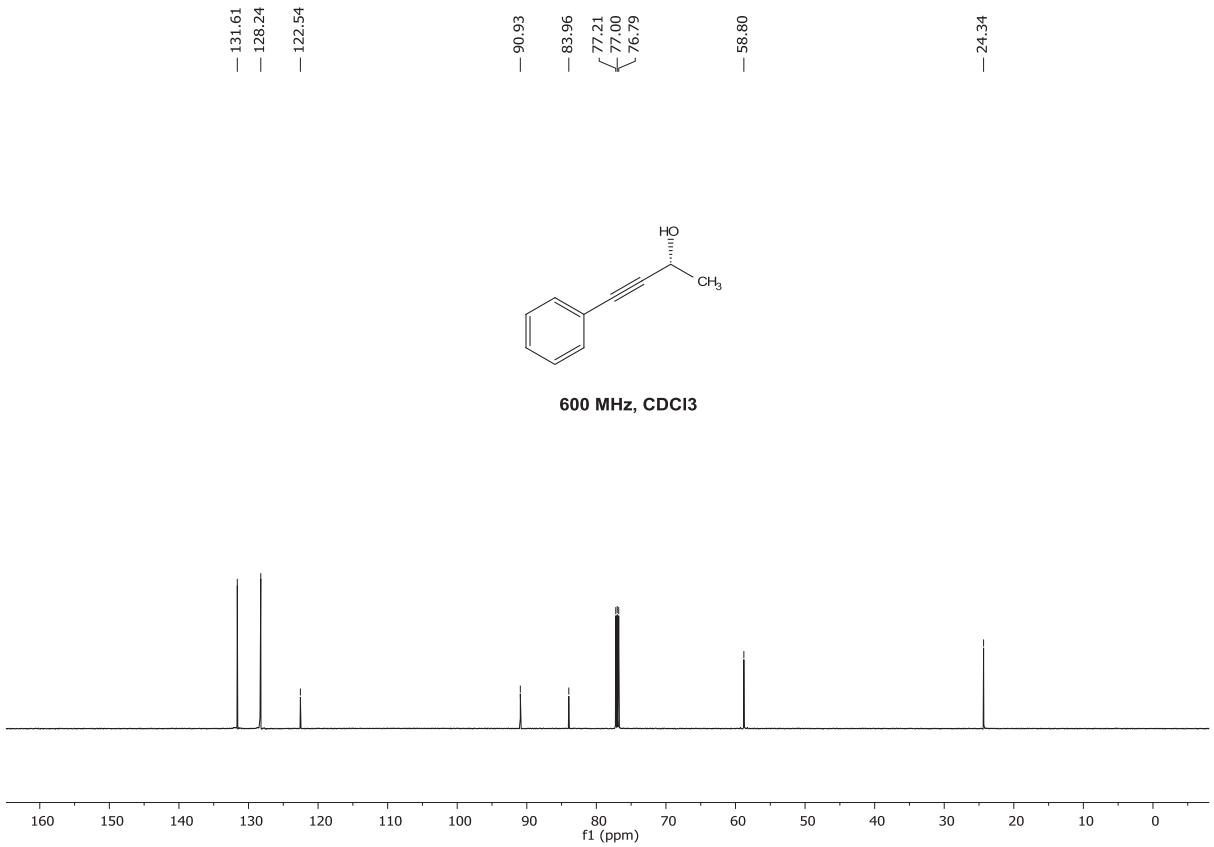

(*S*)-2-Phenyloxirane, 5. Conversion as determined by GC and ^{1}H-NMR, 98% yield. The optical purity of **5** was assessed by GC analysis, using the following method: initial temperature 40 °C hold for 4 min., ramp 15 °C/min to 180 °C hold for 10 min, post run 180 °C for 1 min. (*R*)-isomer, t_R 7.694 min; (*S*)-isomer, t_R 8.109 min., 98% *ee*. The configuration was assigned by comparison with the commercial available (*R*)-(+)-2-phenyloxirane. The NMR spectra are in accordance with the reported data.[1]

[1]W. Li, X. Sun, L. Zhou and G. Hou, *J. Org. Chem.*, 2009, **74**, 1397–1399.

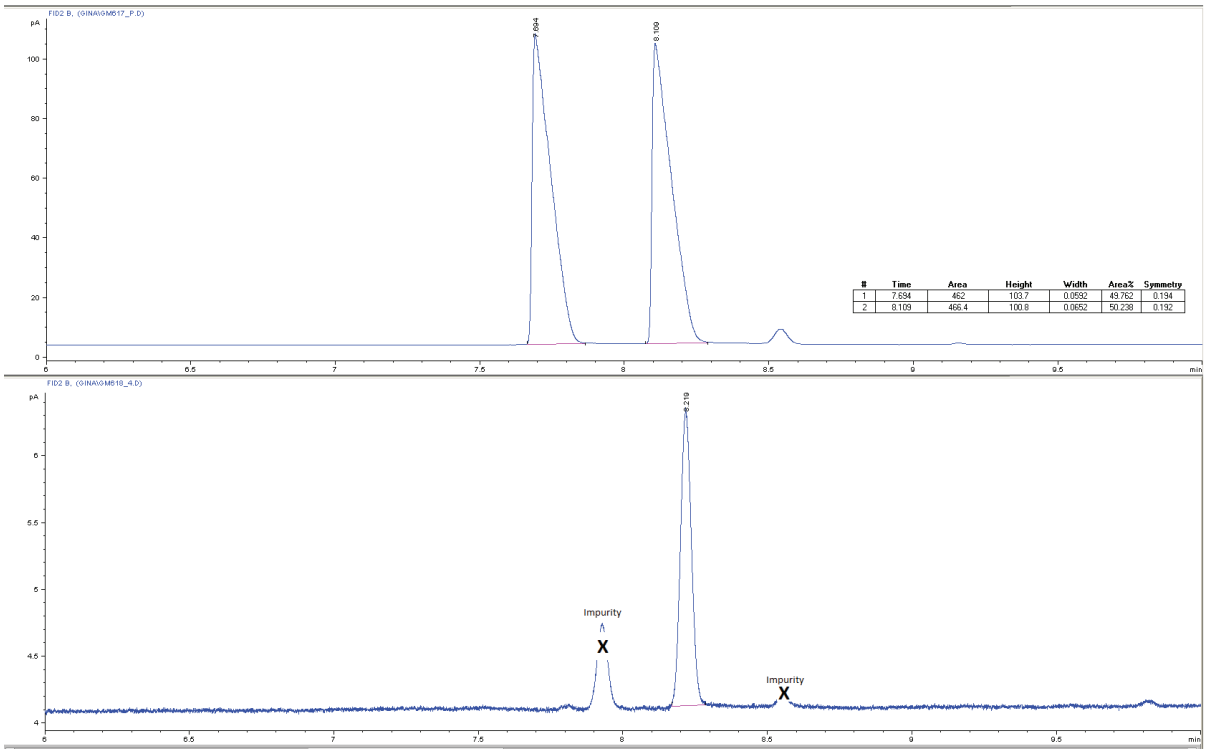

S11. DNA and protein sequences

Primer sequences

Primer 1: tttaagaaggagatatacatATGAAACATCACCATCACCATCACGCAGAAATTGGTACG

Primer 2: tttattcagcagacgataCGCGGCCGCTTTCGCCGC

Primer 3: cagcggcgaaagcggccgcgATGTCTAACCGTTTGGATG

Primer 4: gctttgttagcagccggatcCTATTGAGCAGTGTAGCC

Primer 5: GATCCGGCTGCTAACAAAG

Primer 6: CGCGGCCGCTTTCGCCGC

DNA sequence of *halotag-lbadh*

sequence encoding for the HaloTag^{TM}: green; spacer: red, *Lb*ADH: blue

ATGAAACATCACCATCACCATCACGCAGAAATTGGTACGGGATTTCCGTTTGACCCGCATTATGTG
GAGGTTCTGGGTGAACGCATGCACTACGTGGATGTTGGTCCGCGCGATGGCACACCGGTGCTGTTT
CTGCATGGTAATCCGACCTCCAGCTATGTTTGGCGCAACATTATTCCGCATGTCGCCCCAACGCATC
GCTGTATTGCCCCAGATCTCATTGGCATGGGCAAAAGCGACAAACCGGATTTGGGCTACTTCTTCG
ACGATCACGTACGGTTTATGGACGCCTTTATCGAGGCTCTGGGACTCGAGGAAGTAGTGCTGGTTA
TTCATGACTGGGGCTCTGCATTAGGCTTTCACTGGGCTAAACGGAACCCAGAACGCGTCAAGGGGA
TTGCCTTCATGGAGTTCATCCGTCCGATTCCGACCTGGGATGAATGGCCCGAATTTGCCCGTGAAAC
CTTTCAGGCGTTTCGTACCACGGATGTTGGCCGTAAGCTCATCATCGACCAAAACGTGTTCATTGAG

GGCACTCTTCCCATGGGAGTAGTGCGTCCTTTAACCGAAGTCGAGATGGACCACTATCGCGAACCC
TTCCTGAATCCGGTTGATCGCGAACCGCTGTGGCGCTTCCCGAATGAGCTGCCTATTGCTGGTGAAC
CGGCGAATATCGTGGCACTTGTGGAAGAATACATGGATTGGCTGCATCAGAGTCCAGTCCCTAAGC
TGTTGTTTTGGGGTACACCTGGCGTGTTGATTCCGCCTGCAGAAGCTGCTCGCTTAGCGAAAAGCTT
GCCCAACTGCAAAGCGGTCGATATTGGGCCAGGTCTGAACCTGTTACAGGAGGATAACCCGGATCT
GATCGGGAGTGAAATCGCGCGTTGGCTGTCAACTCTGGAAATCTCGGGTCTTGCAGAAGCAGCGGC
CAAAGAAGCTGCGGCCAAAGAGGCAGCCGCGAAAGAAGCAGCGGCGAAAGCGGCCGCGATGTCT
AACCGTTTGGATGGTAAGGTAGCAATCATTACAGGTGGTACGTTGGGTATCGGTTTAGCTATCGCC
ACGAAGTTCGTTGAAGAAGGGGCTAAGGTCATGATTACCGGCCGGCACAGCGATGTTGGTGAAAA
AGCAGCTAAGAGTGTCGGCACTCCTGATCAGATTCAATTTTTCCAACATGATTCTTCCGATGAAGA
CGGCTGGACGAAATTATTCGATGCAACGGAAAAAGCCTTTGGCCCAGTTTCTACATTAGTTAATAA
CGCTGGGATCGCGGTTAACAAGAGTGTCGAAGAAACCACGACTGCTGAATGGCGTAAATTATTAG
CCGTCAACCTTGATGGTGTCTTCTTCGGTACCCGATTAGGGATTCAACGGATGAAGAACAAAGGCT
TAGGGGCTTCCATCATCAACATGTCTTCGATCGAAGGCTTTGTGGGTGATCCTAGCTTAGGGGCTTA
CAACGCATCTAAAGGGGCCGTACGGATTATGTCCAAGTCAGCTGCCTTAGATTGTGCCCTAAAGGA
CTACGATGTTCGGGTAAACACTGTTCACCCTGGCTACATCAAGACACCATTGGTTGATGACCTACC
AGGGGCCGAAGAAGCGATGTCACAACGGACCAAGACGCCAATGGGCCATATCGGTGAACCTAACG
ATATTGCCTACATCTGTGTTTACTTGGCTTCTAACGAATCTAAATTTGCAACGGGTTCTGAATTCGT
AGTTGACGGTGGCTACACTGCTCAATAG

Amino acid sequence of HaloTag-*Lb*ADH

sequence for the HaloTag™: green; spacer: red, *Lb*ADH: blue

MKHHHHHHAEIGTGFPFDPHYVEVLGERMHYVDVGPRDGTPVLFLHGNPTSSYVWRNIIPHVAPTHRC
IAPDLIGMGKSDKPDLGYFFDDHVRFMDAFIEALGLEEVVLVIHDWGSALGFHWAKRNPERVKGIAFM
EFIRPIPTWDEWPEFARETFQAFRTTDVGRKLIIDQNVFIEGTLPMGVVRPLTEVEMDHYREPFLNPVDR
EPLWRFPNELPIAGEPANIVALVEEYMDWLHQSPVPKLLFWGTPGVLIPPAEAARLAKSLPNCKAVDIG
PGLNLLQEDNPDLIGSEIARWLSTLEISGLAEAAAKEAAAKEAAAKEAAAKAAAMSNRLDGKVAIITGG
TLGIGLAIATKFVEEGAKVMITGRHSDVGEKAAKSVGTPDQIQFFQHDSSDEDGWTKLFDATEKAFGPV
STLVNNAGIAVNKSVEETTTAEWRKLLAVNLDGVFFGTRLGIQRMKNKGLGASIINMSSIEGFVGDPSL
GAYNASKGAVRIMSKSAALDCALKDYDVRVNTVHPGYIKTPLVDDLPGAEEAMSQRTKTPMGHIGEP
NDIAYICVYLASNESKFATGSEFVVDGGYTAQ

2.4 HaloTag-*Pp*BFD in a flow cascade with HaloTag-*Lb*ADH

Results presented in this chapter were published as:

Closing the gap for efficient immobilization of biocatalysts in continuous processes:

HaloTag™ fusion enzymes for a continuous enzymatic cascade towards a vicinal chiral diol

J. Döbber, T. Gerlach, H. Offermann, D. Rother and M. Pohl

Green Chemistry

2018, volume 20, issue 2, pages 544 – 552

DOI: 10.1039/C7GC03225K

Context:

This chapter focuses on the immobilization of a HaloTag-*Pp*BFD variant for the implementation in a two-step continuous cascade with the previously established HaloTag-*Lb*ADH-module. The production of a vicinal chiral diol was targeted by employing consecutive plug-flow reactors, which contained respective biocatalysts. Here, specifically toxicity of benzaldehyde towards the *Pp*BFD variant, different pH-optima, cross-reactivities of the *Lb*ADH with the aldehyde substrates employed in the carboligation step as well as great differences in the catalytic activity of both enzymes had to be managed. The results further prove the usefulness of the HaloTag™ immobilization approach to achieve fast modularization of single reaction steps within reaction sequences and to enhance efficiency of such cascades.

Contributions:

J. Döbber planned and performed the experiments. T. Gerlach helped to identify optimal carboligation conditions by testing different benzaldehyde and acetaldehyde ratios in batch. H. Offermann helped with the hollow fiber module for acetaldehyde removal and with integration of the pH-stat. D. Rother gave valuable input on the cascade set-up. M. Pohl conceptually planned and supervised the project. J. Döbber and M. Pohl wrote the manuscript.

Green Chemistry

PAPER

View Article Online
View Journal | View Issue

Cite this: *Green Chem.*, 2018, **20**, 544

Closing the gap for efficient immobilization of biocatalysts in continuous processes: HaloTag™ fusion enzymes for a continuous enzymatic cascade towards a vicinal chiral diol†

J. Döbber, T. Gerlach, H. Offermann, D. Rother and M. Pohl *

Compartmentalization of biocatalysts is an effective tool to integrate biocatalytic steps in continuous (chemo)enzymatic cascades. Therefore, efficient covalent immobilization techniques are of utmost importance, which enable a fast and selective immobilization of the enzyme directly from crude cell extracts. Here we demonstrate that the HaloTag™ mediates the covalent immobilization of such fusion enzymes in only a few minutes contact time with the respective modified carrier in a packed-bed reactor, thereby enabling enzyme immobilization directly in the flow setup. In this study, we evaluated this concept for a continuous enzymatic cascade towards a chiral vicinal diol by combining a variant of the benzoylformate decarboxylase from *Pseudomonas putida* (*Pp*BFD) and the alcohol dehydrogenase from *Lactobacillus brevis* (*Lb*ADH). Limitations in *Pp*BFD stability were overcome by optimization of buffer salt, cofactor concentration and choice of a different substrate. For optimal *Lb*ADH activity, excess acetaldehyde was removed in-line. This optimization lead to a high operational stability of the individual cascade steps up to several weeks and resulting in the efficient stereoselective production of (1*S*,2*S*)-1-phenylpropane-1,2-diol with high conversion up to 99%, high stereoselectivities (ee/ic) up to 96% and space–time yields up to 1850 g L^{-1} d^{-1}.

Received 28th October 2017,
Accepted 22nd December 2017

DOI: 10.1039/c7gc03225k

rsc.li/greenchem

1 Introduction

In the last two decades, continuous processes were developed as an advanced modular concept for the multistep synthesis of chemical compounds. The high level of safety, the possibility for automation, and profound process reliability has made continuous processes appealing not only for industry. Furthermore, continuous flow chemistry has compelling advantages over traditional batch reactions especially in the field of multistep synthesis, where a high degree of process control is required to prevent undesired formation of by-products.[1,2] With the help of flow concepts, reactants can precisely be introduced into the system at the required time and place and intermediate product work-up becomes unnecessary.

In a certain way, multistep synthesis in flow mimics basic biological principles since metabolic pathways rely on compartmentalization of biocatalysts and a constant flux of metabolites between them.[3] Nowadays, the implementation of such enzymatic cascades for the production of valuable compounds and especially the artificial combination of different biocatalysts have become a key concept in the field of biocatalysis.[4] However, only few examples of artificial enzymatic cascade reactions have been conducted in a continuous mode[5,6] and the majority of reports describes continuous single-step enzymatic transformations.[4,7–11]

Despite enzymatic single-step or cascade reactions, the effective retention of the active biocatalyst in a defined compartment is decisive and represents the major bottleneck for the broad implementation of biocatalysis in continuous processes. The simplest approach would be the retention of whole recombinant cells carrying the desired biocatalyst.[12] However, the natural cell membrane constitutes an additional diffusion barrier that could hamper the passage of certain substrates and products. Furthermore, undesired by-products can be formed through other catalytic activities present in the host cell. In contrast, the immobilization of pure enzymes often requires expensive and time-consuming chromatographic purification steps. Afterwards, the purified enzyme can be immobilized in different ways including binding to a carrier, cross-linking, and entrapment.[13] Here, covalent immobilization strategies are preferred over non-covalent interactions since a more stable immobilization with reduced enzyme leaching is

IBG-1: Biotechnology, Forschungszentrum Jülich GmbH, D-52425 Jülich, Germany. E-mail: ma.pohl@fz-juelich.de; Fax: +49-2461-613870; Tel: +49-02461-614388

†Electronic supplementary information (ESI) available. See DOI: 10.1039/c7gc03225k

achieved. However, covalent immobilization concepts are often based on for example randomized cross-linking approaches including cross-linking agents such as glutaraldehyde[14] or epoxy-activated resins.[15,16] Therefore, strategies using a targeted immobilization concept are to be preferred, since they enable a homogeneous spatial orientation of the enzyme on the carrier and a minimal influence on its activity through a maximal distance between immobilization site and active site.

One targeted approach is the application of an epoxy-modified resin, carrying additional metal ion-chelator groups for the selective binding of a His-tagged enzyme from crude cell extracts followed by subsequent covalent immobilization *via* the epoxy groups.[17] Such concepts were recently successfully investigated for continuous flow applications but the covalent immobilization step required up to 24 h incubation time at low temperature (4 °C).[9]

In comparison, the commercially available HaloTag™ system (Promega) represents a promising alternative for the one-step purification and immobilization of enzymes directly from crude cell extracts. The HaloTag™ is a variant of the haloalkane dehalogenase from *Rhodococcus* spec. and generates a covalent ester bond to matrices carrying a terminal chloroalkane residue (Scheme 1).[18] Recently, we have demonstrated the usefulness of this fusion tag for biocatalysis using the thiamine diphosphate (ThDP)-dependent enzyme benzaldehyde lyase from *Pseudomonas fluorescens* (*Pf*BAL) as an example. We could demonstrate the fast immobilization directly from crude cell extracts within minutes at room temperature and the usefulness of this concept for the efficient recycling of the immobilized biocatalyst.[18] The fast immobilization subsequently motivated us to use the technology for a direct loading of a plug-flow reactor in flow immediately prior to the desired reaction. This was just recently demonstrated using a HaloTag fusion of *Lactobacillus brevis* alcohol dehydrogenase (*Lb*ADH[19]) in flow for the reduction of a broad range of aromatic ketones to the corresponding secondary alcohols. Regeneration of the expensive redoxcofactor NADPH was successfully realized using 2-propanol as a cosubstrate which is oxidized to acetone by the *Lb*ADH thereby recycling the redoxcofactor through reduction of $NADP^+$.[20,33]

Here we demonstrate coupling of the recently optimized *Lb*ADH module to a biocatalytic carboligation step in flow, thereby emphasizing the modular concept. In the first step, a variant of the thiamine diphosphate (ThDP)-dependent benzoylformate decarboxylase from *Pseudomonas putida* (*Pp*BFD L476Q)[21,22] with enhanced carboligase activity as well as improved stereoselectivity compared to the wild-type enzyme was used to produce the intermediate product (*S*)-2-hydroxy-1-phenylpropane-1-one ((*S*)-HPP), which was subsequently reduced to (1*S*,2*S*)-1-phenylpropane-1,2-diol ((*S*,*S*)-PPD) using the *Lb*ADH (see Scheme 2). A similar reaction cascade using wildtype *Pp*BFD and *Lb*ADH has earlier been described using sequential batch reactions.[23,24] Besides, the respective 2-step cascade was successfully realized in batch using both enzymes as whole cell biocatalysts.[25]

In this study, we point out the immobilization of both enzymes directly from crude cell extract on HaloLink™ Resin in plug-flow reactors followed by the optimization of the 2-step flow cascade using reaction engineering to enhance the stability of the *Pp*BFD variant in flow, to increase the product concentration, and to cope with cross-reactivity of the *Lb*ADH with excess acetaldehyde from the first carboligation step. The optimized cascade resulted in the formation of the target product (1*S*,2*S*)-1-phenylpropane-1,2-diol (*S*,*S*-PPD) with high stereoselectivity and high space-time yields.

2 Results and discussion

2.1 Production and characterization of fusion enzymes

The HaloTag™ was genetically fused to the N-terminus of both enzymes resulting in the fusion enzymes HaloTag-*Pp*BFD L476Q and HaloTag-*Lb*ADH. The N-termini were chosen based on the crystal structures in both cases as an appropriate fusion site, because such constructs offered a maximal distance between active site and the immobilization site. To test potential negative effects of the HaloTag™, first experiments concerned the recombinant enzyme production in *E. coli* BL21 (DE3). As was already recently described for the tetrameric HaloTag-*Pf*BAL[26] and HaloTag-*Lb*ADH,[34] also the production

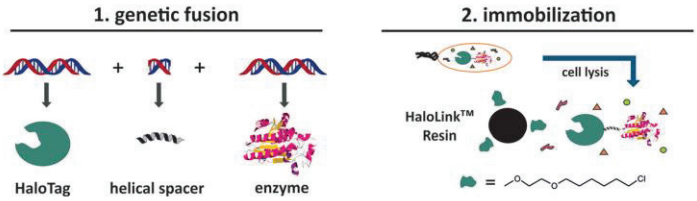

Scheme 1 The HaloTag™ concept for immobilization of enzymes. The DNA encoding for the HaloTag is fused to the DNA encoding the target enzyme. In this study, we additionally used a spacer consisting of a helix forming peptide sequence to separate the HaloTag from the enzyme. The resulting fusion enzyme is produced in *E. coli* cells and immobilization is directly performed from *E. coli* crude cell extracts. Immobilization was performed on commercially available HaloLink™ Resin (Promega) which consists of a sepharose carrier (indicated in black) exposing chloroalkane residues (indicated in green). Such chloroalkane residues are specifically recognized by the HaloTag and a covalent bond is established for immobilization of fusion enzymes.

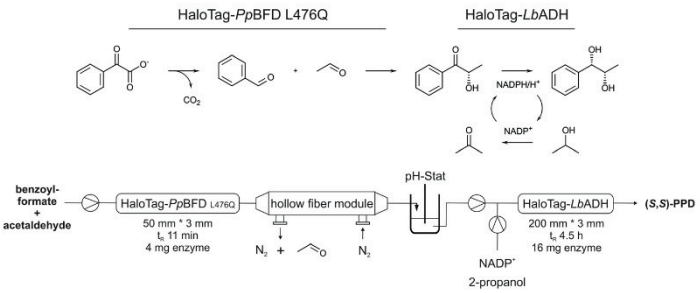

Scheme 2 Enzymatic 2-step cascade for the continuous production of (*S*,*S*)-PPD. In the first step, catalyzed by immobilized HaloTag-*Pp*BFD L476Q, benzoylformate is decarboxylated to benzaldehyde and carbon dioxide. The resulting benzaldehyde is then further converted to (*S*)-HPP by a carboligation in the presence of excess acetaldehyde. Afterwards, residual acetaldehyde is removed by membrane-supported stripping using a hollow fiber module and the pH is automatically adjusted to pH 7.0 with a pH-Stat. In the second step catalyzed by immobilized HaloTag-*Lb*ADH, (*S*)-HPP is reduced to (*S*,*S*)-PPD under consumption of NADPH, which is produced from the cheaper oxidized cofactor $NADP^+$ using 10 vol% 2-propanol as a cosubstrate for cofactor regeneration. See Fig. S2 in the ESI† for more information on the setup.

of the tetrameric HaloTag-*Pp*BFD L476Q was not negatively influenced by the fusion despite the high molecular weight of the HaloTag (33 kDa), which is demonstrated by the intense protein bands in samples of the crude cell extracts using SDS PAGE analysis (Fig. 1). This observation is in line with previous reports showing that the HaloTag does generally not negatively influence the production of fusion proteins.[27] Rather its beneficial effect on the recombinant production and the solubility of the fusion partner have been reported.[28]

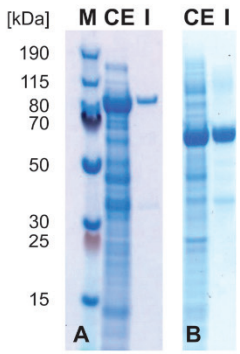

Fig. 1 Production of HaloTag fusion enzymes and purity after immobilization in flow from crude cell extracts. A: HaloTag-*Pp*BFD L476Q (93 kDa per monomer); B: HaloTag-*Lb*ADH (63 kDa per monomer) (modified from ref. 34); M: PageRuler™ plus prestained protein standard (thermo scientific); CE: crude cell extract after production of HaloTag fusion enzymes in *E. coli* BL21 (DE3); I: shows the respective protein fraction immobilized in flow on 10 mg of wet HaloLink™ resin after cleavage of the covalently bound enzyme through saponification (see experimental 4.2).

Afterwards, both fusion enzymes were immobilized on HaloLink™ Resin in batch to compare the initial rate activities of the immobilizates and the free reference enzymes without tag (Fig. 2). For HaloTag-*Pp*BFD L476Q a residual activity of 65% was found. This is in line with earlier results obtained for the similar ThDP-dependent enzyme HaloTag-*Pf*BAL (60%)[26] but significantly higher compared to the residual activity of HaloTag-*Lb*ADH (35%).[34] In general, an activity loss after immobilization is often observed probably due to the reduced degree of flexibility caused by the fixation to a solid support. Therewith inactivation observed *via* the HaloTag™ is in the same range as for other covalent immobilization methods.[15,29–31] In the present case, the tetrameric quaternary structure of the enzymes has to be considered as well.

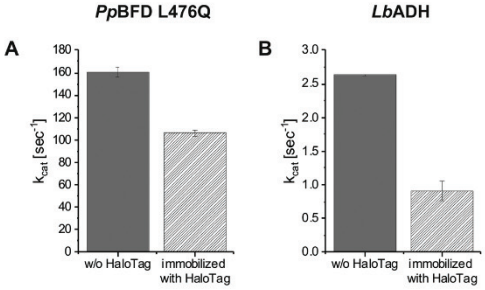

Fig. 2 Activity of immobilized HaloTag fusion enzymes. Initial rate activities (given in k_{cat} [sec^{-1}]) of immobilized fusion enzymes were compared to the activity of the non-immobilized reference enzyme without HaloTag. A: HaloTag-*Pp*BFD L476Q: the decarboxylation of benzoylformate was measured (see section 4.3). B: HaloTag-*Lb*ADH: the reduction of benzaldehyde was followed (see section 4.3) (data was previously determined[34]). Error bars represent the variance of three activity measurements from the same sample.

Consequently, each tetramer carries four individual HaloTags, which may cause a steric hindrance accompanied with a loss of activity. Since *Pf*BAL and *Pp*BFD share the same size (*ca.* 60 kDa per subunit) and quaternary structure, the HaloTag™ making up more than one third of the total size of these fusion enzymes, obviously influences the residual activity after immobilization of *Pf*BAL and the *Pp*BFD variant similarly. Besides, the subunits of *Lb*ADH are with 30 kDa only half of the size and here the HaloTag™ makes up more than one half of the size of the fusion enzyme. Thus, the influence of the tag seems to depend on the overall structure of the fusion enzyme as well as the relative sizes of both fusion partners. However, in both cases active fusion enzymes were obtained, demonstrating the generic concept of the HaloTag strategy.

2.2 Immobilization in flow

Due to the high affinity of the HaloTag™ to terminal chloroalkane groups as for example exposed on the HaloLink™ Resin,[26] we aimed for the direct immobilization of both enzymes in flow as was already previously shown.[34] For this purpose, HaloLink™ Resin was filled into two Omnifit® columns for the preparation of a biocatalytic packed-bed reactor (PBR). Then, the crude cell extracts containing the respective HaloTag™ fusion enzyme were pumped through the respective reactor with a residence time of about 11 min (see section 4.2). After washing, the resin was analyzed to evaluate the purity as well as the amount of bound fusion enzyme on the carrier. As shown in Fig. 1, the immobilizates (I) contained predominantly the target enzymes with only minimal impurities. For both enzyme immobilizates the same contaminating protein band (*ca.* 30 kDa) was found, which fits well to the size of the HaloTag (33 kDa). Since the tag was fused N-terminally to both enzymes, the formation of truncated fusion enzymes during the recombinant production may explain this result.

In total, 4 mg of HaloTag-*Pp*BFD L476Q and 4 mg of HaloTag-*Lb*ADH bound to 360 mg of wet HaloLink™ Resin inside the reactor, indicating the successful one-step purification and covalent immobilization in flow directly from crude cell extracts. Although the same enzyme mass (4 mg) was immobilized in both columns, 1.4-times more HaloTag-*Lb*ADH was bound on a molar basis due to the differences in the molecular weight as discussed above. Probably, the size of the fusion enzyme influences the total enzyme loading since neighboring chloroalkane ligands exposed on the carrier surface may be sterically blocked by big fusion enzymes.

Tag-based immobilization approaches for continuous reaction setups were just recently also evaluated by other groups.[6,9] For example, Peschke *et al.* evaluated a set of different orthogonal tags and successfully implemented a continuous enzymatic cascade consisting of different oxidoreductases in a microfluidic device. Therefore, the authors immobilized the enzymes on magnetic beads prior to loading the microfluidic reactor with the beads.[6] In this study with HaloTag fusion enzymes we developed this concept further, demonstrating the fast immobilization of different enzymes inside packed-bed reactors directly from crude cell extracts. The same protocol for immobilization can be applied for different enzymes without further need for optimization and without complex equipment.

2.3 The first cascade step towards (*S*)-HPP

The first cascade step includes the stereoselective carboligation of benzaldehyde and acetaldehyde towards (*S*)-2-hydroxy-1-phenylpropane-1-one ((*S*)-HPP) catalyzed by the HaloTag-*Pp*BFD L476Q (see Scheme 2). The reaction was conducted in aqueous buffer (see section 4.5), where the solubility of benzaldehyde is limited to around 40 mM. In preliminary experiments, we determined that at least a three-fold excess of acetaldehyde (120 mM) is needed to obtain maximal activity and a high conversion to (*S*)-HPP (data not shown). As demonstrated in Fig. 3, the first continuous carboligation step gave 99% conversion in the first 24 h, before the conversion dropped drastically. In a first hypothesis, we assumed an inactivating effect of both aldehydes on the activity of the *Pp*BFD variant. However, preliminary results pointed towards a much higher impact of benzaldehyde in comparison to acetaldehyde (data not shown). To reduce the benzaldehyde concentration inside the PBR, benzoylformate was used as an alternative substrate, which is *in situ* decarboxylated to benzaldehyde by the same enzyme.[21] Consequently, the benzaldehyde concentration inside the reactor would be constantly low since arising benzaldehyde would directly be converted to (*S*)-HPP. However, as demonstrated in Fig. 3, the stability of the enzyme increased only slightly by this approach, indicating negative influences of further factors. The next hypothesis concerned the applied *Pp*BFD-variant, which was identified from two different screenings of a random mutagenesis library.[21,22] One was targeted towards the better acceptance of *ortho*-substituted benzal-

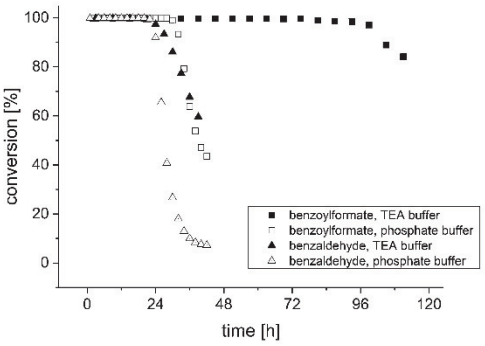

Fig. 3 Stability of immobilized HaloTag-*Pp*BFD L476Q in continuous processes. The continuous carboligation starting from benzaldehyde or benzoylformate (40 mm), respectively, and acetaldehyde (120 mm) towards (*S*)-HPP was analyzed in the presence of different buffering compounds (potassium phosphate and triethanolamine (TEA), each 50 mM, pH 7.0). The corresponding substrate solution was passed with a residence time of 11 min through a 5 cm Omnifit® column containing 4 mg of immobilized HaloTag-*Pp*BFD L476Q.

dehydes for the production of (*S*)-2-HPP derivatives[21] and the second was performed to increase the carboligase activity of wild type (wt) *Pp*BFD towards (*S*)-2-HPP.[22] From both screenings, variant L476Q was one of the best hits, revealing also a significant higher stereoselectivity of 96% for the mixed carboligation of benzaldehyde and acetaldehyde compared to the wt enzyme (83% ee[22,32]). However, up to now this improved *Pp*BFD-variant was not applied in further carboligation studies. Thus, stability studies under reaction conditions were missing. Position 476 is part of a loop close to the ThDP-binding site. It was assumed that the higher carboligase activity of this variant originated from a higher flexibility of this loop induced through the mutation L476Q. However, the same effect could also impair the ThDP-binding.[21]

For wt*Pp*BFD the loss of cofactor in cofactor-free phosphate buffer was earlier shown to reduce the enzyme half-life from 36 days to 3 days in the absence of aldehyde substrates, which further impair the stability.[32] Under these conditions the L476Q-variant exhibited a half-life of only 150 min.[21] Since the cofactor ThDP is bound noncovalently in the active site *via* the diphosphate group, we hypothesized that the use of phosphate buffer might destabilize the binding of ThDP additionally through a competitive effect caused by the phosphate buffer. Therefore, the phosphate buffer was exchanged against triethanolamine (TEA) buffer. As shown in Fig. 3, this and the use of benzoylformate had a strong stabilizing effect while the combination of benzaldehyde and triethanolamine buffer did not enhance the stability markedly. With the optimal combination of benzoylformate and triethanolamine buffer, continuous production with a conversion higher than 99% and an ee >96% was possible for up to 4 days.

In a next step, the substrate concentration was increased to 100 mM benzoylformate and 300 mM acetaldehyde, which was possible due to the considerably better solubility of benzoylformate in aqueous solutions compared to benzaldehyde. As a result, the continuous production of (*S*)-HPP dropped again after 24 h, which is shown in Fig. 4. Most probably, the increased amount of benzoylformate led to higher concentrations of benzaldehyde, which consequently inactivated the *Pp*BFD variant faster. To stabilize the enzyme, the ThDP concentration in the buffer was increased from 0.15 mM to 1 mM since the stability of ThDP-binding seemed to be crucial for the L476Q-variant. As demonstrated in Fig. 4, this modification led to a significant stabilization of the *Pp*BFD variant enabling finally the continuous production of (*S*)-HPP (>96% ee) with almost full conversion for 3 days starting from 100 mM benzoylformate and 300 mM acetaldehyde, which resulted in an excellent space–time yield of 1850 g L^{-1} d^{-1} and an enzyme specific productivity of 488 $g_{product}$ g_{enzyme}^{-1} (see Table 1). In comparison, Iding *et al.* studied the continuous production of (*S*)-HPP with purified wt*Pp*BFD in an enzyme membrane reactor and achieved a space–time yield of 34.2 g L^{-1} d^{-1} starting from 10 mM benzaldehyde and 500 mM acetaldehyde.[32] With our optimized set-up involving the immobilized *Pp*BFD variant L476Q and the PBR, we achieved a 50 times higher space–time yield and a 10-times higher product concentration (100 mM) with only a three-fold excess of acetaldehyde.

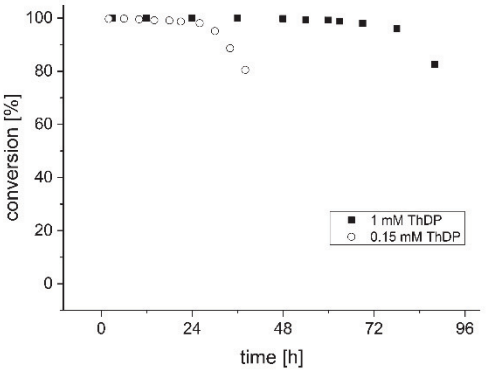

Fig. 4 Effect of ThDP on the stability of immobilized HaloTag-*Pp*BFD L476Q in continuous processes. The continuous carboligation of benzoylformate (100 mM) and acetaldehyde (300 mM) was analyzed in the presence of different ThDP concentrations. The corresponding substrate solution was passed with a residence time of 11 min through a 5 cm Omnifit® column containing 4 mg of immobilized HaloTag-*Pp*BFD L476Q.

2.4 Combining both cascade steps

In the second cascade step, (*S*)-HPP was stereoselectively reduced to (1*S*,2*S*)-1-phenylpropan-1,2-diol ((*S*,*S*)-PPD) catalyzed by immobilized HaloTag-*Lb*ADH under consumption of NADPH. Due to the three-fold excess of acetaldehyde in the first cascade step, acetaldehyde (200 mM) was still present at the efflux of the first column. Since *Lb*ADH prefers acetaldehyde over (*S*)-HPP,[21] acetaldehyde must be removed after the first cascade step to avoid a reduction of the *Lb*ADH activity with respect to the desired diol formation (see Fig. S1 in ESI†). Therefore a hollow fiber module was directly connected to the efflux of the first reactor to perform a membrane supported stripping of acetaldehyde by a reversed nitrogen flow. Thereby the right balance of pressure between the liquid and the gas phase was crucial for the efficient removal of acetaldehyde. By applying a backpressure of 0.3 bar to the liquid phase, we could efficiently prevent nitrogen from entering the liquid solution and *vice versa*.

In addition, we observed an alkaline pH shift from pH 7.0 to pH 8.5 after the first cascade step due to the decarboxylation of benzoylformate. However, a pH of 7.0 is required to ensure maximal activity of the *Lb*ADH.[19] Therefore, the efflux from the hollow fiber module was fed into a reservoir connected to a pH-stat to keep the pH at 7.0.

Via a T-piece the (*S*)-HPP solution from the reservoir was mixed in an equal ratio with a solution containing the redox cofactor $NADP^+$ and the cosubstrate 2-propanol. 2-Propanol is oxidized to acetone by the *Lb*ADH thereby regenerating the

Table 1 Summary of both cascade steps for the continuous production of (*S*,*S*)-PPD. ic (isomer content) is defined as the fraction of a diastereomer in a mixture of multiple stereoisomers

Unit	Conversion [%]	Stereoselectivity [%]	Product concentration [mM]	Space–time yield [g L^{-1} d^{-1}]	Operational stability [d]	Enzyme specific productivity [$g_{product}$ g_{enzyme}^{-1}]	TTN of NADPH [$mol_{product}$ $mol_{cofactor}^{-1}$]
1st step	>99	ee >96	100	1850	3	488	—
2nd step	>97	ic >96[a]	50	38	>14	>48	100

[a] Total distribution of all PPD stereoisomers: (*S*,*S*)-PPD: 96.3%; (*S*,*R*)-PPD: 2.4%; (*R*,*R*)-PPD: 1.2%; (*R*,*S*)-PPD: 0.1%.

cofactor NADPH. Due to this concept, the direct use of NADPH is not required and the much cheaper oxidized cofactor $NADP^+$ can be used instead, which reduces the overall process costs.

2.5 The whole cascade towards (*S*,*S*)-PPD

The *Lb*ADH activity towards the reduction of (*S*)-HPP is much lower compared to the first cascade step.[21,24] Therefore, we had to adjust the amount of enzyme present in the PBR as well as the residence time for the second cascade step. Furthermore, a high conversion of (*S*)-HPP requires an excess of the cosubstrate 2-propanol to shift the equilibrium towards product formation.[20] As a first start, 10 vol% 2-propanol was used corresponding to a 25-fold excess over the substrate (*S*)-HPP. Then, the residence time as well as the enzyme amount was optimized. By applying a column-length of 20 cm containing 16 mg immobilized HaloTag-*Lb*ADH and a residence time of 4.5 h a conversion of (*S*)-HPP >97% to (*S*,*S*)-PPD was obtained (Fig. 5). After 3 days, the first cascade step was stopped due to the inactivation of the immobilized *Pp*BFD L476Q (see above) but the second cascade step was still continued because of the installed reservoir system. Fig. 5 further illustrates the continuous operation of the second cascade step for 14 days with no loss of activity and an overall isomer content (ic; definition see section 4.4) > 96% for the target (*S*,*S*)-PPD diastereomer (see Table 1). This stresses the very high stability of the immobilized HaloTag-*Lb*ADH. Overall, a space–time yield of 38 g L^{-1} d^{-1}, a total turnover number (TTN) of NADPH of 100 $mol_{product}$ $mol_{cofactor}^{-1}$ and an enzyme specific productivity higher than 48 $g_{product}$ g_{enzyme}^{-1} was achieved. After these 14 days, the experiment was stopped although the immobilized HaloTag-*Lb*ADH was still fully active.

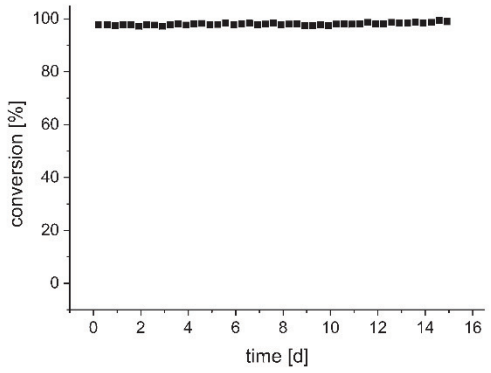

Fig. 5 Continuous production of (*S*,*S*)-PPD. The cascade for the production of (*S*,*S*)-PPD was performed as explained in Scheme 2. The intermediate product (*S*)-HPP was produced first with immobilized *Pp*BFD L476Q starting from 100 mM benzoylformate and 300 mM acetaldehyde (buffer: 50 mM TEA, 1 mM ThDP, 2.5 mM $MgSO_4$, Fig. 4). Afterwards, acetaldehyde was removed with a hollow fiber module and the pH was automatically adjusted in a reservoir. 2-Propanol and $NADP^+$ were introduced *via* a T-piece to result in a substrate solution consisting of 50 mM (*S*)-HPP, 0.5 mM $NADP^+$, 10% (v/v) 2-propanol, 50 mM TEA, pH 7.0, 2.5 mM $MgSO_4$, 1 mM ThDP for the second cascade step. This solution was pumped through a 20 cm Omnifit® column containing 16 mg of immobilized HaloTag-*Lb*ADH. A residence time of 4.5 h was applied.

3 Conclusion

The HaloTag™ system represents a useful strategy for the efficient *in situ* immobilization of enzymes directly from crude cell extracts. Due to the high affinity of this tag, immobilization proceeds rapidly directly in flow inside the reactor prior to the intended reaction. Consequently, no additional process step or equipment is needed, which simplifies the implementation of continuous biocatalytic production processes effectively. Furthermore, the operation of the performed reactions up to several weeks reveals the stable covalent binding of the fusion enzymes and the successful compartmentalization. Still, remaining bottlenecks are enzyme stability in case of the *Pp*BFD L476Q most probably due to aldehyde-induced inactivation and weak ThDP binding as well as low activity in case of the *Lb*ADH towards the substrate (*S*)-HPP. Nevertheless, a high space–time yield of 1850 g L^{-1} d^{-1} with an operational stability of 3 days and an enzyme specific productivity of 488 $g_{product}$ g_{enzyme}^{-1} was achieved for the first cascade step whereas the second cascade step was operated with a space–time yield of 38 g L^{-1} d^{-1} accompanied with an operational stability higher than 14 d and an enzyme specific productivity higher than 48 $g_{product}$ g_{enzyme}^{-1}.

4 Experimental

4.1 Construction of expression plasmids, cell cultivation and enzyme purification

The expression plasmids pET22b-*halotag-ppbfd L476Q* and pET22b-*halotag-lbadh* were constructed with the Gibson Assembly ® Cloning Kit (NEB, Frankfurt, Germany). The DNA sequence encoding for the HaloTag and the linker for the connection to both fusion enzymes was synthesized as linear fragments (Eurofins Genomics, Ebersberg, Germany). Specific overhangs for the integration of this sequence into pET22b which was opened by restriction digestion with NdeI were introduced by PCR (Primer A/B). After successful ligation, the DNA sequences encoding for the *Pp*BFD L476Q and *Lb*ADH were amplified and again, specific overhangs were introduced for the integration into pET22b-*halotag* by PCR (Primer C/D for amplification of *lbadh*, Primer E/F for amplification of *ppbfd L476Q*). pET22b-*halotag* was linearized by PCR, too (Primer G/H) and ligation was performed according to instructions given in the manual of the Gibson Assembly® Cloning Kit.

E. coli BL21 (DE3) cells were transformed with the vector pET22b-*halotag-ppBFD L476Q* as well as pET22b-*halotag-lbadh*, respectively, and production of the respective fusion enzyme was performed in LB medium upon induction with IPTG at 20 °C. For cell disruption, HaloTag-*Pp*BFD L476Q containing cells were suspended in 50 mM potassium phosphate buffer, pH 7.0, containing 2.5 mM $MgSO_4$ and 0.15 mM ThDP, whereas for HaloTag-*Lb*ADH containing cells a buffer containing 50 mM potassium phosphate, pH 7.0, with 1 mM $MgCl_2$ was used. A detailed protocol about the cell cultivation and disruption is described elsewhere.[26] The resulting crude cell extract was frozen at −20 °C and lyophilized (Alpha 1-4 LD plus, Christ, Osterode am Harz, Germany). The lyophilized crude cell extract was stored at −20 °C for further use.

Cloning, cell cultivation, and chromatographic purification of untagged *Lb*ADH[33] and *Pp*BFD L476Q[21] were performed as described elsewhere.

4.2 Immobilization of HaloTag fusion enzymes

Immobilization was performed on HaloLink™ Resin (Promega, Madison, WI, USA). For immobilization of HaloTag-*Pp*BFD L476Q, lyophilized crude cell extract (40 mg ml^{-1}) was dissolved in 50 mM potassium phosphate or triethanolamine buffer, pH 7.0, containing 2.5 mM $MgSO_4$ and either 0.15 mM or 1 mM ThDP, respectively. For immobilization of HaloTag-*Lb*ADH, 25 mg ml^{-1} were dissolved in 50 mM potassium phosphate buffer, pH 7.0, containing 1 mM $MgCl_2$. For immobilizations in batch, 0.5% (v/v) Triton X-100 was added to the buffer to prevent adhesion of the carrier to the plastic of 1.5 mL microreaction tubes. 200 µl of the HaloLink™ slurry were transferred into a 1.5 ml microreaction tube (Eppendorf, Hamburg, Germany) and washed three times with 1 ml of the corresponding buffer (see above) depending on the immobilized fusion enzyme. After the last washing step, the resin was suspended in 100 µl of the corresponding buffer and 100 µl of the prepared crude cell extract solution (see above) was added. This mixture was incubated for 1 h at 25 °C and 1200 rpm in a ThermoMixer® (Eppendorf, Hamburg, Germany). The immobilization was stopped by short centrifugation for a few seconds in a benchtop minicentrifuge to pellet the HaloLink™ Resin. Afterwards, the resin was washed three times with 1 ml of the corresponding buffer and the immobilizates were directly used or stored at 4 °C.

For the immobilization in flow, HaloLink™ Resin was filled into an Omnifit® Column (glass column, internal diameter 3 mm, length 5 cm (V = 0.35 ml) or 20 cm (V = 1.4 ml), Diba, Danbury, CT, USA) and beads were sedimented by applying low pressure with a suction lifter for pipettes. The column was connected to an Asia Syringe Pump (Syrris, Royston, United Kingdom) and the resin was washed first with deionized water to remove residual ethanol (HaloLink™ Resin is stored in 20 vol% ethanol) and afterwards equilibrated with five column volumes of the corresponding buffer (see above). Depending on the size of the column, 1 ml of the resulting crude cell extract solution per cm of column length was used for immobilization of the corresponding fusion enzyme. The immobilization steps were performed with a flow rate of 30 µl min^{-1} at room temperature. Afterwards, the column was washed with the corresponding buffer with 60 µl min^{-1} until the UV-absorption at 280 nm of the flow-through at the outlet of the column reached zero. UV-absorption was measured off-line (UV1800 spectrophotometer, Shimadzu, Duisburg, Germany) and the corresponding buffer was used as a control.

Enzyme purity after immobilization was checked by SDS-PAGE as previously described.[26] The method is based on the saponification of the ester bond connecting the HaloTag with the HaloLink™ Resin.

4.3 Determination of protein concentration and activity assays

Protein concentrations of free and immobilized enzymes were determined with the BC Assay Protein Quantitation Kit (Interchim) as described elsewhere.[26] To measure the amount of enzymes immobilized in flow inside the plug-flow reactor, the bed of the reactor was removed and the amount of protein was determined with this assay.

For characterization of immobilized HaloTag-*Pp*BFD L476Q compared to the non-immobilized reference enzyme without HaloTag, the activity was determined by following the decarboxylation of benzoylformate to benzaldehyde. Assays were performed with 50 mM benzoylformate in 50 mM potassium phosphate buffer, pH 7.0, 2.5 mM $MgSO_4$, 0.5 mM ThDP and 0.004 µg of enzyme in a total volume of 1 ml. The reaction mixture was incubated at 20 °C and 1200 rpm in a ThermoMixer® (Eppendorf, Hamburg, Germany) and samples (20 µl each) were taken over 2.5 min. Benzoylformate and benzaldehyde were detected by HPLC (see below). One Unit (U) of specific activity is defined as the amount of enzyme in mg which catalyzes the formation of 1 µmol benzaldehyde per minute under the described conditions.

For characterization of immobilized HaloTag-*Lb*ADH, the activity was determined by following the reduction of benzaldehyde to benzyl alcohol. Assays were performed with 20 mM benzaldehyde in 50 mM potassium phosphate, pH 7.0, 1 mM $MgCl_2$ and 20 mM NADPH in a total volume of 1 ml. The assay was incubated at 25 °C and 1200 rpm in a ThermoMixer® (Eppendorf, Hamburg, Germany) and samples (20 µl each) were taken over 15 min. 100 µg of immobilized HaloTag-*Lb*ADH and 20 µg of free, untagged *Lb*ADH, respectively, were used for one assay. Benzaldehyde and benzyl alcohol were detected by HPLC (see below). One Unit (U) of specific activity is defined as the amount of enzyme in mg which catalyzes the formation of 1 µmol benzyl alcohol per minute under the described conditions.

4.4 HPLC and GC analytics

HPLC analytics were performed on a Chiralpak IE column using an Agilent 1260 Infinity Quarternary LC system (Agilent Technologies, Santa Clara, CA, USA) equipped with a 1260 Diode Array Detector. Samples (20 µl) were diluted in acetonitrile containing 100 µl L^{-1} toluene as an internal standard. For the detection of benzoylformate, benzaldehyde, and benzyl alcohol, a mobile phase consisting of 50% (v/v) acetonitrile and 50% (v/v) deionized water both containing 0.075% (v/v) trifluoroacetic acid and 1% (w/v) diethylamine with a flow of 1 ml min^{-1} at 20 °C was used. Benzoylformate and benzaldehyde were detected at 250 nm with retention times of about 3.2 min and 5.2 min, respectively. Benzyl alcohol and toluene were detected at 215 nm with retention times of about 3.9 min and 6.3 min, respectively.

To follow the cascade reaction, the column was operated with an isocratic mobile phase consisting of 35% (v/v) acetonitrile and 65% (v/v) deionized water and a flow rate of 1 ml min^{-1} at 20 °C. (*S*)-HPP, (*R*)-HPP, and benzaldehyde were detected at 250 nm with retention times of about 6.3 min, 6.7 min and 8.2 min whereas PPD stereoisomers and toluene were detected at 215 nm with retention times of about 4.1 min and 13.5 min, respectively, according to the respective standards.

The presence of acetaldehyde was analyzed by GC (6890 Series GC system, Agilent Technologies, Santa Clara, CA, USA). 1 µl of an aqueous sample was injected onto a CP-Chirasil-DEX CB column (Varian; 25 m × 0.25 mm × 0.25 mm) and temperature was hold for 5 min at 80 °C. Detection was performed with a flame ionization detector using hydrogen as a carrier gas. The retention time of acetaldehyde was 1.5 min.

The absolute configuration of all four PPD stereoisomers was assigned *via* GC analysis based on respective standards as described elsewhere.[23] The term ic describes the target isomer content and is given as the percent fraction of the target (*S*,*S*)-PPD isomer (I_t) in a mixture of all four possible PPD isomers (I):

$$ic = (I_t / \sum I) \times 100$$

4.5 Final cascade set-up

The substrate solution containing 100 mM benzoylformate and 300 mM acetaldehyde in 50 mM triethanolamine, pH 7.0, 1 mM ThDP, and 2.5 mM $MgSO_4$ was pumped with 30 µl min^{-1} (Micro HPLC pump, Thales Nano, Budapest, Hungary) through an Omnifit® column (50 mm × 3 mm; t_R 11 min) containing 4 mg of HaloTag-*Pp*BFD L476Q immobilized in flow on HaloLink™ Resin (see above), applying a back pressure of 2 bar. The efflux of this column was then passed through a Celgard X50 Liqui-Cel® MiniModule® (3 M, St Paul, USA) hollow fiber module where membrane-supported stripping of acetaldehyde was performed with a nitrogen flow of 20 L_n h^{-1}. Therefore, a back pressure of 0.3 bar was applied to the hollow fiber module. Afterwards, the resulting solution was pumped into a 100 ml reservoir connected to a pH-Stat module including a 691 pH Meter, 665 Dosimat and a 614 Impulsomat (Metrohm, Herisau, Switzerland). The pH was automatically adjusted to pH 7.0 using 2% (v/v) aqueous HCl. Then, a solution of 1 mM $NADP^+$ and 20% 2-propanol was mixed with the solution from the reservoir *via* a T-piece by applying a pumping speed for both solutions of 2.5 µl min^{-1} (Asia Syringe Pump, Syrris, Royston, United Kingdom). The corresponding solution was consequently passed through an Omnifit® column (200 mm × 3 mm; t_R 4.5 h) containing 16 mg of HaloTag-*Lb*ADH previously immobilized in flow on HaloLink™ Resin (see above) with a pumping speed of 5 µl min^{-1}. A back pressure of 2 bar was applied to the column. Furthermore, all steps were performed at room temperature.

Conflicts of interest

There are no conflicts to declare.

Acknowledgements

This project was funded by the German Federal Ministry of Education and Research (BMBF) within the project "Molecular Interaction Engineering" (funding code 031A095).

References

1 J. Wegner, S. Ceylan and A. Kirschning, *Adv. Synth. Catal.*, 2012, **354**, 17–57.
2 I. R. Baxendale, *J. Chem. Technol. Biotechnol.*, 2013, **88**, 519–552.
3 R. Yuryev, S. Strompen and A. Liese, *Beilstein J. Org. Chem.*, 2011, **7**, 1449–1467.
4 J. H. Schrittwieser, S. Velikogne, M. Hall and W. Kroutil, *Chem. Rev.*, 2017, DOI: 10.1021/acs.chemrev.7b00033.
5 P. Gruber, M. P. C. Marques, B. O'Sullivan, F. Baganz, R. Wohlgemuth and N. Szita, *Biotechnol. J.*, 2017, **12**, 1700030.

6 T. Peschke, M. Skoupi, T. Burgahn, S. Gallus, I. Ahmed, K. S. Rabe and C. M. Niemeyer, *ACS Catal.*, 2017, 7, 7866–7872.
7 L. Tamborini, D. Romano, A. Pinto, M. Contente, M. C. Iannuzzi, P. Conti and F. Molinari, *Tetrahedron Lett.*, 2013, **54**, 6090–6093.
8 F. Le Joubioux, N. Bridiau, M. Sanekli, M. Graber and T. Maugard, *J. Mol. Catal. B: Enzym.*, 2014, **109**, 143–153.
9 M. Planchestainer, M. L. Contente, J. Cassidy, F. Molinari, L. Tamborini and F. Paradisi, *Green Chem.*, 2017, **19**, 372–375.
10 A. Brahma, B. Musio, U. Ismayilova, N. Nikbin, S. B. Kamptmann, P. Siegert, G. E. Jeromin, S. V. Ley and M. Pohl, *Synlett*, 2016, 262–266.
11 L. Tamborini, P. Fernandes, F. Paradisi and F. Molinari, *Trends Biotechnol.*, 2017, 1–16.
12 J. Wachtmeister and D. Rother, *Curr. Opin. Biotechnol.*, 2016, **42**, 169–177.
13 R. A. Sheldon and S. van Pelt, *Chem. Soc. Rev.*, 2013, **42**, 6223–6235.
14 I. Migneault, C. Dartiguenave, M. J. Bertrand and K. C. Waldron, *BioTechniques*, 2004, **37**, 790–802.
15 C. Mateo, V. Grazú, B. C. C. Pessela, T. Montes, J. M. Palomo, R. Torres, F. López-Gallego, R. Fernández-Lafuente and J. M. Guisán, *Biochem. Soc. Trans.*, 2007, **35**, 1593–1601.
16 C. Mateo, O. Abian, G. Fernández-lorente, B. C. C. Pessela, V. Grazú, J. M. Guisán and R. Fernández-Lafuente, in *Immobilized Enzyme Cells*, ed. J. M. Guisan, Humana Press, 2006, pp. 47–64.
17 C. Mateo, B. C. C. Pessela, V. Grazu, R. Torres, F. López-Gallego, J. M. Guisan and R. Fernandez-Lafuente, in *Immobilization of Enzymes and Cells*, ed. J. M. Guisan, Humana Press, Totowa, NJ, 2006, pp. 117–128.
18 L. P. Encell, R. Friedman Ohana, K. Zimmerman, P. Otto, G. Vidugiris, M. G. Wood, G. V. Los, M. G. McDougall, C. Zimprich, N. Karassina, R. D. Learish, R. Hurst, J. Hartnett, S. Wheeler, P. Stecha, J. English, K. Zhao, J. Mendez, H. A. Benink, N. Murphy, D. L. Daniels, M. R. Slater, M. Urh, A. Darzins, D. H. Klaubert, R. F. Bulleit and K. V. Wood, *Curr. Chem. Genomics*, 2012, **6**, 55–71.
19 B. Riebel, *PhD thesis*, Heinrich-Heine University Düsseldorf, 1996.
20 S. Leuchs and L. Greiner, *Chem. Biochem. Eng. Q.*, 2011, **25**, 267–281.
21 B. Lingen, J. Grötzinger, D. Kolter, M. R. Kula and M. Pohl, *Protein Eng.*, 2002, **15**, 585–593.
22 B. Lingen, D. Kolter-Jung, P. Dünkelmann, R. Feldmann, J. Grötzinger, M. Pohl and M. Müller, *ChemBioChem*, 2003, **4**, 721–726.
23 D. Kihumbu, T. Stillger, W. Hummel and A. Liese, *Tetrahedron: Asymmetry*, 2002, **13**, 1069–1072.
24 J. Kulig, R. C. Simon, C. A. Rose, S. M. Husain, M. Häckh, S. Lüdeke, K. Zeitler, W. Kroutil, M. Pohl and D. Rother, *Catal. Sci. Technol.*, 2012, **2**, 1580–1589.
25 J. Wachtmeister, A. Jakoblinnert and D. Rother, *Org. Process Res. Dev.*, 2016, **20**, 1744–1753.
26 J. Döbber and M. Pohl, *J. Biotechnol.*, 2017, **241**, 170–174.
27 R. F. Ohana, L. P. Encell, K. Zhao, D. Simpson, M. R. Slater, M. Urh and K. V. Wood, *Protein Expression Purif.*, 2009, **68**, 110–120.
28 C. Sun, Y. Li, S. E. Taylor, X. Mao, M. C. Wilkinson and D. G. Fernig, *PeerJ*, 2015, **3**, e1060.
29 D. H. Zhang, L. J. Peng, Y. Wang and Y. Q. Li, *Colloids Surf., B*, 2015, **129**, 206–210.
30 R. A. Sheldon, *Appl. Microbiol. Biotechnol.*, 2011, **92**, 467–477.
31 B. Tural, T. Tarhan and S. Tural, *J. Mol. Catal. B: Enzym.*, 2014, **102**, 188–194.
32 H. Iding, T. Dünnwald, L. Greiner, A. Liese, M. Müller, P. Siegert, J. Grötzinger, A. S. Demir and M. Pohl, *Chemistry*, 2000, **6**, 1483–1495.
33 L. Kulishova, *PhD thesis*, Heinrich-Heine University Düsseldorf, 2010.
34 J. Döbber, M. Pohl, S. V. Ley and B. Musio, *Reaction Chemistry & Engineering*, 2017, DOI: 10.1039/c7re00173h.

Electronic Supplementary

Closing the gap for efficient immobilization of biocatalysts in continuous processes:

HaloTag™ fusion enzymes for a continuous enzymatic cascade towards a vicinal chiral diol

Table of contents

I Primer Sequences

Primer A: tttaagaaggagatatacatATGAAACATCACCATCACCATCACGCAGAAATTGGTACG

Primer B: tttattcagcagacgataCGCGGCCGCTTTCGCCGC

Primer C: cagcggcgaaagcggccgcgATGTCTAACCGTTTGGATG

Primer D: gctttgttagcagccggatcCTATTGAGCAGTGTAGCC

Primer E: cagcggcgaaagcggccgcgATGGCTTCGGTACACGGCACCAC

Primer F: gctttgttagcagccggatcTTAAGATCTCTTCACCGGGCTTAC

Primer G: GATCCGGCTGCTAACAAAG

Primer H: CGCGGCCGCTTTCGCCGC

II DNA sequences encoding for the corresponding fusion enzymes

- green sequences encode for the HaloTag™
- red sequences encode for the helical linker
- blue sequences encode for the corresponding enzyme

II.I *halotag-ppbfd L476Q*

ATGAAACATCACCATCACCATCACGCAGAAATTGGTACGGGATTTCCGTTTGACCCGCATTATGTG
GAGGTTCTGGGTGAACGCATGCACTACGTGGATGTTGGTCCGCGCGATGGCACACCGGTGCTGTTT
CTGCATGGTAATCCGACCTCCAGCTATGTTTGGCGCAACATTATTCCGCATGTCGCCCCAACGCATC
GCTGTATTGCCCCAGATCTCATTGGCATGGGCAAAAGCGACAAACCGGATTTGGGCTACTTCTTCG
ACGATCACGTACGGTTTATGGACGCCTTTATCGAGGCTCTGGGACTCGAGGAAGTAGTGCTGGTTA
TTCATGACTGGGGCTCTGCATTAGGCTTTCACTGGGCTAAACGGAACCCAGAACGCGTCAAGGGGA
TTGCCTTCATGGAGTTCATCCGTCCGATTCCGACCTGGGATGAATGGCCCGAATTTGCCCGTGAAAC
CTTTCAGGCGTTTCGTACCACGGATGTTGGCCGTAAGCTCATCATCGACCAAAACGTGTTCATTGAG
GGCACTCTTCCCATGGGAGTAGTGCGTCCTTTAACCGAAGTCGAGATGGACCACTATCGCGAACCC
TTCCTGAATCCGGTTGATCGCGAACCGCTGTGGCGCTTCCCGAATGAGCTGCCTATTGCTGGTGAAC
CGGCGAATATCGTGGCACTTGTGGAAGAATACATGGATTGGCTGCATCAGAGTCCAGTCCCTAAGC
TGTTGTTTTGGGGTACACCTGGCGTGTTGATTCCGCCTGCAGAAGCTGCTCGCTTAGCGAAAAGCTT
GCCCAACTGCAAAGCGGTCGATATTGGGCCAGGTCTGAACCTGTTACAGGAGGATAACCCGGATCT
GATCGGGAGTGAAATCGCGCGTTGGCTGTCAACTCTGGAAATCTCGGGTCTTGCAGAAGCAGCGGC
CAAAGAAGCTGCGGCCAAAGAGGCAGCCGCGAAAGAAGCAGCGGCGAAAGCGGCCGCGATGGCT
TCGGTACACGGCACCACATACGAACTCTTGCGACGTCAAGGCATCGATACGGTCTTCGGCAATCCT
GGCTCGAACGAGCTCCCGTTTTTGAAGGACTTTCCAGAGGACTTTCGATACATCCTGGCTTTGCAGG
AAGCGTGTGTGGTGGGCATTGCAGACGGCTATGCGCAAGCCAGTCGGAAGCCGGCTTTCATTAACC
TGCATTCTGCTGCTGGTACCGGCAATGCTATGGGTGCACTCAGTAACGCCTGGAACTCACATTCCCC
GCTGATCGTCACTGCCGGCCAGCAGACCAGGGCGATGATTGGCGTTGAAGCTCTGCTGACCAACGT
CGATGCCGCCAACCTGCCACGACCACTTGTCAAATGGAGCTACGAGCCCGCAAGCGCAGCAGAAG
TCCCTCATGCGATGAGCAGGGCTATCCATATGGCAAGCATGGCGCCACAAGGCCCTGTCTATCTTT
CGGTGCCATATGACGATTGGGATAAGGATGCTGATCCTCAGTCCCACCACCTTTTTGATCGCCATGT
CAGTTCATCAGTACGCCTGAACGACCAGGATCTCGATATTCTGGTGAAAGCTCTCAACAGCGCATC
CAACCCGGCGATCGTCCTGGGCCCGGACGTCGACGCAGCAAATGCGAACGCAGACTGCGTCATGTT
GGCCGAACGCCTCAAAGCTCCGGTTTGGGTTGCGCCATCCGCTCCACGCTGCCCATTCCCTACCCGT
CATCCTTGCTTCCGTGGATTGATGCCAGCTGGCATCGCAGCGATTTCTCAGCTGCTCGAAGGTCACG
ATGTGGTTTTGGTAATCGGCGCTCCAGTGTTCCGTTACCACCAATACGACCCAGGTCAATATCTCAA
ACCTGGCACGCGATTGATTTCGGTGACCTGCGACCCGCTCGAAGCTGCACGCGCGCCAATGGGCGA
TGCGATCGTGGCAGACATTGGTGCGATGGCTAGCGCTCTTGCCAACTTGGTTGAAGAGAGCAGCCG
CCAGCTCCCAACTGCAGCTCCGGAACCCGCGAAGGTTGACCAAGACGCTGGCCGACTTCACCCAGA
GACAGTGTTCGACACACTGAACGACATGGCCCCGGAGAATGCGATTTACCTGAACGAGTCGACTTC
AACGACCGCCCAAATGTGGCAGCGCCTGAACATGCGCAACCCTGGTAGCTACTACTTCTGTGCAGC
TGGCGGACTGGGCTTCGCCCTGCCTGCAGCAATTGGCGTTCAACTCGCAGAACCCGAGCGACAAGT
CATCGCCGTCATTGGCGACGGATCGGCGAACTACAGCATTAGTGCGTTGTGGACTGCAGCTCAGTA
CAACATCCCCACTATCTTCGTGATCATGAACAACGGCACCTACGGTGCGTTGCGATGGTTTGCCGG
CGTTCTCGAAGCAGAAAACGTTCCTGGGCAGGATGTGCCAGGGATCGACTTCCGCGCACTCGCCAA
GGGCTATGGTGTCCAAGCGCTGAAAGCCGACAACCTTGAGCAGCTCAAGGGTTCGCTACAAGAAG
CGCTTTCTGCCAAAGGCCCGGTACTTATCGAAGTAAGCACCGTAAGCCCGGTGAAGAGATCTTAA

II.II *halotag-lbadh*

ATGAAACATCACCATCACCATCACGCAGAAATTGGTACGGGATTTCCGTTTGACCCGCATTATGTG
GAGGTTCTGGGTGAACGCATGCACTACGTGGATGTTGGTCCGCGCGATGGCACACCGGTGCTGTTT
CTGCATGGTAATCCGACCTCCAGCTATGTTTGGCGCAACATTATTCCGCATGTCGCCCCAACGCATC
GCTGTATTGCCCCAGATCTCATTGGCATGGGCAAAAGCGACAAACCGGATTTGGGCTACTTCTTCG
ACGATCACGTACGGTTTATGGACGCCTTTATCGAGGCTCTGGGACTCGAGGAAGTAGTGCTGGTTA
TTCATGACTGGGGCTCTGCATTAGGCTTTCACTGGGCTAAACGGAACCCAGAACGCGTCAAGGGGA
TTGCCTTCATGGAGTTCATCCGTCCGATTCCGACCTGGGATGAATGGCCCGAATTTGCCCGTGAAAC
CTTTCAGGCGTTTCGTACCACGGATGTTGGCCGTAAGCTCATCATCGACCAAAACGTGTTCATTGAG
GGCACTCTTCCCATGGGAGTAGTGCGTCCTTTAACCGAAGTCGAGATGGACCACTATCGCGAACCC
TTCCTGAATCCGGTTGATCGCGAACCGCTGTGGCGCTTCCCGAATGAGCTGCCTATTGCTGGTGAAC
CGGCGAATATCGTGGCACTTGTGGAAGAATACATGGATTGGCTGCATCAGAGTCCAGTCCCTAAGC
TGTTGTTTTGGGGTACACCTGGCGTGTTGATTCCGCCTGCAGAAGCTGCTCGCTTAGCGAAAAGCTT
GCCCAACTGCAAAGCGGTCGATATTGGGCCAGGTCTGAACCTGTTACAGGAGGATAACCCGGATCT
GATCGGGAGTGAAATCGCGCGTTGGCTGTCAACTCTGGAAATCTCGGGTCTTGCAGAAGCAGCGGC
CAAAGAAGCTGCGGCCAAAGAGGCAGCCGCGAAAGAAGCAGCGGCGAAAGCGGCCGCGATGTCT

AACCGTTTGGATGGTAAGGTAGCAATCATTACAGGTGGTACGTTGGGTATCGGTTTAGCTATCGCC
ACGAAGTTCGTTGAAGAAGGGGCTAAGGTCATGATTACCGGCCGGCACAGCGATGTTGGTGAAAA
AGCAGCTAAGAGTGTCGGCACTCCTGATCAGATTCAATTTTTCCAACATGATTCTTCCGATGAAGA
CGGCTGGACGAAATTATTCGATGCAACGGAAAAAGCCTTTGGCCCAGTTTCTACATTAGTTAATAA
CGCTGGGATCGCGGTTAACAAGAGTGTCGAAGAAACCACGACTGCTGAATGGCGTAAATTATTAG
CCGTCAACCTTGATGGTGTCTTCTTCGGTACCCGATTAGGGATTCAACGGATGAAGAACAAAGGCT
TAGGGGCTTCCATCATCAACATGTCTTCGATCGAAGGCTTTGTGGGTGATCCTAGCTTAGGGGCTTA
CAACGCATCTAAAGGGGCCGTACGGATTATGTCCAAGTCAGCTGCCTTAGATTGTGCCCTAAAGGA
CTACGATGTTCGGGTAAACACTGTTCACCCTGGCTACATCAAGACACCATTGGTTGATGACCTACC
AGGGGCCGAAGAAGCGATGTCACAACGGACCAAGACGCCAATGGGCCATATCGGTGAACCTAACG
ATATTGCCTACATCTGTGTTTACTTGGCTTCTAACGAATCTAAATTTGCAACGGGTTCTGAATTCGT
AGTTGACGGTGGCTACACTGCTCAATAG

III Protein sequences

- green: sequence of the HaloTag™
- red: sequence of the helical linker
- blue: sequence of the corresponding enzyme

III.I HaloTag-*Pp*BFD L476Q

MKHHHHHHAEIGTGFPFDPHYVEVLGERMHYVDVGPRDGTPVLFLHGNPTSSYVWRNIIPHVAPTHRC
IAPDLIGMGKSDKPDLGYFFDDHVRFMDAFIEALGLEEVVLVIHDWGSALGFHWAKRNPERVKGIAFM
EFIRPIPTWDEWPEFARETFQAFRTTDVGRKLIIDQNVFIEGTLPMGVVRPLTEVEMDHYREPFLNPVDR
EPLWRFPNELPIAGEPANIVALVEEYMDWLHQSPVPKLLFWGTPGVLIPPAEAARLAKSLPNCKAVDIG
PGLNLLQEDNPDLIGSEIARWLSTLEISGLAEAAAKEAAAKEAAAKEAAAKAAAMASVHGTTYELLRR
QGIDTVFGNPGSNELPFLKDFPEDFRYILALQEACVVGIADGYAQASRKPAFINLHSAAGTGNAMGALS
NAWNSHSPLIVTAGQQTRAMIGVEALLTNVDAANLPRPLVKWSYEPASAAEVPHAMSRAIHMASMAP
QGPVYLSVPYDDWDKDADPQSHHLFDRHVSSSVRLNDQDLDILVKALNSASNPAIVLGPDVDAANAN
ADCVMLAERLKAPVWVAPSAPRCPFPTRHPCFRGLMPAGIAAISQLLEGHDVVLVIGAPVFRYHQYDP
GQYLKPGTRLISVTCDPLEAARAPMGDAIVADIGAMASALANLVEESSRQLPTAAPEPAKVDQDAGRL
HPETVFDTLNDMAPENAIYLNESTSTTAQMWQRLNMRNPGSYYFCAAGGLGFALPAAIGVQLAEPERQ
VIAVIGDGSANYSISALWTAAQYNIPTIFVIMNNGTYGALRWFAGVLEAENVPGQDVPGIDFRALAKGY
GVQALKADNLEQLKGSLQEALSAKGPVLIEVSTVSPVKRS

III.II HaloTag-*Lb*ADH

MKHHHHHHAEIGTGFPFDPHYVEVLGERMHYVDVGPRDGTPVLFLHGNPTSSYVWRNIIPHVAPTHRC
IAPDLIGMGKSDKPDLGYFFDDHVRFMDAFIEALGLEEVVLVIHDWGSALGFHWAKRNPERVKGIAFM
EFIRPIPTWDEWPEFARETFQAFRTTDVGRKLIIDQNVFIEGTLPMGVVRPLTEVEMDHYREPFLNPVDR
EPLWRFPNELPIAGEPANIVALVEEYMDWLHQSPVPKLLFWGTPGVLIPPAEAARLAKSLPNCKAVDIG
PGLNLLQEDNPDLIGSEIARWLSTLEISGLAEAAAKEAAAKEAAAKEAAAKAAAMSNRLDGKVAIITGG
TLGIGLAIATKFVEEGAKVMITGRHSDVGEKAAKSVGTPDQIQFFQHDSSDEDGWTKLFDATEKAFGPV
STLVNNAGIAVNKSVEETTTAEWRKLLAVNLDGVFFGTRLGIQRMKNKGLGASIINMSSIEGFVGDPSL
GAYNASKGAVRIMSKSAALDCALKDYDVRVNTVHPGYIKTPLVDDLPGAEEAMSQRTKTPMGHIGEP
NDIAYICVYLASNESKFATGSEFVVDGGYTAQ

IV Effect of acetaldehyde on the production of (*S*,*S*)-PPD

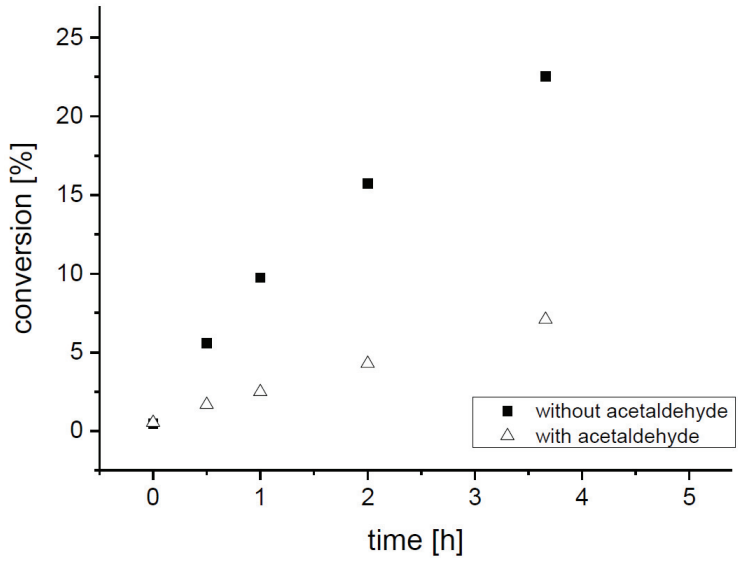

Figure S1: Production of (*S*,*S*)-PPD catalyzed by HaloTag-*Lb*ADH in the presence of acetaldehyde. The reduction of (*S*)-HPP towards (S,S)-PPD was analyzed in batch using immobilized HaloTag-*Lb*ADH. (*S*)-HPP resulting from the carboligation of benzoylformate and acetaldehyde was used either without removal of residual acetaldehyde or after removal by membrane supported stripping. Assay: 20 mM (*S*)-HPP containing either 40 mM or no acetaldehyde, 10 % (v/v) isopropanol, 0.5 mM NAPH, 50 mM TEA, 0.15 mM ThDP, 2.5 mM $MgSO_4$, V = 1 ml, 25 °C, 1200 rpm.

V Photograph of flow setup

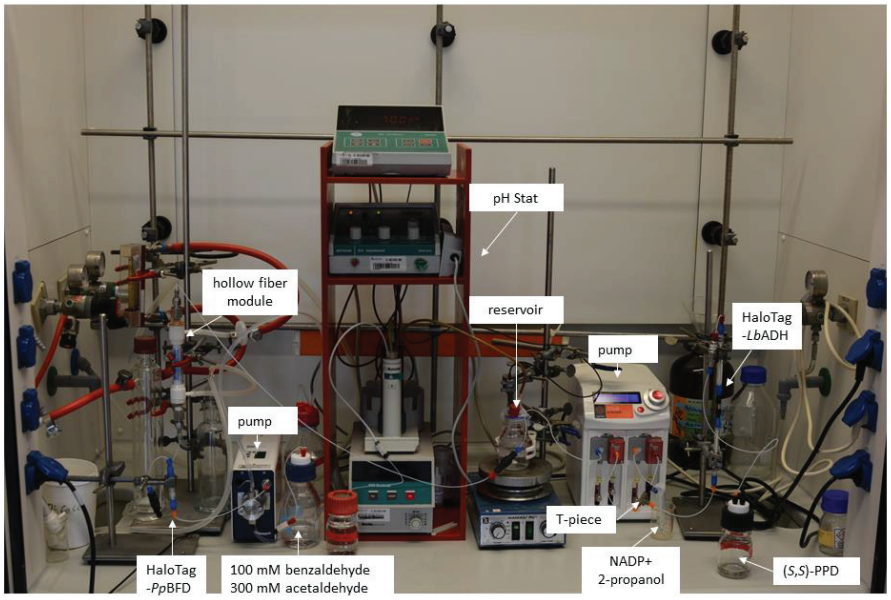

Figure S2: Enzymatic 2-step cascade for the continuous production of (S,S)-PPD. In the first step catalyzed by immobilized HaloTag-PpBFD L476Q, benzoylformate is decarboxylated towards benzaldehyde and carbon dioxide. The resulting benzaldehyde is then further converted into (S)-HPP by a carboligation in the presence of excess acetaldehyde. Afterwards, residual acetaldehyde is removed by membrane supported stripping using a hollow fiber module and the pH is automatically adjusted to pH 7.0 with a pH-Stat. In the second step catalyzed by immobilized HaloTag-LbADH, (S)-HPP is reduced to (S,S)-PPD under consumption of NADPH, which is produced from the cheaper oxidized cofactor NADP+ using 10 vol% 2-propanol as a cosubstrate for cofactor regeneration.

2.5 HaloTag-*Ec*DERA

Results presented in this chapter are part of a cooperation with the group of Thomas Classen at the Institute of Bioorganic Chemistry, HHU Düsseldorf. As final studies have to be performed by the cooperation partner the respective manuscript could not be finalized until this thesis was submitted. Thus, this chapter comprises a manuscript draft focusing on the results obtained by Johannes Döbber. Where necessary for an understanding, the results of others were included, which was indicated respectively.

Context:

Results in this chapter focus on the application of immobilized HaloTag-*Ec*DERA in cooperation with J. Bramski et al. (see below). In a first step, the design of this fusion enzyme was optimized to enable maximal catalytic activity by investigating spacer sequences, which separate the HaloTag™ and the *Ec*DERA. In a second step, best variants were used for the easy preparation of plug-flow reactors to achieve high control about *Ec*DERA-catalyzed aldol reactions. Therefore, this study provides tools to modulate catalytic activity of respective immobilizates. Furthermore, the continuous reaction system allowed synthesis of products that are otherwise not accessible in batch.

Contributions:

J. Döbber[1], J. Bramski[2], T. Gerlach[1] and D. Hahn[1] performed the experiments. J. Döbber planned and constructed different fusion enzyme designs and developed a suitable enzyme assay to analyze fusion enzyme variants. D. Hahn assisted in the construction of fusion enzymes and T. Gerlach helped to establish a suitable assay as well as to measure activity of immobilized variants. Protocols and material for the immobilization of HaloTag-*Ec*DERA in flow were provided by J. Döbber and continuous reactions as well as purification of free *Ec*DERA were performed by J. Bramski. T. Classen[2], J. Pietruszka[2] and M. Pohl[1] conceptually planned and supervised the project.

[1] Group of Martina Pohl, IBG-1: Biotechnology, Forschungszentrum Jülich, Germany
[2] Group of Thomas Classen, Institute of Bioorganic Chemistry, Heinrich-Heine-Universität Düsseldorf im Forschungszentrum Jülich, Germany

2.5.1 Introduction

2-Deoxyribose-5-phosphate aldolase from *E. coli* (*Ec*DERA) is a promising catalyst for the formation of C-C bonds (Dean et al., 2007). It catalyzes the asymmetric aldol reaction of several aldehydes but reveals highest activity when acetaldehyde is used as a donor molecule (Barbas et al., 1990; Chen et al., 1992). A major drawback for the application of *Ec*DERA is its irreversible inactivation in the presence of higher acetaldehyde concentrations hampering the long-term use of this enzyme (Hoffee et al., 1965). However, recent studies revealed that catalyst inactivation occurs via modification of an essential active site lysine and can be overcome by mutation of a specific cysteine present at position 47 of the enzyme (Bramski et al., 2017; Dick et al., 2016).

Therefore, optimized *Ec*DERA variants for further synthetic applications are now available but the production of some compounds remains challenging. Especially, the access to mono aldol products is in some cases difficult, since the *Ec*DERA is able to directly catalyze the sequential addition of two acetaldehyde molecules to one acceptor substrate (Gijsen and Wong, 1994). To achieve only mono aldol products, a high reaction control, specifically of the contact time between enzymes and substrates is crucial. Such a control is difficult to achieve in batch reactions. Instead, continuous reaction concepts would allow a higher level of control, since residence times of substrates and products inside the reactor can exactly be adjusted (Baxendale, 2013; Tamborini et al., 2018).

However, the use of biocatalysts in continuous reactions demands for efficient compartmentalization concepts in the first place. To address this issue, enzyme immobilization can be a solution and recently, the simple loading of plug-flow reactors in flow using HaloTag™ fusion enzymes was successfully demonstrated (Döbber et al., 2018a; Döbber et al., 2018b). The HaloTag™ can be genetically fused to the enzyme of interest and mediates the covalent binding to carriers exposing chloroalkane residues directly from crude cell extracts in flow. On the contrary, fusion of an additional tag may influence the catalytic activity of the enzyme and strategies have to be developed to allow optimal performance after immobilization. In case of steric hindrance by the tag, an optimal orientation of the HaloTag™ and sufficient distance to the fused enzyme can enhance activity after immobilization. Therefore, spacer sequences separating both fusion partners might be crucial. Several reports underlined that linker rigidity as well as length influence interaction of fusion partners and can be used to efficiently establish spatial distance from each other (Arai et al., 2001; Li et al., 2016).

In this study, *Ec*DERA was immobilized via the HaloTag™ and a continuous reaction system allowing selective access of mono aldol compounds was developed. Since high enzyme stability is necessary to implement continuous reactions for long-term use, a variant of this enzyme (*Ec*DERA C47M) with increased resistance against high acetaldehyde concentrations was selected. In a first step, different HaloTag™ fusion enzyme designs were analyzed to achieve optimal orientation of the fusion partners to each other and to enable high catalytic activity of the immobilized enzyme. In a second step, best variants were chosen for continuous reactions and to find appropriate reaction conditions yielding solely mono aldol reaction products.

2.5.2 Methods

Construction of expression plasmids and production of enzymes

The expression plasmid for the production of HaloTag-*Ec*DERA containing the spacer sequence 20aa – 4r was constructed as described previously by amplifying the DNA encoding for *Ec*DERA C47M and integrating it into pET22b, which already contained the DNA encoding for the HaloTag™ and the corresponding spacer (Döbber et al., 2018b). The backbone of this expression plasmid was subsequently used to integrate the oligonucleotide encoding the spacer sequences as listed in Table 2.5-1. A PCR was performed with primers A and B (see SI) to open the circular plasmid at the position between both sequences encoding for the HaloTag™ and the *Ec*DERA, respectively, but without amplifying the part encoding the spacer sequence. DNA sequences encoding for each spacer were ordered as linear, single-stranded DNA primers (eurofinsgenomics, München, Germany) with specific overhangs for the constructed plasmid backbone (see SI). Ligation was performed with the NEBuilder® HiFi DNA Assembly Cloning Kit (NEB, Frankfurt, Germany) according to the manufacturer´s instructions resulting in the construction of all expression plasmids. Further detailed information about all sequences is given in the SI. Production of fusion enzymes and preparation of lyophilized crude cell extracts was performed according to established protocols as mentioned elsewhere but as buffer for sonification 10 mM TEA, pH 7 was used (Döbber and Pohl, 2017).
Construction of expression plasmids, production and chromatographic purification via anion exchange chromatography of free *Ec*DERA C47M was described previously (Dick, 2016).

Table 2.5-1: Spacer sequences used to separate HaloTag-*Ec*DERA fusion enzymes.

spacer	protein sequence
25 aa – 5f	$A(GGGGS)_5A$
25 aa – 4f1r	$A(EAAAK)(GGGGS)_4A$
25 aa – 3f2r	$A(EAAAK)(GGGGS)_2(EAAAK)(GGGGS)A$
25aa – 2f3r	$A(EAAAK)(GGGGS)_2(EAAAK)_2A$
25 aa – 1f4r	$A(EAAAK)(GGGGS)(EAAAK)_3A$
25 aa – 5r	$A(EAAAK)_5A$
20 aa – 4r	$A(EAAAK)_4A$
30 aa – 6r	$A(EAAAK)_6A$
35 aa – 7r	$A(EAAAK)_7A$

Immobilization of HaloTag-EcDERA fusion enzymes

Immobilization of fusion enzymes was performed directly from crude cell extracts on HaloLink™ Resin (Promega, USA). A crude cell extract solution consisting of 25 mg of lyophilized crude cell extract per ml of buffer (100 mM TEA, pH 7.0) was prepared. For immobilization in batch, HaloLink™ Resin was equilibrated with the same buffer (3x 1ml) supplemented with 0.1 vol% Triton X-100 and 200 µl of crude cell extract solution were mixed with 50 µl of resin. After 1h of incubation at 25 °C and 1200 rpm in a ThermoMixer® (Eppendorf, Hamburg, Germany), the resin was washed three times with 1 ml of buffer supplemented with 0.1 vol% Triton x-100. For immobilization in flow, 5 ml of crude cell extract solution (see above) were pumped through a 5 cm Omnifit® glass column containing HaloLink™ Resin as described previously (Döbber et al., 2018a). The amount of bound proteins was determined with the BC Assay Protein Quantitation Kit (Interchim, France).

Activity assay

The activity of free and immobilized *Ec*DERA was analyzed by following the cleavage of 2-deoxyribose-5-phosphate (DRP) into glyceraldehyde and acetaldehyde. To monitor this reaction, alcohol dehydrogenase from *S. cerevisiae* (*Sc*ADH, Sigma Aldrich, Germany) was applied to catalyze the reduction of acetaldehyde to ethanol under consumption of NADH. The decrease of NADH was determined spectrophotometrically by following the absorption of NADH at 340 nm. In a 3 ml quartz cuvette, DRP (0.4 mM), NADH (0.2 mM), *Sc*ADH (0.1 mg/ml) and *Ec*DERA (either free or immobilized HaloTag™ fusion enzyme, protein concentration: around 20 µg/ml) were mixed and TEA buffer, pH 7.0, supplemented with 0.1 vol% Triton X-100 was used. The assay was performed in a total volume of 3 ml at 25 °C for 90 sec. To keep immobilizates suspended, the assay mixture was stirred by a magnetic stirrer. One Unit (U) of specific activity is defined as the amount of enzyme (either free or bound on the HaloLink™ Resin) in mg which catalyzes the formation of 1 µmol glyceradehyde per minute under the described conditions.

Reactions in flow

For reactions in flow, HaloTag-*Ec*DERA (C47M, 25aa – 5r) was immobilized as described above in a 5 cm Omnifit® glass column. To prepare the reaction solution, a stock solution of acetaldehyde was made using gastight Hamilton® syringes (Hamilton Company, USA) previously cooled on ice to be as exact as possible. Then, hexanal and acetaldehyde were mixed in TEA buffer (100 mM, pH 7.0, concentrations see Table 2.5-2) and connected to the column using a syringe pump (Legato 100, KD Scientific, MA, USA). The column was tempered via a water bath and 25 °C were adjusted. Concentrations of hexanal and acetaldehyde as well as pumping speed were varied to find optimal conditions for 3-hydroxy-octanal production (see Table 2.5-2)

Analytics

To follow the reaction, 500 µl of sample were taken and products were extracted three times with 1 ml ethylacetate. After drying with $MgSO_4$, samples were applied to GC (TRACE™ GC, Thermo Scientific, Germany) using a FS-HYDRODEX β-3P column (length/ID: 25 m/0.25 mm, Macherey-Nagel, Düren, Germany). The column was hold 5 min at 60 °C, then the column was heated 5 °C/min until 200 °C were reached and again hold for 2 min. Retention times were as follows: hexanal, 6.6 min; 2-octenal: 16.7 min, 3-hydroxy-octanal, 22.6 min; 3,5-dihydroxy-decanal, 33.5 min.
Enantiomeric excess of 3-hydroxy-octanal enantiomers was determined according to Bisterfeld, 2016.

2.5.3 Results and Discussion

The synthesis of mono aldol products catalyzed by *Ec*DERA was targeted in this study. As shown in Figure 2.5-1, the production of (*R*)-3-hydroxy-octanal starting from hexanal and acetaldehyde was selected as a model reaction. However, *Ec*DERA directly catalyzes the sequential aldol addition towards (*R*,*R*)-3,5-dihydroxy-decanal. Therefore, a high control about the contact time between substrates and enzyme is crucial to solely produce the target compound (*R*)-3-hydroxy-octanal.

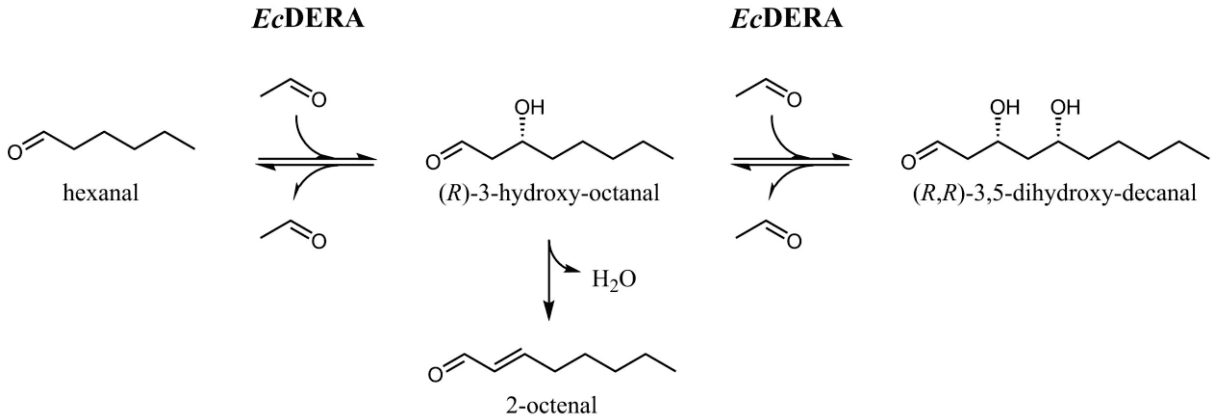

Figure 2.5-1: *Ec*DERA-catalyzed aldol addition starting from hexanal and acetaldehyde. *Ec*DERA catalyzes the sequential aldol addition leading to (*R*)-3-hydroxy-octanal as an intermediate product and to the final bis-aldol compound (*R*,*R*)-3,5-dihydroxy-octanal. 2-octenal arises as a by-product.

As a consequence, the construction of a continuous reaction system was aimed whereby *Ec*DERA should be immobilized in a plug-flow reactor to enable adjustment of the contact time between substrates and enzyme, which only lead to the mono aldol product (*R*)-3-hydroxy-octanal. Since such plug-flow reactors can easily be established with the HaloTag™-based immobilization approach (Döbber et al., 2018a; Döbber et al., 2018b), the HaloTag™ was genetically fused to the N-terminus of

*Ec*DERA[1]. Initial investigations on the activity of immobilized HaloTag-*Ec*DERA fusion enzymes revealed a very low residual activity (data not shown) and consequently, we focused on strategies to optimize catalytic activity of respective immobilizates. We hypothesized that low enzymatic activity resulted from an unfavorable orientation of the HaloTag™ in respective fusion enzymes causing negative interference on the activity of *Ec*DERA. According to Li and coworkers, spacer sequences have a great impact on the general interaction of single subunits in fusion enzymes and the length, rigidity and flexibility of these sequences can influence the overall orientation of the individual proteins to each other (Li et al., 2016). Based on this study, we selected two different spacer motifs: (*i*) the rigid (r) helix forming motif EAAAK and (*ii*) the flexible (f) motif GGGGS. In a first approach, these different motifs were combined with each other to yield spacer sequences of different rigidity and flexibility. Each spacer sequence contained five motifs indicating that the spacer length was kept constant at 25 amino acids (aa) but a different set of rigid and flexible motifs. As demonstrated in Figure 2.5-2, this led in total to six different fusion enzyme constructs. The most flexible spacer sequence 25 aa – 5f contained five repetitions of the flexible motif GGGGS which led to the spacer sequence $(GGGGS)_5$. In the remaining spacer sequences, rigidity was enhanced stepwise by exchange of single flexible motifs against the rigid motif EAAAK until no flexible sequence was left in the last spacer 25 aa- 5r ($(EAAAK)_5$). Overall, highest activity was achieved for constructs containing only rigid (5r) or flexible (5f) motifs while combination of the different motifs was less tolerated. In these constructs with highest activity, residual activity ranged around 12.5 % in comparison to the free *Ec*DERA without HaloTag™ whereas spacer sequences with a mixed set of both motifs revealed a residual activity down to 9 %. Therefore, we aimed to further optimize the catalytic activity of respective immobilizates and targeted the distance between HaloTag™ and *Ec*DERA as a potential factor contributing to reduced activity. Previous studies verified that distance between fusion partners can be enhanced proportionally with increasing repetitions of the rigid motif EAAAK (Arai et al., 2001). Consequently, we established several fusion enzyme constructs with different repetitions of the selected rigid motif leading to overall spacer sizes between 20 and 35 amino acids (aa). As shown in Figure 2.5-3, longer rigid spacer, like 30 aa – 6r, led to a clear increase in activity after immobilization of HaloTag-*Ec*DERA. However, this trend stops with even longer spacers of 30 aa and 35 aa where no further increase of activity was observed. The residual activity in comparison to the untagged *Ec*DERA without HaloTag™ was thereby enhanced up to 15 %. In summary, these experiments underline that a higher distance between the fusion partners is beneficial which indicates a potential steric hindrance of the HaloTag™ on the activity of *Ec*DERA. In addition, further factors might be involved in the activity reduction after immobilization, since activity could only be restored up to 15 % by this approach. Probably, factors such as the microenvironment established by the carrier or reduced enzyme flexibility due to the fixation on a support might contribute as well (Liese and Hilterhaus, 2013).

[1] A variant of *Ec*DERA was used containing the mutation C47M to enable higher stability towards acetaldehyde.

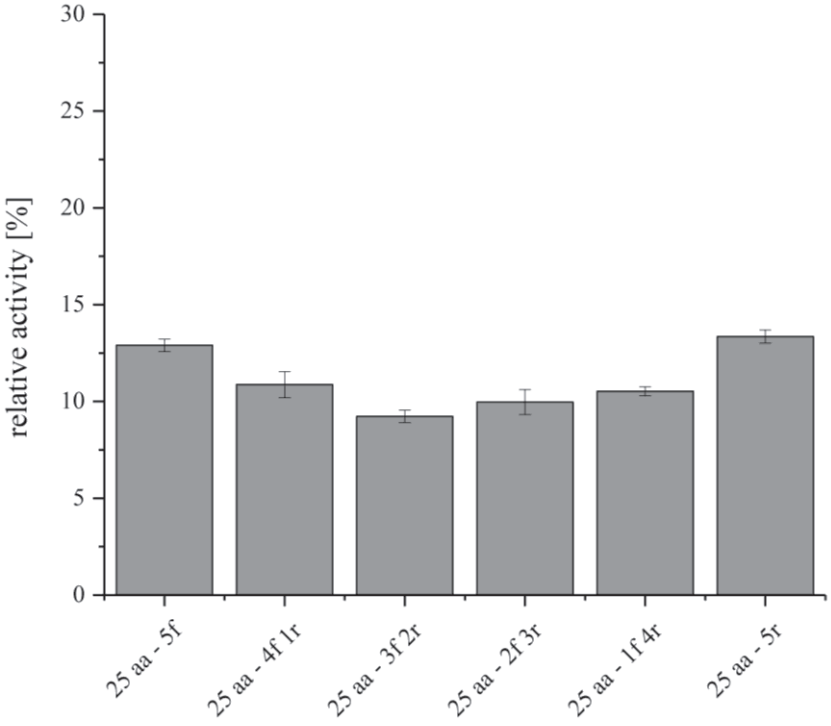

Figure 2.5-2: Effect of spacer rigidity and flexibility on the activity of immobilized HaloTag-*Ec*DERA. The spacer motifs EAAAK (rigid motif, r) and GGGGS (flexible motif, f) were combined with each other and integrated into HaloTag-*Ec*DERA fusion enzymes. Each spacer consisted of 5 motifs (different number of r or f) to give a total length of 25 amino acids (aa). After immobilization, the activity of each construct was analyzed by following the conversion of 2-deoxyribose-5-phospate into glyceraldehyde and acetaldehyde and compared to the activity of soluble *Ec*DERA without HaloTag™ (activity of soluble *Ec*DERA = 100 %). Detailed information about the spacer sequences is given in the experimental section. Error bars represent the variance of three activity measurements from the same sample.

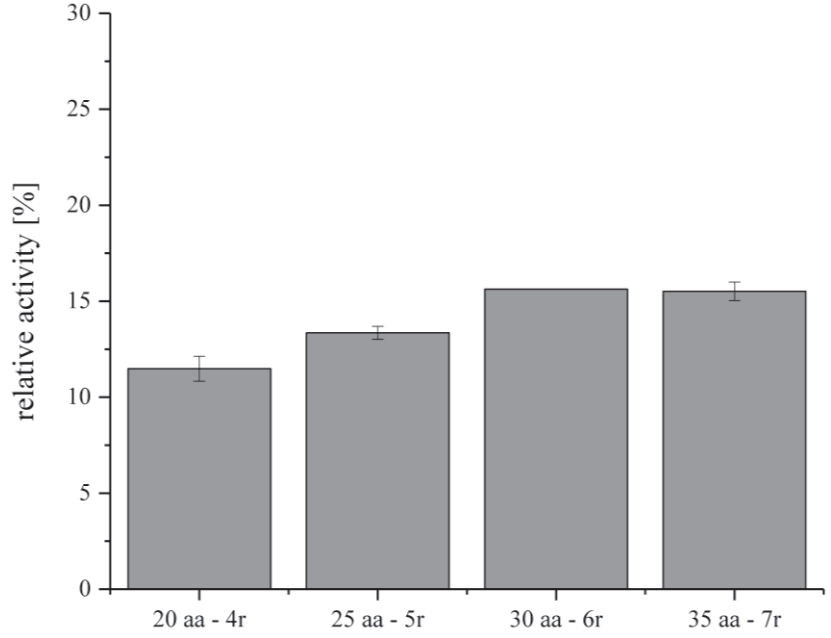

Figure 2.5-3: Effect of spacer length on the activity of immobilized HaloTag-*Ec*DERA. A different number of rigid motifs (r) was inserted into HaloTag-*Ec*DERA fusion enzymes yielding different lengths between 20 and 35 amino acids (aa). After immobilization, the activity of each construct was analyzed by following the conversion of 2-deoxyribose-5-phospate into glyceraldehyde and acetaldehyde and compared to the activity of soluble *Ec*DERA without HaloTag™ (activity of soluble *Ec*DERA = 100 %). Detailed information about the spacer sequences is given in the experimental section. Error bars represent the variance of three activity measurements from the same sample.

After optimization of the fusion enzyme design and partial restoring of catalytic activity, the production of mono aldol compounds was focused. As mentioned above, *Ec*DERA catalyzes the sequential addition of two acetaldehyde molecules to various aldehyde acceptors. Therefore, the synthesis of exclusively mono aldol products is challenging and requires a high control about the contact time between substrates and enzyme. To achieve this, the HaloTag™ immobilization strategy was employed for the fast and easy construction of plug-flow reactors as demonstrated previously (Döbber et al., 2018a; Döbber et al., 2018b). A crude cell extract solution containing HaloTag-*Ec*DERA (C 47M, 25aa – 5r) fusion enzymes was simply pumped through a plug-flow reactor previously filled with HaloLink™ Resin thereby covalently immobilizing HaloTag-*Ec*DERA fusion enzymes. Then, aldol formation was analyzed and synthesis of (*R*)-3-hydroxy-octanal starting from hexanal and acetaldehyde served as a model reaction. In general, mono aldol production was influenced by the residence time as well as the concentration and ratio of the substrates. As shown in Table 2.5-2, best results were achieved so far by applying a residence time of 7 min. Under these conditions, higher amounts of the target compound (*R*)-3-hydroxy-octanal were produced with an excess of acetaldehyde whereas higher substrate concentrations additionally led to increased production of the bis-aldol compound (*R*,*R*)-3,5-dihydroxy-decanal. In all cases, the *ee* of (*R*)-3-hydroxy-octanal was > 90 %. These results suggest that flow conditions can be adjusted such that only mono aldol product is produced. However, with increasing conversion above 50 % the probability for bis-aldol formation increases. In such cases, especially enzymes at the end of the plug-flow reactor would face a higher concentration of (*R*)-3-hydroxy-octanal in comparison to hexanal, which could shift the reaction towards bis-aldol formation. Therefore, full conversion with exclusively mono aldol products might be difficult to achieve although investigations are currently performed to further optimize the described reaction. If full conversion cannot be reached, the overall strategy has to be adapted. A solution could be the separation of the unreacted substrates hexanal and acetaldehyde from the target mono aldol compound in flow. Then, (*R*)-3-hydroxy-octanal would constantly be removed while substrates could be recycled and recirculated for a reentry into the plug-flow reactor. In such a reaction concept, the formation of the bis-aldol compound 3,5-dihydroxy-decanal would be detrimental and must be prevented to enable high purity of the mono aldol compound and low contamination of the unreacted substrates intended for recycling. However, suitable strategies for in-line separation of unreacted substrates from the reaction products have to be developed first. Second, the naturally high reactivity and instability of the substrates hexanal and acetaldehyde could prevent successful recycling. Therefore, additional investigations on these issues have to elucidate optimal strategies for most efficient mono aldol synthesis.

Table 2.5-2: Reaction optimization for the continuous production of (*R*)-3-hydroxy-octanal by immobilized HaloTag-*Ec*DERA. Aldol reaction of hexanal and acetaldehyde towards (*R*)-3-hydroxy-octanal (mono aldol product) was investigated under different conditions using HaloTag-*Ec*DERA (C47M, 25 aa – 5r). Side products formed during this reaction are listed (double aldol product = 3,5-dihydroxy-decanal; 2-octenal). Reactions were performed at the Institute of Bioorganic Chemistry, HHU Düsseldorf, by Julia Bramski. Experiments were performed in duplicate.

	reaction conditions			**results**			
entry	**residence time [min]**	**hexanal [mM]**	**acetaldehyde [mM]**	**hexanal [%]**	**mono aldol product [%]**	**double aldol product [%]**	**2-octenal [%]**
#1	7	200	160	46 ± 0.01	**48 ± 0.05**	5 ± 0.004	1 ± 0.001
#2	7	50	150	41 ± 0.01	**54 ± 0.05**	3 ± 0.004	2 ± 0.002
#3	7	200	600	22 ± 0.01	**64 ± 0.02**	13 ± 0.003	2 ± 0.002

2.5.4 Supporting information

DNA and protein sequences

a) DNA sequences to allow integration of different spacer in HaloTag-*Ec*DERA fusion enzymes

PCR primer to produce linear plasmid backbone:

Primer A: ATGACTGATCTGAAAGCAAGCAGCC

Primer B: ACCCGAGATTTCCAGAGTTG

Spacer ordered as linear fragment with overhangs (spacer, red; overhangs, blue and green)

25aa – 5f

aactctggaaatctcgggtgcaggcggcggtgggagtggtggcggcggatcgggcggtggaggtagtggcggcggcggcagcg
gtggtggtggctcagctatgactgatctgaaagcaag

25aa – 4f1r

aactctggaaatctcgggtgcggaggcggcggcaaaaggtggtggcggcagtggcggcggtggttctggaggcggagggagtgg
aggtggtggctccgccatgactgatctgaaagcaag

25aa – 3f2r

aactctggaaatctcgggtgcggaagccgccgcaaaaggaggtggtggaagtggcggtggcgggtctgaggctgcggcaaaagg
cggtggcggctcggccatgactgatctgaaagcaag

25aa – 2f 3r

aactctggaaatctcgggtgctgaagcagccgcgaaaggcggtggcggtagtggtggtggaggctcagaggcggcagcaaaagaa
gcggccgctaaagcgatgactgatctgaaagcaag

25aa – 1f4r

aactctggaaatctcgggtgcagaagctgcggcaaaaggtggcggtggaagtgaagcggcggccaaagaagcagcagcgaaaga
agcggcagcaaaggcgatgactgatctgaaagcaag

25aa – 5r

aactctggaaatctcgggtgccgaagcggcggccaaagaggccgcagcaaaagaggcagctgccaaagaggcggcagcgaaag
aagctgccgctaaagcaatgactgatctgaaagcaag

20aa – 6r

aactctggaaatctcgggtgccgaagctgccgccaaagaggctgcagcgaaggaagcggctgccaaagaggcagcggcgaaaga
agccgcagcgaaagaagcggcagccaaagcgatgactgatctgaaagcaag

20 aa – 7r

aactctggaaatctcgggtgccgaagcagcggcgaaagaagcggcagcgaaagaggctgctgcgaaggaagcagccgccaaag
aggccgcagccaaggaagcggctgcgaaagaagccgctgcgaaagcaatgactgatctgaaagcaag

b) DNA sequence encoding for HaloTag-*Ec*DERA C47M

The open reading frame encoding for HaloTag-*Ec*DERA with spacer 20 aa – 4r is listed below. Different colors indicate DNA fragments encoding for different fusion enzyme components: HaloTag™, green; spacer 20aa – 4r, red; *Ec*DERA C47M, blue. All other fusion enzyme construct contained the same fragments encoding for the HaloTag™ and *Ec*DERA C47M but different spacer sequences as given above.

atgaaacatcaccatcaccatcacgcagaaattggtacgggatttccgtttgacccgcattatgtggaggttctgggtgaacgcatgcactacgtggat
gttggtccgcgcgatggcacaccggtgctgtttctgcatggtaatccgacctccagctatgtttggcgcaacattattccgcatgtcgccccaacgcat
cgctgtattgccccagatctcattggcatgggcaaaagcgacaaaccggatttgggctacttcttcgacgatcacgtacggtttatggacgcctttatc
gaggctctgggactcgaggaagtagtgctggttattcatgactggggctctgcattaggctttcactgggctaaacggaacccagaacgcgtcaagg
ggattgccttcatggagttcatccgtccgattccgacctgggatgaatggcccgaatttgcccgtgaaacctttcaggcgtttcgtaccacggatgttg
gccgtaagctcatcatcgaccaaaacgtgttcattgagggcactcttcccatgggagtagtgcgtcctttaaccgaagtcgagatggaccactatcgc
gaacccttcctgaatccggttgatcgcgaaccgctgtggcgcttcccgaatgagctgcctattgctggtgaaccggcgaatatcgtggcacttgtgga
agaatacatggattggctgcatcagagtccagtccctaagctgttgttttggggtacacctggcgtgttgattccgcctgcagaagctgctcgcttagc
gaaaagcttgcccaactgcaaagcggtcgatattgggccaggtctgaacctgttacaggaggataacccggatctgatcgggagtgaaatcgcgc
gttggctgtcaactctggaaatctcgggtcttgcagaagcagcggccaaagaagctgcggccaaagaggcagccgcgaaagaagcagcggcga
aagcggccgcgatgactgatctgaaagcaagcagcctgcgtgcactgaaattgatggacctgaccaccctgaatgacgacgacaccgacgagaa
agtgatcgccctgtgtcatcaggccaaaactccggtcggcaataccgccgctatcatgatctatcctcgctttatcccgattgctcgcaaaactctgaa
agagcagggcaccccggaaatccgtatcgctacggtaaccaacttcccacacggtaacgacgacatcgacatcgcgctggcagaaacccgtgcg
gcaatcgcctacggtgctgatgaagttgacgttgtgttcccgtaccgcgcgctgatggcgggtaacgagcaggttggttttgacctggtgaaagcct
gtaaagaggcttgcgcggcagcgaatgtactgctgaaagtgatcatcgaaaccggcgaactgaaagacgaagcgctgatccgtaaagcgtctgaa
atctccatcaaagcgggtgcggacttcatcaaaacctctaccggtaaagtggctgtgaacgcgacgccggaaagcgcgcgcatcatgatggaagt
gatccgtgatatgggcgtagaaaaaaccgttggtttcaaaccggcgggcggcgtgcgtactgcggaagatgcgcagaaatatctcgccattgcaga
tgaactgttcggtgctgactgggcagatgcgcgtcactaccgctttggcgcttccagcctgctggcaagcctgctgaaagcgctgggtcacggcga
cggtaagagcgccagcagctactaa

b) Protein sequence encoding for HaloTag-*Ec*DERA C47M

The protein sequence of HaloTag-*Ec*DERA C47M containing spacer 20aa – 4r is given below. Different colors indicate different fusion enzyme components: HaloTag™, green; spacer 20aa – 4r, red; *Ec*DERA C47M, blue. All other fusion enzyme constructs contained the same sequence of the HaloTag™ and *Ec*DERA C47M but different spacer sequences as given in Table 2.5-1.

MKHHHHHHAEIGTGFPFDPHYVEVLGERMHYVDVGPRDGTPVLFLHGNPTSSYVWRNIIPHVAPTHRC
IAPDLIGMGKSDKPDLGYFFDDHVRFMDAFIEALGLEEVVLVIHDWGSALGFHWAKRNPERVKGIAFM
EFIRPIPTWDEWPEFARETFQAFRTTDVGRKLIIDQNVFIEGTLPMGVVRPLTEVEMDHYREPFLNPVDR
EPLWRFPNELPIAGEPANIVALVEEYMDWLHQSPVPKLLFWGTPGVLIPPAEAARLAKSLPNCKAVDIG
PGLNLLQEDNPDLIGSEIARWLSTLEISGLAEAAAKEAAAKEAAAKEAAAKAAAMTDLKASSLRALKL
MDLTTLNDDDTDEKVIALCHQAKTPVGNTAAIMIYPRFIPIARKTLKEQGTPEIRIATVTNFPHGNDDIDI
ALAETRAAIAYGADEVDVVFPYRALMAGNEQVGFDLVKACKEACAAANVLLKVIIETGELKDEALIRK
ASEISIKAGADFIKTSTGKVAVNATPESARIMMEVIRDMGVEKTVGFKPAGGVRTAEDAQKYLAIADEL
FGADWADARHYRFGASSLLASLLKALGHGDGKSASSY

3 General Discussion

In the following chapters, the results mentioned in section 2 will be comparatively discussed to evaluate the HaloTag™-based immobilization approach and tag-based immobilization strategies in general. Where appropriate, unpublished results were added to further evaluate the usefulness of these techniques for biocatalysis.

3.1 Overview of results

Chapter 2.1 describes a first proof of concept to achieve the one-step purification and immobilization of biocatalysts with the HaloTag™ immobilization strategy. The *Pf*BAL was selected as a model enzyme and the speed of immobilization, the obtained purity as well as the storage and operational stability of produced immobilizates were investigated.

Chapter 2.2 reports on the optimization of a two-step enzymatic cascade for the production of chiral 1,2-amino alcohols by immobilizing the *Pp*BFD and the *Bm*TA. Experiments focused on the separation of both reaction steps to allow consecutive batch reactions under optimal conditions for each step. Furthermore, the recycling of both immobilized enzymes was targeted to enhance respective productivities.

Chapter 2.3 is based on the transfer of the HaloTag™ immobilization concept from applications in batch to continuous reaction systems. The easy construction of plug-flow reactors by immobilizing HaloTag™ fusion enzymes in flow was investigated and the usefulness of established protocols was evaluated for the continuous production of chiral alcohols employing immobilized HaloTag-*Lb*ADH. Furthermore, the modularity of such flow modules was analyzed to establish a two-step chemo-enzymatic reaction cascade towards a chiral epoxide.

In chapter 2.4, investigations on the modular combination of biocatalytic flow modules, which were established using the HaloTag™ immobilization approach, were intensified and the development of a continuous two-step enzymatic cascade towards chiral vicinal diols was targeted. Factors influencing stability of immobilized enzymes (here *Pp*BFD and *Lb*ADH) were analyzed and the flow concept was used to guarantee optimal conditions for each step by removing or introducing compounds and reactants, respectively, exactly at the time and place required.

Chapter 2.5 reports on further intensification of the HaloTag™ immobilization strategy and describes the development of tools to enhance the residual activity of immobilized enzymes. The *Ec*DERA was selected as a model enzyme and different spacer sequences connecting the HaloTag™ with the aldolase were analyzed to find optimal orientation of both fusion partners to each other. In a second step, immobilized aldolases were employed to access mono aldol products in a continuous reaction system.

3.2 Selected Model enzymes

As mentioned in the introduction, a huge variety of different immobilization methods has been developed to address the specific requirements of individual biocatalysts. The potential of an immobilization method can only be determined based on the evaluation of an appropriate set of biocatalysts reflecting the diversity among enzymes with respect to structure, size and cofactors. As shown in Table 3.2-1, the enzymes selected for this thesis differ in size, the number of subunits and the requirement of cofactors. One of these cofactors (NADPH) must be actively regenerated, whereas the regeneration of the other occurs during the respective catalytic cycle (see 1.5). The smallest enzyme is *Ec*DERA which has a subunit size of 28 kDa and occurs as monomer and dimers. In comparison, the tetrameric *Pf*BAL is more than four times bigger and is generally the largest selected model enzyme.

Table 3.2-1: Model enzymes selected in this thesis for evaluation of tag-based immobilization strategies

enzyme	source	size per subunit	active structure	cofactors
2-deoxyribose-5-phosphate aldolase (DERA)	*E. coli*	28 kDa (260 aa)	monomer/dimer	-
alcohol dehydrogenase (ADH)	*L. brevis*	27 kDa (250 aa)	tetramer	$NADP^+$/ $NADPH + H^+$; Mg^{2+}
ω-transaminase (TA)	*B. megaterium*	53 kDa (470 aa)	tetramer	PLP
benzoylformate decarboxylase (BFD)	*P. putida*	56 kDa (530 aa)	tetramer	ThDP; Mg^{2+}
benzaldehyde lyase (BAL)	*P. fluorescens*	59 kDa (560 aa)	tetramer	ThDP; Mg^{2+}

3.3 One-step purification and immobilization

3.3.1 Production of fusion enzymes

The fusion of an additional peptide or protein can sometimes lead to the production of completely insoluble recombinant enzymes, although the wild type enzyme without tag was soluble (Krauss et al., 2017). Therefore, the success of tag-based immobilization strategies greatly depends on the effect of

the respective tags on the soluble production of fusion enzymes in microbial hosts. As mentioned in section 2 and as summarized in Figure 3.3-1, all HaloTag™ fusion enzymes were successfully produced in a soluble form and high expression levels were achieved. Figure 3.3-1 shows an intense protein band in respective SDS-PAGE pictures at the position corresponding to the size of one monomer of each fusion enzyme. As can be deduced from the intensity of the signals for the recombinant fusion enzymes, HaloTag-*Ec*DERA, HaloTag-*Lb*ADH, and HaloTag-*Pp*BFD showed the highest titers.

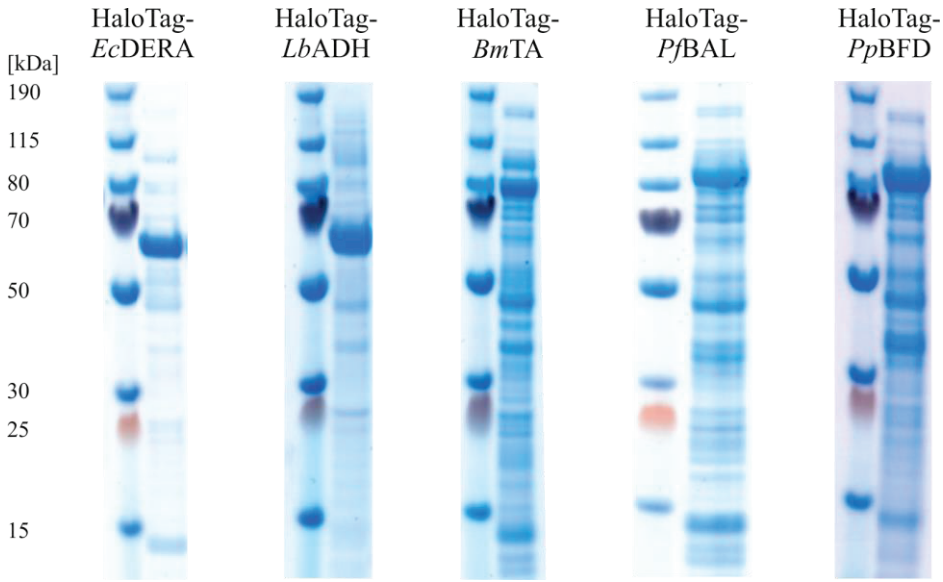

Figure 3.3-1: Heterologous production of HaloTag™ fusion enzymes in *E. coli*. The HaloTag™ was fused to the N-terminus of the selected model enzymes (*Ec*DERA = desoxyribose-5-phosphate aldolase from *E. coli*, 64.5 kDa; *Lb*ADH = alcohol dehydrogenase from *L. brevis*, 63.5 kDa; *Bm*Ta = ω-transaminase from *B. megaterium*, 89.7 kDa; *Pf*BAL = benzaldehyde lyase from *P. fluorescens*, 95.7 kDa; *Pp*BFD = benzoylformate decarboxylase from *P. putida*, 93.4 kDa). The picture shows the soluble crude cell extract after cell lysis and centrifugation. PageRuler™ Plus Prestained Ladder (ThermoFischer Scientific, Germany) was used as a protein marker.

Overall, the observation of good expression yields matches with previous reports, which highlight the potential of the HaloTag™ to rather improve the soluble production of fusion enzymes in bacterial expression systems (Ohana et al., 2009; Peterson and Kwon, 2013; Sun et al., 2015). In general, the fusion of certain tags such as the maltose-binding protein (MBP) or the N-utilization substance (NusA) are common strategies in molecular biology to induce the soluble production of insoluble proteins (Costa et al., 2014). To assess the solubility enhancing effect of the HaloTag™ in comparison to these commonly applied tags, a comparative study was performed by fusion of more than 20 human proteins to the HaloTag™ as well as to further tags like MBP (Ohana et al., 2009). While MBP resulted in the soluble production of around 50 % of the constructed fusion enzymes, the HaloTag™ induced efficient production of more than 70 % of the investigated proteins indicating the great potential of the HaloTag™ for such applications. Although the exact solubility-enhancing mechanism is yet unclear, a chaperon-like activity or the attraction of chaperones are discussed. (Douette et al., 2005; Nallamsetty

and Waugh, 2007). In case of the HaloTag™, the authors referred to a great intrinsic stability and a reduced tendency to induce aggregation but exact explanations remain elusive (Ohana et al., 2009). Therefore, the HaloTag™ can be considered as a suitable fusion partner with respect to the production of corresponding fusion enzymes and may also enable improved production of biocatalysts with insufficient expression yields in microbial host strains.

3.3.2 Immobilization of fusion enzymes

Binding on the HaloLink™ Resin

A great challenge in enzyme immobilization is the establishment of covalent bonds under conditions that do not affect the enzyme´s activity and stability. Of utmost importance is the time required to establish such bonds. For example, the covalent immobilization of enzymes via epoxy groups exposed on carriers takes up to several days due to the low reactivity of such reactions (Mateo et al., 2007a). During such a long incubation time, activity and stability of the enzyme may be negatively influenced. Furthermore, the general conditions required for covalent bond formation may be unfavorable, too. For example, functional groups present in enzymes or carriers and targeted for covalent bond formation need in some cases extreme pH values to render these groups reactive. An example is the binding of enzymes to glyoxyl-modified supports. (Mateo et al., 2013). Such supports expose aldehyde groups and are used for the formation of Schiff bases with amino groups present in enzymes. Therefore, an alkaline pH is required to activate the amino groups. In comparison, the immobilization of HaloTag™ fusion enzymes is possible directly from a crude cell extract solution after cell lysis. As exemplarily shown in chapter 2.1, all fusion enzymes studied in this thesis bound covalently within minutes to the employed HaloLink™ Resin. This allows immobilization in a physiological environment with optimal pH and temperature keeping potential stress factors for the biocatalyst at a minimum. Despite the use of different cofactors like ThDP or PLP and various buffering compounds of standard use in biochemistry such as phosphate ions, triethanolamine or Tris, a successful immobilization on HaloLink™ Resin was always achieved within a few minutes of contact time (see section 2). As mentioned in the introduction (see 1.4.2), this high affinity was also reported previously and binding kinetics were characterized to range in the same order of magnitude as streptavidin and biotin (HaloTag™: $2.7*10^6$ $M^{-1}s^{-1}$; Streptavidin: $8.5*10^6$ $M^{-1}s^{-1}$) (Los et al., 2008). This additionally allowed easy loading of packed-bed reactors in flow. Chapter 2.3 and 2.4 clearly indicate that such reactors could be loaded by simply pumping a crude cell extract solution through the packed-bed in the fully assembled reactor setup, which simplifies the immobilization even further. No additional equipment or further process steps are needed to establish continuous reaction systems and immobilization can be performed directly before the intended reaction. Besides, immobilization can

potentially be automated with the help of suitable pumps which perform loading and washing steps without the need for any external adjustments.

A further point for evaluation is the protein load achieved after immobilization. Therefore, a comparative analysis of all achieved carrier loadings is shown in Table 3.3-1, based on the same amount of lyophilized crude cell extract and HaloLink™ Resin, respectively.

Table 3.3-1: Comparison of protein load achieved after immobilization of different HaloTag™ fusion enzymes. 5 mg of lyophilized crude cell extract were added to 50 µl of HaloLink™ Resin in a total volume of 250 µl at 25 °C and 1200 rpm in a Thermomixer. The protein load per ml of HaloLink™ Resin is given and was determined with the BCA assay. For abbreviation of enzymes see Figure 3.3-1. Detailed information about the immobilization of all enzymes is given in section 2: 2.1: *Pf*BAL; 2.2: *Bm*TA; 2.3: *Lb*ADH, 2.4: *Pp*BFD, 2.5: *Ec*DERA. Experiments were performed in duplicate.

	HaloTag-*Ec*DERA	HaloTag-*Lb*ADH	HaloTag-*Bm*TA	HaloTag-*Pp*BFD	HaloTag-*Pf*BAL
load [mg/ml]	5.1 ± 0.05	13 ± 0.6	2.4 ± 0	6.8 ± 0.3	2.7 ± 0.06
size	monomer/dimer 28 kDa	tetramer 27 kDa	tetramer 53 kDa	tetramer 56 kDa	tetramer 59 kDa

As shown in Table 3.3-1, the protein load varied in a range from 2.4 mg/ml observed for HaloTag-*Bm*TA to 13 mg/ml achieved for HaloTag-*Lb*ADH, which might be due to different factors. First of all, the size of the enzyme can lead to different loads after immobilization since larger fusion enzymes might potentially block neighboring chloroalkane binding ligands thereby reducing the overall protein load. However, the size of the fusion enzyme cannot be the only reason to explain the observed differences. *Lb*ADH forms a tetramer but the achieved protein load is almost three times higher in comparison to the dimeric *Ec*DERA with comparable subunit size. Furthermore, the molecular weights of *Pp*BFD and *Pf*BAL are similar but the protein load obtained with *Pp*BFD was two-times higher. Therefore, additional effects must be considered. Besides size, the concentration of the respective fusion enzyme in the crude cell extract is an important factor, too, and lower concentrations of the fusion enzymes would consequently lead to lower protein loads, if the amount of resin and the contact time are kept constant. As demonstrated in Figure 3.3-1, HaloTag-*Bm*TA and HaloTag-*Pf*BAL revealed the lowest expression yields. This most probably explains why for these enzymes the lowest protein loads were observed (Table 3.3-1). Nevertheless, the protein load achieved after immobilization of HaloTag-*Ec*DERA, which features the lowest molecular weight and a very high expression yield, is lower than expected. Therefore, it can be assumed that the properties of the enzyme fused to the HaloTag™ might influence the affinity towards the resin as well. As proposed by Liese and coworkers, the charge or polarity of the carrier surface might induce repulsion or attraction of fusion enzymes with a specific surface charge and consequently affect binding of HaloTag™ fusion enzymes (Liese and Hilterhaus, 2013). Furthermore, both fusion partners might interact with each

other and could disturb each other in their catalytic activity leading not only to reduced catalytic activity of the enzyme but also to lowered binding affinity of the HaloTag™. To sum up, size, expression yield, and the specific structure of the fusion enzymes might contribute to the protein load observed after immobilization.

Considering the amount of crude cell extract applied, general conclusions concerning the binding efficiency in relation to the total amount of applied fusion enzymes can be drawn. Related to 1 ml of HaloLink™ Resin, 100 mg of lyophilized crude cell extract were applied for each immobilization. Since buffering salts account to the weight of lyophilized crude cell extracts as well, the total protein amount employed for each immobilization probably ranged around 50 mg. The exact proportion of the HaloTag™ fusion enzymes in the crude cell extract can hardly be estimated but most probably ranged between 10 % (e.g. HaloTag-*Bm*TA) and 50 % (e.g. HaloTag-*Ec*DERA) based on the SDS-PAGE pictures shown in Figure 3.3-1. If a fusion enzyme content of 10 % is assumed for HaloTag-*Bm*TA and HaloTag-*Pf*BAL, around 50 % of all employed fusion enzymes would have bound on the carrier (2.4 mg and 2.7 mg, respectively, out of 5 mg employed fusion enzymes, see Table 3.3-1). This estimation is supported by the binding studies shown in chapter 2.1. In this experiment, 300 µg of purified HaloTag-*Pf*BAL were employed for immobilization but the protein load did not exceed 150 µg although the amount of HaloLink™ Resin used in this experiment should have had the capacity to bind at least 350 µg of HaloTag™ fusion enzyme[1]. In addition, also for HaloTag-*Pp*BFD and HaloTag-*Ec*DERA no complete binding of all employed fusion enzymes can be expected. Only in the case of HaloTag-*Lb*ADH, complete binding of all employed fusion enzymes was potentially prevented due to full saturation of the carrier which has got a binding capacity of at least 7 mg/ml[1] but a protein load of 13 mg/ml was observed. Although the exact reasons for the incomplete binding remains to be elucidated, a general hypothesis could be that the surface of the carrier is rapidly covered by fusion enzymes, which subsequently prevents the binding of further fusion enzymes. However, further investigations are necessary to explain this phenomenon.

Purity after immobilization

Tag-based immobilization methods enable the targeted binding of respective biocatalysts from crude mixtures thereby achieving a simultaneous purification (see 1.4.2). However, the purity is determined by the affinity of further proteins towards the carrier in comparison to the affinity as well as the concentration of the target fusion enzyme present in the crude cell extract (Lichty et al., 2005). Especially, poor production of the target enzyme leads to a higher competition for potential binding sites and consequently, to a lower purity, if unspecific binding of host cell proteins occurs. In the chapters above, the high affinity of the HaloTag™ and the good protein production in *E. coli* were

[1] Technical Manual HaloLink™ Resin, Promega Corporation, Madison, WI, USA; accessed February 2018: The HaloLink™ Resin has a binding capacity of 7 mg/ml. In the mentioned experiment, 50 µl of resin was used, which would correspond to a binding capacity of 350 µg.

already discussed, which provides the basis for the high purity observed for immobilized HaloTag™ fusion enzymes in this thesis (see section 2). In addition, the HaloLink™ Resin consists of Sepharose® beads, which is a commercially available form of cross-linked agarose and often used for protein purification such as size exclusion chromatography (Ahmed, 2004). The reason for its frequent application for chromatographic purposes in protein biochemistry is its availability from cheap and renewable resources as well as its low unspecific protein binding, which further explains the high purity achieved after immobilization. However, one additional weak protein band with a molecular weight between 30 and 40 kDa often appears in respective SDS-PAGE pictures (e.g. in chapter 2.1 or 2.4) suggesting that this band might correspond to truncated HaloTag™ fusion enzymes (HaloTag™ 34 kDa). Since this band was always observed at the same position in respective SDS-PAGE gels, truncation seemed to occur in the same manner in all cases. Probably, this truncation leads to the production of a functional HaloTag™ capable of binding to the HaloLink™ Resin. The reason can either be a termination of expression or a proteolysis of respective fusion enzymes (Zuker, 2003). In both cases, it is likely that the DNA or amino acid sequence at the end of the HaloTag™ triggered such events since termination or lysis at other positions would have led to inactive HaloTag™ protein or to fragments of a bigger molecular weight. In most of the fusion enzymes, this sequence consists of a repetitive motif $A(EAAAK)_4A$, which was chosen to establish a spatial distance between both fusion partners (Arai et al., 2001). This sequence was analyzed with different bioinformatic tools to evaluate either proteolysis or termination of expression. First, the amino acid sequence of HaloTag™ fusion enzymes was submitted to the web server PROSPER, a tool for predicting potential cleavage sites (Song et al., 2012). This analysis gave no specific preference for enzymatic cleavage at this site indicating that proteolysis might not explain the observed results. Second, termination of expression was investigated. The just mentioned spacer sequence could either be involved in termination of transcription or translation. Since termination of translation strongly depends on stop codons not present in this sequence (Petry et al., 2008), a potential termination of transcription is more likely. Transcription of DNA into RNA in bacteria can either be terminated by specific hairpin motifs followed by uridine rich sequences or by a specific protein named Rho (Porrua et al., 2016). Rho binds to the nascent transcript but binding sequences are not specific so it cannot be determined, whether such a mechanism could provoke fusion enzyme truncation. In contrast, secondary structures such as hairpins of DNA and their corresponding RNA sequences can be predicted with bioinformatics tools. Figure 3.3-2 shows predictions of the spacer sequence produced with two different bioinformatics tools. Both tools predict the formation of several hairpin structures in the corresponding RNA sequence. Although uridine-rich sequences are missing after these hairpin structures at the initial RNA sequence of respective model enzymes, such secondary structures might explain the occurrence of truncated fusion enzymes. Therefore, further experiments might target this hypothesis by for example completely removing any spacer sequences to analyze the effect on the formation of truncated fusion enzymes.

Nevertheless, the HaloTag™ enabled the covalent immobilization of several model enzymes within minutes from crude cell extracts under mild conditions, proving its usefulness in establishing respective immobilization bonds. However, the activity of the immobilized biocatalysts is an important factor as well and will be discussed in the following chapter.

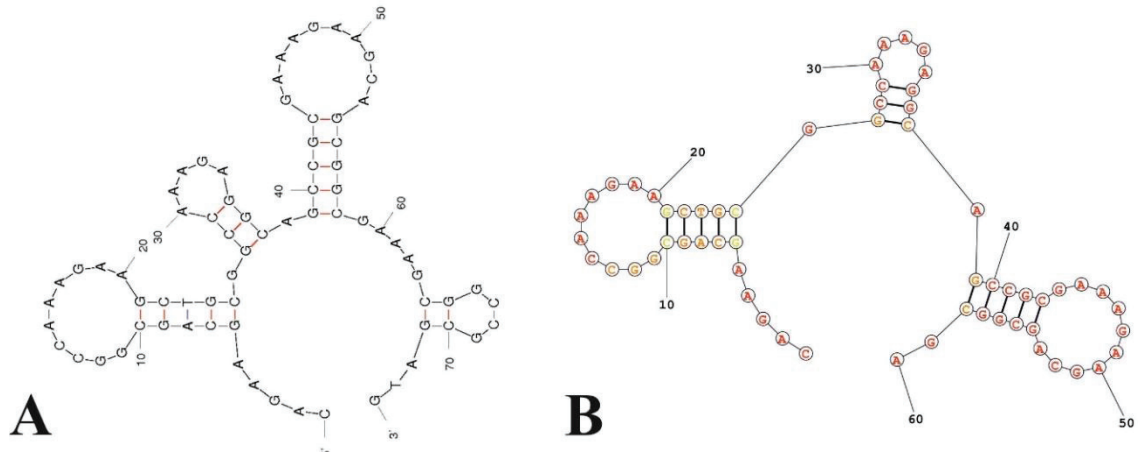

Figure 3.3-2: RNA-fold prediction of DNA spacer sequence A(EAAAK)$_4$A mainly used in this thesis to separate fusion partners in HaloTag™ fusion enzymes. A: Bioinformatic prediction tool: "Predict a Secondary Structure Web Server" offered by the Mathews group, Department of Biochemistry & Biophysics, University of Rochester, New York, USA, accessed via: https://rna.urmc.rochester.edu/ - February 2018. B: Bioinformatic prediction tool: "The mfold web server" (Zuker, 2003), The RNA Institute, University of Albany, New York, USA, accessed via: http://unafold.rna.albany.edu/ - February 2018.

3.4 Activity of immobilized fusion enzymes

3.4.1 Characterization of model enzymes

An important measure for the evaluation of every immobilization method is the activity of respective fusion enzymes in comparison to their free counterparts. As mentioned in the introduction (see 1.4.1), covalent immobilization strategies targeting amino acid side chains for immobilization permits only limited control about the immobilization site and residues essential for the catalytic activity may be altered, which might impair activity drastically.

As mentioned in section 2 and summarized in Figure 3.4-1, the residual activity of the investigated fusion enzymes after immobilization ranged between 10 % and 75 %. Interestingly, the size of the fusion enzymes correlated with the observed activities of the immobilized enzymes. *Bm*TA, *Pp*BFD as well as *Pf*BAL are composed of relatively large subunits of 52 - 58 kDa without HaloTag™ and each of them forms a tetramer in its active conformation (see 1.5). Despite these high molecular weights, more than 50 % of residual activity was retained in the immobilizates compared to the free enzyme without the HaloTag™. In comparison, *Lb*ADH forms a tetramer as well but has smaller subunits of only 27 kDa (see 1.5.2). However, the residual activity reached only 50 % compared to the larger fusion enzymes. Finally, the lowest residual activity of around 10 % was found for *Ec*DERA which is

characterized by the lowest complexity since it has small subunits, exists as monomers as well as dimers and needs no additional cofactors for catalytic activity (see 1.5.4).

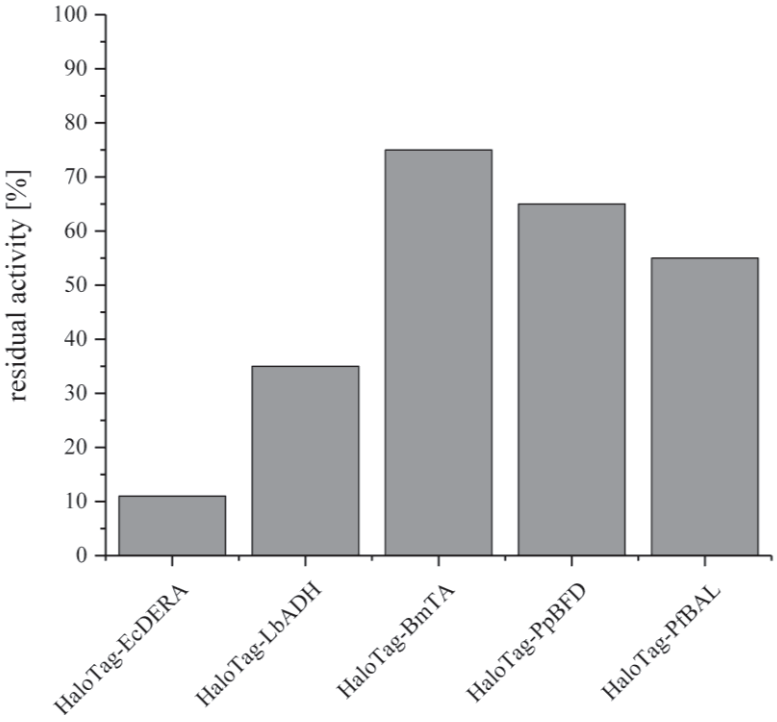

Figure 3.4-1: Residual activity of HaloTag™ fusion enzymes in comparison to their free counterparts without HaloTag™. Activity of free reference enzymes was defined as 100 % and activity was compared in aqueous buffered systems. For further information see section 2.

In general, a loss of activity after immobilization can be due to several reasons including for example mass-transfer limitations, reduced flexibility or an unfavorable microenvironment established by the used carrier (Guisan, 2006; Liese and Hilterhaus, 2013). Particularly for tag-based immobilization strategies, the tag may negatively interfere with the conformation of the biocatalyst due to its big size thereby reducing catalytic activity. Such interference could impair smaller enzymes more pronouncedly than larger ones. However, this does not explain the differences observed for *Pf*BAL, *Pp*BFD and *Bm*TA, since all of them from tetramers of comparable size. Furthermore, chapter 2.1 showed that free HaloTag-*Pf*BAL fusion enzymes were even more active than the reference enzyme without HaloTag™. In this particular case, loss of activity was only observed after immobilization indicating that steric interference may not be the only reason to explain the loss of activity. To develop further hypotheses, a general idea about how immobilization proceeds in case of the selected model enzymes is required. The HaloTag™ was fused to the N-terminus of the selected model enzymes. As each monomer of a model enzyme carries one HaloTag™, there are one to two (*Ec*DERA) or four HaloTags™ (*Bm*TA, *Pp*BFD, *Pf*BAL, *Lb*ADH) present in the final quaternary structure. In the selected model enzymes, the N-termini are arranged in a mirror-symmetrical manner indicating that

the associated HaloTags™ are positioned oppositely (Hasson et al., 1998; Heine et al., 2004; Mosbacher et al., 2005; Niefind et al., 2003; van Oosterwijk et al., 2016). For example, two N-termini of *Pf*BAL are exposed on one site of the tetrameric enzyme complex while the other two are grouped on the opposite site (Mosbacher et al., 2005). Consequently, binding of fusion enzymes to the HaloLink™ Resin will probably occur only via one site, while HaloTags™ exposed on the opposite will not be involved. This leads to the assumption that only a portion of subunits are covalently immobilized, whereas the adjacent subunits are bound to each other by non-covalent interactions. The rigidification of single subunits by covalent attachment may therefore compromise the functional interaction in a multimeric enzyme, thereby reducing the catalytic activity either by partial dissociation of the oligomer or by influencing the interaction of active sites in the oligomeric enzymes (Frank et al., 2007). According to this hypothesis, model enzymes displaying strong intermolecular subunit interactions should retain a higher residual activity. To assess such subunit interactions, the interface areas between subunits could be a potential measure since large interface areas are stabilized by a larger number of non-covalent interactions (Andrews et al., 2014). Such data was already published for each model enzyme and is summarized in Table 3.4-1.

Table 3.4-1: Interface areas between subunits of model enzymes used in this thesis. *Ec*DERA forms a dimer and consequently possesses only one interface area. For *Lb*ADH, all interface areas along all three interaction sites in the tetramer are listed. *Pf*BAL, *Pp*BFD and *Bm*TA form dimers of dimers. Therefore, the interfaces of two monomers forming a dimer and between the dimers forming a tetramer are listed. Abbreviations for model enzymes see Figure 3.3-1.

model enzyme	residual activity [%]	interface area [Å^2]	reference
*Ec*DERA	10	444	Heine et al., 2004
*Lb*ADH	35	289, 1641, 1652	Niefind et al., 2003
*Pf*BAL	55	1790 (between dimers) 3270 (within dimer)	Mosbacher et al., 2005
*Pp*BFD	65	1601 (between dimers) 3475 (within dimer)	Andrews et al., 2014
*Bm*TA	75	2850 (between dimers) 5700 (within dimer)	van Oosterwijk et al., 2016

As shown, the interface areas correlate with the observed residual activity, with the largest interface area and highest residual activity for *Bm*TA and the lowest values for both parameters for *Ec*DERA. One can expect that enzymes with larger subunits exhibit larger interface areas but this argument does not hold for *Bm*TA, which has almost the same subunit size as the selected ThDP-dependent enzymes but a much larger interface area between the subunits. This could point towards a distortion of subunit interaction upon immobilization in case of *Pp*BFD and *Pf*BAL and could explain higher residual

activities for *Bm*TA with stronger subunit interactions. However, a major drawback of this hypothesis is that the need for oligomerization to enable catalytic activity in case of *Ec*DERA and *Lb*ADH is questionable. While at least dimerization in the other model enzymes is a prerequisite for catalytic activity, since the active sites are formed at the interface of two subunits, active sites in *Ec*DERA and *Lb*ADH are principally not influenced by the quaternary structure. (Andrews et al., 2014; Heine et al., 2004; Mosbacher et al., 2005; Niefind et al., 2003; van Oosterwijk et al., 2016). On the contrary, a potential influence of oligomerization on the catalytic activity cannot be excluded completely. In addition, the importance for oligomerization was proven in related enzymes of *Lb*ADH and *Ec*DERA. For example, dissociation of several alcohol dehydrogenases resulted in a complete loss of activity (Cheng et al., 1968; Pauly and Pfleiderer, 1977) and oligomerization in several aldolases was found to preserve their catalytic mechanism (Katebi and Jernigan, 2015). To summarize this discussion, based on the five examples studied in this thesis the loss of activity cannot be fully explained and the higher residual activity of bigger model enzymes could also be simply accidental. Most probably, several effects contribute to lower catalytic activity after immobilization such as steric hindrance of the tag, influences on the quaternary structure or an unfavorable microenvironment established by the selected carrier.

The residual activities discussed above refer to the comparison of immobilized HaloTag™ enzymes with soluble, non-immobilized reference enzymes without HaloTag™ in aqueous buffered systems. However, chapter 2.3 revealed the influence of the reaction conditions when comparing free and immobilized enzymes. Under aqueous reaction conditions, a huge difference between free and immobilized *Lb*ADH was found but in the presence of THF and 2-propanol, both formulations of the biocatalyst performed similarly. These findings indicate that immobilization can lead to stabilization against deactivating factors such as organic co-solvents, while free enzymes are directly exposed, which in turn influences the initial rate activity. Therefore, a comparison of both catalyst formuations under applied reaction conditions is necessary to fully evaluate the potential of immobilized biocatalysts.

Nevertheless, enzyme inactivation upon immobilization is often observed (see 1.4). To further evaluate the HaloTag™-based immobilization, a comparison with already published results about the covalent immobilization of the selected model enzymes is necessary. Such publications exist for almost all of the selected model enzymes except for the *Bm*TA. For both ThDP-dependent enzymes, several covalent immobilization approaches were reported. For example, *Pf*BAL and *Pp*BFD were immobilized on epoxy-functionalized supports resulting in residual activities of around 1 % and 30 %, respectively (Tural et al., 2013; Tural et al., 2014). In addition, *Pp*BFD was covalently immobilized on polymethacrylat and silica beads leading to activities of 5 % and 70 % in comparison to the free reference enzymes (Hilterhaus et al., 2008; Peper et al., 2011). In comparison, the immobilization of *Lb*ADH on amino-epoxy Sepabeads® yielded immobilizates with 15 % residual activity and further cross-linking with glutaraldehyde led to almost complete deactivation of the catalyst (Hildebrand and

Lütz, 2006). Only the immobilization of *Ec*DERA on mesocellular foams or in ultrathin films did not reduce enzymatic activity after covalent binding to the respective supports (Subrizi et al., 2014; Wang et al., 2011; Wang et al., 2012). Compared to these results, the HaloTag™-based covalent immobilization approach led in most of the cases to comparable or even higher residual activities, indicating its ability to enable covalent and site-directed immobilization under mild conditions with low interference on the enzyme´s activity. However, in some cases a huge loss of activity could not be prevented. Therefore, strategies were studied to influence the residual activity, which are discussed in the next chapter.

3.4.2 Strategies to influence the residual activity of immobilizates

Several options exist for intervention in case of low catalytic activity as observed for HaloTag-*Lb*ADH or HaloTag-*Ec*DERA. First of all, the HaloTag™ can be added to both termini of an enzyme (Encell et al., 2012). If available, crystal structure data may help to choose the appropriate terminus. For example, a C-terminal fusion of the HaloTag™ to *Lb*ADH was not considered since the C-termini are deeply buried within the active tetramer and also participate in magnesium binding (Niefind et al., 2003). Likewise, mutations at the C-terminal end of the *Ec*DERA resulted in a huge loss of activity and consequently, the N-terminus was chosen for tag fusion (Heine et al., 2001). However, crystal structures and mutagenesis studies reported for *Ec*DERA did not provide complete certainty that specific termini might not be suitable for respective fusions. Since in case of HaloTag-*Ec*DERA a huge loss of activity was observed upon fusion to the N-terminus, the HaloTag™ fusion to the C-terminus of *Ec*DERA was tested. However, this did not alter any important parameter such as heterologous production, immobilization as well as residual activity (unpublished results, experiments performed by J. Döbber). Therefore, this fusion construct was not further investigated.

Instead, the effect of the spacer structures on the activity after immobilization was analyzed. In general, spacer sequences can be varied according to two different measures: spacer length and rigidity (Chen et al., 2013; Yu et al., 2015). Both of these parameters determine to what extent fusion partners might interact with each other. Generally, long and rigid linkers establish separation of both fusion partners while short and flexible ones will allow a higher degree of subunit interaction. Further studies additionally reported the successful modulation of linker flexibility as well as rigidity by combining sequence motifs known to establish either rigid or flexible spacers (Li et al., 2016). As presented in chapter 2.5, ten different linker sequences were integrated into HaloTag-*Ec*DERA fusion enzymes leading to the conclusion that highly flexible as well as rigid motifs have the same effect and that long, rigid spacers are able to slightly enhance the residual activity. All together, these results indicate that interferences caused by the HaloTag™ are probably only a minor contributing factor for low residual activity since a high spatial separation of both fusion partners led only to slightly enhanced activity. To further evaluate the effect of spacer sequences, the same spacers of different flexibility and rigidity

were introduced into HaloTag-*Lb*ADH fusion enzymes as well. These unpublished results are displayed in Figure 3.4-2.

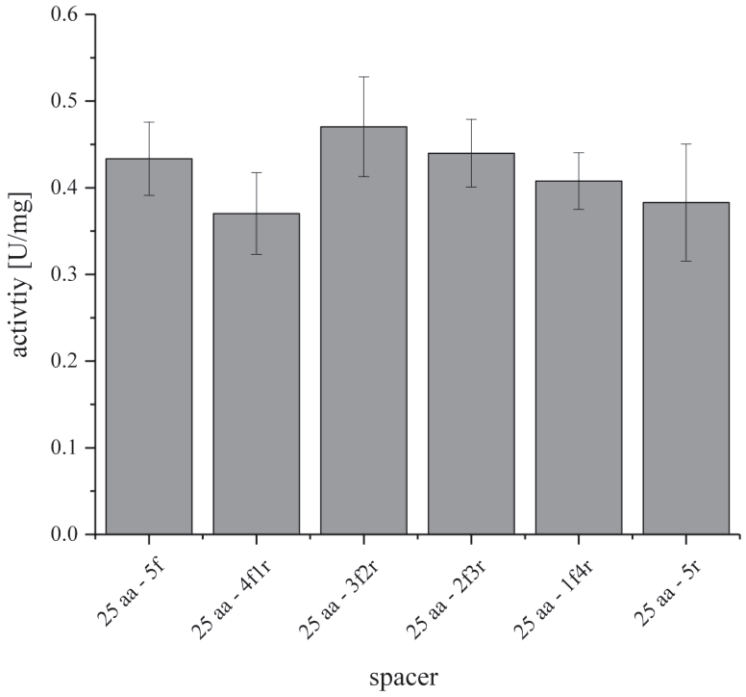

Figure 3.4-2: Effect of spacer flexibility on HaloTag-*Lb*ADH fusion enzymes. The spacer motifs EAAAK (rigid motif, r) and GGGGS (flexible motif, f) were combined with each other and integrated into HaloTag-*Lb*ADH fusion enzymes. Each spacer consisted of 5 motifs (different number of r or f) to give a total length of 25 amino acids (aa). Activity assay were performed as described in chapter 2.3. Detailed information about spacer sequences and construction of HaloTag-*Lb*ADH fusion enzymes are given in chapter 2.5.

As demonstrated in Figure 3.4-2, the spacer flexibility had almost no effect on the activity of HaloTag-*Lb*ADH after immobilization and similar activities were observed for all different constructs. The effect of different spacer length was not yet investigated. Based on the data obtained so far it can be concluded that the spacer sequence seems to contribute only to a small extent to the residual activity observed after immobilization. This might point towards low steric interference of the HaloTag^{TM} on the investigated fusion enzymes since a higher degree of separation between fusion partners does not lead to highly enhanced activity. However, only ten different spacer structures were investigated, which covers only a small range of potential spacer structures (George and Heringa, 2002). Furthermore, the exact interaction of the fusion partner in the selected model enzymes upon insertion of different spacer sequences was not resolved and still remains unknown. Therefore, a more profound analysis of suitable spacer structures including the resolution of the interaction between fusion partners may reveal deeper insights into the impact of spacer sequences.

Finally, the choice of the carrier influences the performance of immobilized biocatalysts (Cao, 2006b; Liese and Hilterhaus, 2013; Sheldon, 2007). Porosity, morphology or surface properties are only some

of important factors which affect the properties of immobilized biocatalysts. In particular, the activity depends on the micro-environment established by the carrier. As already mentioned above, the surface charge of carriers for example readjusts the local pH by attraction or rejection of protons or may also attract or reject fusion enzymes (Liese and Hilterhaus, 2013). In addition, the carrier surface might also influence the conformation of the biocatalyst upon binding (Cao, 2006b). As a consequence, the carrier choice is crucial and has to match the catalysts requirements. The HaloTag™-based immobilization technology allows such adaptations since binding only depends on chloroalkane binding ligands exposed on respective carriers (Encell et al., 2012). In theory, a huge range of different carrier materials would be possible provided that functionalization with corresponding chloroalkane binding ligands can be achieved. Therefore, additional experiments might target the development of further carrier types to identify optimal immobilization supports with lowest interference on catalytic activity.

3.5 Operational performance of immobilized enzymes

3.5.1 Stability and recyclability

Enzyme immobilization may enhance the stability of biocatalysts (Sheldon and van Pelt, 2013). However, this does not hold for every immobilization approach and the final stability after immobilization cannot be predicted. Generally, a higher enzyme stability can be induced mainly via two different effects (Mateo et al., 2007b). First, immobilization may establish a protective micro-environment where inactivation is reduced. For example, porous carriers or polymers surrounding enzymes can help to protect the enzyme against mechanic stress or reduce the contact with inactivating interfaces like gas bubbles (Bolivar et al., 2006; Bommarius and Karau, 2005). Second, multi-point attachments to the carrier and covalent inter-subunit bonds, e.g. via disulfide bonds, increase the conformational rigidification and thus the (thermal) stability (Klibanov, 1979; Klibanov, 1983). Besides, fixation of enzymes to a support generally prevents aggregation thereby enhancing the operational stability of enzymes (Singh et al., 2013). Keeping these stabilization strategies in mind, single-point immobilizations of enzymes on the surface of carriers as in case of the HaloTag™ mediated immobilization are consequently not expected to contribute much to the stabilization of enzymes. Since binding is mediated by the tag, multi-point attachments will not occur and as discussed above, immobilization of multimeric enzymes will probably proceed predominantly via one binding site. Nevertheless, a high stability of immobilized catalysts was observed in some cases in this thesis. As shown in 2.1, immobilized HaloTag-*Pf*BAL revealed high storage stability over several months at 4 °C but repetitive batch experiments showed that it was inactivated in the presence of aldehydes. Such aldehyde induced inactivation was already reported for the soluble *Pf*BAL which revealed a half-life below 30 minutes in the presence of benzaldehyde concentrations above 4 mM (Schwarz, 2010). Based on these data, recycling of *Pf*BAL seemed to be unlikely but immobilized

HaloTag-*Pf*BAL still retained 60 % of its activity after incubation for 1 h in a solution containing 10 mM benzaldehyde and 60 mM acetaldehyde, indicating a higher stability in comparison to the non-immobilized *Pf*BAL (see 2.1). The higher stability can be explained by efficient washing steps with fresh buffer solution between the repetitive batches. Partial reactivation after removal of aldehyde substrates was also reported for non-immobilized *Pf*BAL (Schwarz, 2010) but washing of immobilizates can be performed much more intensively in comparison to soluble enzymes. Aldehyde-induced inactivation was also observed for HaloTag-*Pp*BFD during the continuous production of (*S*)-HPP (see 2.4). Although much higher aldehyde concentrations were tolerated and the enzyme was stabilized by addition of ThDP, a huge decay of activity after continuous use of several days in a plug-flow reactor could not be prevented. In general, inactivation in the presence of aldehydes is often reported for ThDP-dependent enzymes, although the sensitivity strongly varies between different enzymes (Gocke, 2007; Iding et al., 2000; Schwarz, 2010). Several hypotheses for inactivation were developed including for example Schiff base formations with lysine residues (Schwarz, 2010), but the exact mechanism still remains elusive. The inactivation mechanisms are probably diverse among ThDP-dependent enzymes and can potentially be targeted through protein engineering. However, reaction engineering strategies, which keep the concentration of aldehydes low (fed-batch, enzyme membrane reactor) are additional appropriate tools to preserve enzyme activity. Here, immobilization improved the handling of the biocatalyst and in case of reversible inactivation phenomena, as observed for *Pf*BAL, an immobilized and insoluble enzyme can be washed much easier to restore activity.

In comparison, exceptional stability was observed for the immobilized HaloTag-*Lb*ADH. As demonstrated in 2.3 and 2.4, the immobilized HaloTag-*Lb*ADH was successfully used for the continuous production of several chiral alcohols with constant activity over several weeks. The enzyme revealed a high stability under aqueous conditions as well in the presence of THF and 2-propanol of which the latter was used for cofactor regeneration. Generally, several reports confirm the high stability also of the non-immobilized, untagged *Lb*ADH but stability drastically depends on the applied conditions (Leuchs and Greiner, 2011). Besides temperature and pH, the type and concentration of the buffer salt as well as the concentration of magnesium ions result in half-lifes ranging from 20 – 1000 h (Leuchs et al., 2013). Likewise, the addition of ionic liquids or organic solvents such as methyl *tert*-butyl ether (MTBE) and acetonitrile has a great impact, too, and again results in highly different half-lifes (Dreyer and Kragl, 2008; Kohlmann et al., 2011; Schumacher et al., 2006; Villela Filho et al., 2003). Under standard conditions (50 mM potassium phosphate buffer, pH 7, 1 mM $MgCl_2$), Leuchs and coworkers reported a half-life of around 80 h for the soluble form of the *Lb*ADH. Under the same conditions with additional 2-propanol (10 vol%) for cofactor regeneration, immobilized HaloTag-*Lb*ADH showed no activity loss over at least 130 h during the continuous production of (*R*)-phenylethanol (see 2.3). This can be taken as a first hint for a higher stability of the immobilized HaloTag-*Lb*ADH in comparison to the soluble form of the enzyme. In comparison, covalent immobilization on amino-epoxy beads and additional multi-point cross-linking

with glutaraldehyde enhanced the half-life of immobilized *Lb*ADH up to 1260 h while covalent immobilization without cross-linking did not alter stability significantly (Hildebrand and Lütz, 2006). Based on this data from Hildebrand and Lütz, multi-point connections seemed to be a prerequisite for high stability of *Lb*ADH after immobilization. Therefore, it is surprising that the HaloTag™-based immobilization enables similar high stability while only few connections via the HaloTags™ present in the active *Lb*ADH tetramer are established with the support. Although the reasons for the stabilization by the HaloTag™-induced immobilization is not yet clear, it can be concluded that the activity loss observed for HaloTag-*Lb*ADH after immobilization (see 3.4.1) is compensated by the remarkable stability of the established immobilizates.

In addition, the comparison of immobilized HaloTag-*Bm*TA with the soluble enzyme without HaloTag™ revealed that both biocatalyst formulations show a high stability at 30 °C and high shaking speed with almost no activity loss over several weeks (see 2.2). As already discussed in chapter 3.4, the enzyme reveals very large interface areas in comparison to the ThDP-dependent enzymes of similar size. This high interface area possibly allows the establishment of a huge number of non-covalent interactions among the individual subunits leading to a highly stable conformation, which is resistant towards fast thermal denaturation at 30 °C. However, both the free and the immobilized *Bm*TA were impaired by the reaction conditions applied for the reductive amination of (*S*)-HPP. Using the free enzyme, precipitated enzymes were observed in the reaction tubes after 48 h of this reaction (unpublished data). In comparison, recycling of immobilized HaloTag-*Bm*TA was possible indicating a higher stability of the immobilized enzyme under reaction conditions in comparison to the soluble variant. But also in this case, activity was reduced during repetitive use (see 2.2). Most likely, residual amounts of acetaldehyde from the first carboligation step and the selected amino donor isopropylamine might have caused the inactivation of *Bm*TA. Although a good half-life (288 h) of this enzyme was observed in the performed experiments, the considerable low activity towards the reductive amination of (*S*)-HPP required high catalyst loads and long incubation times to reach high conversion. For each batch, incubation for several days was required which consequently challenges enzyme stability and limits the number of possible recycling steps. Therefore, optimization of *Bm*TA for higher activity towards (*S*)-HPP is a prerequisite to enable a higher number of repetitive batches.

For immobilized HaloTag-*Ec*DERA, experiments to analyze the long-term stability in continuous reactions for the production of (*R*)-3-hydroxy-octanal were still under investigation by our cooperation partner[1], when this thesis was written. As mentioned in chapter 1.5.4, long-term use of *Ec*DERA in such applications was restricted by the high susceptibility towards higher concentrations of acetaldehyde (> 200 mM). This problem was overcome by identifying the exact mechanism of this inactivation and by introduction of mutations circumventing inhibition by acetaldehyde (Bramski et al., 2017; Dick et al., 2016). Since this optimized *Ec*DERA variant (C47M) was also selected for fusion with the HaloTag™, a high stability of the immobilized HaloTag-*Ec*DERA can be expected.

[1] Cooperation partner were Julia Bramski, Thomas Classen and Jörg Pietruszka.

Besides stability of the respective enzyme, the binding stability of the HaloTag™ fusion enzymes towards the HaloLink™ Resin is another important criteria for the evaluation of this tag-based immobilization approach. As mentioned for example in chapter 2.1, a mixture of SDS and NaOH was employed to saponify the ester bond which connects the HaloTag™ to the carrier surface to release bound fusion enzymes. The active site of the HaloTag™ is deeply buried inside the enzyme and only accessible via a tunnel, which also explains the length of respective chloroalkane residues (Encell et al., 2012). Therefore, SDS was employed to induce unfolding of the HaloTag™ and subsequent exposure of the respective ester bond. In contrast, incubation of immobilizates under denaturating conditions (0.1 % SDS, 95 °C) without NaOH was not sufficient to specifically release any fusion enzyme (Los et al., 2008; unpublished data). In general, it can be assumed that the high binding stability caused by establishing covalent bonds is even enhanced by the protection of this bond via the surrounding HaloTag™ conformation. Consequently, HaloTag™ fusion enzymes revealed a high binding stability in experiments performed for this thesis. As demonstrated in 2.3 and 2.4, no leakage of HaloTag-*Lb*ADH fusion enzymes was observed under aqueous conditions as well as in the presence of organic co-solvents, which allowed continuous operation up to several weeks. Furthermore, HaloTag-*Pp*BFD, HaloTag-*Pf*BAL or HaloTag-*Bm*TA were successfully recycled in repetitive batch experiments or employed in continuous plug-flow reactors indicating high binding stability also for further model enzymes (see 2.1, 2.2 and 2.4).

3.5.2 Optimized reaction performance through HaloTag™-based immobilization

As discussed above, a high stability of the immobilized model enzymes was observed. In addition, immobilization enabled further advantages leading to enhanced catalyst performance for several applications. As explained in chapter 2.5, *Ec*DERA catalyzes the sequential aldol additions leading to mono-aldol and bis-aldol products (see Figure 2.5-1). In this thesis the mixed aldol reaction of acetaldehyde and hexanal was studied. However, the targeted production of the mono aldol product (*R*)-3-hydroxy-octanal is challenging, since a defined short contact time between the enzyme and respective aldehydes can hardly be adjusted in batch experiments with soluble enzymes. Upon immobilization, continuous reaction set-ups were implemented allowing the use of HaloTag-*Ec*DERA in combination with adjustable residence times in a plug-flow reactor (see Table 2.5-2). This led to the production of solely mono aldol products with almost no bis-aldol compounds which was not yet achieved when applying free and soluble enzymes in batch. However, full conversion was not yet accomplished. Therefore, further investigations of this reaction will be targeted to either enhance the conversion towards exclusively mono aldol compounds or to find alternative strategies which allow a more efficient synthesis of the target product. A potential solution can be the separation of unreacted substrates in flow and subsequent recycling. However, suitable separation strategies have to be developed first.

Furthermore, immobilization of the selected model enzymes had a huge impact on the implementation of multi-step reactions combining different types of biocatalysts as well as non-catalyzed chemical reactions. As mentioned in 1.2.2, the implementation of such cascades is of great importance, since it allows the synthesis of complex compounds without the need for tedious intermediate product purifications and waste generation. Thereby, incompatible reaction conditions can be challenging. In this thesis, different types of catalyst incompatibilities were observed and by applying immobilizates, individual reactions steps were easily separated or compartmented to allow maximal efficiency of each reaction. For example, the implementation of a cascade for the production of amino alcohols involving a carboligation step catalyzed by *Pp*BFD and a subsequent amination step performed by a *Bm*TA (see Figure 2.2-2) was hampered by the activity of both enzymes towards the same substrate (benzaldehyde) leading to undesired side-product formation (benzylamine). This site reaction influenced the thermodynamic equilibrium of the first carboligation step and caused the constant cleavage of (*S*)-HPP by *Pp*BFD. In addition, inactivation of *Bm*TA by the aldehyde substrates (benzaldehyde and acetaldehyde) from the *Pp*BFD-catalyzed step was observed (see 2.2). Here, specifically acetaldehyde was detrimental for the activity of *Bm*TA, which made the complete removal necessary before the transaminase was added. Immobilization of the both enzymes allowed fast and easy separation of both cascade steps by simple centrifugation of the biocatalyst combined with intermediate acetaldehyde evaporation. As a side-effect, the catalyst-specific productivities were enhanced by their successful recycling.

Similarly, the production of (*S*,*S*)-PPD in a two-step enzymatic cascade was efficiently enabled by compartmentalization of immobilized catalysts in consecutive plug-flow reactors (see 2.4). In this cascade, immobilized HaloTag-*Pp*BFD was employed for the production of (*S*)-HPP, which was subsequently reduced by immobilized HaloTag-*Lb*ADH towards (*S*,*S*)-PPD. Due to established flow concept, reactants and compounds could either be introduced or removed exactly at the time and place required, enabling highly efficient reaction steps: The *Lb*ADH reveals much higher activity for the reduction of acetaldehyde in comparison to the intermediate cascade product (*S*)-HPP (Kulig et al., 2012) and therefore, removal of acetaldehyde by a hollow-fiber module successfully prevented high side-product formation of ethanol and loss of redox equivalents. In contrast, 2-propanol, which was essential for cofactor regeneration in the second reduction step, was introduced into the flow stream after the first step, thereby preventing contact with the immobilized *Pp*BFD. Otherwise, activity of this enzyme would have been reduced since ThDP dependent enzymes were generally shown to be less active in 2-propanol (Gerhards et al., 2012).

Despite these cascades involving two different biocatalysts, the combination of enzymes with chemical reaction steps is challenging as well since required reaction conditions often deviate substantially (see 1.2.2). Such problems were also experienced for the production of chiral epoxides (see 2.3). After the formation of chiral alcohols catalyzed by the *Lb*ADH, highly alkaline conditions were required for spontaneous epoxide formation. Again, the immobilization of the *Lb*ADH via the

HaloTag™ strategy enabled successful separation of both reactions and high *Lb*ADH stability was maintained since the pH was only enhanced in a separated reactor compartment. All these examples demonstrate the implementation of improved reaction set-ups through the immobilization of respective enzymes. This enabled access to instable intermediate compounds through the establishment of flow concepts and the separation of individual cascade steps either in batch or in flow, which is absolutely necessary to achieve optimal stability and activity of the respective biocatalysts.

3.6 Economic evaluation of the HaloTag™-based immobilization strategy

The immobilization of enzymes is mainly employed to enable improved biocatalyst performance under application related conditions, which enables higher catalyst specific productivities, higher operational stability or the use of several reaction set-ups including continuous reactions for more efficient product synthesis (see 1.4). Therefore, the evaluation of immobilization strategies has to consider the production costs for respective immobilizates as well, since these will finally decide about the feasibility of an immobilization approach. According to Tufvesson et al., the costs for an immobilized biocatalyst comprise several contributing factors encompassing (*i*) enzyme costs, (*ii*) required equipment and labor as well as (*iii*) the costs for the carrier (Tufvesson et al., 2011). Regarding the enzyme costs, production of HaloTag™ fusion enzymes will probably result in an additional metabolic burden on the microbial host cell due to the size of this tag (34 kDa). Consequently, less energy and resources could potentially be available, resulting in lowered catalytic activity per cell mass. However, high expression yields were observed for the heterologous production of the selected model enzymes in *E. coli* (see 3.3.1). The HaloTag™ may in some cases even promote the production of some biocatalysts due to its solubility enhancing effects, suggesting that in such cases similar amounts of active biocatalysts can be achieved (Ohana et al., 2009; Sun et al., 2015). In addition, the final biocatalyst formulation has a huge impact on the enzyme´s price, too (Tufvesson et al., 2011; see 1.3). Especially, enzyme purification enhances the price drastically, while whole cells and crude cell extracts are considerably cheaper. Since the HaloTag™-based immobilization strategy allows purification and immobilization in one step, crude cell extract formulations containing respective fusion enzymes are sufficient and the need for expensive purification steps prior to immobilization becomes obsolete. Taking these arguments into account, reasonable costs for the production of respective fusion enzymes can be expected and by circumventing expensive purification steps, enzyme costs are even reduced.

In addition, the amount of labor and equipment, which has to be invested for immobilizing HaloTag™ fusion enzymes is considerably low. Binding of HaloTag™ fusion enzymes takes place under mild conditions without the help of any additional equipment or chemicals and simple mixing is sufficient (see 3.3.2). In comparison, traditional covalent immobilization strategies depend on additional cross-linkers like glutaraldehyde (Migneault et al., 2004) or involve blocking steps of unreacted functional

groups on the carrier surface (Hildebrand and Lütz, 2006), which makes them consequently much more labor-intensive. Furthermore, the HaloTag™ is characterized by a high affinity towards respective supports thereby enabling a short and therefore cheap immobilization process, while other covalent immobilization strategies require long incubation times up to several days (see 3.3.2). Finally, immobilization can be performed in a continuous manner which allows automation and the reduction of labor costs (see 2.3 and 2.4). As a consequence, costs for labor and equipment are considerably low and the costs for HaloTag™-based immobilizates will mainly be determined by the expenses for the carrier.

Currently, the HaloLink™ Resin, which was used as a carrier in this thesis, is sold by Promega. The main focus of this product lies on applications in the field of cell imaging and identification of protein-protein interactions (Los et al., 2008). Consequently, it targets a relatively small market and is probably produced in a small scale accompanied with a high price. However, product prices are also a function of scale (Tufvesson et al., 2011), which would allow reduced carrier costs if production would occur in a larger scale targeting a bigger market.

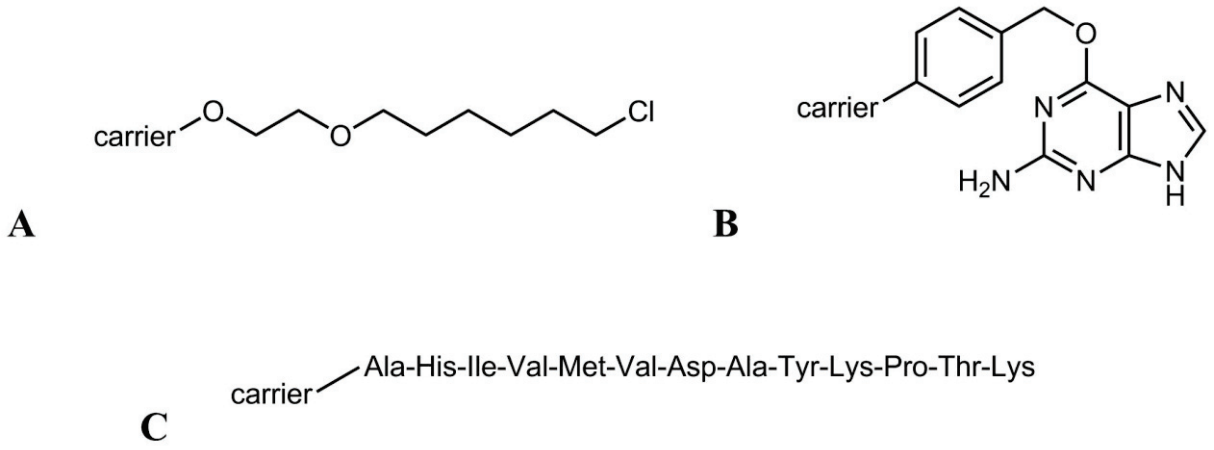

Figure 3.6-1: Ligands for tag-mediated covalent immobilization. Binding ligands of the HaloTag™ (Encell et al., 2012) (A), the SNAP-tag (Gautier et al., 2008) (B) and the SpyCatcher (Zakeri et al., 2012) (C) are displayed.

As shown in Figure 3.6-1, the structure of the chloroalkane ligand, which has to be exposed on respective carriers for efficient immobilization is rather simple. In comparison, further fusion tags enabling covalent immobilization such as SNAP-tag or SpyCatcher recognize more complex structures like benzylguanine moieties or a 15 amino acid long peptide sequence, respectively, which renders functionalization of supports for HaloTag™ binding less expensive. Furthermore, carrier functionalization is also required for further immobilization strategies which are based on the reaction of reactive functional groups with amino acid residues of the biocatalyst. Potential carriers can be theoretically composed of any material or (bio)polymer allowing functionalization as well as high catalyst activity and therefore, cheap or abundant materials can be selected. In addition, the respective

chloroalkane ligand shown in Figure 3.6-1 is already commercially available as a building block with different functionalizations (sold as HaloTag™ Ligand Building Blocks by Promega), which further simplifies the development of new carriers.

To further decrease carrier costs, immobilization supports are often reused after inactivation of the bound enzymes (see 1.4.3). So far, such concepts were not developed for the HaloTag™ immobilization concept but would principally be possible. As shown for example in 2.1, the targeted release of HaloTag™ fusion enzymes was performed by treatment with SDS and NaOH leaving a terminal hydroxyl group exposed on the HaloLink™ Resin. If methods would be developed to reinstall a terminal chlorine instead without harming the carrier material, the carrier could be reused and immobilization of fresh HaloTag™ fusion enzymes could occur[1]. Therefore, the HaloTag™ technology has the potential to enable enzyme immobilization on cheap and reusable carriers.

Besides these cost contributing factors, the time to develop a suitable immobilization method and intellectual property issues have to be considered as well. To achieve an optimal immobilization result, conventional covalent immobilization methods usually require the selection of suitable non-essential functional groups on the biocatalyst's surface for binding to the support, tests of various carrier materials followed by the optimization of binding conditions. These preliminary investigations demand investment of time and resources, which contribute to the costs for immobilization as well and often represent a barrier, which hampers implementation of immobilized enzymes in the field of biocatalysis (see 1.4.3). In comparison, the HaloTag™-based immobilization requires initial investigations and optimization like selection of appropriate carriers or fusion sites as well (see 3.4.2), but fewer resources have to be invested for binding studies. As demonstrated in this thesis, the HaloTag™-based immobilization can be regarded as a generic method, as the five different fusion enzymes studied in this thesis could be immobilized by the same protocol (see 3.3.2). On the contrary, the Promega Corporation holds the rights and patents[2] on this technology which restricts the unlimited access to this immobilization method for commercial applications. As a consequence, an additional investment is needed to acquire respective licenses, which has to be considered in an economical evaluation, too.

To conclude, the HaloTag™ technology has the possibility to become an economically viable immobilization method but suitable carriers of reasonable price have to be established first.

[1] For example, the use of thionyl chloride is well-known for the formation of alkyl chlorides from alcohols (Bissinger and Kung, 1947).

[2] Several patents have been filed for various applications, for example EP 3179252 A1-3.

3.7 Alternative tags mediating one-step purification and immobilization

3.7.1 Carbohydrate-binding modules

As presented in Table 1.4-2, a huge variety of further tags exists that are potentially useful for the one-step purification and immobilization of biocatalysts. Therefore, additional tags were selected in this thesis and evaluated according to the parameters discussed above. Among these, carbohydrate-binding modules (CBMs) mediating the non-covalent binding to different carbohydrates like cellulose and chitin (see 1.4.2) were intensively studied. The results are described in the Bachelor thesis of Carmen Prince and the Master thesis of Tim Gerlach (Gerlach, 2017; Prince, 2017) and will be briefly summarized in this chapter.

The carbohydrate-active enzyme database (CAZy) currently contains ten thousands of different CBMs (CAZypedia Consortium, 2018). Each of them recognizes and binds to specific forms of carbohydrates comprising small monosaccharides up to insoluble polysaccharides like cellulose (see 1.4.2). Therefore, the selection of appropriate CBMs is difficult. Since several publications reported the successful use of the CBM from the xylanase 10 A from *C. fimi* in biocatalysis (Kopka et al., 2015; Ong et al., 1989), this CBM was fused to *Pf*BAL and the alcohol dehydrogenase from *Ralstonia* sp. (*R*ADH) (Kulig et al., 2013). However, the fusion of this CBM to respective model enzymes led to massive production of inclusion bodies (unpublished results). Such formation of inclusion bodies is often observed for CBM-fusions and represents a general problem, while the exact underlying mechanisms are not yet understood (Krauss et al., 2017). However, CBMs often exhibit hydrophobic areas for the binding to carbohydrates (Creagh et al., 1996) and aggregation via these hydrophobic areas might explain the formation of inclusion bodies during recombinant protein production. Therefore, the project of Carmen Prince was initiated to find CBMs that are more suitable for the intended immobilization approach by enabling the efficient production of fusion enzymes. For this purpose, the CBM of cipA from *Chlostridium thermocellum* (CBM-cipA) and the CBM of cipC from *Chlostridium cellulolyticum* were selected. (Morag et al., 1995; Shimon et al., 2000). Briefly, cips integrate several enzymes with carbohydrate activity on one scaffold. This scaffold contains an additional CBM to guide the whole complex of enzymes towards carbohydrate substrates like cellulose. The pyruvate decarboxylase from *Acetobacter pasteurianus* (*Ap*PDC) (Gocke et al., 2009) was selected as a model enzyme and both CBMs were fused to the N- as well as to the C-terminus of this enzyme.

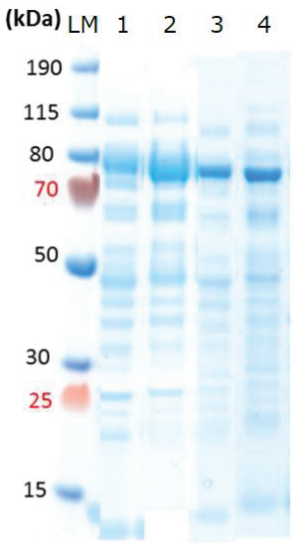

Figure 3.7-1: Production of CBM-fusion enzymes in *E. coli*. The CBMs of cipA from *Chlostridium thermocellum* and cipC from *Chlostridium cellulolyticum* were fused to the *Ap*PDC and respective fusion enzymes (80 kDa) were produced in *E. coli* BL21 (DE3). After cell lysis, the soluble crude cell extract was analyzed by SDS-PAGE. 1: CBM-cipA fused to the N-terminus, 2: CBM-cipA fused to the C-terminus, 3: CBM-cipC fused to the N-terminus, 4: CBM-cipC fused to the C-terminus. PageRuler^{TM} Plus Prestained Ladder (ThermoFischer Scientific, Germany) was used as a protein marker.

As shown in Figure 3.7-1, the fusion of these two different CBMs to the N- as well as to the C-terminus of the *Ap*PDC resulted in soluble fusion enzyme variants. However, the expression yields were reduced by roughly 50 % compared to those obtained for HaloTag^{TM} fusion enzymes (see Figure 3.3-1). These findings indicate that the selected CBMs were more suitable with respect to the heterologous production but still resulted in weak production of the fusion enzymes. Next, the immobilization of the fusion enzymes on Avicel® cellulose was investigated. As demonstrated in Figure 3.7-2, the CBMs mediated the fast binding of the respective fusion enzymes directly from crude cell extracts. Overall, a high purity was achieved but fusion of the CBM to the C-terminus led to much better results. These findings support the hypothesis about the potential influence of the spacer structures on the production of fusion enzymes since the same spacer sequences as selected for HaloTag^{TM} fusion enzymes were used for the construction of CBM fusion enzymes (spacer 20 aa – 4r, see 2.5). As discussed in 3.3.2, some spacer sequences might terminate transcription by the formation of hairpin motifs and therefore induce truncation of fusion enzymes. As a consequence, termination of transcription at the spacer sequence would lead to the accumulation of functional CBMs during the expression of genes encoding for N-terminal CBM fusions whereas this would not occur during the production of C-terminal CBM fusions. Since additional protein bands having the same size as the corresponding CBM (20 kDa) appear only for N-terminal fusions after immobilization from crude cell extracts (see Figure 3.7-2), this hypothesis seems likely. Furthermore, CBM fusion enzymes, which are naturally occurring in the production host *E. coli*, could also lower the purity after immobilization.

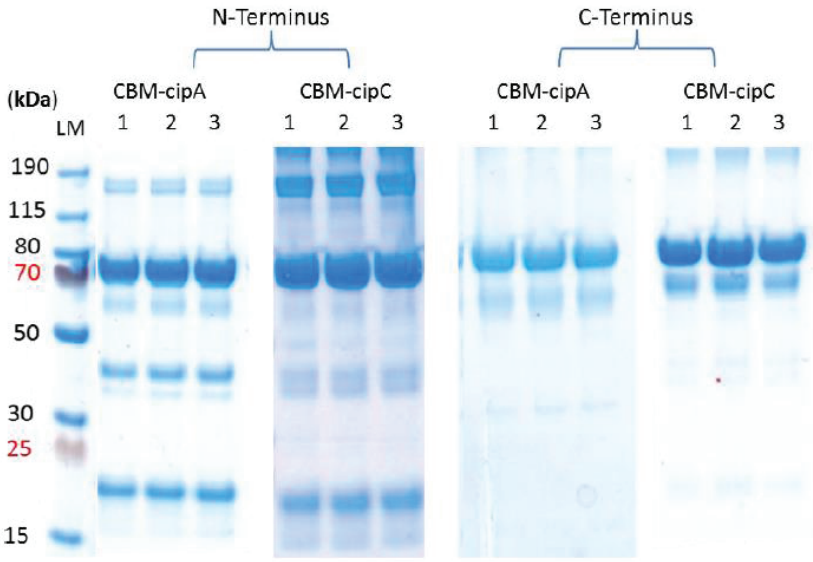

Figure 3.7-2: Purity of CBM fusion enzymes immobilized on Avicel® cellulose. Crude cell extract solutions containing respective fusion enzymes (CBM-cipA or CBM-cipC fused to the N- or C-terminus of the *Ap*PDC; 80 kDa each) were incubated for 30 min with Avicel® cellulose. Bound proteins were released by incubation with SDS and analyzed by SDS-PAGE, Experiments were performed in triplicate (1, 2, 3). PageRuler^{TM} Plus Prestained Ladder (ThermoFischer Scientific, Germany) was used as a protein marker.

Next, residual activity of the immobilized fusion enzymes was investigated. Overall, the activity of the established immobilizates ranged between 30 – 70 % in comparison to the free reference enzyme without CBM. In addition, CBMs revealed high binding stability during repetitive batch experiments but aldehyde-based inactivation of the *Ap*PDC occurred under the selected reaction conditions (Prince, 2017).

Due to these promising results, a second project was established to analyze the performance of the identified CBMs under application-related conditions and to establish a continuous enzymatic cascade (Gerlach, 2017). Therefore, the CBM of cipC was fused to the N-terminus of *Pp*BFD and *Lb*ADH to establish a two-step enzymatic cascade for the production of a vicinal diol as it was already established with the HaloTag^{TM} strategy (see 2.4). Initial characterization of the fusion enzymes revealed good expression yields and a high purity after immobilization on Avicel®. In addition, residual activities measured for *Pp*BFD were comparable to those observed for HaloTag^{TM} fusion enzymes (CBM strategy: 60 %, HaloTag^{TM} strategy: 65 %) but *Lb*ADH fusion enzymes showed lower activity in comparison to corresponding HaloTag^{TM} fusions (CBM strategy: 15 %, HaloTag strategy: 35 %). It is surprising that similar residual activities were observed although both tags differ from each other. The selected CBMs are much smaller (CBMs: 20 kDa, HaloTag^{TM}: 34 kDa) and their surface is probably more hydrophobic due to the hydrophobic binding patches (Shimon et al., 2000). If the tag would be mainly responsible for the observed loss of activity, for example due to steric hindrance, tags with different size and polarity should influence the residual activity in a different manner. Of course, experimental data are not sufficient to yield a clear picture but they may support the hypothesis proposed above that the tag-induced distortion of the enzyme's quaternary structure is one factor

amongst others, which generally lowers activities of enzymes in tag-based immobilization approaches. (see 3.4.1).

To establish a continuous enzymatic cascade, CBM fusion enzymes were immobilized on cellulose membranes for the construction of a catalytically-active membrane reactor. Both fusion enzymes were successfully immobilized in flow accompanied with a high purity after immobilization. However, the cascade could not be established since CBM-*Pp*BFD fusion enzymes rapidly desorbed under flow conditions. In comparison, binding of the CBM-*Lb*ADH fusion to the membrane was much more stable as it was shown for the reduction of model substrates like acetophenone or benzaldehyde using 2-propanol for cofactor regeneration, respectively.

In summary, CBMs allow the one-step purification and immobilization of respective fusion enzymes on cheap and abundant carriers like cellulose. However, negative effects on the heterologous production as well as low binding stability on cellulose carriers were observed under reaction conditions, which yields the HaloTag™ as a more appropriate candidate for tag-based immobilization approaches.

3.7.2 The Aldehyde-tag

Preliminary immobilization experiments were also performed with the Aldehyde-tag (unpublished data). As shown in Figure 3.7-3, the Aldehyde-tag enables the introduction of an unnatural aldehyde moiety into proteins. A short peptide sequence fused to the enzyme of interest is recognized by a second enzyme, a formylglycine generating enzyme (FGE), which converts a cysteine within the peptide sequence into an aldehyde bearing formylglycine (Carrico et al., 2007). This approach was followed, since covalent immobilization would be possible with minor interference on the enzyme´s structure by adding only a short peptide sequence to one terminus. To establish this approach, the corresponding peptide sequence was fused to the *Pf*BAL and the *R*ADH. In a next step, coproduction of the modified model enzymes and the FGE occurred in *E. coli* BL21 (DE3) cells. Then, the commercially available Affi-Gel® Hz (Bio Rad, Germany) was selected as an appropriate carrier, because it consists of small particles exposing hydrazide groups on the surface. This carrier was selected, because condensation of aldehydes with hydrazines yield hydrazones, which are more stable than Schiff bases formed with primary amines (O'Shannessy, 1990). However, all immobilization attempts failed and the formation of a formylglycine moiety within the model enzyme could not be proven. Therefore, this immobilization approach was not further investigated.

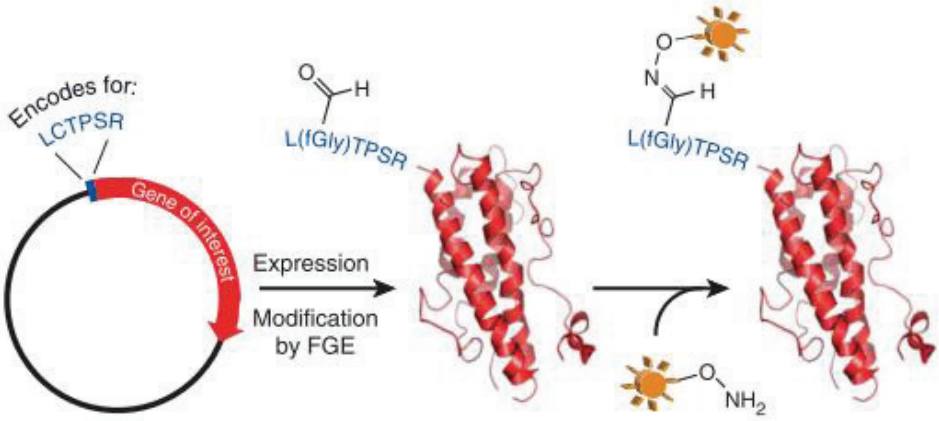

Figure 3.7-3: Tag-mediated post-translational incorporation of aldehydes into proteins. A short peptide sequence, which is fused to the protein of interest, is recognized by the formylglycine-generating enzyme (FGE). The cysteine within this sequence is converted into a formylglycine (fGly), which can be used for further bioconjugation (see 1.4.2). Figure was taken from Carrico et al., 2007.

4 Conclusion and outlook

This thesis provides new solutions for the field of enzyme immobilization. Tag-based immobilization strategies were evaluated to find alternative methods that allow the easy formation of pure immobilizates for a broad range of enzymes with high catalytic activity and tightly bound biocatalysts. While CBM-tags suffered from low expression yields and low binding strength of respective fusion enzymes, the HaloTag™ was identified as the most suitable candidate and enabled efficient immobilization of five different model enzymes. This tag did not impair the heterologous production of the fusion enzymes and high yields of the recombinant enzymes were achieved. Covalent immobilization proceeds rapidly from crude cell extracts under mild conditions resulting in tightly bound biocatalysts with high purity. All enzymes were immobilized using the same protocol, thus the HaloTag™-based immobilization strategy can be regarded as a generic method. Although, the residual activity of the established immobilizates is case-specific, it exceeded 50 % specifically for the three largest enzymes tested.

This technology allows the easy implementation of different reaction concepts from repetitive batch to continuous mode including the easy reuse of respective immobilizates. Biocatalytic continuous flow modules can be prepared easily without the need for additional equipment or specific knowledge. Furthermore, multi-step reaction sequences can be performed under optimal conditions for each step due to easy biocatalyst compartmentalization, thereby increasing the overall efficiency of such cascades.

To conclude, the HaloTag™ immobilization approach is a simple and broadly applicable method. It combines strong biocatalyst binding with high residual activity and additionally allows purification and immobilization in one step. As a consequence, this concept has the potential to accelerate tedious and time-consuming development of immobilized biocatalysts and to result in an enhanced implementation of immobilizates in various applications and processes.

In next steps, the establishment of a larger toolbox with various inexpensive carriers should be targeted to further promote the HaloTag™ immobilization approach. First, the development of additional materials functionalized with the required chloroalkane binding ligand can be focused to allow the identification of optimal immobilization supports for each biocatalyst. Second, different forms of carriers, such as membranes or particles with higher porosity can lead to additional possibilities of reaction set-ups as well as enhanced biocatalyst protection and stability, respectively. Finally, suitable methods for carrier recycling should be developed to reduce the overall costs for enzyme immobilization.

5 References

Abdelhamid MAA, Motomura K, Ikeda T, Ishida T, Hirota R, Kuroda A. 2014. Affinity purification of recombinant proteins using a novel silica-binding peptide as a fusion tag. *Appl. Microbiol. Biotechnol.* **98**:5677–5684.

Aguilera J, Gomes AR, Olaru I. 2013. Principles for the risk assessment of genetically modified microorganisms and their food products in the European Union. *Int. J. Food Microbiol.* **167**:2–7.

Ahmed H. 2004. Principles and Reactions of Protein Extraction, Purification, and Characterization. Boca Raton: CRC Press.

Anastas P, Eghbali N. 2010. Green Chemistry: Principles and Practice. *Chem. Soc. Rev.* **39**:301–312.

Anastas PT, Warner JC. 1998. Green Chemistry: Theory and Practice. New York: Oxford University Press.

Anderson NG. 2012. Using Continuous Processes to Increase Production. *Org. Process Res. Dev.* **16**:852–869.

Andrews FH, Rogers MP, Paul LN, McLeish MJ. 2014. Perturbation of the monomer-monomer interfaces of the benzoylformate decarboxylase tetramer. *Biochemistry* **53**:4358–4367.

Arai R, Ueda H, Kitayama A, Kamiya N, Nagamune T. 2001. Design of the linkers which effectively separate domains of a bifunctional fusion protein. *Protein Eng.* **14**:529–532.

Arnold FH. 1996. Directed evolution: Creating biocatalysts for the future. *Chem. Eng. Sci.* **51**:5091–5102.

Arnold FH. 2017. Directed Evolution: Bringing New Chemistry to Life. *Angew. Chemie - Int. Ed.*

Arora B, Mukherjee J, Gupta MN. 2014. Enzyme promiscuity: using the dark side of enzyme specificity in white biotechnology. *Sustain. Chem. Process.* **2**.

Auld DS, Bergman T. 2008. Medium- and short-chain dehydrogenase/reductase gene and protein families : The role of zinc for alcohol dehydrogenase structure and function. *Cell. Mol. Life Sci.* **65**:3961–3970.

Babtie A, Tokuriki N, Hollfelder F. 2010. What makes an enzyme promiscuous? *Curr. Opin. Chem. Biol.* **14**:200–207.

Bahulekar R, Ayyangar NR, Ponrathnam S. 1991. Polyethyleneimine in immobilization of biocatalysts. *Enzyme Microb. Technol.* **13**:858–868.

Barbas CF, Wang YF, Wong CH. 1990. Deoxyribose-5-phosphate aldolase as a synthetic catalyst. *J. Am. Chem. Soc.* **112**:2013–2014.

Barbosa O, Ortiz C, Berenguer-Murcia Á, Torres R, Rodrigues RC, Fernandez-Lafuente R. 2015. Strategies for the one-step immobilization–purification of enzymes as industrial biocatalysts. *Biotechnol. Adv.* **33**:435–456.

Baxendale IR. 2013. The integration of flow reactors into synthetic organic chemistry. *J. Chem. Technol. Biotechnol.* **88**:519–552.

Baxendale IR, Deeley J, Griffiths-Jones CM, Ley SV, Saaby S, Tranmer GK. 2006a. A flow process for the multi-step synthesis of the alkaloid natural product oxomaritidine: a new paradigm for molecular assembly. *Chem. Commun.* **24**:2566–2568.

Baxendale IR, Griffiths-Jones CM, Ley SV, Tranmer GK. 2006b. Microwave-Assisted Suzuki Coupling Reactions with an Encapsulated Palladium Catalyst for Batch and Continuous-Flow Transformations. *Chem. - A Eur. J.* **12**:4407–4416.

Beck G. 2002. Synthesis of Chiral Drug Substances. *Synlett* **6**:837–850.

Beckett D, Kovaleva E, Schatz PJ. 1999. A minimal peptide substrate in biotin holoenzyme synthetase-catalyzed biotinylation. *Protein Sci.* **8**:921–929.

Berglund P, Humble MS, Branneby C. 2012. C–X Bond Formation: Transaminases as Chiral Catalysts: Mechanism, Engineering, and Applications. In: Carreira, E, Yamamoto, H, editors. *Compr. Chirality*. Amsterdam: Elsevier, Vol. 7, pp. 390–401.

Bernhardt R, Urlacher VB. 2014. Cytochromes P450 as promising catalysts for biotechnological application: chances and limitations. *Appl. Microbiol. Biotechnol.* **98**:6185–6203.

Bhosale SH, Rao MB, Deshpande VV. 1996. Molecular and industrial aspects of glucose isomerase. *Microbiol. Rev.* **60**:280–300.

Bilal M, Asgher M, Iqbal H. 2016. Polyacrylamide Gel-Entrapped Fungal Manganese Peroxidase from *Ganoderma lucidum* IBL-05 with Enhanced Catalytic, Stability, and Reusability Characteristics. *Protein Pept. Lett.* **23**:812–818.

Bissinger WE, Kung FE. 1947. A Study of the Reaction of Alcohols with Thionyl Chloride. *J. Am. Chem. Soc.* **69**:2158–2163.

Bisterfeld C. 2016. Rationales Design der Acetaldehyd-abhängigen Aldolasen und deren Anwendung in der organischen Synthese; Heinrich-Heine-Universität Düsseldorf.

Blackmond DG. 2010. The origin of biological homochirality. *Cold Spring Harb. Perspect. Biol.* **2**:a002147.

Bolivar JM, Nidetzky B. 2012. Oriented and selective enzyme immobilization on functionalized silica carrier using the cationic binding module Z basic2: design of a heterogeneous D-amino acid oxidase catalyst on porous glass. *Biotechnol. Bioeng.* **109**:1490–1498.

Bolivar JM, Wiesbauer J, Nidetzky B. 2011. Biotransformations in microstructured reactors: more than flowing with the stream? *Trends Biotechnol.* **29**:333–342.

Bolivar JM, Wilson L, Ferrarotti SA, Fernandez-Lafuente R, Guisan JM, Mateo C. 2006. Stabilization of a formate dehydrogenase by covalent immobilization on highly activated glyoxyl-agarose supports. *Biomacromolecules* **7**:669–673.

Bommarius AS, Karau A. 2005. Deactivation of Formate Dehydrogenase (FDH) in Solution and at Gas-Liquid Interfaces. *Biotechnol. Prog.* **21**:1663–1672.

Bommarius AS, Riebel BR. 2004. Biocatalysis: Fundamentals and Applications. Weinheim, FRG: Wiley-VCH Verlag GmbH & Co. KGaA.

Boraston AB, Bolam DN, Gilbert HJ, Davies GJ. 2004. Carbohydrate-binding modules: fine-tuning polysaccharide recognition. *Biochem. J.* **382**:769–781.

Bornscheuer UT, Huisman GW, Kazlauskas RJ, Lutz S, Moore JC, Robins K. 2012. Engineering the third wave of biocatalysis. *Nature* **485**:185–194.

Both P, Busch H, Kelly PP, Mutti FG, Turner NJ, Flitsch SL. 2016. Whole-Cell Biocatalysts for Stereoselective C-H Amination Reactions. *Angew. Chemie - Int. Ed.* **55**:1511–1513.

Botyanszki Z, Tay PKR, Nguyen PQ, Nussbaumer MG, Joshi NS. 2015. Engineered catalytic biofilms: Site-specific enzyme immobilization onto *E. coli* curli nanofibers. *Biotechnol. Bioeng.* **112**:2016–2024.

Bradshaw CW, Fu H, Shen GJ, Wong CH. 1992a. A *Pseudomonas* sp. alcohol dehydrogenase with broad substrate specificity and unusual stereospecificity for organic synthesis. *J. Org. Chem.* **57**:1526–1532.

Bradshaw CW, Hummel W, Wong CH. 1992b. *Lactobacillus kefir* alcohol dehydrogenase: a useful catalyst for synthesis. *J. Org. Chem.* **57**:1532–1536.

Brahma A, Musio B, Ismayilova U, Nikbin N, Kamptmann SB, Siegert P, Jeromin GE, Ley SV, Pohl M. 2016. An orthogonal biocatalytic approach for the safe generation and use of HCN in a multistep continuous preparation of chiral O-acetylcyanohydrins. *Synlett* **27**:262–266.

Bramski J, Dick M, Pietruszka J, Classen T. 2017. Probing the acetaldehyde-sensitivity of 2-deoxy-ribose-5-phosphate aldolase (DERA) leads to resistant variants. *J. Biotechnol.* **258**:56–58.

Bray MR, Johnson PE, Gilkes NR, McIntosh LP, Kilburn DG, Warren RA. 1996. Probing the role of tryptophan residues in a cellulose-binding domain by chemical modification. *Protein Sci.* **5**:2311–2318.

Breuer M, Ditrich K, Habicher T, Hauer B, Keßeler M, Stürmer R, Zelinski T. 2004. Industrial methods for the production of optically active intermediates. *Angew. Chemie - Int. Ed.* **43**:788–824.

Buthe A. 2011. Entrapment of Enzymes in Nanoporous Sol–Gels. In: Wang, P, editor. *Nanoscale Biocatal. Methods Protoc.* Humana Press, pp. 223–237.

Caddow AJ, Concoby B. 2004. Enzyme Safety and Regulatory Considerations. In: Aehle, W, editor. *Enzym. Ind. Prod. Appl.* 2nd ed. Weinheim, FRG: Wiley-VCH Verlag GmbH & Co. KGaA, pp. 399–411.

Calvelage S, Dörr M, Höhne M, Bornscheuer UT. 2017. A Systematic Analysis of the Substrate Scope of (*S*)- and (*R*)-Selective Amine Transaminases. *Adv. Synth. Catal.* **359**:4235–4243.

Cao L. 2006a. Adsorption-based Immobilization. In: *Carrier-bound Immobil. Enzym. Princ. Appl. Des.* Weinheim, FRG: Wiley-VCH Verlag GmbH & Co. KGaA, pp. 53–168.

Cao L. 2006b. Carrier-bound Immobilized Enzymes: Principles, Application and Design. Weinheim, FRG: Wiley-VCH Verlag GmbH & Co. KGaA 563 p.

Cao L. 2006c. Enzyme Entrapment. In: *Carrier-bound Immobil. Enzym. Princ. Appl. Des.* Weinheim, FRG: Wiley-VCH Verlag GmbH & Co. KGaA, pp. 317–395.

Cao L. 2006d. Enzyme Encapsulation. In: *Carrier-bound Immobil. Enzym. Princ. Appl. Des.* Weinheim, FRG: Wiley-VCH Verlag GmbH & Co. KGaA, pp. 397–448.

Cao L. 2006e. Covalent Enzyme Immobilization. In: *Carrier-bound Immobil. Enzym. Princ. Appl. Des.* Weinheim, FRG: Wiley-VCH Verlag GmbH & Co. KGaA, pp. 169–316.

Carrico IS, Carlson BL, Bertozzi CR. 2007. Introducing genetically encoded aldehydes into proteins. *Nat. Chem. Biol.* **3**:321–322.

Carvalho CCR, Fonseca RMM. 2007. Bacterial Whole Cell Biotransformations: In Vivo Reactions Under In Vitro Conditions. *Dyn. Biochem. Process Biotechnol. Mol. Biol.* **1**:32–39.

Cascón O, Richter G, Allemann RK, Wirth T. 2013. Efficient Terpene Synthase Catalysis by Extraction in Flow. *Chempluschem* **78**:1334–1337.

CAZypedia Consortium. 2018. Ten years of CAZypedia: a living encyclopedia of carbohydrate-active enzymes. *Glycobiology* **28**:3–8.

Chen B, Lim S, Kannan A, Alford SC, Sunden F, Herschlag D, Dimov IK, Baer TM, Cochran JR. 2016. High-throughput analysis and protein engineering using microcapillary arrays. *Nat. Chem. Biol.* **12**:76–81.

Chen L, Dumas DP, Wong CH. 1992. Deoxyribose 5-phosphate aldolase as a catalyst in asymmetric aldol condensation. *J. Am. Chem. Soc.* **114**:741–748.

Chen WP. 1980. Glucose isomerase. *Process Biochem.* **15**:30–41.

Chen X, Zaro JL, Shen W-C. 2013. Fusion protein linkers: property, design and functionality. *Adv. Drug Deliv. Rev.* **65**:1357–1369.

Cheng L-Y, McKinley-McKee JS, Greenwood CT, Hourston DJ. 1968. II. The dissociation of the alcohol dehydrogenases. *Biochem. Biophys. Res. Commun.* **31**:761–767.

Choi J-M, Han S-S, Kim H-S. 2015. Industrial applications of enzyme biocatalysis: Current status and future aspects. *Biotechnol. Adv.* **33**:1443–1454.

Cohen SN, Chang ACY, Boyer HW, Helling RB. 1973. Construction of Biologically Functional Bacterial Plasmids In Vitro. *Proc. Natl. Acad. Sci.* **70**:3240–3244.

Constantinou A, Ghiotto F, Lam KF, Gavriilidis A. 2014. Stripping of acetone from water with microfabricated and membrane gas-liquid contactors. *Analyst* **139**:266–272.

Cosp A, Dresen C, Pohl M, Walter L, Röhr C, Müller M. 2008. α,β-Unsaturated Aldehydes as Substrates for Asymmetric C-C Bond Forming Reactions with Thiamin Diphosphate (ThDP)-Dependent Enzymes. *Adv. Synth. Catal.* **350**:759–771.

Costa S, Almeida A, Castro A, Domingues L. 2014. Fusion tags for protein solubility, purification and immunogenicity in *Escherichia coli*: the novel Fh8 system. *Front. Microbiol.* **5**.

Crabb WD, Shetty JK. 1999. Commodity scale production of sugars from starches. *Curr. Opin. Microbiol.* **2**:252–256.

Creagh AL, Ong E, Jervis E, Kilburn DG, Haynes CA. 1996. Binding of the cellulose-binding domain of exoglucanase Cex from *Cellulomonas fimi* to insoluble microcrystalline cellulose is entropically driven. *Proc. Natl. Acad. Sci. U. S. A.* **93**:12229–12234.

Cronan JE. 1990. Biotination of proteins in vivo. A post-translational modification to label, purify, and study proteins. *J. Biol. Chem.* **265**:10327–10333.

Dach R, Song JJ, Roschangar F, Samstag W, Senanayake CH. 2012. The Eight Criteria Defining a Good Chemical Manufacturing Process. *Org. Process Res. Dev.* **16**:1697–1706.

Dean SM, Greenberg WA, Wong CH. 2007. Recent advances in aldolase-catalyzed asymmetric synthesis. *Adv. Synth. Catal.* **349**:1308–1320.

Demir AS, Dünnwald T, Iding H, Pohl M, Müller M. 1999. Asymmetric benzoin reaction catalyzed by benzoylformate decarboxylase. *Tetrahedron: Asymmetry* **10**:4769–4774.

Demir AS, Şeşenoglu Ö, Eren E, Hosrik B, Pohl M, Janzen E, Kolter D, Feldmann R, Dünkelmann P, Müller M. 2002. Enantioselective Synthesis of α-Hydroxy Ketones via Benzaldehyde Lyase-Catalyzed C−C Bond Formation Reaction. *Adv. Synth. Catal.* **344**:96–103.

Demir AS, Ayhan P, Igdir AC, Duygu AN. 2004. Enzyme catalyzed hydroxymethylation of aromatic aldehydes with formaldehyde. Synthesis of hydroxyacetophenones and (*S*)-benzoins. *Tetrahedron* **60**:6509–6512.

Demir AS, Pohl M, Janzen E, Müller M. 2001. Enantioselective synthesis of hydroxy ketones through cleavage and formation of acyloin linkage. Enzymatic kinetic resolution via C–C bond cleavage. *J. Chem. Soc. Perkin Trans. 1* 633–635.

Demir AS, Seşenoglu O, Dünkelmann P, Müller M. 2003. Benzaldehyde lyase-catalyzed enantioselective carboligation of aromatic aldehydes with mono- and dimethoxy acetaldehyde. *Org. Lett.* **5**:2047–2050.

Denard CA, Hartwig JF, Zhao H. 2013. Multistep One-Pot Reactions Combining Biocatalysts and Chemical Catalysts for Asymmetric Synthesis. *ACS Catal.* **3**:2856–2864.

Denesyuk AI, Denessiouk KA, Korpela T, Johnson MS. 2002. Functional attributes of the phosphate group binding cup of pyridoxal phosphate-dependent enzymes. *J. Mol. Biol.* **316**:155–172.

Dick M. 2016. Strukturelle Untersuchungen zur Aktivität und Stabilität in Acetaldehyd-abhängigen Aldolasen; Heinrich-Heine-Universität Düsseldorf.

Dick M, Hartmann R, Weiergräber OH, Bisterfeld C, Classen T, Schwarten M, Neudecker P, Willbold D, Pietruszka J. 2016. Mechanism-based inhibition of an aldolase at high concentrations of its natural substrate acetaldehyde: structural insights and protective strategies. *Chem. Sci.* **7**:4492–4502.

DiCosimo R, McAuliffe J, Poulose AJ, Bohlmann G. 2013. Industrial use of immobilized enzymes. *Chem. Soc. Rev.* **42**:6437–6474.

Diener M, Kopka B, Pohl M, Jaeger K-E, Krauss U. 2016. Fusion of a Coiled-Coil Domain Facilitates the High-Level Production of Catalytically Active Enzyme Inclusion Bodies. *ChemCatChem* **8**:142–152.

Döbber J, Pohl M, Ley SV., Musio B. 2018a. Rapid, selective and stable HaloTag-*Lb*ADH immobilization directly from crude cell extract for the continuous biocatalytic production of chiral alcohols and epoxides. *React. Chem. Eng.* **3**:8–12.

Döbber J, Gerlach T, Offermann H, Rother D, Pohl M. 2018b. Closing the gap for efficient immobilization of biocatalysts in continuous processes: HaloTag™ fusion enzymes for a continuous enzymatic cascade towards a vicinal chiral diol. *Green Chem.* **20**:544–552.

Döbber J, Pohl M. 2017. HaloTag™: Evaluation of a covalent one-step immobilization for biocatalysis. *J. Biotechnol.* **241**:170–174.

Dobritzsch D, König S, Schneider G, Lu G. 1998. High resolution crystal structure of pyruvate decarboxylase from *Zymomonas mobilis*. Implications for substrate activation in pyruvate decarboxylases. *J. Biol. Chem.* **273**:20196–20204.

Domínguez de María P, Hollmann F. 2015. On the (Un)greenness of biocatalysis: Some challenging figures and some promising options. *Front. Microbiol.* **6**:6–10.

Domínguez de María P, Pohl M, Gocke D, Gröger H, Trauthwein H, Stillger T, Walter L, Müller M. 2007. Asymmetric Synthesis of Aliphatic 2-Hydroxy Ketones by Enzymatic Carboligation of Aldehydes. *European J. Org. Chem.* **2007**:2940–2944.

Domínguez de María P, Stillger T, Pohl M, Kiesel M, Liese A, Gröger H, Trauthwein H. 2008. Enantioselective C-C Bond Ligation Using Recombinant *Escherichia coli*-Whole-Cell Biocatalysts. *Adv. Synth. Catal.* **350**:165–173.

Domínguez de María P, Stillger T, Pohl M, Wallert S, Drauz K, Gröger H, Trauthwein H, Liese A. 2006. Preparative enantioselective synthesis of benzoins and (*R*)-2-hydroxy-1-phenylpropanone using benzaldehyde lyase. *J. Mol. Catal. B Enzym.* **38**:43–47.

Douette P, Navet R, Gerkens P, Galleni M, Lévy D, Sluse FE. 2005. *Escherichia coli* fusion carrier proteins act as solubilizing agents for recombinant uncoupling protein 1 through interactions with GroEL. *Biochem. Biophys. Res. Commun.* **333**:686–693.

Dreßen A, Hilberath T, Mackfeld U, Rudat J, Pohl M. 2017. Phenylalanine ammonia lyase from *Arabidopsis thaliana* (AtPAL2): A potent MIO-enzyme for the synthesis of non-canonical aromatic alpha-amino acids. Part II: Application in different reactor concepts for the production of (*S*)-2-chloro-phenylalanine. *J. Biotechnol.* **258**:158–166.

Dreyer S, Kragl U. 2008. Ionic liquids for aqueous two-phase extraction and stabilization of enzymes. *Biotechnol. Bioeng.* **99**:1416–1424.

Duggleby RG, Kaplan H. 1975. A competitive labeling method for the determination of the chemical properties of solitary functional groups in proteins. *Biochemistry* **14**:5168–5175.

Duggleby RG. 2006. Domain relationships in thiamine diphosphate-dependent enzymes. *Acc. Chem. Res.* **39**:550–557.

Dünkelmann P, Kolter-Jung D, Nitsche A, Demir AS, Siegert P, Lingen B, Baumann M, Pohl M, Müller M. 2002. Development of a donor-acceptor concept for enzymatic cross-coupling

reactions of aldehydes: the first asymmetric cross-benzoin condensation. *J. Am. Chem. Soc.* **124**:12084–12085.

Dünnwald T, Demir AS, Siegert P, Pohl M, Müller M. 2000. Enantioselective Synthesis of (*S*)-2-Hydroxypropanone Derivatives by Benzoylformate Decarboxylase Catalyzed C−C Bond Formation. *European J. Org. Chem.* **2000**:2161–2170.

Edwards JO, Pearson G. 1962. The Factors Determining Nucleophilic Reactivities. *J. Am. Chem. Soc.* **84**:16–24.

Eklund H, Ramaswamy S. 2008. Medium- and short-chain dehydrogenase/reductase gene and protein families: Three-dimensional structures of MDR alcohol dehydrogenases. *Cell. Mol. Life Sci.* **65**:3907–3917.

Encell LP, Friedman Ohana R, Zimmerman K, Otto P, Vidugiris G, Wood MG, Los GV, McDougall MG, Zimprich C, Karassina N, Learish RD, Hurst R, Hartnett J, Wheeler S, Stecha P, English J, Zhao K, Mendez J, Benink HA, Murphy N, Daniels DL, Slater MR, Urh M, Darzins A, Klaubert DH, Bulleit RF, Wood KV. 2012. Development of a dehalogenase-based protein fusion tag capable of rapid, selective and covalent attachment to customizable ligands. *Curr. Chem. Genomics* **6**:55–71.

Engel S, Vyazmensky M, Berkovich D, Barak Z, Merchuk J, Chipman DM. 2005. Column flow reactor using acetohydroxyacid synthase I from *Escherichia coli* as catalyst in continuous synthesis of *R*-phenylacetyl carbinol. *Biotechnol. Bioeng.* **89**:733–40.

Engelmark Cassimjee K, Kadow M, Wikmark Y, Svedendahl Humble M, Rothstein ML, Rothstein DM, Bäckvall J-E. 2014. A general protein purification and immobilization method on controlled porosity glass: biocatalytic applications. *Chem. Commun.* **50**:9134.

Enoki J, Meisborn J, Müller A-C, Kourist R. 2016. A Multi-Enzymatic Cascade Reaction for the Stereoselective Production of γ-Oxyfunctionalyzed Amino Acids. *Front. Microbiol.* **7**:1–8.

Erdmann V. 2018. Synthetic enzyme cascades for the synthesis of amino alcohols and tetrahydroisoquinolines; Rheinisch-Westfälische Technische Hochschule Aachen.

Erdmann V, Mackfeld U, Rother D, Jakoblinnert A. 2014. Enantioselective, continuous (*R*)- and (*S*)-2-butanol synthesis: achieving high space-time yields with recombinant *E. coli* cells in a micro-aqueous, solvent-free reaction system. *J. Biotechnol.* **191**:106–112.

Faber K. 2018. Biotransformations in Organic Chemistry 7th ed. Springer International Publishing.

Ferloni C, Heinemann M, Hummel W, Daussmann T, Büchs J. 2004. Optimization of enzymatic gas-phase reactions by increasing the long-term stability of the catalyst. *Biotechnol. Prog.* **20**:975–978.

Fessner W-D, Schneider A, Held H, Sinerius G, Walter C, Hixon M, Schloss JV. 1996. The Mechanism of Class II, Metal-Dependent Aldolases. *Angew. Chemie - Int. Ed.* **35**:2219–2221.

Finn RD, Mistry J, Tate J, Coggill P, Heger A, Pollington JE, Gavin OL, Gunasekaran P, Ceric G, Forslund K, Holm L, Sonnhammer ELL, Eddy SR, Bateman A. 2010. The Pfam protein families database. *Nucleic Acids Res.* **38**:D211–D222.

Fischer E. 1894. Einfluss der Configuration auf die Wirkung der Enzyme. *Berichte der Dtsch. Chem. Gesellschaft* **27**:2985–2993.

Fitzpatrick DE, Ley S V. 2016. Engineering chemistry: integrating batch and flow reactions on a single, automated reactor platform. *React. Chem. Eng.* **1**:629–635.

Frank RAW, Leeper FJ, Luisi BF. 2007. Structure, mechanism and catalytic duality of thiamine-dependent enzymes. *Cell. Mol. Life Sci.* **64**:892–905.

Fraser JE, Bickerstaff GF. 1997. Entrapment in Calcium Alginate. In: Bickerstaff, GF, editor.

Immobil. Enzym. Cells. Methods Biotechnol. vol. 1. New Jersey: Humana Press, pp. 61–66.

Frese M-A, Dierks T. 2009. Formylglycine Aldehyde Tag-Protein Engineering through a Novel Post-translational Modification. *ChemBioChem* **10**:425–427.

Fuchs SM, Raines RT. 2009. Polyarginine as a multifunctional fusion tag. *Protein Sci.* **14**:1538–1544.

García-Fruitós E, Villaverde A. 2010. Friendly production of bacterial inclusion bodies. *Korean J. Chem. Eng.* **27**:385–389.

Garcia-Galan C, Berenguer-Murcia Á, Fernandez-Lafuente R, Rodrigues RC. 2011. Potential of Different Enzyme Immobilization Strategies to Improve Enzyme Performance. *Adv. Synth. Catal.* **353**:2885–2904.

Garrabou X, Castillo JA, Guérard-Hélaine C, Parella T, Joglar J, Lemaire M, Clapés P. 2009. Asymmetric self- and cross-aldol reactions of glycolaldehyde catalyzed by D-fructose-6-phosphate aldolase. *Angew. Chemie - Int. Ed.* **48**:5521–5525.

Gautier A, Juillerat A, Heinis C, Corrêa IR, Kindermann M, Beaufils F, Johnsson K. 2008. An Engineered Protein Tag for Multiprotein Labeling in Living Cells. *Chem. Biol.* **15**:128–136.

Gefflaut T, Blonski C, Perie J, Willson M. 1995. Class I aldolases: substrate specificity, mechanism, inhibitors and structural aspects. *Prog. Biophys. Mol. Biol.* **63**:301–340.

George RA, Heringa J. 2002. An analysis of protein domain linkers: their classification and role in protein folding. *Protein Eng.* **15**:871–879.

Gerhards T, Mackfeld U, Bocola M, von Lieres E, Wiechert W, Pohl M, Rother D. 2012. Influence of organic solvents on enzymatic asymmetric carboligations. *Adv. Synth. Catal.* **354**:2805–2820.

Gerlach T. 2017. Construction of biocatalytically active membranes through CBM-mediated immobilization of enzymes; Rheinisch-Westfälische Technische Hochschule Aachen.

Gijsen HJM, Wong C-H. 1994. Unprecedented Asymmetric Aldol Reactions with Three Aldehyde Substrates Catalyzed by 2-Deoxyribose-5-phosphate Aldolase. *J. Am. Chem. Soc.* **116**:8422–8423.

Gocke D. 2007. New and optimised thiamine diphosphate (ThDP)-dependent enzymes for carboligation; Heinrich-Heine-Universität Düsseldorf.

Gocke D, Graf T, Brosi H, Frindi-Wosch I, Walter L, Müller M, Pohl M. 2009. Comparative characterisation of thiamin diphosphate-dependent decarboxylases. *J. Mol. Catal. B Enzym.* **61**:30–35.

Gocke D, Walter L, Gauchenova E, Kolter G, Knoll M, Berthold CL, Schneider G, Pleiss J, Müller M, Pohl M. 2008. Rational protein design of ThDP-dependent enzymes - Engineering stereoselectivity. *ChemBioChem* **9**:406–412.

Gong Y, Pan L. 2015. Recent advances in bioorthogonal reactions for site-specific protein labeling and engineering. *Tetrahedron Lett.* **56**:2123–2132.

Gonzalez B, Vicuna R. 1989. Benzaldehyde lyase, a novel thiamine PPi-requiring enzyme, from *Pseudomonas fluorescens* biovar I. *J. Bacteriol.* **171**:2401–2405.

de Gonzalo G, Lavandera I, Faber K, Kroutil W. 2007. Enzymatic Reduction of Ketones in "Micro-aqueous" Media Catalyzed by ADH-A from *Rhodococcus ruber*. *Org. Lett.* **9**:2163–2166.

Groboillot AF, Champagne CP, Darling GD, Poncelet D, Neufeld RJ. 1993. Membrane formation by interfacial cross-linking of chitosan for microencapsulation of *Lactococcus lactis*. *Biotechnol. Bioeng.* **42**:1157–1163.

Gröger H, Hummel W. 2014. Combining the "two worlds" of chemocatalysis and biocatalysis towards multi-step one-pot processes in aqueous media. *Curr. Opin. Chem. Biol.* **19**:171–179.

Gruber P, Marques MPC, O'Sullivan B, Baganz F, Wohlgemuth R, Szita N. 2017. Conscious coupling: The challenges and opportunities of cascading enzymatic microreactors. *Biotechnol. J.* **12**.

Guillén D, Sánchez S, Rodríguez-Sanoja R. 2010. Carbohydrate-binding domains: multiplicity of biological roles. *Appl. Microbiol. Biotechnol.* **85**:1241–1249.

Guisan JM ed. 2006. Immobilization of Enzymes and Cells. *Methods Biotechnol. Vol 22* 2nd ed. Totowa, NJ: Humana Press. Vol. 22 450p.

Gunsalus CF, Stanier RY, Gunsalus IC. 1953. The enzymatic conversion of mandelic acid to benzoic acid. III. Fractionation and properties of the soluble enzymes. *J. Bacteriol.* **66**:548–553.

Gupta RD. 2016. Recent advances in enzyme promiscuity. *Sustain. Chem. Process.* **4**.

Guzik U, Hupert-Kocurek K, Wojcieszyńska D. 2014. Immobilization as a Strategy for Improving Enzyme Properties-Application to Oxidoreductases. *Molecules* **19**:8995–9018.

Hammer SC, Kubik G, Watkins E, Huang S, Minges H, Arnold FH. 2017. Anti-Markovnikov alkene oxidation by metal-oxo–mediated enzyme catalysis. *Science* **358**:215–218.

Hänisch J, Wältermann M, Robenek H, Steinbüchel A. 2006. The *Ralstonia eutropha* H16 phasin PhaP1 is targeted to intracellular triacylglycerol inclusions in *Rhodococcus opacus* PD630 and *Mycobacterium smegmatis* mc2155, and provides an anchor to target other proteins. *Microbiology* **152**:3271–3280.

Hanson RL, Davis BL, Chen Y, Goldberg SL, Parker WL, Tully TP, Montana MA, Patel RN. 2008. Preparation of (*R*)-Amines from Racemic Amines with an (*S*)-Amine Transaminase from *Bacillus megaterium*. *Adv. Synth. Catal.* **350**:1367–1375.

Hartmann M. 2005. Ordered Mesoporous Materials for Bioadsorption and Biocatalysis. *Chem. Mater.* **17**:4577–4593.

Hartmeier W. 1985. Immobilized biocatalysts - From simple to complex systems. *Trends Biotechnol.* **3**:149–153.

Hasson MS, Muscate A, McLeish MJ, Polovnikova LS, Gerlt JA, Kenyon GL, Petsko GA, Ringe D. 1998. The crystal structure of benzoylformate decarboxylase at 1.6 Å resolution: diversity of catalytic residues in thiamin diphosphate-dependent enzymes. *Biochemistry* **37**:9918–9930.

Hegeman GD. 1966. Synthesis of the enzymes of the mandelate pathway by *Pseudomonas putida*. I. Synthesis of enzymes by the wild type. *J. Bacteriol.* **91**:1140–1154.

Hegeman GD. 1970. Benzoylformate decarboxylase (*Pseudomonas putida*). In: Tabor, H, Tabor, CW, editors. *Methods Enzymol.* Academic Press, pp. 674–678.

Heine A, DeSantis G, Luz JG, Mitchell M, Wong CH, Witson IA. 2001. Observation of covalent intermediates in an enzyme mechanism at atomic resolution. *Science* **294**:369–374.

Heine A, Luz JG, Wong CH, Wilson IA. 2004. Analysis of the class I aldolase binding site architecture based on the crystal structure of 2-Deoxyribose-5-phosphate aldolase at 0.99 Å resolution. *J. Mol. Biol.* **343**:1019–1034.

Hildebrand F, Lütz S. 2006. Immobilization of alcohol dehydrogenase from *Lactobacillus brevis* and its application in a plug-flow reactor. *Tetrahedron Asymmetry* **17**:3219–3225.

Hilterhaus L, Minow B, Müller J, Berheide M, Quitmann H, Katzer M, Thum O, Antranikian G, Zeng AP, Liese A. 2008. Practical application of different enzymes immobilized on sepabeads. *Bioprocess Biosyst. Eng.* **31**:163–171.

Hoarau M, Badieyan S, Marsh ENG. 2017. Immobilized enzymes: understanding enzyme – surface interactions at the molecular level. *Org. Biomol. Chem.* **15**:9539–9551.

Hoffee P, Rosen OM, Horecker BL. 1965. The Mechanism of Action of Aldolases. VI. Crystallization of Deoxyribose 5-Phosphate Alodolase and the number of Active Sites. *J. Biol. Chem.* **240**:1512–1516.

Höhne M, Bornscheuer UT. 2009. Biocatalytic routes to optically active amines. *ChemCatChem* **1**:42–51.

Höhne M, Kühl S, Robins K, Bornscheuer UT. 2008. Efficient asymmetric synthesis of chiral amines by combining transaminase and pyruvate decarboxylase. *ChemBioChem* **9**:363–365.

Homaei AA, Sariri R, Vianello F, Stevanato R. 2013. Enzyme immobilization: an update. *J. Chem. Biol.* **6**:185–205.

Honda T, Tanaka T, Yoshino T. 2015. Stoichiometrically Controlled Immobilization of Multiple Enzymes on Magnetic Nanoparticles by the Magnetosome Display System for Efficient Cellulose Hydrolysis. *Biomacromolecules* **16**:3863–3868.

Huisman GW, Collier SJ. 2013. On the development of new biocatalytic processes for practical pharmaceutical synthesis. *Curr. Opin. Chem. Biol.* **17**:284–292.

Hummel W, Gröger H. 2014. Strategies for regeneration of nicotinamide coenzymes emphasizing self-sufficient closed-loop recycling systems. *J. Biotechnol.* **191**:22–31.

Iding H, Dünnwald T, Greiner L, Liese A, Müller M, Siegert P, Grötzinger J, Demir AS, Pohl M. 2000. Benzoylformate decarboxylase from *Pseudomonas putida* as stable catalyst for the synthesis of chiral 2-hydroxy ketones. *Chem. - A Eur. J.* **6**:1483–1495.

Iyer PV, Ananthanarayan L. 2008. Enzyme stability and stabilization—Aqueous and non-aqueous environment. *Process Biochem.* **43**:1019–1032.

Jakoblinnert A, Rother D. 2014. A two-step biocatalytic cascade in micro-aqueous medium: using whole cells to obtain high concentrations of a vicinal diol. *Green Chem.*:3472–3482.

Jansonius JN. 1998. Structure, evolution and action of vitamin B6-dependent enzymes. *Curr. Opin. Struct. Biol.* **8**:759–769.

Jegannathan KR, Nielsen PH. 2013. Environmental assessment of enzyme use in industrial production – a literature review. *J. Clean. Prod.* **42**:228–240.

Jeromin GE. 2009. Superabsorbed alcohol dehydrogenase-a new catalyst for asymmetric reductions. *Biotechnol. Lett.* **31**:1717–1721.

Jesionowski T, Zdarta J, Krajewska B. 2014. Enzyme immobilization by adsorption: a review. *Adsorption* **20**:801–821.

Jiang M, Zhang L, Wang F, Zhang J, Liu G, Gao B, Wei D. 2017. Novel Application of Magnetic Protein: Convenient One-Step Purification and Immobilization of Proteins. *Sci. Rep.* **7**.

John RA. 1995. Pyridoxal phosphate-dependent enzymes. *Biochim. Biophys. Acta* **1248**:81–96.

Jordan F. 2003. Current mechanistic understanding of thiamin diphosphate-dependent enzymatic reactions. *Nat. Prod. Rep.* **20**:184–201.

Jörnvall H, Hedlund J, Bergman T, Oppermann U, Persson B. 2010. Superfamilies SDR and MDR: From early ancestry to present forms. Emergence of three lines, a Zn-metalloenzyme, and distinct variabilities. *Biochem. Biophys. Res. Commun.* **396**:125–130.

Jörnvall H, Landreh M, Östberg LJ. 2015. Alcohol dehydrogenase, SDR and MDR structural stages, present update and altered era. *Chem. Biol. Interact.* **234**:75–79.

Jörnvall H, Persson B, Krook M, Atrian S, Gonzàlez-Duarte R, Jeffery J, Ghosh D. 1995. Short-chain dehydrogenases/reductases (SDR). *Biochemistry* **34**:6003–6013.

Jörnvall H, Persson M, Jeffery J. 1981. Alcohol and polyol dehydrogenases are both divided into two protein types, and structural properties cross-relate the different enzyme activities within each type. *Proc. Natl. Acad. Sci. U. S. A.* **78**:4226–4230.

Kallberg Y, Oppermann U, Jörnvall H, Persson B. 2002. Short-chain dehydrogenases/reductases (SDRs). Coenzyme-based functional assignments in completed genomes. *Eur. J. Biochem.* **269**:4409–4417.

Kallenberg AI, van Rantwijk F, Sheldon RA. 2005. Immobilization of Penicillin G Acylase: The Key to Optimum Performance. *Adv. Synth. Catal.* **347**:905–926.

Kan SBJ, Lewis RD, Chen K, Arnold FH. 2016. Directed evolution of cytochrome c for carbon – silicon bond formation: Bringing silicon to life. *Science* **354**:1048–1052.

Kara S, Schrittwieser JH, Hollmann F. 2013a. Strategies for Cofactor Regeneration in Biocatalyzed Reductions. In: Brenna, E, editor. *Synth. Methods Biol. Act. Mol.* Weinheim, Germany: Wiley-VCH Verlag GmbH & Co. KGaA, pp. 209–238.

Kara S, Spickermann D, Schrittwieser JH, Weckbecker A, Leggewie C, Arends IWCE, Hollmann F. 2013b. Access to Lactone Building Blocks via Horse Liver Alcohol Dehydrogenase-Catalyzed Oxidative Lactonization. *ACS Catal.* **3**:2436–2439.

Kara S, Spickermann D, Schrittwieser JH, Leggewie C, van Berkel WJH, Arends IWCE, Hollmann F. 2013c. More efficient redox biocatalysis by utilising 1,4-butanediol as a "smart cosubstrate." *Green Chem.* **15**:330–335.

Katebi AR, Jernigan RL. 2015. Aldolases Utilize Different Oligomeric States To Preserve Their Functional Dynamics. *Biochemistry* **54**:3543–3554.

Kazenwadel F, Biegert E, Wohlgemuth J, Wagner H, Franzreb M. 2016. A 3D-printed modular reactor setup including temperature and pH control for the compartmentalized implementation of enzyme cascades. *Eng. Life Sci.* **16**:560–567.

Kelly SA, Pohle S, Wharry S, Mix S, Allen CCR, Moody TS, Gilmore BF. 2018. Application of ω-Transaminases in the Pharmaceutical Industry. *Chem. Rev.* **118**:349–367.

Keppler A, Gendreizig S, Gronemeyer T, Pick H, Vogel H, Johnsson K. 2003. A general method for the covalent labeling of fusion proteins with small molecules in vivo. *Nat. Biotechnol.* **21**:86–89.

Kihumbu D, Stillger T, Hummel W, Liese A. 2002. Enzymatic synthesis of all stereoisomers of 1-phenylpropane-1,2-diol. *Tetrahedron Asymmetry* **13**:1069–1072.

Kirsch JF, Eichele G, Ford GC, Vincent MG, Jansonius JN, Gehring H, Christen P. 1984. Mechanism of action of aspartate aminotransferase proposed on the basis of its spatial structure. *J. Mol. Biol.* **174**:497–525.

Kirschning A, Kupracz L, Hartwig J. 2012. New Synthetic Opportunities in Miniaturized Flow Reactors with Inductive Heating. *Chem. Lett.* **41**:562–570.

Klein J, Ziehr H. 1990. Immobilization of microbial cells by adsorption. *J. Biotechnol.* **16**:1–15.

Klermund L, Poschenrieder ST, Castiglione K. 2017. Biocatalysis in Polymersomes: Improving Multienzyme Cascades with Incompatible Reaction Steps by Compartmentalization. *ACS Catal.* **7**:3900–3904.

Klibanov AM. 1979. Enzyme stabilization by immobilization. *Anal. Biochem.* **93**:1–25.

Klibanov AM. 1983. Approaches to enzyme stabilization. *Biochem. Soc. Trans.* **11**:19–20.

Klibanov AM. 1997. Why are enzymes less active in organic solvents than in water? *Trends Biotechnol.* **15**:97–101.

Kluger R, Tittmann K. 2008. Thiamin diphosphate catalysis: enzymic and nonenzymic covalent

intermediates. *Chem. Rev.* **108**:1797–833.

Kocienski PJ. 2005. Protecting Groups 3rd ed. New York: Thieme.

Kohlmann C, Robertz N, Leuchs S, Dogan Z, Lütz S, Bitzer K, Na'amnieh S, Greiner L. 2011. Ionic liquid facilitates biocatalytic conversion of hardly water soluble ketones. *J. Mol. Catal. B Enzym.* **68**:147–153.

Kohls H, Steffen-Munsberg F, Höhne M. 2014. Recent achievements in developing the biocatalytic toolbox for chiral amine synthesis. *Curr. Opin. Chem. Biol.* **19**:180–92.

Kopka B, Diener M, Wirtz A, Pohl M, Jaeger K-E, Krauss U. 2015. Purification and simultaneous immobilization of *Arabidopsis thaliana* hydroxynitrile lyase using a family 2 carbohydrate-binding module. *Biotechnol. J.* **10**:811–819.

Koszelewski D, Göritzer M, Clay D, Seisser B, Kroutil W. 2010a. Synthesis of Optically Active Amines Employing Recombinant ω-Transaminases in *E. coli* Cells. *ChemCatChem* **2**:73–77.

Koszelewski D, Lavandera I, Clay D, Rozzell D, Kroutil W. 2008. Asymmetric synthesis of optically pure pharmacologically relevant amines employing ω-transaminases. *Adv. Synth. Catal.* **350**:2761–2766.

Koszelewski D, Pressnitz D, Clay D, Kroutil W. 2009. Deracemization of mexiletine biocatalyzed by ω-transaminases. *Org. Lett.* **11**:4810–4812.

Koszelewski D, Tauber K, Faber K, Kroutil W. 2010b. ω-Transaminases for the synthesis of non-racemic alpha-chiral primary amines. *Trends Biotechnol.* **28**:324–332.

Krasňan V, Stloukal R, Rosenberg M, Rebroš M. 2016. Immobilization of cells and enzymes to LentiKats®. *Appl. Microbiol. Biotechnol.* **100**:2535–2553.

Krauss U, Jäger VD, Diener M, Pohl M, Jaeger K-E. 2017. Catalytically-active inclusion bodies—Carrier-free protein immobilizates for application in biotechnology and biomedicine. *J. Biotechnol.* **258**:136–147.

Kroutil W, Rueping M. 2014. Introduction to ACS Catalysis Virtual Special Issue on Cascade Catalysis. *ACS Catal.* **4**:2086–2087.

Kuhn D, Kholiq MA, Heinzle E, Bühler B, Schmid A. 2010. Intensification and economic and ecological assessment of a biocatalytic oxyfunctionalization process. *Green Chem.* **12**:815–827.

Kühne W. 1876. Ueber das Verhalten verschiedener organisirter und sog. ungeformter Fermente. *Verhandlungen des naturhistorisch-medicinischen Vereins zu Heidelb.*:190–193.

Kuiper SM, Nallani M, Vriezema DM, Cornelissen JJLM, van Hest JCM, Nolte RJM, Rowan AE. 2008. Enzymes containing porous polymersomes as nano reaction vessels for cascade reactions. *Org. Biomol. Chem.* **6**:4315–4318.

Kulig J, Frese A, Kroutil W, Pohl M, Rother D. 2013. Biochemical characterization of an alcohol dehydrogenase from *Ralstonia* sp. *Biotechnol. Bioeng.* **110**:1838–1848.

Kulig J, Simon RC, Rose CA, Husain SM, Häckh M, Lüdeke S, Zeitler K, Kroutil W, Pohl M, Rother D. 2012. Stereoselective synthesis of bulky 1,2-diols with alcohol dehydrogenases. *Catal. Sci. Technol.* **2**:1580–1589.

Kumada Y, Hamasaki K, Shiritani Y, Nakagawa A, Kuroki D, Ohse T, Choi DH, Katakura Y, Kishimoto M. 2009. Direct immobilization of functional single-chain variable fragment antibodies (scFvs) onto a polystyrene plate by genetic fusion of a polystyrene-binding peptide (PS-tag). *Anal. Bioanal. Chem.* **395**:759–765.

Kumada Y, Tokunaga Y, Imanaka H, Imamura K, Sakiyama T, Katoh S, Nakanishi K. 2006. Screening and Characterization of Affinity Peptide Tags Specific to Polystyrene Supports for the Orientated Immobilization of Proteins. *Biotechnol. Prog.* **22**:401–405.

Kurlemann N, Liese A. 2004. Immobilization of benzaldehyde lyase and its application as a heterogeneous catalyst in the continuous synthesis of a chiral 2-hydroxy ketone. *Tetrahedron Asymmetry* **15**:2955–2958.

Ladenstein R, Winberg J-O, Benach J. 2008. Medium- and short-chain dehydrogenase/reductase gene and protein families : Structure-function relationships in short-chain alcohol dehydrogenases. *Cell. Mol. Life Sci.* **65**:3918–35.

Laurenti E, dos Santos Vianna Jr. A. 2016. Enzymatic microreactors in biocatalysis: history, features, and future perspectives. *Biocatalysis* **1**:148–165.

Leuchs S, Greiner L. 2011. Alcohol Dehydrogenase from *Lactobacillus brevis*: A Versatile Robust Catalyst for Enantioselective Transformations. *Chem. Biochem. Eng. Q.* **25**:267–281.

Leuchs S, Na'amnieh S, Greiner L. 2013. Enantioselective reduction of sparingly water-soluble ketones: continuous process and recycle of the aqueous buffer system. *Green Chem.* **15**:167–176.

Levy I, Shoseyov O. 2002. Cellulose-binding domains. *Biotechnol. Adv.* **20**:191–213.

Ley SV. 2012. On Being Green: Can Flow Chemistry Help? *Chem. Rec.* **12**:378–390.

Li G, Huang Z, Zhang C, Dong BJ, Guo RH, Yue HW, Yan LT, Xing XH. 2016. Construction of a linker library with widely controllable flexibility for fusion protein design. *Appl. Microbiol. Biotechnol.* **100**:215–225.

Li H, Moncecchi J, Truppo MD. 2015. Development of an Immobilized Ketoreductase for Enzymatic (*R*)-1-(3,5-Bis(trifluoromethyl)phenyl)ethanol Production. *Org. Process Res. Dev.* **19**:695–700.

Lichty JJ, Malecki JL, Agnew HD, Michelson-Horowitz DJ, Tan S. 2005. Comparison of affinity tags for protein purification. *Protein Expr. Purif.* **41**:98–105.

Liese A, Zelinski T, Kula MR, Kierkels H, Karutz M, Kragl U, Wandrey C. 1998. A novel reactor concept for the enzymatic reduction of poorly soluble ketones. *J. Mol. Catal. - B Enzym.* **4**:91–99.

Liese A, Hilterhaus L. 2013. Evaluation of immobilized enzymes for industrial applications. *Chem. Soc. Rev.* **42**:6236–6249.

Lindqvist Y, Schneider G, Ermler U, Sundström M. 1992. Three-dimensional structure of transketolase, a thiamine diphosphate dependent enzyme, at 2.5 Å resolution. *EMBO J.* **11**:2373–2379.

Lingen B, Grötzinger J, Kolter D, Kula MR, Pohl M. 2002. Improving the carboligase activity of benzoylformate decarboxylase from *Pseudomonas putida* by a combination of directed evolution and site-directed mutagenesis. *Protein Eng.* **15**:585–593.

Lingen B, Kolter-Jung D, Dünkelmann P, Feldmann R, Grötzinger J, Pohl M, Müller M. 2003. Alteration of the substrate specificity of benzoylformate decarboxylase from *Pseudomonas putida* by directed evolution. *ChemBioChem* **4**:721–726.

Liu Y, Cao A. 2017. Encapsulating Proteins in Nanoparticles: Batch by Batch or One by One. In: Kumar, CV, editor. *Methods Enzymol.* 1st ed. Elsevier Inc., Vol. 590, pp. 1–31.

Lombard V, Golaconda Ramulu H, Drula E, Coutinho PM, Henrissat B. 2014. The carbohydrate-active enzymes database (CAZy) in 2013. *Nucleic Acids Res.* **42**:490–495.

Los GV, Encell LP, McDougall MG, Hartzell DD, Karassina N, Zimprich C, Wood MG, Learish R, Ohana RF, Urh M, Simpson D, Mendez J, Zimmerman K, Otto P, Vidugiris G, Zhu J, Darzins A, Klaubert DH, Bulleit RF, Wood KV. 2008. HaloTag: a novel protein labeling technology for cell imaging and protein analysis. *ACS Chem. Biol.* **3**:373–382.

Lu L, Xu S, Zhao R, Zhang D, Li Z, Li Y, Xiao M. 2012. Synthesis of galactooligosaccharides by CBD fusion β-galactosidase immobilized on cellulose. *Bioresour. Technol.* **116**:327–333.

Lvov Y, Antipov AA, Mamedov A, Möhwald H, Sukhorukov GB. 2001. Urease Encapsulation in Nanoorganized Microshells. *Nano Lett.* **1**:125–128.

Malik MS, Park E-S, Shin J-S. 2012. Features and technical applications of ω-transaminases. *Appl. Microbiol. Biotechnol.* **94**:1163–1171.

Mallin H, Wulf H, Bornscheuer UT. 2013. A self-sufficient Baeyer–Villiger biocatalysis system for the synthesis of ε-caprolactone from cyclohexanol. *Enzyme Microb. Technol.* **53**:283–287.

Mateo C, Grazú V, Pessela BCC, Montes T, Palomo JM, Torres R, López-Gallego F, Fernández-Lafuente R, Guisán JM. 2007a. Advances in the design of new epoxy supports for enzyme immobilization–stabilization. *Biochem. Soc. Trans.* **35**:1593–1601.

Mateo C, Fernandez-Lorente G, Rocha-Martin J, Bolivar JM, Guisan JM. 2013. Oriented Covalent Immobilization of Enzymes on Heterofunctional-Glyoxyl Supports. In: Guisan, JM, editor. *Immobil. Enzym. Cells. Methods Mol. Biol.* Totowa, NJ: Humana Press. Methods in Molecular Biology, Vol. 1051, pp. 73–88.

Mateo C, Palomo JM, Fernandez-Lorente G, Guisan JM, Fernandez-Lafuente R. 2007b. Improvement of enzyme activity, stability and selectivity via immobilization techniques. *Enzyme Microb. Technol.* **40**:1451–1463.

Matsuda T, Yamanaka R, Nakamura K. 2009. Recent progress in biocatalysis for asymmetric oxidation and reduction. *Tetrahedron: Asymmetry* **20**:513–557.

McAuliffe JC. 2012. Industrial Enzymes and Biocatalysis. In: Kent, JA, editor. *Handb. Ind. Chem. Biotechnol.* Boston, MA: Springer US, pp. 1183–1227.

McLean BW, Bray MR, Boraston AB, Gilkes NR, Haynes CA, Kilburn DG. 2000. Analysis of binding of the family 2a carbohydrate-binding module from *Cellulomonas fimi* xylanase 10A to cellulose: specificity and identification of functionally important amino acid residues. *Protein Eng.* **13**:801–809.

Means GE, Feeney RE. 1990. Chemical modifications of proteins: history and applications. *Bioconjug. Chem.* **1**:2–12.

Mehta PK, Hale TI, Christen P. 1993. Aminotransferases: demonstration of homology and division into evolutionary subgroups. *Eur. J. Biochem.* **214**:549–561.

Meldal M, Schoffelen S. 2016. Recent advances in covalent, site-specific protein immobilization. *F1000Research* **5**.

Michael Green N. 1990. Avidin and streptavidin. In: Wilchek, M, Bayer, EA, editors. *Avidin-Biotin Technol.* Elsevier. Methods in Enzymology, Vol. 184, pp. 51–67.

Migneault I, Dartiguenave C, Bertrand MJ, Waldron KC. 2004. Glutaraldehyde: Behavior in aqueous solution, reaction with proteins, and application to enzyme crosslinking. *Biotechniques* **37**:790–802.

Morag ELY, Lapidot A, Govorko D, Lamed R, Wilchek M, Bayer EA, Shoham Y. 1995. Expression, Purification, and Characterization of the Cellulose- Binding Domain of the Scaffoldin Subunit from the Cellulosome of *Clostridium thermocellum*. *Appl. Environ. Microbiol.* **61**:1980–1986.

Mosbacher TG, Mueller M, Schulz GE. 2005. Structure and mechanism of the ThDP-dependent benzaldehyde lyase from *Pseudomonas fluorescens*. *FEBS J.* **272**:6067–6076.

Mozzarelli A, Bettati S. 2006. Exploring the pyridoxal 5'-phosphate-dependent enzymes. *Chem. Rec.* **6**:275–287.

Müller M, Gocke D, Pohl M. 2009. Thiamin diphosphate in biological chemistry: exploitation of diverse thiamin diphosphate-dependent enzymes for asymmetric chemoenzymatic synthesis. *FEBS J.* **276**:2894–904.

Muller YA, Schulz GE. 1993. Structure of the thiamine- and flavin-dependent enzyme pyruvate oxidase. *Science* **259**:965–967.

Muller YA, Lindqvist Y, Furey W, Schulz GE, Jordan F, Schneider G. 1993. A thiamin diphosphate binding fold revealed by comparison of the crystal structures of transketolase, pyruvate oxidase and pyruvate decarboxylase. *Structure* **1**:95–103.

Musa MM, Phillips RS. 2011. Recent advances in alcohol dehydrogenase-catalyzed asymmetric production of hydrophobic alcohols. *Catal. Sci. Technol.* **1**:1311–1323.

Musio B, Gala E, Ley SV. 2018. Real-Time Spectroscopic Analysis Enabling Quantitative and Safe Consumption of Fluoroform during Nucleophilic Trifluoromethylation in Flow. *ACS Sustain. Chem. Eng.* **6**:1489–1495.

Nallamsetty S, Waugh DS. 2007. Mutations that alter the equilibrium between open and closed conformations of *Escherichia coli* maltose-binding protein impede its ability to enhance the solubility of passenger proteins. *Biochem. Biophys. Res. Commun.* **364**:639–644.

Nawaz MA, Aman A, Rehman HU, Bibi Z, Ansari A, Islam Z, Khan IA, Qader SAU. 2016. Polyacrylamide Gel-Entrapped Maltase: An Excellent Design of Using Maltase in Continuous Industrial Processes. *Appl. Biochem. Biotechnol.* **179**:383–397.

Newman SG, Jensen KF. 2013. The role of flow in green chemistry and engineering. *Green Chem.* **15**:1456–1472.

Niefind K, Müller J, Riebel B, Hummel W, Schomburg D. 2003. The crystal structure of *R*-specific alcohol dehydrogenase from *Lactobacillus brevis* suggests the structural basis of its metal dependency. *J. Mol. Biol.* **327**:317–328.

Niefind K, Riebel B, Müller J, Hummel W, Schomburg D. 2000. Crystallization and preliminary characterization of crystals of *R*-alcohol dehydrogenase from *Lactobacillus brevis*. *Acta Crystallogr. Sect. D Biol. Crystallogr.* **56**:1696–1698.

O'Brien M, Baxendale IR, Ley SV. 2010. Flow Ozonolysis Using a Semipermeable Teflon AF-2400 Membrane To Effect Gas−Liquid Contact. *Org. Lett.* **12**:1596–1598.

O'Shannessy DJ. 1990. Hydrazido-derivatized supports in affinity chromatography. *J. Chromatogr.* **510**:13–21.

Ohana RF, Encell LP, Zhao K, Simpson D, Slater MR, Urh M, Wood KV. 2009. HaloTag7: a genetically engineered tag that enhances bacterial expression of soluble proteins and improves protein purification. *Protein Expr. Purif.* **68**:110–120.

Ong E, Gilkes NR, Warren RAJ, Miller RC, Kilburn DG. 1989. Enzyme Immobilization Using the Cellulose-Binding Domain of a *Cellulomonas Fimi* Exoglucanase. *Nat. Biotechnol.* **7**:604–607.

van Oosterwijk N, Willies S, Hekelaar J, Terwisscha van Scheltinga AC, Turner NJ, Dijkstra BW. 2016. Structural Basis of the Substrate Range and Enantioselectivity of Two (*S*)-Selective ω-Transaminases. *Biochemistry* **55**:4422–4431.

Park E, Kim M, Shin J. 2012. Molecular determinants for substrate selectivity of ω-transaminases. *Appl Microbiol. Biotechnol.* **93**:2425–2435.

Pauly HE, Pfleiderer G. 1977. Conformational and functional aspects of the reversible dissociation and denaturation of glucose dehydrogenase. *Biochemistry* **16**:4599–4604.

Pellis A, Cantone S, Ebert C, Gardossi L. 2018. Evolving biocatalysis to meet bioeconomy challenges and opportunities. *N. Biotechnol.* **40**:154–169.

Peper S, Kara S, Long WS, Liese A, Niemeyer B. 2011. Immobilization and characterization of benzoylformate decarboxylase from *Pseudomonas putida* on spherical silica carrier. *Bioprocess Biosyst. Eng.* **34**:671–680.

Peschke T, Rabe KS, Niemeyer CM. 2017a. Orthogonal Surface Tags for Whole-Cell Biocatalysis. *Angew. Chemie - Int. Ed.* **56**:2183–2186.

Peschke T, Skoupi M, Burgahn T, Gallus S, Ahmed I, Rabe KS, Niemeyer CM. 2017b. Self-Immobilizing Fusion Enzymes for Compartmentalized Biocatalysis. *ACS Catal.* **7**:7866–7872.

Peternel Š, Komel R. 2011. Active Protein Aggregates Produced in *Escherichia coli*. *Int. J. Mol. Sci.* **12**:8275–8287.

Peterson SN, Kwon K. 2013. The HaloTag: Improving Soluble Expression and Applications in Protein Functional Analysis. *Curr. Chem. Genomics* **6**:8–17.

Petry S, Weixlbaumer A, Ramakrishnan V. 2008. The termination of translation. *Curr. Opin. Struct. Biol.* **18**:70–77.

Pierre AC. 2004. The sol-gel encapsulation of enzymes. *Biocatal. Biotransformation* **22**:145–170.

Plutschack MB, Pieber B, Gilmore K, Seeberger PH. 2017. The Hitchhiker's Guide to Flow Chemistry. *Chem. Rev.* **117**:11796–11893.

Pohl M, Lingen B, Müller M. 2002. Thiamin-diphosphate-dependent enzymes: new aspects of asymmetric C-C bond formation. *Chem. - A Eur. J.* **8**:5288–5295.

Polakovič M, Švitel J, Bučko M, Filip J, Neděla V, Ansorge-Schumacher MB, Gemeiner P. 2017. Progress in biocatalysis with immobilized viable whole cells: systems development, reaction engineering and applications. *Biotechnol. Lett.* **39**:667–683.

Porrua O, Boudvillain M, Libri D. 2016. Transcription Termination: Variations on Common Themes. *Trends Genet.* **32**:508–522.

Prakash S, Chang TMS. 1995. Preparation and in vitro analysis of microencapsulated genetically engineered *E. coli* DH5 cells for urea and ammonia removal. *Biotechnol. Bioeng.* **46**:621–626.

Prelog V. 1964. Specification of the stereospecificity of some oxido-reductases by diamond lattice sections. *Pure Appl. Chem.* **9**:119–130.

Prince C. 2017. Nutzung von carbohydrate-binding modules als Tags für die Enzymimmobilisierung; Fachhochschule Jülich.

Qin S, Yin H, Yang C, Dou Y, Liu Z, Zhang P, Yu H, Huang Y, Feng J, Hao J, Hao J, Deng L, Yan X, Dong X, Zhao Z, Jiang T, Wang H-W, Luo S-J, Xie C. 2016. A magnetic protein biocompass. *Nat. Mater.* **15**:217–226.

Racker E. 1952. Enzymatic synthesis and breakdown of desoxyribose phosphate. *J. Biol. Chem.* **196**:347–365.

Rao NN, Lütz S, Würges K, Minör D. 2009. Continuous Biocatalytic Processes. *Org. Process Res. Dev.* **13**:607–616.

Reetz MT. 2017. Recent Advances in Directed Evolution of Stereoselective Enzymes. In: Alcalde, M, editor. *Dir. Enzym. Evol. Adv. Appl.* Springer International Publishing, pp. 69–99.

Rehm FBH, Chen S, Rehm BHA. 2018. Bioengineering toward direct production of immobilized enzymes: A paradigm shift in biocatalyst design. *Bioengineered* **9**:6–11.

Reizman BJ, Jensen KF. 2016. Feedback in Flow for Accelerated Reaction Development. *Acc. Chem. Res.* **49**:1786–1796.

Richins RD, Mulchandani A, Chen W. 2000. Expression, immobilization, and enzymatic characterization of cellulose-binding domain-organophosphorus hydrolase fusion enzymes. *Biotechnol. Bioeng.* **69**:591–596.

Riebel B. 1996. Biochemische und molekularbiologische Charakterisierung neuer mikrobieller

NAD(P)-abhängiger Alkoholdehydrogenasen.; Heinrich-Heine-Universität Düsseldorf.

Roberge DM, Zimmermann B, Rainone F, Gottsponer M, Eyholzer M, Kockmann N. 2008. Microreactor Technology and Continuous Processes in the Fine Chemical and Pharmaceutical Industry: Is the Revolution Underway? *Org. Process Res. Dev.* **12**:905–910.

Robertson K. 2017. Using flow technologies to direct the synthesis and assembly of materials in solution. *Chem. Cent. J.* **11**.

Rodríguez C, Borzęcka W, Sattler JH, Kroutil W, Lavandera I, Gotor V. 2014. Steric vs. electronic effects in the *Lactobacillus brevis* ADH-catalyzed bioreduction of ketones. *Org. Biomol. Chem.* **12**:673–681.

Roldán R, Sanchez-Moreno I, Scheidt T, Hélaine V, Lemaire M, Parella T, Clapés P, Fessner W-D, Guérard-Hélaine C. 2017. Breaking the Dogma of Aldolase Specificity: Simple Aliphatic Ketones and Aldehydes are Nucleophiles for Fructose-6-phosphate Aldolase. *Chem. - A Eur. J.* **23**:5005–5009.

Rother C, Nidetzky B. 2014. Enzyme Immobilization by Microencapsulation: Methods, Materials, and Technological Applications. In: Flickinger, MC, editor. *Encycl. Ind. Biotechnol.* Hoboken, NJ, USA: John Wiley & Sons, Inc., pp. 1–21.

Rozzell JD. 1999. Commercial scale biocatalysis: myths and realities. *Bioorg. Med. Chem.* **7**:2253–2261.

Rulli G, Heidlindemann M, Berkessel A, Hummel W, Gröger H. 2013. Towards catalyst compartimentation in combined chemo- and biocatalytic processes: Immobilization of alcohol dehydrogenases for the diastereoselective reduction of a β-hydroxy ketone obtained from an organocatalytic aldol reaction. *J. Biotechnol.* **168**:271–276.

Rutter WJ. 1964. Evolution of Aldolases. *Fed. Proc.* **23**:1248–57.

Santiago-Hernández JA, Vásquez-Bahena JM, Calixto-Romo MA, Xoconostle-Cázares GB, Ortega-López J, Ruíz-Medrano R, Montes-Horcasitas MC, Hidalgo-Lara ME. 2006. Direct immobilization of a recombinant invertase to Avicel by *E. coli* overexpression of a fusion protein containing the extracellular invertase from *Zymomonas mobilis* and the carbohydrate-binding domain CBDCex from *Cellulomonas fimi*. *Enzyme Microb. Technol.* **40**:172–176.

Sato H, Hummel W, Gröger H. 2015. Cooperative catalysis of noncompatible catalysts through compartmentalization: wacker oxidation and enzymatic reduction in a one-pot process in aqueous media. *Angew. Chemie - Int. Ed.* **54**:4488–4492.

Savile CK, Janey JM, Mundorff EC, Moore JC, Tam S, Jarvis WR, Colbeck JC, Krebber A, Fleitz FJ, Brands J, Devine PN, Huisman GW, Hughes GJ. 2010. Biocatalytic Asymmetric Synthesis of Chiral Amines from Ketones Applied to Sitagliptin Manufacture. *Science* **329**:305–309.

Schaber SD, Gerogiorgis DI, Ramachandran R, Evans JMB, Barton PI, Trout BL. 2011. Economic Analysis of Integrated Continuous and Batch Pharmaceutical Manufacturing: A Case Study. *Ind. Eng. Chem. Res.* **50**:10083–10092.

Schauer-Vukasinovic V, Daunert S. 1999. Purification of recombinant proteins based on the interaction between a phenothiazine-derivatized column and a calmodulin fusion tail. *Biotechnol. Prog.* **15**:513–516.

Schindler JF, Naranjo PA, Honaberger DA, Chang CH, Brainard JR, Vanderberg LA, Unkefer CJ. 1999. Haloalkane dehalogenases: steady-state kinetics and halide inhibition. *Biochemistry* **38**:5772–5778.

Schlange A, dos Santos AR, Kunz U, Turek T. 2011. Continuous preparation of carbon-nanotube-supported platinum catalysts in a flow reactor directly heated by electric current. *Beilstein J. Org. Chem.* **7**:1412–1420.

Schlieben NH, Niefind K, Müller J, Riebel B, Hummel W, Schomburg D. 2005. Atomic resolution structures of *R*-specific alcohol dehydrogenase from *Lactobacillus brevis* provide the structural bases of its substrate and cosubstrate specificity. *J. Mol. Biol.* **349**:801–813.

Schmid A, Dordick JS, Hauer B, Kiener A, Wubbolts M, Witholt B. 2001. Industrial biocatalysis today and tomorrow. *Nature* **409**:258–268.

Schmidt S, Castiglione K, Kourist R. 2017. Overcoming the Incompatibility Challenge in Chemoenzymatic and Multi-Catalytic Cascade Reactions. *Chem. - A Eur. J.*:1–15.

Schmidt TG, Skerra A. 1993. The random peptide library-assisted engineering of a C-terminal affinity peptide, useful for the detection and purification of a functional Ig Fv fragment. *Protein Eng.* **6**:109–22.

Schmidt TGM, Koepke J, Frank R, Skerra A. 1996. Molecular Interaction Between the Strep-tag Affinity Peptide and its Cognate Target, Streptavidin. *J. Mol. Biol.* **255**:753–766.

Schomburg I, Jeske L, Ulbrich M, Placzek S, Chang A, Schomburg D. 2017. The BRENDA enzyme information system–From a database to an expert system. *J. Biotechnol.* **261**:194–206.

Schrittwieser JH, Velikogne S, Hall M, Kroutil W. 2018. Artificial Biocatalytic Linear Cascades for Preparation of Organic Molecules. *Chem. Rev.* **118**:270–348.

Schroer K, Lütz S. 2009. A Continuously Operated Bimembrane Reactor Process for the Biocatalytic Production of (2*R*,5*R*)-Hexanediol. *Org. Process Res. Dev.* **13**:1202–1205.

Schroer K, Mackfeld U, Tan IAW, Wandrey C, Heuser F, Bringer-Meyer S, Weckbecker A, Hummel W, Daußmann T, Pfaller R, Liese A, Lütz S. 2007. Continuous asymmetric ketone reduction processes with recombinant *Escherichia coli*. *J. Biotechnol.* **132**:438–444.

Schumacher J, Eckstein M, Kragl U. 2006. Influence of water-miscible organic solvents on kinetics and enantioselectivity of the (*R*)-specific alcohol dehydrogenase from *Lactobacillus brevis*. *Biotechnol. J.* **1**:574–581.

Schwarz M. 2010. Einflussfaktoren auf die Stabilität und Aktivität der Benzaldehydlyase aus *Pseudomonas fluorescens* in Carboligasereaktionen mit aromatischen Aldehyden; Heinrich-Heine-Universität Düsseldorf.

Sehl T, Hailes HC, Ward JM, Menyes U, Pohl M, Rother D. 2014. Efficient 2-step biocatalytic strategies for the synthesis of all nor(pseudo)ephedrine isomers. *Green Chem.* **16**:3341–3348.

Sehl T, Hailes HC, Ward JM, Wardenga R, von Lieres E, Offermann H, Westphal R, Pohl M, Rother D. 2013. Two steps in one pot: enzyme cascade for the synthesis of nor(pseudo)ephedrine from inexpensive starting materials. *Angew. Chemie - Int. Ed.* **52**:6772–6775.

Serdakowski AL, Dordick JS. 2008. Enzyme activation for organic solvents made easy. *Trends Biotechnol.* **26**:48–54.

Sheldon RA. 2007. Enzyme Immobilization: The Quest for Optimum Performance. *Adv. Synth. Catal.* **349**:1289–1307.

Sheldon RA. 2011. Characteristic features and biotechnological applications of cross-linked enzyme aggregates (CLEAs). *Appl. Microbiol. Biotechnol.* **92**:467–477.

Sheldon RA. 2017. The E factor 25 years on: the rise of green chemistry and sustainability. *Green Chem.* **19**:18–43.

Sheldon RA, Woodley JM. 2018. Role of Biocatalysis in Sustainable Chemistry. *Chem. Rev.* **118**:801–838.

Sheldon RA, van Pelt S. 2013. Enzyme immobilisation in biocatalysis: why, what and how. *Chem. Soc. Rev.* **42**:6223–6235.

Shimon LJW, Pagès S, Belaich A, Belaich JP, Bayer EA, Lamed R, Shoham Y, Frolow F. 2000. Structure of a family IIIa scaffoldin CBD from the cellulosome of *Clostridium cellulolyticum* at 2.2 Å resolution. *Acta Crystallogr. Sect. D Biol. Crystallogr.* **56**:1560–1568.

Shpigel E, Goldlust A, Efroni G, Avraham A, Eshel A, Dekel M, Shoseyov O. 1999. Immobilization of recombinant heparinase I fused to cellulose-binding domain. *Biotechnol. Bioeng.* **65**:17–23.

Sierra MA, de la Torre MC. 2004. Dead Ends and Detours. Weinheim, FRG: Wiley-VCH Verlag GmbH & Co. KGaA 290 p.

Silverman R. 2002. Group Transfer Reactions: Hydrolysis, Amination, Phosphorylation. In: Silverman, RB, editor. *Org. Chem. Enzym. React.* Academic Press, pp. 39–94.

Simon RC, Richter N, Busto E, Kroutil W. 2014. Recent developments of cascade reactions involving ω-transaminases. *ACS Catal.* **4**:129–143.

Singh R, Tiwari M, Singh R, Lee J-K. 2013. From Protein Engineering to Immobilization: Promising Strategies for the Upgrade of Industrial Enzymes. *Int. J. Mol. Sci.* **14**:1232–1277.

Sletten EM, Bertozzi CR. 2011. Bioorthogonal Reactions. *Acc. Chem. Res.* **44**:666–676.

Smith DB, Johnson KS. 1988. Single-step purification of polypeptides expressed in *Escherichia coli* as fusions with glutathione S-transferase. *Gene* **67**:31–40.

Smith SW. 2009. Chiral Toxicology: It's the Same Thing…Only Different. *Toxicol. Sci.* **110**:4–30.

Song J, Tan H, Perry AJ, Akutsu T, Webb GI, Whisstock JC, Pike RN. 2012. PROSPER: an integrated feature-based tool for predicting protease substrate cleavage sites. *PLoS One* **7**.

Stanier RY. 1948. The Oxidation of Aromatic Compounds by Fluorescent *Pseudomonads*. *J. Bacteriol.* **55**:477–494.

Stankiewicz A, Moulijn JA. 2000. Process Intensification: Transformin Chemical Engineering. *Chem. Eng. Prog.* **96**:22–33.

Stemmer WPC. 1994. Rapid evolution of a protein in vitro by DNA shuffling. *Nature* **370**:389–391.

Stepankova V, Bidmanova S, Koudelakova T, Prokop Z, Chaloupkova R, Damborsky J. 2013. Strategies for Stabilization of Enzymes in Organic Solvents. *ACS Catal.* **3**:2823–2836.

Stillger T, Bönitz M, Villela Filho M, Liese A. 2002. Überwindung von thermodynamischen Limitierungen in substratgekoppelten Cofaktorregenerierungsverfahren. *Chemie Ing. Tech.* **74**:1035–1039.

Straathof AJJ, Panke S, Schmid A. 2002. The production of fine chemicals by biotransformations. *Curr. Opin. Biotechnol.* **13**:548–556.

Stura EA, Ghosh S, Garcia-Junceda E, Chen L, Wong C -H, Wilson IA. 1995. Crystallization and preliminary crystallographic data for class I deoxyribose-5-phosphate aldolase from *Escherichia coli*: an application of reverse screening. *Proteins* **22**:67–72.

Subrizi F, Crucianelli M, Grossi V, Passacantando M, Botta G, Antiochia R, Saladino R. 2014. Versatile and Efficient Immobilization of 2-Deoxyribose-5-phosphate Aldolase (DERA) on Multiwalled Carbon Nanotubes. *ACS Catal.* **4**:3059–3068.

Sührer I, Langemann T, Lubitz W, Weuster-Botz D, Castiglione K. 2015. A novel one-step expression and immobilization method for the production of biocatalytic preparations. *Microb. Cell Fact.* **14**.

Sun C, Li Y, Taylor SE, Mao X, Wilkinson MC, Fernig DG. 2015. HaloTag is an effective expression and solubilisation fusion partner for a range of fibroblast growth factors. *PeerJ* **3**.

Tamborini L, Fernandes P, Paradisi F, Molinari F. 2018. Flow Bioreactors as Complementary Tools

for Biocatalytic Process Intensification. *Trends Biotechnol.* **36**:73–88.

Taniguchi K, Nomura K, Hata Y, Nishimura T, Asami Y, Kuroda A. 2007. The Si-tag for immobilizing proteins on a silica surface. *Biotechnol. Bioeng.* **96**:1023–1029.

Tischer W, Wedekind F. 1999. Immobilized Enzymes: Methods and Applications. In: Fessner, WD, editor. *Biocatal. - From Discov. to Appl. Top. Curr. Chem. vol 200.* Berlin Heidelberg: Springer, pp. 95–126.

Tosa T, Mori T, Fuse N, Chibata I. 1966a. Studies on continuous enzyme reactions. II. Preparation of DEAE-cellulose-aminoacylase column and continuous optical resolution of acetyl-DL-methionine. *Enzymologia* **31**:225–238.

Tosa T, Mori T, Fuse N, Chibata I. 1966b. Studies on continuous enzyme reactions. I. Screening of carriers for preparation of water-insoluble aminoacylase. *Enzymologia* **31**:214–224.

Tosa T, Mori T, Fuse N, Chibata I. 1967. Studies on continuous enzyme reactions. 3. Enzymatic properties of the DEAE-cellulose-aminoacylase complex. *Enzymologia* **32**:153–168.

Truppo MD. 2017. Biocatalysis in the Pharmaceutical Industry: The Need for Speed. *ACS Med. Chem. Lett.* **8**:476–480.

Truppo MD, Strotman H, Hughes G. 2012. Development of an Immobilized Transaminase Capable of Operating in Organic Solvent. *ChemCatChem* **4**:1071–1074.

Tufvesson P, Lima-Ramos J, Nordblad M, Woodley JM. 2011. Guidelines and cost analysis for catalyst production in biocatalytic processes. *Org. Process Res. Dev.* **15**:266–274.

Tural B, Tarhan T, Tural S. 2014. Covalent immobilization of benzoylformate decarboxylase from *Pseudomonas putida* on magnetic epoxy support and its carboligation reactivity. *J. Mol. Catal. B Enzym.* **102**:188–194.

Tural B, Tural S, Ertaş E, Yalınkılıç İ, Demir AS. 2013. Purification and covalent immobilization of benzaldehyde lyase with heterofunctional chelate-epoxy modified magnetic nanoparticles and its carboligation reactivity. *J. Mol. Catal. B Enzym.* **95**:41–47.

Vemmer M, Patel A V. 2013. Review of encapsulation methods suitable for microbial biological control agents. *Biol. Control* **67**:380–389.

Villela Filho M, Stillger T, Müller M, Liese A, Wandrey C. 2003. Is log P a Convenient Criterion to Guide the Choice of Solvents for Biphasic Enzymatic Reactions? *Angew. Chemie - Int. Ed.* **42**:2993–2996.

Vogel C, Pleiss J. 2014. The modular structure of ThDP-dependent enzymes. *Proteins* **82**:2523–2537.

Wachtmeister J, Jakoblinnert A, Rother D. 2016. Stereoselective Two-Step Biocatalysis in Organic Solvent: Toward All Stereoisomers of a 1,2-Diol at High Product Concentrations. *Org. Process Res. Dev.* **20**:1744–1753.

Wachtmeister J, Rother D. 2016. Recent advances in whole cell biocatalysis techniques bridging from investigative to industrial scale. *Curr. Opin. Biotechnol.* **42**:169–177.

Walde P, Ichikawa S. 2001. Enzymes inside lipid vesicles: preparation, reactivity and applications. *Biomol. Eng.* **18**:143–177.

Wang A, Gao W, Zhang F, Chen F, Du F, Yin X. 2012. Amino acid-mediated aldolase immobilisation for enhanced catalysis and thermostability. *Bioprocess Biosyst. Eng.* **35**:857–863.

Wang A, Wang M, Wang Q, Chen F, Zhang F, Li H, Zeng Z, Xie T. 2011. Stable and efficient immobilization technique of aldolase under consecutive microwave irradiation at low temperature. *Bioresour. Technol.* **102**:469–474.

Ward J, Wohlgemuth R. 2010. High-Yield Biocatalytic Amination Reactions in Organic Synthesis.

Curr. Org. Chem. **14**:1914–1927.

Wegner J, Ceylan S, Kirschning A. 2012. Flow chemistry - A key enabling technology for (multistep) organic synthesis. *Adv. Synth. Catal.* **354**:17–57.

Wichmann R, Wandrey C, Bückmann AF, Kula M. 1981. Continuous enzymatic transformation in an enzyme membrane reactor with simultaneous NAD(H) regeneration. *Biotechnol. Bioeng.* **23**:2789–2802.

Widmann M, Radloff R, Pleiss J. 2010. The Thiamine diphosphate dependent Enzyme Engineering Database: a tool for the systematic analysis of sequence and structure relations. *BMC Biochem.* **11**:9.

Wiesbauer J, Bolivar JM, Mueller M, Schiller M, Nidetzky B. 2011. Oriented Immobilization of Enzymes Made Fit for Applied Biocatalysis: Non-Covalent Attachment to Anionic Supports using Zbasic2 Module. *ChemCatChem* **3**:1299–1303.

Wilcocks R, Ward OP, Collins S, Dewdney NJ, Hong Y, Prosen E. 1992. Acyloin formation by benzoylformate decarboxylase from *Pseudomonas putida*. *Appl. Environ. Microbiol.* **58**:1699–1704.

Wilcocks R, Ward OP. 1992. Factors affecting 2-hydroxypropiophenone formation by benzoylformate decarboxylase from *Pseudomonas putida*. *Biotechnol. Bioeng.* **39**:1058–1063.

Wiles C, Watts P. 2012. Continuous flow reactors: a perspective. *Green Chem.* **14**:38–54.

Wohlgemuth R. 2009. The locks and keys to industrial biotechnology. *N. Biotechnol.* **25**:204–213.

Wohlgemuth R. 2010. Biocatalysis—key to sustainable industrial chemistry. *Curr. Opin. Biotechnol.* **21**:713–724.

Wohlgemuth R, Plazl I, Žnidaršič-Plazl P, Gernaey K V., Woodley JM. 2015. Microscale technology and biocatalytic processes: opportunities and challenges for synthesis. *Trends Biotechnol.* **33**:302–314.

Wong C, G. W. 1994. C-C Bond Formation. In: Wong, CH, Whitesides, GM, editors. *Enzym. Synth. Org. Chem.* Oxford: Elsevier, pp. 195–251.

Wong SS, Jameson DM. 2011. Chemistry of Protein and Nucleic Acid Cross-Linking and Conjugation 2nd ed. CRC Press.

Worrall DM, Goss NH. 1989. The formation of biologically active beta-galactosidase inclusion bodies in Escherichia coli. *Aust. J. Biotechnol.* **3**:28–32.

Xu GY, Ong E, Gilkes NR, Kilburn DG, Muhandiram DR, Harris-Brandts M, Carver JP, Kay LE, Harvey TS. 1995. Solution structure of a cellulose-binding domain from *Cellulomonas fimi* by nuclear magnetic resonance spectroscopy. *Biochemistry* **34**:6993–7009.

Xu X, Guo Z, Zhang H, Vikbjerg AF, Damstrup ML. 2006. Chemical and enzymatic interesterification of lipids for use in food. In: Gunstone, FD, editor. *Modifying Lipids Use Food*. Cambridge: Woodhead Publishing, pp. 234–272.

Yan C, Parmeggiani F, Jones EA, Claude E, Hussain SA, Turner NJ, Flitsch SL, Barran PE. 2017. Real-Time Screening of Biocatalysts in Live Bacterial Colonies. *J. Am. Chem. Soc.* **139**:1408–1411.

Yoshino T, Matsunaga T. 2006. Efficient and Stable Display of Functional Proteins on Bacterial Magnetic Particles Using Mms13 as a Novel Anchor Molecule. *Appl. Environ. Microbiol.* **72**:465–471.

Young TS, Schultz PG. 2010. Beyond the Canonical 20 Amino Acids: Expanding the Genetic Lexicon. *J. Biol. Chem.* **285**:11039–11044.

Yu K, Liu C, Kim B-G, Lee D-Y. 2015. Synthetic fusion protein design and applications. *Biotechnol. Adv.* **33**:155–164.

Yuryev R, Strompen S, Liese A. 2011. Coupled chemo(enzymatic) reactions in continuous flow. *Beilstein J. Org. Chem.* **7**:1449–1467.

Zajkoska P, Rebroš M, Rosenberg M. 2013. Biocatalysis with immobilized *Escherichia coli*. *Appl. Microbiol. Biotechnol.* **97**:1441–1455.

Zakeri B, Fierer JO, Celik E, Chittock EC, Schwarz-Linek U, Moy VT, Howarth M. 2012. Peptide tag forming a rapid covalent bond to a protein, through engineering a bacterial adhesin. *Proc. Natl. Acad. Sci. U. S. A.* **109**:690–697.

Zaks A. 1991. Enzymes in Organic Solvents. In: Dordick, JS, editor. *Biocatal. Ind.* Boston, MA: Springer US, pp. 161–180.

Zhang DH, Peng LJ, Wang Y, Li YQ. 2015. Lipase immobilization on epoxy-activated poly(vinyl acetate-acrylamide) microspheres. *Colloids Surfaces B Biointerfaces* **129**:206–210.

Zhang X-H, Liu Z-Q, Xue Y-P, Wang Y-S, Yang B, Zheng Y-G. 2018. Production of *R*-Mandelic Acid Using Nitrilase from Recombinant *E. coli* Cells Immobilized with Tris(Hydroxymethyl)Phosphine. *Appl. Biochem. Biotechnol.* **184**:1024–1035.

Zheng R-C, Zheng Y-G, Shen Y-C. 2010. Acrylamide, Microbial Production by Nitrile Hydratase. In: Flickinger, MC, editor. *Encycl. Ind. Biotechnol.* Hoboken, NJ, USA: John Wiley & Sons, Inc., pp. 26–36.

Zheng Y-G, Yin H-H, Yu D-F, Chen X, Tang X-L, Zhang X-J, Xue Y-P, Wang Y-J, Liu Z-Q. 2017. Recent advances in biotechnological applications of alcohol dehydrogenases. *Appl. Microbiol. Biotechnol.* **101**:987–1001.

Zhou Z, Hartmann M. 2013. Progress in enzyme immobilization in ordered mesoporous materials and related applications. *Chem. Soc. Rev.* **42**:3894–912.

Zuker M. 2003. Mfold web server for nucleic acid folding and hybridization prediction. *Nucleic Acids Res.* **31**:3406–3415.

Danksagung

Viele Menschen haben mich im Laufe dieser Arbeit unterstützt und mitgeholfen, diese Arbeit zu ermöglichen. Daher möchte ich mich an dieser Stelle dafür bedanken:

Es ist nicht immer einfach, die Zusammenhänge der Forschungswelt zu verstehen und dabei gleichzeitig den Fokus auf das Wesentliche zu behalten. Daher bin ich meiner Doktormutter Prof. Martina Pohl sehr dankbar dafür, dass sie mir an den nötigen Stellen den richtigen Weg gezeigt und gleichzeitig genügend Luft und Freiheiten zur Entfaltung gelassen hat. In den seltenen Fällen, in denen Martina nicht zur Verfügung stand, wurde sie hervorragend durch Jun.-Prof. Dörte Rother vertreten, wofür ich ebenfalls sehr dankbar bin. Genauso dankbar bin ich allerdings auch Frau Prof. Vlada Urlacher für die Zeit und Arbeit, welche die Begutachtung und Prüfung dieser Arbeit kosten wird.

Generell bietet das IBG-1: Biotechnologie am Forschungszentrum Jülich hervorragende Bedingungen für eine erfolgreiche Promotion, was hauptsächlich an den Personen liegt, die dieses Institut gestalten und pflegen. Daher bin ich Prof. Wolfgang Wiechert dankbar dafür, dass ich diese Arbeit in so einer gelungenen Atmosphäre durchführen konnte. Genauso danke ich aber auch allen anderen, die an diesem Institut mitwirken: Marianne Hess für die tolle Unterstützung bei allen organisatorischen Fragen, der gesamten Verwaltung, der Werkstatt und der IT.

Doch auch ohne die tägliche Unterstützung von allen Mitgliedern der Biokatalyse und Biosensorgruppe wäre diese Arbeit nicht zu Stande gekommen. Hervorheben möchte ich hier aber mehrere Personen: Dr. Jochen Wachtmeister war in dieser Zeit ein großes Vorbild. Seine Ratschläge waren immer hilfreich und ohne ihn, wäre mir der Einstieg in die Promotion nicht so leicht gefallen. Genauso hilfreich war die Unterstützung von Dr. Zaira Maugeri, die mich bei vielen chemischen Fragestellungen unterstützt hat. Rückblickend ist wahrscheinlich zudem kein Tag vergangen, an dem das tolle Team der Technikerinnen nicht für mich da gewesen wäre. Besondere Unterstützung habe ich dabei in allen Lebenslagen von Heike Offermann erhalten, genauso dankbar bin ich aber auch Ursula Mackfeld, Doris Hahn, Ilona Frindi-Wosch und Lilia Arnold. Abschließend möchte ich nun noch Carmen Prince und Tim Gerlach danken, die als Bachelor- und Masterstudenten viel Zeit und Arbeit in Teile dieser Arbeit investiert haben.

Meinen Kooperationspartnern danke ich außerdem für tolle Zusammenarbeit: Prof. Steven Ley und Dr. Gina Musio von der Universität Cambridge, Dr. Thomas Classen und Julia Bramski vom IBOC, Prof. Matthias Franzreb und Barbara Schmieg vom KIT sowie Prof. Tanja Gulder und Catharina Seel von der TU München.

Nicht nur über diesen Zeitraum der Arbeit, sondern generell und immer haben mich meine Familie und meine Freundin Christina bisher unterstützt. Für eure ständige Hilfe und Verfügbarkeit bei allen Problemen bin ich euch sehr dankbar.